MALAYSIAN JOURNAL OF SCIENCE

Vol. 43 • No 1 • March 2024

MALAYSIAN JOURNAL OF SCIENCE

MJS

ISSN 1394-3065

MJS is indexed in Scopus, Google Scholar, Chemical Abstracts Service Database, ASEAN Citation Index (ACI), and MYCite.

MALAYSIAN JOURNAL OF SCIENCE
MJS
ISSN 1394-3065

Regular Issue

Malaysian Journal of Science 43 (1): 1-10 (Jan 2024) https://mjs.um.edu.my

PHYSICOCHEMICAL PROPERTIES OF HERBAL SOAP MADE FROM AVERRHOA BILIMBI LEAF AND FLOS LONICERAE

Siti Nurul 'Ain Hj Zaiton[1a]*, Hairul Amiza Azman[2a], Norhafini Hambali[3b], Munirah Onn[4a], Saiful Najmee Mohamad[5a], Haikal Mustafa[6c]

Abstract: Malaysian herbs, *Averrhoa Bilimbi*, and *Flos Lonicerae*, are widely known in traditional Chinese medicine. Both are used as natural remedies for jaundice treatment in newborns. Formulating herbal bath soap by the saponification method is proposed because newborn babies are poor feeders. Today, a lot of chemicals are used in soap production. Users will have a wide range of issues due to chemicals like parabens and triclosan. As a result, soap is made from herbs without chemicals. This herbal soap uses two herbs, *Averrhoa Bilimbi* leaf and *Flos Lonicerae*. Paper journals examining these herbs' physicochemical properties are scarce in Malaysia. After the herbal soap has been successfully created, it will be examined for its physicochemical properties. The antioxidant activity and total phenolic content (TPC), of *Averrhoa Bilimbi* leaf extract and *Flos Lonicerae* extract were all tested. The antibacterial activity, heavy metal and pH tests were also validated the suitability of this herbal soap for skin application. According to the findings, *Averrhoa Bilimbi* leaf extract had a TPC value of 24.49 mg GAE/g compared to 4.96 mg GAE/g for *Flos Lonicerae* extract. *Averrhoa Bilimbi* leaf required a slightly higher concentration of 0.0588 g/mL extract to inhibit 50% of the DPPH assay compared to *Flos Lonicerae* plant extract, which required 0.0315 g/mL. Since there was no evidence of any bacterial growth, the herbal soap was effective against all the tested bacterial strains. The heavy metal test showed the soap does not contain any lead, mercury or arsenic and exhibits a pH value which close to the range for suitable skin application.

Keywords: *Physicochemical properties, herbal soap, averrhoa bilimbi leaf, flos lonicerae*

1. Introduction

The use of plants as lead compounds for drug development or refined herbal remedies has always played a critical role in the development of medicines and healthcare preparations (Ekpo et al., 2009). In China, the herbal treatment has been practiced for quite some time and is still very demanding. According to Ayobami et al. (2017), it is possible to formulate topical herbal remedies such as soaps, ointments, creams, lotions, gels or crude/solvent extracts from plants that contain bioactive (antimicrobial) principles for the care and treatment of skin infections as an alternative to synthetic antibiotics. Throughout history, people have taken baths in herbal waters and added other bathing additives that were believed to be beneficial. Nowadays, the use of natural product-based therapies such as herbal soap is very popular. In layman's terms, soap is any substance used with water. Often, it is used to clean skin, clothing, dishes, floors, and walls of soil or grease. According to Warra et al. (2011), from a scientific standpoint, soap is a mixture of sodium or potassium salts of various naturally occurring fatty acids. Unlike synthetic soaps, natural herbal soaps are prepared without artificial surfactants, and contain natural substances, essential oils, or plant extracts as functional ingredients.

As reviewed by Alhassan et al. (2016), *Averrhoa Bilimbi* is one of the important medicinal plants that has been widely used in the traditional system of medicines for various treatments. The tree belongs to the genus *Averrhoa* and the family Oxalidaceae, also known as "Bilimbi", "Cucumber Tree" or "Tree Sorrel" (Ismail et al., 2019; Sutrisna et al., 2019). It functions as a postpartum preventive medicine as well as an antibiotic, antiscorbutic, and astringent. Additionally, it can be used to treat syphilis, rheumatism, diabetes, boils, itches, mumps, and inflammation of the rectum. According to research done by Gogoi et al. (2010), the ripe fruit of *Averrhoa Carambola Linn*, which is related to *Averrhoa Bilimbi* and used to cure infective jaundice, including dyspepsia, is effective in treating this condition. *Lonicerae Flos* is a semi-evergreen climber with fragrant and paired flowers (Li et al., 2018). It has been used as a tea and traditional Chinese medicine remedy in China for more than 1,500 years. It was widely grown in Hunan Province and was a well-known traditional Chinese herbal medicine that was used as a heat-clearing medication and an alexipharmic agent (Zheng et al., 2022). *Lonicerae Flos* primarily contains biologically active substances such as terpenoids, flavonoids, iridoid glycosides, and derivatives

Authors information:
[a]Faculty of Applied Sciences, Universiti Teknologi MARA Cawangan Johor, Kampus Pasir Gudang, Johor, MALAYSIA. E-mail: siti6687@uitm.edu.my[1]; hairulamiza@uitm.edu.my[2]; munirah591@uitm.edu.my[4]; snajmee@uitm.edu.my[5]
[b]College of Engineering, Universiti Teknologi MARA Cawangan Johor, Kampus Pasir Gudang, Johor, MALAYSIA. E-mail: norhafini@uitm.edu.my[3]
[c]College of Engineering, Universiti Teknologi MARA Cawangan Terengganu, Kampus Bukit Besi, Tengganu, MALAYSIA. E-mail: haikal4757@uitm.edu.my[6]
*Corresponding Author: siti6687@uitm.edu.my

Received: October 6, 2022
Accepted: March 3, 2023
Published: March 31, 2024

DOI:https//doi.org/10.22452/mjs.vol43no1.1
Malaysian Journal of Science 43(1): 1-10 (March 2024)

of caffeic acid. Plant extracts have been shown to have a variety of biological properties, including anti-inflammatory, anti-cancer, antioxidant, antiallergenic, immunomodulating, and antibacterial action (Tang et al., 2018).

Antioxidants have gained recognition as scientifically fascinating compounds because of their many health benefits, such as their anti-inflammatory and anti-aging effects. Studies on antioxidants conducted in vivo or in vitro have shown a variety of findings about the prevention of illnesses. As a result, the use of antioxidants in pharmacology, cosmetics, and medicine gained significance (Zehiroglu & Ozturk, 2019). Antioxidants are helpful in extending the shelf life of consumer goods because they are effective bio-regulators, oxidation suppressors, and bio-regulators. Antioxidant-active components are present in manufactured natural herbal soaps, however, it is unclear how this affects shelf life (Adigun et al., 2019).

The microbes (bacteria, fungi, protozoa, archaea) that inhabit and exist in the human body have significant implications for health. According to the body places they dwell, these microorganisms are assumed to have co-evolved with humans. They serve a variety of tasks for the host, from digesting to immunological protection. Understanding how antibacterial products affect the microbial skin communities of people living in rural areas of developing countries is crucial as the availability and adoption of these products increase globally (Yu et al., 2018). Skin and wound bacterial infections can significantly reduce a patient's quality of life and even result in death in some cases. One of the main concerns in their management is the spread of resistant strains outside of hospitals and into the general population as a result of the increasing antibiotic resistance of bacterial pathogenic diseases. The discovery of innovative medicinal drugs that are effective and secure is encouraged by this pattern. The pharmaceutical industry frequently fails in its fight against germs because it primarily on libraries of synthetic compounds as a source for therapeutic discovery. Contrarily, numerous organic substances, as well as complete, complex plant extracts, are efficient in this area, inactivating resistant bacterial strains or reducing their pathogenicity. Natural products like herbs have not only antibacterial but also anti-inflammatory effects and may support tissue regeneration and wound healing (Bittner et al., 2021).

According to the American Cleaning Institute (2019), pH indicates whether a substance is acidic or alkaline. In soap preparation, soap quality is greatly influenced by pH. Warra (2013) claims that soaps with pH levels below five and significantly above 10 are harsh on the hands and skin. Additionally, by definition, soap is the salt of a weak acid (fatty acid) and a weak base, and because soap is generally alkaline in aqueous solutions, its pH is typically above 7. The statement is supported by Tokosh and Baig (1995), who state that all soap-based formulations should produce alkaline pH solutions. Incomplete alkaline hydrolysis has caused the pH to be high, indicating that a large percentage of matters are unclear and unresolvable during the saponification process.

Phytochemical compounds such as flavonoids and phenolic compounds have been well-known for their benefits for human health or for their ability to cure or prevent diseases for many years. Commonly known as secondary metabolites, these compounds have at least one hydroxyl group on their aromatic ring (Tungmunnithum et al., 2018). There are more than 8000 naturally occurring phenolic compounds present in plants. In addition to flavonoids and many other phenolic compounds found in herbs and nutrients. These phytochemical substances have been reported to act as effective antioxidants, anti-cancer agents, antibacterial agents, cardioprotective agents, anti-inflammation agents, immune system enhancing agents, and skin protection (Kumar et al., 2013; Chen et al., 2015; Dzialo et al., 2016; Ahmed et al., 2016; Andreu, 2018; Meng et al., 2018).

In this study, the Malaysian herbs *Averrhoa Bilimbi* and *Flos Lonicerae*, which are widely used in traditional Chinese medicine, were used to treat jaundice in newborn babies naturally. Because babies are not good eaters when they are newborn, herbal bath soap made from *Averrhoa Bilimbi* and *Flos Lonicerae* is made using saponification. Soap frequently contains many chemicals that may not suit babies' skin. Thus, this study aimed to produce herbal soap without using chemicals. Aside from that, studies on the antioxidant activity and total phenolic content of *Averrhoa Bilimbi* and *Flos Lonicerae* herbs are scarce in Malaysia. Thus, after the solvent extraction process, both *Averrhoa Bilimbi* and *Flos Lonicerae* extracts were quantified for their antioxidant activity and total phenolic content. The soap produced was further tested for antimicrobial activity, heavy metals, and pH to validate its suitability for skin application.

2. Methodology

Preparation of Herbal Soap

The tropical *Averrhoa Bilimbi* tree is a common species in Malaysia. The leaves of *Averrhoa Bilimbi* were washed and dried under the sun for one to two months, depending on the weather. Meanwhile, the dried *Flos Lonicerae* was bought from the store. Both dried *Averrhoa Bilimbi* and *Flos Lonicerae* were pounded into a fine powder. Virgin coconut and lavender essential oils were added to a glycerin-free SLS solution. An equal portion of both *Flos Lonicerae* and *Averrhoa Bilimbi* leaf powders were then added to the solution. After being poured into a silicone mold, the solution was dried at room temperature. The soap must be completely dry below room temperature to prevent fungus from growing on the surface of the soap.

Physicochemical Test

The extraction process of both dried *Averrhoa Bilimbi* and *Flos Lonicerae* is conducted before the antioxidant activity and total phenolic content of the herbs can be quantified. Physicochemical testing for the herbal soap has been carried out in the UiTM Pasir Gudang, Johor laboratory, with some tests being outsourced to independent labs.

DOI:https//doi.org/10.22452/mjs.vol43no1.1
Malaysian Journal of Science 43(1): 1-10 (March 2024)

Extraction

The extraction process was done using a Soxhlet extractor and a rotary evaporator. The samples of *Averrhoa Bilimbi* and *Flos Lonicerae* were weighed. These samples were placed in an extraction thimble that was about ¾ full. A round bottom flask of the Soxhlet extractor was filled with 200 mL of methanol-water solvent. After being inserted into the extractor fitting, the thimbles were linked to the top of the flask with a round bottom. The condenser is then connected to the extractor fitting's top. For an 8-hour extraction period, the heater is put on to heat the methanol.

A round-bottom flask containing methanol and extraction solution was placed in a rotary evaporator after extraction to separate the oil further. The oil separation process was obtained to make sure no more solvent (methanol) was in the solution. The extraction of samples was transferred to bottles wrapped in aluminium foil and stored in a 2°C refrigerator.

Antioxidant Activity Test

The basic scavenging impact on the stable DPPH free radical activity was tested as part of the antioxidant activity test. The approach outlined by Veeru et al. (2009) was followed for the antioxidant activity procedure with some modifications. 1.0 mL of 0.002% DPPH in methanol was added into 1.0 mL of sample extract. A 30-minute storage period at room temperature was performed on the mixture in the dark. The absorbance of the mixture was measured at 517 nm by using methanol as the blank. The control was a solution containing 1.0 mL of methanol and 1.0 mL of 0.002% DPPH. The free-radical scavenging activities in terms of % inhibition can be calculated by the following equation:

$$\% \text{ inhibition} = [(A_0 - A_e) / A_0] \times 100\%$$

where A_0 is the absorbance value of the control while A_e is the absorbance of the extract. Tests were conducted on five concentrations of sample extracts to determine the % inhibition of each extract. To compare the antioxidant activity of the phenolic content, the IC_{50} value was used. This value represents the concentration of sample extract required to inhibit 50% of the free radical present in the DPPH solution.

Phenolic Contents Determination

Using Follin-Ciocalteu reagent, the Follin-Ciocalteu method is used to assess the phenolic acid concentration and total content of the sample extract. Based on Ibrahim et al. (2010), with slight adjustments, the following procedure was carried out: 1.0 mL of sample extract was combined with 3.0 mL of 20% sodium carbonate, 0.5 mL of the Follin-Ciocalteu reagent, and 10 mL of distilled water. The resulting mixture was kept at room temperature for a 2-hour reaction period. Following two hours, methanol was used as a blank in place of the sample extract to measure absorbance at 765 nm. The phenolic acid concentration is measured by comparing it to a constructed standard curve. On the other hand, the sample extract's total phenolic content was determined by applying the equation below:

$$C = cx (V/m)$$

where

c - concentration of gallic acid (mg GAE/mL) from a standard curve

C - total phenolic content (mg GAE/g) from the sample extract

m - dry weight of sample (g)

V - volume of the sample extract (mL)

Microbiology Test

Sample of the herbal soap was sent to Chemical Laboratory (Malaysia) Sdn Bhd for microbiology test.

pH Testing

The pH of the herbal soap was determined using pH meter model PH300 purchased from Eutech.

3. Findings

In this work, the saponification technique was used to turn *Averrhoa Bilimbi* leaf and the *Flos Lonicerae* plant into herbal soap product for easy application on the skin. Both extracts were tested for antioxidant activity and total phenolic content. The herbal soap was further tested for the antibacterial activity, toxicity and pH tests. This is to verify the heavy metal content and to ensure the pH falls within the suitable range for skin application.

Antioxidant Activity

Antioxidants are becoming increasingly popular as illness preventative and therapy options. Antioxidants are chemicals that interact with free radicals and neutralise them, preventing cellular harm. Many plants exhibit antioxidant activities that can be therapeutically beneficial, based on their therapeutic potential as an antioxidant in lowering such free radicals. Antioxidants' therapeutic potential in treating conditions including cancer, diabetes, and neurological disorders that are linked to oxidative stress has received a lot of attention recently. In this study, the antioxidant activity of both *Averrhoa Bilimbi* leaf and *Flos Lonicerae* plant extracts was examined in light of their ability to scavenge stable DPPH free radical activity. A percent inhibition versus concentration curve was constructed for each test solution, and the sample concentration necessary to achieve 50% inhibition was determined and given as an IC_{50} value. Figure 1 shows the amount of each *Flos Lonicerae* and *Averrhoa Bilimbi* leaf extract required for 50% inhibition of DPPH activity (IC_{50}). *Averrhoa Bilimbi* leaf required a slightly higher concentration of 0.0588 g/mL extract to inhibit 50% of DPPH assay compared to *Flos Lonicerae* plant extract which required 0.0315 g/mL. This suggest that *Flos Lonicerae* plant extract exhibited slightly higher antioxidant activity compared to *Averrhoa Bilimbi* leaf extract.

The findings of this investigation were in line with those of a previous study by Lan et al. (2007), who discovered that the aqueous, methanolic, and 70% ethanolic extracts of *Flos*

DOI:https//doi.org/10.22452/mjs.vol43no1.1
Malaysian Journal of Science 43(1): 1-10 (March 2024)

Lonicerae have the ability to scavenge DPPH radicals and reduce Fe^{3+} to Fe^{2+}. As a significant contributor to this activity, this study also identified a crucial *Flos Lonicerae* ingredient termed chlorogenic acid, which was purified using HPLC from a 70% ethanolic extract. This implies that the extract of *Flos Lonicerae* might be employed as a natural source of antioxidants for the treatment of particular disorders (Lan et al., 2007). Rahman et al. (2014) investigation's into the antioxidant properties of the *Averrhoa Bilimbi* ethanolic extract revealed that the concentration of the extracts increased the reducing power of the crude ethanol extracts, and the *Averrhoa Bilimbi* extracts demonstrated moderate free radical scavenging activity against DPPH with an IC_{50} value of 635.066 ± 8.4102 g/mL. (Rahman et al., 2014). This suggest that both *Averrhoa Bilimbi* leaf and the *Flos Lonicerae* plant exhibit antioxidant activities that can be therapeutically beneficial, based on their therapeutic potential as an antioxidant in lowering such free radicals.

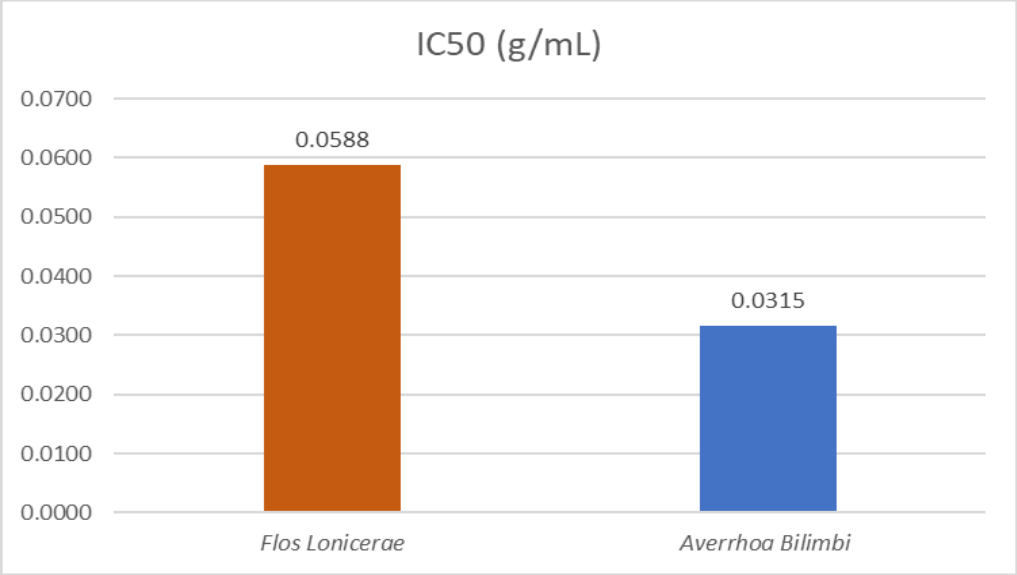

Figure 1. Free radical scavenging activity (IC_{50}) in *Flos Lonicerae* and *Averrhoa Bilimbi* leaf.

Phenolic Content

The total phenolic content (TPC) of both the methanolic extract of *Averrhoa Bilimbi* leaf and the *Flos Lonicerae* plant were investigated in this study. Phenolic compounds, which have low toxicity, are a form of secondary metabolite. These compounds can take the form of polyphenol structures, which include aromatic rings with hydroxyl groups, as well as simpler structures like phenolic acids and phenolic alcohols that consist of just one phenol ring. A phenolic molecule typically contains at least one phenyl ring, but a more reactive residue, such as methyl, hydroxyl, or acetyl, can replace it (Setyawan et al., 2021). TPC concentrations were calculated using the Follin Ciocalteu method. A spectrophotometer operating at a wavelength of 765 nm can be used to identify blue complexes, which are the foundation of the Follin Ciocalteu technique. Gallic acid equivalents were used to quantify the amounts of TPC in methanolic extracts (GAE). The results showed that *Flos Lonicerae* extract had a TPC value of 5.0 mg GAE/g, while *Averrhoa Bilimbi* leaf extract had a TPC value of 24.5 mg GAE/g (refer Figure 2). *Averrhoa Bilimbi* leaf ethanolic extract contained a greater value of TPC, 39.03 ± 0.25mg GAE/g, according to a study by Setyawan et al. (2021). The kind of solvent employed for the extraction had an impact on the value of TPC that was recovered. This is because the number of phenolic groups in a substance affects how it responds to the Folin-Ciocalteu reagent. The compatibility of phenolic compounds with the solvent system is closely related to a sample where its phenolic compounds are extracted, according to the "like-dissolves-like" idea. (Othman et al., 2014). The phytochemical screening of the *Averrhoa Bilimbi* extractives revealed the presence of flavonoid, tannin, and phenol, according to Hasanuzzaman et al. (2013). It has been demonstrated that plant-derived polyphenols such as flavonoids, tannins, and phenolic acids have a range of biological effects, including antioxidant activity. According to phytochemical screening, the flavonoids and tannins included in the plant extract from *Averrhoa Bilimbi* may be the cause of the extract's antioxidant action. According to the same study, the total phenolic content of several *Averrhoa Bilimbi* extracts ranges from 50.23 to 68.67 mg of GAE/g (Hasanuzzaman et al., 2013).

Flos Lonicerae, on the other hand, was found to contain 16 phenolic acids, the majority of which are caffeic acid derivatives. Neochlorogenic acid, caffeic acid, chlorogenic acid, isochlorogenic acid A-C, and cynarin are the primary phenolic acids found in *Flos Lonicerae* (Li et al., 2019). Among the naturally occurring substances with antioxidative strength are phenolic acids, which react with free radicals to form a new radical that is stabilized by the resonance action of the aromatic nucleus. The potential for antioxidant activity may be stronger in phenolic acids that have a second hydroxy group in the ortho or para position. Numerous

DOI:https//doi.org/10.22452/mjs.vol43no1.1
Malaysian Journal of Science 43(1): 1-10 (March 2024)

investigations have shown that variations in phenolic acid concentration are always significantly correlated with changes in antioxidant intensity. Chlorogenic acid and caffeic acid, the two most researched elements in *Flos Lonicerae*, have both been demonstrated to have strong anti-inflammatory and antioxidant capabilities both in vitro and in vivo by removing harmful free radicals from the body (Li et al., 2019). Another study discovered that the chlorogenic acid in *Flos Lonicerae* shields mice from acute liver damage brought on by intraperitoneal injection of carbon tetrachloride as well as alcohol-induced chemical liver injury (CCl_4) (Li et al., 2019). It can be concluded that both *Averrhoa Bilimbi* leaf and the *Flos Lonicerae* plant are a good source of phytochemicals that exhibits many pharmacological activities.

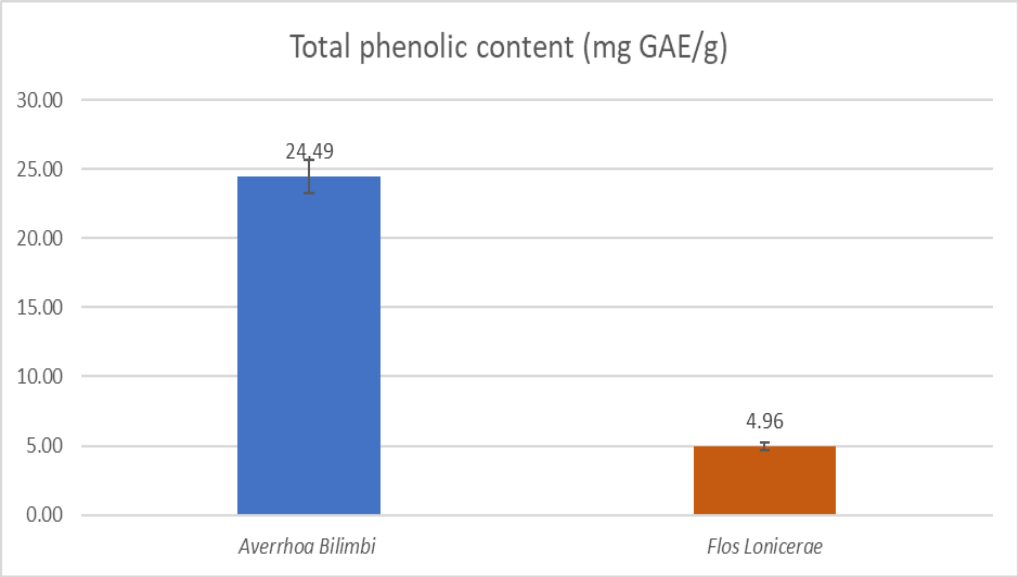

Figure 2. Total phenolic content (mg GAE/g) in *Flos Lonicerae* and *Averrhoa Bilimbi* leaf.

Microbiology Testing

The goal of the current study was to assess the antimicrobial activity of herbal soap against *Escherichia coli*, *Salmonella*, *Typhimurium*, *Staphylococcus aureus*, and *Enterococcus* sp. in vitro. The soap was made using the saponification process and contains extracts of *Averrhoa Bilimbi* leaf and *Flos Lonicerae*. According to Table 1, the herbal soap was efficient against all of the tested bacterial strains since no bacterial growth was seen. Compared to the National Pharmaceutical Regulatory Agency (NPRA) criteria, the total plate count test revealed relatively low bacteria growth of 30 cfu/g. The presence of hydrophilic and hydrophobic antibacterial components from extracts of *Averrhoa Bilimbi* leaf and *Flos Lonicerae* revealed that the herbal soap has antibacterial efficacy against some bacteria. In this study, the antibacterial activity of the herbal soap could be associated with the antioxidant activity and phenolic content of both the extracts of *Averrhoa Bilimbi* leaf and *Flos Lonicerae*. This conclusion was also consistent with prior research that suggested *Averrhoa Bilimbi's* antibacterial activity was linked to the presence of bioactive flavonoids such as apigenin and luteolin (Zakaria et al., 2007). In a different investigation, it was discovered that the ethanol extracts, water extracts with alcohol precipitating solution, and water extracts of *Flos Lonicerae* were highly inhibitory against a range of pathogens, including *Pseudomonas aeruginosa*, *Bacillus subtilis*, *Staphylococcus aureus*, *Candida albicans, and Shigella dysenteriae* (Li et al., 2019).

Table 1. Antibacterial test on jaundice soap containing *Averrhoa Bilimbi* leaf and *Flos Lonicerae.*

Parameter Test	Results	NPRA Specification
Total plate count, cfu/g	30	≤ 5 x 10^4
Total Yeast & Mould Count, cfu/g	No growth <10	≤ 5 x 10^2
E. coli in 1g	Not present in 1g	Not present in 1g
Staphylococcus aureus in 1g	Not present in 1g	Not present in 1g
Salmonella in 10g	Not present in 10g	Not present in 10g
Enterobacteriaceae and certain other gram-negative bacteria	Absent	≤ 5 x 10^2

Heavy Metal Test and pH

The goal of this investigation was to find out how much heavy metals were in the herbal soap. There are concerns about the existence of hazardous compounds in herbal soap, which can be dangerous to children, particularly babies. It is noteworthy that babies have fragile skin and poor skin barriers, which makes them more vulnerable to skin damage and compels particular care (Kuo et al., 2020). Heavy metals such as mercury, lead and arsenic were

DOI:https//doi.org/10.22452/mjs.vol43no1.1
Malaysian Journal of Science 43(1): 1-10 (March 2024)

not discovered in this product, as stated in Table 2. This is due to the ingredients used in the herbal soap where only glycerine, essential oil, and plant extract were used in the saponification procedure.

The acidic pH of the skin's surface is known to play a role in maintaining the homeostasis and permeability of the stratum corneum. Acidic pH seems to have the most important effects on the process of keratinocyte differentiation, the formation and function of epidermal lipids and the corneocyte lipid envelope, and the maintenance of the skin microbiome. Most people agree that products that go on the skin should be acidic and have a pH between 4 and 6 (Lukić et al., 2021). The pH of the herbal soap formulation has the pH of 7.82 (refer Figure 3). Skin products should have a pH that is as close to this range as feasible to reduce irritation. Even though the readings are not within the pH range, but the pH of this herbal soap is close to the recommended range.

Table 2. Heavy metal test on herbal soap containing *Averrhoa Bilimbi* leaf and *Flos Lonicerae*.

Parameter Test	Results	NPRA Specification
Lead as Pb, ppm	Not detected (<0.01)	≤ 10
Mercury as Hg, ppm	Not detected (<0.005)	≤ 0.5
Arsenic as As, ppm	Not detected (<0.005)	≤ 5.0

Figure 3. pH testing on herbal soap

4. Conclusion

As a conclusion, the herbal soap containing *Averrhoa Bilimbi* leaf and *Flos Lonicerae* by saponification method is successfully produced and its physicochemical properties have been investigated. The total phenolic content (TPC) value for *Averrhoa Bilimbi* leaf extract was 24.49 mg GAE/g as opposed to 4.96 mg GAE/g for *Flos Lonicerae* extract. Compared to *Flos Lonicerae* plant extract, which needed 0.0315 g/mL, *Averrhoa Bilimbi* leaf required a slightly greater quantity of 0.0588 g/mL extract to achieve 50% inhibition of the DPPH assay. The herbal soap proved efficient against all of the tested bacterial strains because there was no sign of bacterial development. Natural goodness from organic nature is present in herbal soaps, making them healthy for the skin. The created herbal soap contains no heavy metal and possesses a pH value which close to the recommended range.

5. Acknowledgement

This effort would not have been feasible without the financial assistance of the G-Best Phase 2 UiTM Johor Branch. We would also want to thank the Science Officer and Assistant Engineer of the laboratory at the College of Engineering at the UiTM Johor Branch Pasir Gudang Campus.

6. References

Adigun, O., Manful, C., Prieto Vidal, N., Mumtaz, A., Pham, T. H., Stewart, P., Nadeem, M., Keough, D., & Thomas, R. (2019). Use of natural antioxidants from newfoundland wild berries to improve the shelf life of natural herbal soaps. *Antioxidants (Basel, Switzerland)*, 8(11), 536. https://doi.org/10.3390/antiox8110536

Ahmed, S. I., Hayat, M. Q., Tahir, M., Mansoor, Q., Ismail, M., Keck, K., & Bates, R. B. (2016). Pharmacologically active flavonoids from the anti-cancer, antioxidant and antimicrobial extracts of Cassia angustifolia Vahl. *BMC Complementary and Alternative Medicine.* 16(460), 1-9. https://doi.org/10.1186/s12906-016-1443-z

Alhassan, A. M., & Ahmed, Q. U. (2016). Averrhoa bilimbi Linn: A review of its ethnomedicinal uses, hytochemistry and pharmacology. *Journal of Pharmacy & Biollied Sciences.* 8(4), 265-271. https://doi.org/10.4103/0975-7406.199342

American Cleaning Institute (2019) The science of soap: an introduction to the science of how things get clean. https://www.cleaninginstitute.org/sites/default/files/assets/1/AssetManager/Science ofSoap.pdf

Andreu, L., Nuncio-Jáuregui, N., Carbonell-Barrachina, Á. A., Legua, P., & Hernández, F. (2018). Antioxidant properties and chemical characterization of Spanish Opuntia ficus-indica Mill. cladodes and fruits. *Journal of the Science of Food and Agriculture.* 98, 1566–1573. https://doi.org/10.1002/jsfa.8628

Assimakopoulos, S. F., & Vagianos, C. E. (2009). Bile duct ligation in rats: a reliable model of hepatorenal syndrome? *World Journal of Gastroenterol.* 15. 121.

Aydın, S., Tokaç, M., Taner, G., Arıkök, A. T., Dündar, H. Z., Ozkardeş, A. B., Taşlıpınar, M. Y., Kılıç, M., Başaran, A. A., & Başaran, N. (2013). Antioxidant and antigenotoxic effects of lycopene in obstructive jaundice. *The Journal of surgical*

DOI:https//doi.org/10.22452/mjs.vol43no1.1
Malaysian Journal of Science 43(1): 1-10 (March 2024)

research. *182*(2), 285–295. https://doi.org/10.1016/j.jss.2012.10.031

Ayobami, O. O., Ezekiel, O. A., Doyinsola, D. F., & Lara O. O. (2017). Physicochemical properties and antimicrobial activities of soap formulations containing Senna alata and Eugenia uniflora leaf preparations. *Journal of Medicinal Plants Research,* 11(48), 778-787 https://doi.org/10.5897/JMPR2017.6515

Ayyappan, S., Philip, S., Bharathy, N., Ramesh, V., Kumar, C. N., Swathi, S., & Kumar, A. A. (2015). Antioxidant status in neonatal Jaundice before and after phototherapy. *Journal of Pharmacy & Bioallied Sciences,* 7(Suppl 1), S16–S21. https://doi.org/10.4103/0975-7406.155766

Bittner Fialová, S., Rendeková, K., Mučaji, P., Nagy, M., & Slobodníková, L. (2021). Antibacterial activity of medicinal plants and their constituents in the context of skin and wound infections, considering European legislation and folk medicine—a review. *International Journal of Molecular Sciences*. 22(19), 10746. https://doi.org/10.3390/ijms221910746

Boo, N. Y., Gan, C. Y., Gian, Y. W., Lim, K. S. L., Lim, M. W, & Krishna-Kumar, H. (2011). Malaysian mothers' knowledge & practices on care of neonatal Jaundice. *Med J Malaysia.* 66 (3), 239- 243. PMID 22111448.

Carlsen, M. H., Halvorsen, B. L., Holte, K., Bøhn, S. K., Dragland, S., Sampson, L., Willey, C., Senoo, H., Umezono, Y., Sanada, C., Barikmo, I., Berhe, N., Willett, W. C., Phillips, K. M., Jacobs, D. R., Jr, & Blomhoff, R. (2010). The total antioxidant content of more than 3100 foods, beverages, spices, herbs and supplements used worldwide. *Nutrition journal,* 9*, 3*. https://doi.org/10.1186/1475-2891-9-3

Chen, X., Dang, T. T. T., & Facchini, P. J. (2015) Noscapine comes of age. *Phytochemistry*. 111, 7–13. https://doi.org/10.1016/j.phytochem.2014.09.008

Cruz, A., Padillo, F. J., Túnez, I., Muñoz, C., Granados, J., Pera-Madrazo, C., & Montilla, P. (2001). Melatonin protects against renal oxidative stress after obstructive Jaundice in rats, *Europian Journal of Pharmacology*. 425. 135-139. https://doi.org/10.1016/S0014-2999(01)01173-6

Dantas, A. V. V. C., Farias, L. J. R., de Paula, S. J., Moreira, R. P., da Silva, V. M., Lopes, M. V. O., & Guedes, N. G. (2018). Nursing diagnosis of neonatal jaundice: study of clinical indicators. *J. Pediatric. Nursing.* 39, 6–10. https://doi.org/10.1016/j.pedn.2017.12.001

Dnyaneshwar, M. N., Shekhar, B. Y., Shaijesh, S. W., & Juvekar, R. (2010) Hepatoprotective effect of Averrhoa bilimbi Linn. against carbon tetrachloride induced hepatic damage in rats. *Pharmacologyonline.* 3, 1–6.

Dzialo, M., Mierziak, J., Korzun, U., Preisner, M., Szopa, J., & Kulma, A. (2016). The potential of plant phenolics in prevention and therapy of skin disorders. *International Journal of Molecular Science.* 17(160), 1-41. https://doi.org/10.3390/ijms17020160

Egube, B. A., Ofili, A. N., Isara, A. R., & Onakewhor, J. U. (2013). Neonatal Jaundice and its management: knowledge, attitude, and practice among expectant mothers attending antenatal clinic at University of Benin Teaching Hospital, Benin City, Nigeria. *Nigerian Journal of Clinical Practice.* 16(2):188-194. http://dx.doi.org/10.4103/1119-3077.110147.

Esan, D. T., Muhammad, F., Ogunkorode, A., Obialor, B., & Ramos, C. (2022). Traditional beliefs in the management and prevention of neonatal Jaundice in Ado-Ekiti, Nigeria. *Enfermería Clínica (English Edition), 32 Suppl 1,* S73-S76. https://doi.org/10.1016/j.enfcle.2021.09.006.

Gogoi, J. C., Mohanta, D., & Borah, P. (2010). Hepatoprotective Activity of Averrhoa Carambola, Cajanus Cajan and Paederia Foetida against Acetaminophen and D-Galactosamine Induced Hepatotoxicity in Rats. *Journal of Pharmaceutical Research.* 9 (2),76. http://dx.doi.org/10.18579/jpcrkc/2010/9/2/79491

Gonzalez-Correa, J. A., De La Cruz, J. P., Martin-Aurioles, E., Lopez-Egea, M. A., Ortiz, P., & Sanchez de la Cuesta, F. (1997). Effects of S-adenosyl-L-methionine on hepatic and renal oxidative stress in an experimental model of acute biliary obstruction in rats. *Hepatology (Baltimore, Md.)*, 26(1), 121–127. https://doi.org/10.1002/hep.510260116

Govindan, P., & Muthukrishnan, S. (2013). Evaluation of total phenolic content and free radical scavenging activity of Boerhavia erecta. *Journal of Acute Medicine*, 3(3), 103–109. https://doi.org/10.1016/j.jacme.2013.06.003.

Greig, J. D., Krukowski, Z. H., & Matheson, N. A. (1988). Surgical morbidity and mortality in one hundred and twenty-nine patients with obstructive jaundice. *The British journal of surgery*, 75(3), 216–219. https://doi.org/10.1002/bjs.1800750309

Guo, Y. P., Lin, L. G., & Wang, Y. T. (2015). Chemistry and pharmacology of the herb pair Flos Lonicerae japonicae-Forsythiae fructus. *Chinese medicine*, 10, 16. https://doi.org/10.1186/s13020-015-0044-y

Hafizuddin A., Siti M. J., Nurul A. W. I., & Zawiyah D. (2019). Determinants of neonatal jaundice among newborns in Pasir Puteh District, Kelantan. *International Journal of Public Health*

DOI:https//doi.org/10.22452/mjs.vol43no1.1
Malaysian Journal of Science 43(1): 1-10 (March 2024)

and Clinical Sciences. 6(6):109-122. https://doi.org/10.32827/ijphcs.6.6.109

Halliwell, B. (1994). Free radicals, antioxidants and human disease: curiosity, cause or consequence? *The Lancet.* 344. 721. https://doi.org/10.1016/S0140-6736(94)92211-X

Hasanuzzaman, M., Ali, M. R., Hossain, M., Kuri, S., & Islam, M. S. (2013). Evaluation of total phenolic content, free radical scavenging activity and phytochemical screening of different extracts of Averrhoa bilimbi (fruits). *International Current Pharmaceutical Journal*. 2(4), 92–96. https://doi.org/10.3329/icpj.v2i4.14058

Horst, R. K. (2013). Honeysuckle (Lonicera). *Westcott's Plant Disease Handbook*. 909–910. https://doi.org/10.1007/978-1-4020-4585-1_2079

Huang, W., Zhang, J., & Moore, D. D. (2004). A traditional herbal medicine enhances bilirubin clearance by activating the nuclear receptor CAR. *The Journal of clinical investigation.* 113(1), 137–143. https://doi.org/10.1172/JCI18385

Ibrahim, T. A., El-Hefnawy, H. M., & El-Hela, A. A. (2010). Antioxidant potential and phenolic acid content of certain cucurbitaceous plants cultivated in Egypt. *Natural product research*, *24*(16), 1537–1545. https://doi.org/10.1080/14786419.2010.489049

Ismail, S., Marliana, E., & Kosala, K. (2019). Effect of pH increasing of Wuluh Star Fruit (Averrhoa Bilimbi L.) juice on vasodilatation activity. *Journal of Physics: Conference Series*. 1277(1), 012017. https://doi.org/10.1088/1742-6596/1277/1/012017

Kaplan, M., Muraca, M., Hammerman, C., Rubaltelli, F. F., Vilei, M. T., Vreman, H. J., & Stevenson, D. K. (2002). Imbalance between production and conjugation of bilirubin: a fundamental concept in the mechanism of neonatal jaundice. *Pediatrics*. 110(4), e47. https://doi.org/10.1542/peds.110.4.e47

Karatepe O., Acet E., Battal, M., Adas, G., Kemik, A., Altiok, M., Kamali, G., Koculu, S., Cagatay, A., Kamali, S., & Karahan, S. (2010). Effects of glutamine and curcumin on bacterial translocation in jaundiced rats. *World Journal of Gastroenterol.* 16. 4313. http://dx.doi.org/10.3748/wjg.v16.i34.4313

Kennedy, T. A., & Liebler, D.C. (1992). Peroxyl radical scavenging by bcarotene in lipid bilayers, World Journal of Gastroenterol. *Journal of Biological Chemistry*. 267(7). 4658-4663. https://doi.org/10.1016/S0021-9258(18)42884-0

Kumar, S., & Pandey, A. K. (2013). Chemistry and biological activities of flavonoids: An overview. *The Scientific World Journal,* 2013 (162750), 1-16. https://doi.org/10.1155/2013/162750

Kuo, S. H., Shen, C. J., Shen, C. F., & Cheng, C. M. (2020). Role of pH value in clinically relevant diagnosis. *Diagnostics*, 10(2), 1–17. https://doi.org/10.3390/diagnostics10020107

Lan, Wu., Zhaojun, Z., & Zesheng, Z. (2007) Characterization of antioxidant activity of extracts from flos lonicerae. *Drug Development and Industrial Pharmacy*. 33:8, 841-847. https://doi.org/10.1080/03639040701378019.

Li, Y., Li, W., Fu, C., Song, Y., & Fu, Q. (2019). Lonicerae japonicae flos and Lonicerae flos: A systematic review of ethnopharmacology, phytochemistry and pharmacology. *Phytochemistry Reviews.* 19(1), 1–61. https://doi.org/10.1007/s11101-019-09655-7

Linqing, W., Hongying, Z., Wenzeng, L., & Kuntao, L. (2011). The study on antiviral effect of chlorogenic acids from Lonicerae japonicas flos and Lonicerae flos on NDV in vitro. *Chinese Agricultural Science Bulletin.* vol. 27, no. 19, pp. 277–282.

Lukić, M., Pantelić, I., & Savić, S. D. (2021). Towards optimal pH of the skin and topical formulations: From the current state of the art to tailored products. *Cosmetics*, *8*(3). https://doi.org/10.3390/cosmetics8030069

Meng, X. H., Liu, C., Fan, R., Zhu, L. F., Yang, S. X., Zhu, H.T., Wang, D., Yang, C. R., & Zhang, Y. J., (2018). Antioxidative flavan-3-ol dimers from the leaves of Camellia fangchengensis. *Journal of Agriculture and Food Chemistry.* 66, 247–254. https://doi.org/10.1021/acs.jafc.7b04572

Miller, N. J., Sampson, J., Candeias, L.P., Bramley, P. M., Rice-Evans, C. A. (1996). Antioxidant activities of carotenes and xanthophylls, *FEBS Letter.* 384. 240-242. https://doi.org/10.1016/0014-5793(96)00323-7

Mitra, S., & Rennie, J. (2017). Neonatal Jaundice: aetiology, diagnosis and treatment. *British. Journal of Hospital Medicine.* 78 (12), 699-704. https://doi.org/10.12968/hmed.2017.78.12.699

Novo, C., & Welsh, F. (2017). Jaundice. *Surgery.* 35 (12), 675-681. https://doi.org/10.1016/j.mpsur.2017.09.012

Olusanya, B. O., Osibanjo, F. B., Mabogunje, C. A., Slusher, T. M., & Olowe, S. A. (2016). The burden and management of neonatal Jaundice in Nigeria: a scoping review of the literature. *Nigerian Journal Clinical Practice.* 19 (1), 1-17. http://dx.doi.org/10.4103/1119-3077.173703.

Othman, A., Mukhtar, N. J., Ismail, N. S., & Chang, S. K. (2014). Phenolics, flavonoids content and antioxidant activities of 4

DOI:https//doi.org/10.22452/mjs.vol43no1.1
Malaysian Journal of Science 43(1): 1-10 (March 2024)

Malaysian herbal plants. *International Food Research Journal*. 21(2), 759–766.

Panahandeh, G., Khoshdel, A., Sedehi, M., & Aliakbari, A. (2017). Phytotherapy with Hordeum Vulgare: A Randomized Controlled Trial on Infants with Jaundice. *Journal of clinical and diagnostic research: JCDR*. 11(3), SC16–SC19. https://doi.org/10.7860/JCDR/2017/22177.9586

Paur, I., Carlsen, M. H., Halvorsen, B. L., & Blomhoff, R. (2011). Antioxidants in Herbs and Spices: Roles in Oxidative Stress and Redox Signaling. In I. F. F. Benzie (Eds.) et. al., *Herbal Medicine: Biomolecular and Clinical Aspects*. *(2nd ed.). CRC Press/Taylor & Francis.* https://pubmed.ncbi.nlm.nih.gov/22593932/

Peng, C., Hou, X. (2020). Key points of neonatal jaundice, queensland maternity and neonatal clinical guideline, 2018. *Chinese Journal Perinatal Medicine.* 23 (4), 285–288. https://doi.org/10.3760/cma.j.cn113903-20190624-00399

Pincemail, J. (1995). Free radicals and antioxidants in human disease. In: Favier AE, Cadet J, Kalyanaraman B, Fontecave M, Pierre JL, editors. Analysis of free radicals in biological systems. *Basel, Switzerland: Birkhauser Verlag.* 83. https://doi.org/10.1007/978-3-0348-9074-8_7

Qaisiya, M., Coda Zabetta, C. D., Bellarosa, C., & Tiribelli, C. (2014). Bilirubin mediated oxidative stress involves antioxidant response activation via Nrf2 pathway. *Cellular Signalling*. 26. 512-520. http://dx.doi.org/10.1016/j.cellsig.2013.11.029

Rahman, M. M., Habib, M. R., Hasan, M. A., Al Amin, M., Saha, A., & Mannan, A. (2014). Comparative assessment on in vitro antioxidant activities of ethanol extracts of Averrhoa bilimbi, Gymnema sylvestre and Capsicum frutescens. *Pharmacognosy research*. 6(1), 36–41. https://doi.org/10.4103/0974-8490.122915

Sachdeva, M., Murki, S., Oleti, T. P., & Kandraju, H. (2015). Intermittent versus continuous phototherapy for the treatment of neonatal non-hemolytic moderate hyperbilirubinemia in infants more than 34 weeks of gestational age: a randomized controlled trial. *European journal of pediatrics*. 174(2), 177–181. https://doi.org/10.1007/s00431-014-2373-8

Seebaluck-Sandoram, R., Lall, N., Fibrich, B., Blom van Staden, A., Saleem, H., & Mahomoodally, M. F. (2019). Antimicrobial, antioxidant and cytotoxic evaluation of two underutilised food plants: Averrhoa Bilimbi L. (Oxalidaceae) and Phyllanthus acidus L. Skeels (Phyllanthaceae*). Biocatalysis and Agricultural Biotechnology*. 18, 100998. https://doi.org/10.1016/j.bcab.2019.01.036.

Setyawan, H. Y., Sukardi, S., & Nareswari, B. F. (2021). The phytochemical potential of Averrhoa bilimbi - A review. *IOP Conference Series: Earth and Environmental Science*. 733(1). 012091. https://doi.org/10.1088/1755-1315/733/1/01209.

Siu, S.L., Chan, L.W., & Kwong, A.N. (2018). Clinical and biochemical characteristics of infants with prolonged neonatal Jaundice. *Hong Kong Medical Journal*. 24 (3), 270–276. https://doi.org/10.12809/hkmj176990

Sokol, R. J., Devereaux, M., Khandwala, R., & O'Brien, K. (1993). Evidence for involvement of oxygen free radicals in bile acid toxicity to isolated rat hepatocytes. *Hepatology (Baltimore, Md.)*. 17(5), 869–881. https://pubmed.ncbi.nlm.nih.gov/8387948/

Sutrisna E. M., & Tanti A. S., (2015). The combination of belimbing wuluh fruit (Averrhoa bilimbi L.) and leaves of tapak dara (Catharanthus roseus G.) from Indonesia as a candidate hypoglycemic agents and thin layer chromatography profiles. *Biomedical & Pharmacology Journal.* 8(1), 39-46. https://dx.doi.org/10.13005/bpj/580

Tai, F. F. (2001). Neonatal Jaundice- traditional Medicine Approach. *Journal of Pennatologi.* 98-100.

Talib, W. H., Al-Ataby, I. A., Mahmod, A. I., Jawarneh, S., Al Kury, L. T., & Al-Yasari, I. H. (2020). The impact of herbal infusion consumption on oxidative stress and cancer: the good, the bad, the misunderstood. *Molecules (Basel, Switzerland)*. 25(18), 4207. https://doi.org/10.3390/molecules25184207

Tang, Y.-R., Zeng, T., Zafar, S., Yuan, H.-W., Li, B., Peng, C.-Y., Wang, S.-C., Jian, Y.-Q., Qin, Y., Choudhary, M. I., & Wang, W. (2018). Lonicerae Flos: A review of chemical constituents and biological activities. *Digital Chinese Medicine*. 1(2), 173–188. https://doi.org/10.1016/s2589-3777(19)30022-9

Tewari, D., Mocan, A., Parvanov, E. D., Sah, A. N., Nabavi, S. M., Huminiecki, L., Ma, Z. F., Lee, Y. Y., Horbańczuk, J. O., & Atanasov, A. G. (2017). Ethnopharmacological approaches for therapy of jaundice: part ii. Highly used plant species from acanthacea, asteraceae, combretaceae, and fabaceae families, *Frontiers in Pharmacology.* 8, 519. https://doi.org/10.3389/fphar.2017.00519

Thamizh, S. N., Santhi, P. S., Sanjayakumar, Y. R., Venugopalan, T. N., Vasanthakumar, K. G., & Swamy, G. (2015). Hepatoprotective activity of Averrhoa bilimbi fruit in acetaminophen induced hepatotoxicity in wistar albino rats. *J Chem Pharm Res.* 2015;7, 535–40.

DOI:https//doi.org/10.22452/mjs.vol43no1.1
Malaysian Journal of Science 43(1): 1-10 (March 2024)

Thomas, M., Hardikar, W., Greaves, R.F., Tingay, D.G., Loh, T.P., Ignjatovic, V., Newall, F., & Rajapaksa, A.E. (2021). Mechanism of bilirubin elimination in urine: insights and prospects for neonatal Jaundice. *Clinical Chemistry and Laboratory Medicine,* 59, 1025–1033. https://doi.org/10.1515/cclm-2020-1759

Tokosh, R., & Baig, M. A. (1995). Transparent soap formulations and methods of making same. *US Patent* 5529714. https://www.google.com/patents/US5417876

Tungmunnithum, D., Thongboonyou, A., Pholboon, A., & Yangsabai, A. (2018). Flavonoids and other phenolic compounds from medicinal plants for pharmaceutical and medical aspects: an overview. *Medicines.* 5(3), 93. https://doi.org/10.3390/medicines5030093

Veeru, P., Kishor, M. P., & Meenakshi, M. (2009). Screening of medicinal plant extracts for antioxidant activity. *Journal of Medicinal Plants Research.* 3(8), 608-612.

Warra, A. A., Hassan, L. G., Gunu, S. Y., & Jega, S. A. (2011). Cold-process synthesis and properties of soaps prepared from different triacylglycerol sources. *Nigerian Journal of Basic and Applied Sciences*. 18, 315-321. https://doi.org/10.4314/njbas.v18i2.64350

Warra, A., (2013). A report on soap in nigeria using indigenous technology and raw materials. *African Journal of Pure and Applied Chemistry.* 7, 139-145. https://doi.org/10.5897/AJPAC11.016

Yang, S., Li, S., & Yu, J. (2021). Effect of intermittent and persistent blue light irradiation on serum bilirubin in newborns with Jaundice. *China Practical Medicine.* 16(5), 81–83. https://doi.org/10.14163/j.cnki.11-5547/r.2021.05.029.

Yu, J. J., Manus, M. B., Mueller, O., Windsor, S. C., Horvath, J. E., & Nunn, C. L. (2018). Antibacterial soap use impacts skin microbial communities in rural Madagascar. *PLOS ONE*. 13(8). https://doi.org/10.1371/journal.pone.0199899

Zakaria, Z. A., Zaiton, H., Henie, E. F. P., Jais, A. M., & Zainuddin, E. N. (2007). In vitro antibacterial activity of Averrhoa bilimbi L. leaves and fruits extracts. *International Journal of Tropical Medicine*. 2(3), 96-100.

Zehiroglu, C., & Ozturk Sarikaya, S. B. (2019). The importance of antioxidants and place in today's scientific and technological ttudies. *Journal of Food Science and Technology*. 56(11), 4757–4774. https://doi.org/10.1007/s13197-019-03952-x

Zheng, S., Liu, S., Hou, A., Wang, S., Na, Y., Hu, J., Jiang, H., & Yang, L. (2022). Systematic review of lonicerae japonicae flos: A significant food and traditional Chinese medicine. *Frontiers in Pharmacology*. 13. https://doi.org/10.3389/fphar.2022.1013992

DOI:https//doi.org/10.22452/mjs.vol43no1.1
Malaysian Journal of Science 43(1): 1-10 (March 2024)

MALAYSIAN JOURNAL OF SCIENCE
MJS
ISSN 1394-3065

Regular Issue

Malaysian Journal of Science 43 (1): 11-21 (Mar 2024) https://mjs.um.edu.my

ASSESSING LOCAL PORE WATER VELOCITY ALONG PREFERENTIAL FLOW IN EARTHEN DAM USING SALT TRACER

Huong Thi Thu Huynh[1a]*, Son Le Van[2a], Hieu Tran Trong[3a], Luan Phan Thi[4a], Phung Vuong Duc[5a] and Hai Lai Viet[6a]

Abstract: The local pore water velocity along the preferential flow path signifies the hydraulic parameter responsible for erosion within an earthen dam. This study introduces an empirical approach to ascertain the local pore water velocity within the earth dam's leakage zones by monitoring the travel time of the salt tracer through the corresponding electric potential anomalies in the ground. The alignment of electric potential anomalies with the movement of the salt tracer plume over time was confirmed through experiments on a physical model coupled with numerical simulations. The pore water velocity, calculated based on the location of the maximum electric potential anomaly, demonstrated excellent agreement with the experimental value, with an error of under 6%. For illustrative purposes, a field-scale salt tracer test was conducted at a leaking earthen dam in Vietnam. The tracer breakthrough curve originating from the leakage point revealed that the seepage water's travel time is approximately 40 days. The results of electric potential anomalies over time indicate that the pathway of seepage flow from upstream to the leakage point forms a horizontal V-shape, with the local pore water velocity ranging from 1.7 to 9.9x10^{-5} m/s. These local pore water velocities are subsequently compared with the critical seepage velocity to assess in-situ information regarding the internal erosion status of the target dam.

Keywords: *Leakage, internal erosion, salt tracer, electric potential*

1. Introduction

Concentrated seepage resulting from local permeability anomalies in the body and foundation of an earthen dam is one of the primary mechanisms responsible for internal erosion (Foster et al., 2000; Zhang et al., 2016). Statistics based on the International Commission on Large Dams (ICOLD) database, comprising more than 10,000 dams, reveal that seepage erosion accounts for approximately 50% of dam failures (Foster et al., 1998). Detecting abnormal downstream leaks necessitates serious consideration of erosion potential to prevent or mitigate the damage caused by dam failures. Erosion occurs when the seepage water velocity is sufficiently high to transport discrete fine soil particles through the pores. Hence, the local pore water velocity along the preferential flow path serves as a hydraulic parameter for assessing the erosion process within the earthen dam (Goltz et al., 2009).

While geophysical methods for dam investigation, such as radar (Hui & Haitao, 2011; Bigman & Day, 2022), micro-seismic (Hickey et al., 2010), and resistivity (Kukemilks & Wagner, 2021; Zumr et al., 2020), focus on providing a visual representation of the seepage zone, the tracer method is considered an empirical technique that enables the determination of flow path direction and water velocity in the dam body and foundation (Bedmar & Araguas, 2002; Qiu et al., 2022). A tracer test is conducted by introducing artificial tracers like saline, ethanol, or fluorescent substances at a known upstream location and monitoring their concentration over time at target sites such as piezometers and downstream leakage points. The water velocity in the preferential flow can be determined using the tracer concentration curves at the monitoring locations. For instance, Battaglia et al. (2016) located the leakage zone at the Bumbuna dam by analyzing arrival times and tracer recovery in a series of experiments employing fluorescent dyes. Noraee Nejad et al. (2021) utilized a tracer experiment with $NaNO_3$ salt to investigate seepage at Shahghasem dam, determining the primary flow direction of the preferential flow path based on flow velocity calculations from experimental tracer curves. Sampling for tracer analysis is typically deemed essential for detecting tracer movement through the seepage zone. However, sampling locations may not always be accessible for all dams, especially smaller ones. Recent reports have highlighted the use of non-invasive self-potential measurements to monitor the movement of salt tracers through dam seepage zones (Bolève et al., 2011; Ikard et al., 2012). This method relies on variations in the total source current density generated by the transport of salt tracers through preferential flow paths within a dam, producing electric potential signals on the surface in response.

To conduct a more comprehensive assessment of internal erosion status, this paper introduces an experimental approach to determine the pore water velocity along the preferential flow path (local pore water velocity) based on observing the travel time of a salt tracer through self-potential anomalies on the

Authors information:
[a]Vietnam Atomic Energy Institute, Department of Nuclear Techniques, Center for Applications of Nuclear Technique in Industry, Dalat, VIETNAM. E-mail: huonghtt@canti.vn[1]; sonlv@canti.vn[2]; hieutt@canti.vn[3]; luanpt@canti.vn[4]; phungvd@canti.vn[5]; hailv@canti.vn[6]
*Corresponding Author: huonghtt@canti.vn

Received: July 30, 2022
Accepted: April 18, 2023
Published: March 31, 2024

DOI:https//doi.org/10.22452/mjs.vol43no1.2
Malaysian Journal of Science 43(1): 11-21 (Mar 2024)

ground. We investigate the suitability of self-potential anomalies in accordance with the motion of the NaCl salt tracer through a physical model experiment combined with ANSYS/CFX simulation (ANSYS Student 2021 R2). Subsequently, a salt tracer test was carried out at a leaking earthen dam in Vietnam to demonstrate the viability of the proposed approach.

2. Methodology

In the tracer experiment, tracers were injected into known locations upstream. Their occurrence at target sites downstream was monitored over time. Assuming that the adsorption effect is negligible and the tracer is instantaneously injected, the 1D analytical solution describes the tracer concentration at position *x* (m) and time *t* (s) (Evans, 1983):

$$C(x,t) = \frac{M}{A}.\frac{e^{\frac{-(x-v^*t)^2}{4.Dt}}}{\sqrt{4D\pi t}} \quad (1)$$

where *M* (kg) is the mass of the tracer, *A* is the cross-sectional area of the flow (m^2), v^* is the pore water velocity (m/s), and *D* is the dispersion coefficient (m^2/s). Considering the isotropic porous media $D = D_0/(F\phi) + \alpha v^*$, D_0 is the molecular diffusion coefficient of the tracer in solution (m^2/s), and α is the dispersivity (m).

The pore water velocity, or the mean interstitial velocity of water, is defined as the ratio between the Darcy velocity and the effective porosity. The pore water velocity can generally be determined experimentally by the following formula:

$$v^* = \frac{L}{t} \quad (2)$$

where *L* is the distance between injection and observation (m) and *t* is the time determined from the tracer breakthrough curve at the observation (s).

Previous studies have mentioned three concepts of *t* in Equation (1): t_a – the arrival time, t_p – the peak time and t_r – the mean residence time (Figure 1). The mean residence of the tracer is:

$$t_r = \frac{\int Ctdt}{\int Cdt} \quad (3)$$

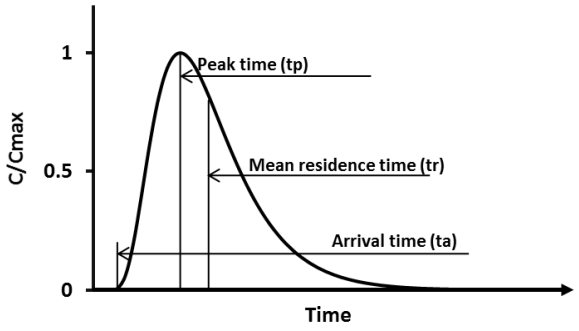

Figure 1. Examples of time characteristics of the tracer breakthrough curve: the arrival time, the peak time, and the mean residence time.

Noraee-Nejad et al. (2021) combined the consideration of the velocity determined from the arrival time (maximum velocity) and the peak time (average velocity) at piezometers to identify the primary flow direction of the preferential flow path at the Shahghasem Dam (Iran). Similarly, various t-concepts were used to assess the water volume in karst caves using the tracer method: Atkinson et al. (1973) proposed to use the peak time; Birk et al. (2004) used the arrival time; Smart (1988), Goldscheider et al. (2008) used the mean residence time; Käss (1998) concluded that when the tracer curve is severely affected by the dispersion process, using the peak time yielded better results.

When sampling locations are unavailable to observe the entire tracer curve, using a salt tracer and monitoring its movement time through the self-potential anomalies on the ground is a viable empirical approach. In this work, NaCl salt was used due to its notable advantages, such as environmental friendliness, low test cost and easy analysis. When the NaCl salt tracer moves through a porous medium, increasing the conductivity of the pore water, the source current density $\vec{j}_s$ (A.m^{-2}) generates the electric potential (Revil & Linde, 2006):

$$\vec{j}_s = \bar{Q}_v\vec{v} - \frac{K_bT}{Fe}\left(2t_{(+)} - 1\right)\nabla\sigma_f \quad (4)$$

$$\nabla.(\sigma\nabla\psi) = \nabla.\vec{j}_s \quad (5)$$

where $\vec{v}$ is the Darcy velocity (m/s); $\bar{Q}_v$ is the excess charge density (C.m^{-3}) determined from the equation $Log_{10}\bar{Q}_v = -9.2349 - 0.8219Log_{10}k$; *k* is the permeability (m^2); $K_b = 1.381\times10^{-23}$ is the Boltzmann constant (J/K); *T* is the absolute temperature (K); $F = \phi^{-m}$ is the formation factor; ϕ is the porosity; $e = 1.6022\times10^{-19}$ is the electron charge (C); $t_{(+)} = 0.38$ is the microscopic Hittorf number of the Na^+ in the pore water.; $\sigma_f = \sigma.F$ is the electrical conductivity of the pore water (S.m^{-1}); σ is the electrical conductivity of the porous

DOI:https//doi.org/10.22452/mjs.vol43no1.2
Malaysian Journal of Science 43(1): 11-21 (Mar 2024)

media (S.m^{-1}); and ψ (V) is the electric potential.

If the actual pore water velocity obtained from the tracer test is greater than the critical value, transport of soil particles within the pore structure can occur. Goltz et al. (2009) modified Wittmann's theoretical approach for the assessment of the critical velocity when taking into account adhesion and frictional forces:

$$v_{crit} = \frac{12\upsilon}{d_p\left(2.7-2.3FF\right)}\left[\sqrt{1+\left(0.21D^s\right)^3\left(2.7-2.3FF\right)\tan\varphi}-1\right] \quad (6)$$

where υ is the dynamic viscosity of water (m^2/s), *FF* = 0.7, d_p is the particle diameter (m), $D^s = d_p\left(\frac{\rho' g}{\upsilon^2}\right)^{1/3}$ with $\rho' = \frac{\rho_{sA}-\rho_w}{\rho_w}$, $\rho_{sA} = \rho_s + \frac{9\times10^{-8}}{d_p{}^2}$, ρ_s is the bulk density of soil (kg/m^3), ρ_w is the water density (kg/m^3), *g* is the gravitational acceleration (m/s^2), and φ is the friction angle.

3. Laboratory Experiment

The correlation between the response time of the electric potential generated by the salt migration and the travel time of water was confirmed by the salt tracer experiment on the physical model combined with numerical simulation.

Physical model

The physical model used in this study is a rectangular box with dimensions of 61.6 cm x 30 cm x 30.8 cm, constructed from 0.8 cm-thick sheet glass. The model was divided into three compartments by two 1 cm thick mica sheets with holes drilled 1 cm in diameter and a distance of 2 cm between holes. Two 10 cm long compartments at the ends act as upstream and downstream reservoirs, while the 38 cm long compartment in the middle is packed with glass beads. Fabric mesh with a mesh diameter of 100 µm was attached to the two shields to prevent glass beads from spilling into the other two compartments. The total height of the glass bead column is 20 cm. The porosity of the middle compartment is 37%. The flow through the porous media is controlled by the water levels of the upstream and downstream. Upstream water was supplied by a water tank located 3 m above the ground and a tube with a diameter of 1 cm. The supplying flow rate was regulated with a valve. The downstream water level was adjusted by changing the outlet height of the 1 cm diameter overflow discharge tube. The experiment used tap water as the fluid with an average conductivity of 2.4x10^{-3} S·m^{-1}. We used laboratory glass beads with a diameter of about 450-500 µm. By measuring the outlet flow rate according to the difference in water level, the permeability was determined to be 1.95x10^{-10} m^2. The experimental system and the sketch of the physical model are shown in Figures 2a and 2b.

The laboratory Cu/$CuSO_4$ electrodes, in combination with a Fluke 87V voltmeter (USA), were used to record the electric potential during the transport of the NaCl tracer. The in-house electrodes operate with a natural drift of 0.02 mV/min (22°C). The dependence of the potential drift on ambient temperature was ignored because the temperature fluctuation in the experiment is insignificant (within 0.1°C). A total of three electrode arrays (four electrodes each array) were inserted into the middle compartment (depth 8.5 cm from the top), and the reference electrode was placed upstream at (x; y) = (0 cm; 14.5 cm). The position of the electrodes is considered in the Cartesian coordinate system with the x-axis parallel to the flow direction and the y-axis perpendicular to it. The electrode arrays have coordinates y = (6.5 cm; 14.5 cm; 22 cm), with the positions of the measuring electrodes along the x-axis being (6.5 cm; 14.5 cm; 23 cm; 31.5 cm), as shown in Figure 2c.

DOI:https//doi.org/10.22452/mjs.vol43no1.2
Malaysian Journal of Science 43(1): 11-21 (Mar 2024)

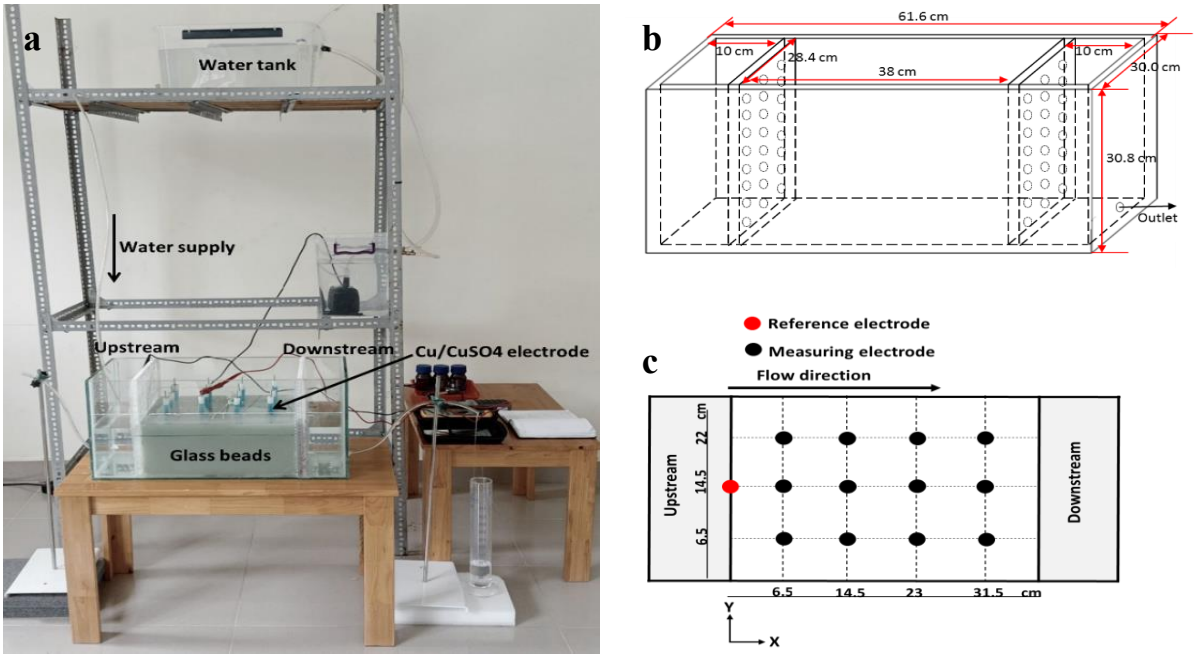

Figure 2. The experimental system: (a) Photo of experimental system; (b) Sketch of physical model; (c) Illustration of electrode position (top view).

Experimental Procedure

The upstream level was maintained at 20 cm, and the tracer experiment was carried out with a flow rate of 0.81 L/min, corresponding to a 17 cm downstream level. The pore water velocity, calculated from the ratio between the Darcy velocity and the effective porosity, was 3.85 cm/min.

After setting the downstream and upstream levels, the experimental system was stabilized for several hours. Before the injection of the tracer, the potential difference between the 12 measuring electrodes and the reference electrode was recorded. This included the signal generated by the steady flow in the model and the difference in internal potential between the electrodes. Simultaneously, the initial conductivity of the water was measured to establish a background value. A total of 120 mL of the salt tracer solution, containing 4.42 g of NaCl, was injected into the upstream reservoir, which had a water volume of 5.68 L. The potential difference between the reference and measuring electrodes was recorded over time using a Fluke 87V voltmeter (USA). The measuring time for the 12 electrodes was 20 seconds, with a measurement frequency of 1 minute. The NaCl concentration over time at the downstream drainage was measured using a conductivity meter, specifically a Hanna HI98197 device (Romania). The linear relationship between the concentration of Cl^- (C, in mg/L) and the conductivity of water (EC, in µS/cm) is represented by the equation C = 0.25EC – 4.49, with an R^2 value of 0.998. The initial electric potential before tracer injection and the natural drift potential were subtracted from the measurement data. The temperature during the experiment remained stable within a range of 21.9°C to 22.1°C.

ANSYS/CFX Simulation

A multi-component numerical model was developed to analyze the concentration distribution of the tracer and correlate it with the variations in the experimental electric potential. This model simulates the movement of the NaCl tracer within the physical model over time and was constructed using the ANSYS/CFX software, specifically the ANSYS Student 2021 R2 version. In this multi-component model, the fluid, comprising multiple components, is treated as an ideal mixture. This means that the fluid's velocity, pressure, and temperature are computed by solving the continuity equation and the Navier-Stokes equations. For this experiment, the fluid system includes two main components: water and a solution of the NaCl tracer. The advection-dispersion equation is solved following the determination of the fluid's velocity field. This process enables the determination of the tracer's movement through the medium, allowing for a detailed examination of its distribution over time.

DOI:https//doi.org/10.22452/mjs.vol43no1.2
Malaysian Journal of Science 43(1): 11-21 (Mar 2024)

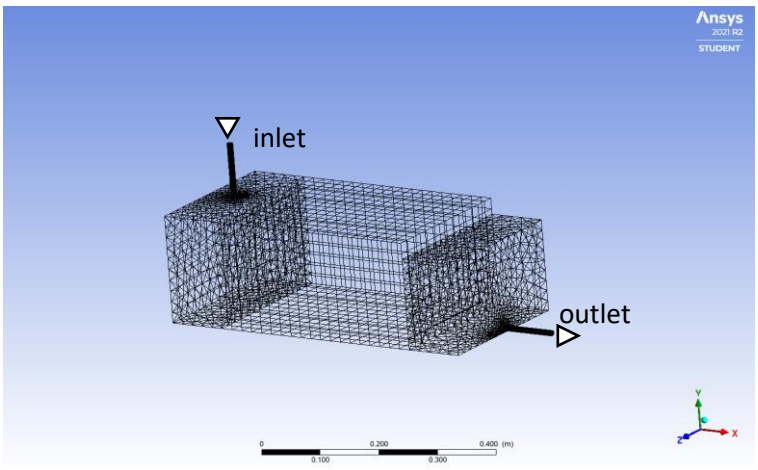

Figure 3. The structured mesh of the model (courtesy of ANSYS, Inc.)

The numerical simulation involved a substantial computational mesh comprising 58,926 elements and 15,934 nodes, as depicted in Figure 3. The simulation process was divided into two main steps to ensure accuracy and comprehensiveness. Initially, the model was brought to a steady state by achieving convergence in the velocity field. This phase was capped at a maximum of 600 iterations, with convergence being determined by meeting the Residual RMS criterion of $1x10^{-4}$. At both the inlet and outlet, velocity boundary conditions were implemented based on experimental data, with the velocity vector directed normally to the boundary surfaces. Furthermore, an open boundary condition was applied at the top of the porous region, designed to permit air to traverse the boundary surface perpendicularly, thus simulating a realistic environmental interaction.

Following the establishment of a steady state, the simulation transitioned to a transient phase to model the injection of the NaCl solution. This phase used the outcome of the steady-state simulation as its input file. Initially, the NaCl solution concentration was set to zero throughout the domain. During the tracer injection period ($0 \leq t \leq t_0$, where t_0 represents the injection stop time), the mass fraction of the tracer in the fluid at the inlet was maintained at 1, with a time step size (Δt) of 0.2 seconds. For times $t > t_0$, the tracer concentration was set to zero, and the time step size was adjusted to 1 second to simulate the cessation of tracer injection, aligning with the experimental procedure.

The maximum number of iterations per time step during the transient simulation was limited to 10, adhering to the same convergence criteria established for the steady-state model. The turbulence effects within the fluid flow were modeled using the k-Epsilon turbulence model, with a default turbulence intensity of 5% at both the inlet and outlet, ensuring a realistic simulation of fluid dynamics within the system.

4. Field-Scale Experiment

The study dam was built in 1997 in the Dong Nai river basin, situated approximately 200 km northeast of Ho Chi Minh City. It is a homogeneous earth-fill dam with a height of 36 m and a crest length of 215 m. The physical characteristics of the soil embankment are shown in Table 1.

Table 1. The physical characteristics of the soil embankment.

Density (kg/m^3)	Particle diameter (m)	Friction angle (degrees)	Hydraulic conductivity (m/s)
1870	$5.0x10^{-6}$	20.0	$2.0x10^{-8}$

According to the company's report, a wet area downstream of the dam becomes evident when the reservoir water level surpasses 604 meters. This area, measuring approximately 7 meters by 3 meters, is located at 595 meters, as illustrated in Figure 4a. In December 2021, in collaboration with the dam supervisor, a ditch was constructed to collect seepage water. This water was then directed into a measurement hole with dimensions of 40 cm by 40 cm by 15 cm to assess the leak's flow rate. The findings indicated that the leakage flow rate was 0.5 liters per minute when the reservoir's water level reached 605 meters.

To ascertain the direction and local pore water velocity of preferential flow paths through the dam, a salt tracer test was conducted. On December 18, 2021, nylon bags filled with NaCl tracer crystals were placed into the reservoir. These bags, positioned 78 meters symmetrically from the leak site (as depicted in Figure 4b), were perforated, allowing the salt crystals to dissolve gradually into the reservoir water. Each bag,

DOI:https//doi.org/10.22452/mjs.vol43no1.2
Malaysian Journal of Science 43(1): 11-21 (Mar 2024)

containing 5 kg of NaCl, was submerged at a depth of 1 meter and spaced 3 meters apart. At the time of the tracer injection, the reservoir water level was recorded at 604.6 meters. Over approximately three hours post-injection, the electrical conductivity and chloride ion (Cl^-) concentration were measured at various distances from the injection point. The leakage site offered the sole opportunity for downstream sampling. Water samples were collected until February 3, 2022, for analysis of conductivity and Cl^- concentration at the Laboratory (VILAS-609) of the Center for the Application of Nuclear Techniques in Industry. To prevent air contact, 300 mL water samples were sealed in plastic bottles. The Cl^- concentration was determined using test method TCVN 6494-1:2011, with a minimum detection limit of 0.01 mg/L. A Hanna HI98197 instrument (Romania) with a resolution of 0.1 µS/cm was used to measure the electrical conductivity of the samples. Prior to the tracer injection, the Cl^- concentration in the reservoir water was 3.80 mg/L and in the leak water was 2.77 mg/L, correlating to conductivities of 66.5 µS/cm and 28.5 µS/cm, respectively.

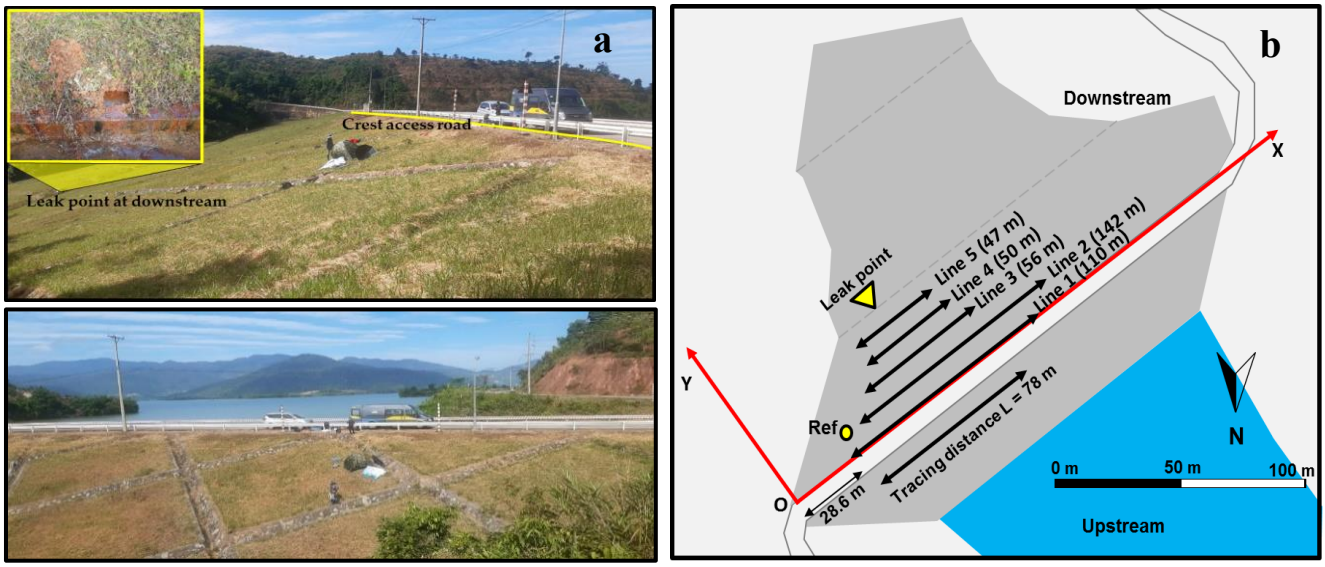

Figure 4. (a) The study dam site; (b) The tracing distance, measuring lines for electric potential (Line 1-5), and reference electrode (Ref) position.

A comprehensive electric potential measurement campaign was conducted at the dam site involving five measuring lines (Line 1-5) before and after the injection of a salt tracer. The initial measurements took place on December 17, 2021, with subsequent sessions on January 5, January 18, and January 26, 2022. These measuring lines were laid out parallel to the toe of the dam downstream, spaced 10 meters apart from each other. To enhance efficiency and reduce the survey time, the length of the measuring lines was decreased moving downstream.

Measurements were carried out using a pair of non-polarized $Cu/CuSO_4$ electrodes, which were connected to a measuring device capable of handling a maximum impedance of 20 MΩ and equipped with a 500 m cable, specifically the ARES II measurement system by GF Instruments. The reference electrode was stationed at the left abutment of the dam (as shown in Figure 4b), while the other electrode was moved to each measurement point along the measuring lines. The average spacing between measurement points was 8 meters, though adjustments were made based on the ground conditions encountered at each site. At every measurement location, a small hole approximately 10 cm deep was dug to ensure contact with moist soil, facilitating accurate measurements.

Given the $Cu/CuSO_4$ electrodes' sensitivity to temperature fluctuations, protective measures were taken to shield the electrodes from direct sunlight during measurements, including a mandatory pre-measurement waiting period of 5 minutes at each point to ensure temperature stabilization. At each measurement point, five readings were taken, with the average relative error recorded at 1.7%. Additionally, the drift potential of the electrodes was assessed at the beginning and end of each measuring line while they were immersed in a bath of saturated $CuSO_4$ solution, registering a potential value around 1 mV.

Consistent with findings from previous research, such as that by Revil et al. (2003), corrections for telluric currents were deemed unnecessary for this study due to the short temporal span and limited geographical scale (below 1 km) of the measurements. Consequently, the collected raw electric potential data were adjusted for the drift potential across each measuring line, ensuring the accuracy of the data analysis.

DOI:https//doi.org/10.22452/mjs.vol43no1.2
Malaysian Journal of Science 43(1): 11-21 (Mar 2024)

5. Results and Discussion

Laboratory Experiment Results

Figure 5a illustrates a comparative analysis between the tracer response curves at the outlet, as obtained from both ANSYS/CFX simulations and experimental observations. The numerical model's accuracy was validated through a root-mean-square error (RMSE) of $1x10^{-4}$ between the simulation outputs and the experimental data. Figure 5b presents a comparison of the experimental electric potential signals recorded at distances of x = 6.5 cm, 14.5 cm, 23 cm, and 31.5 cm with the tracer curves derived from simulation results.

The temporal distribution of electric potential at these measuring positions mirrors the findings of Maineult and Bernabé (2005), showcasing a notable pattern. Immediately following tracer injection, there's a rapid decline in the electric potential to negative values, followed by a swift transition through zero, eventually stabilizing over time. This abrupt shift in electric potential corresponds closely with the arrival times of the water at each measuring point, demonstrating the direct influence of water movement on electric potential signals.

The observed travel times for the water to reach the respective measuring positions were 1.7, 3.8, 6, and 8.2 minutes, correlating to positions x = 6.5 cm, 14.5 cm, 23 cm, and 31.5 cm, respectively. These times align with a calculated pore water velocity (v*) of 3.85 cm/min. Such detailed comparison not only confirms the predictive accuracy of the numerical model but also provides valuable insights into the dynamics of tracer movement and its interaction with the electric potential field within the experimental setup.

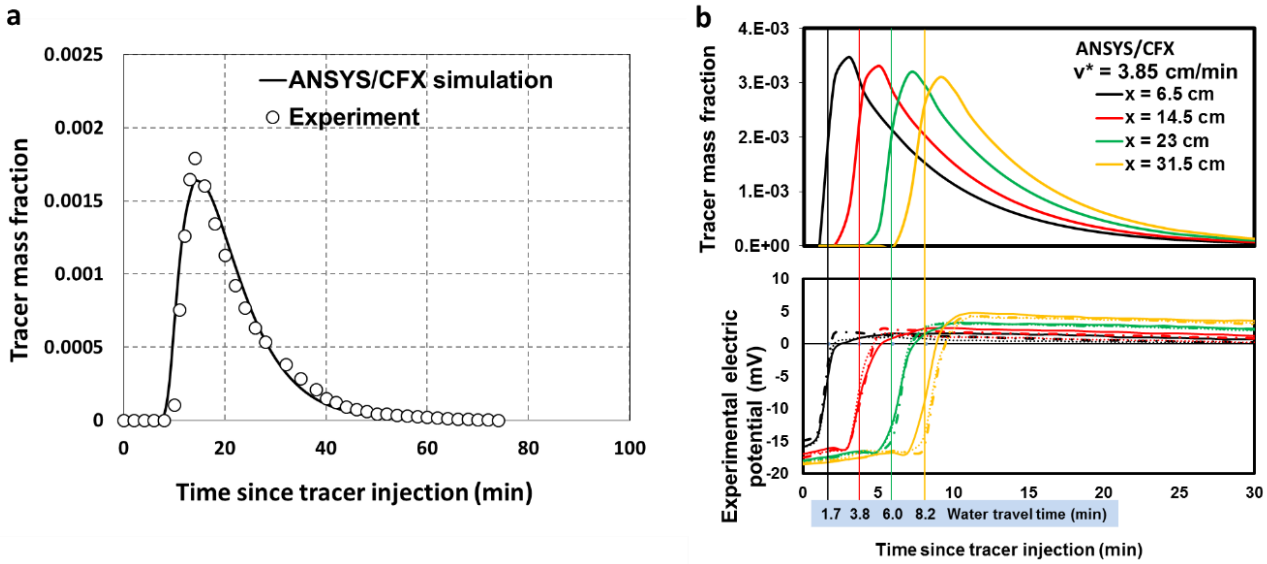

Figure 5. (a) The tracer response curve at the outlet obtained from ANSYS/CFX simulation and experiment; (b) The electric potential signal at measuring positions of *x* = 6.5 cm, 14.5 cm, 23 cm, 31.5 cm. The corresponding tracer curves were determined from the simulation.

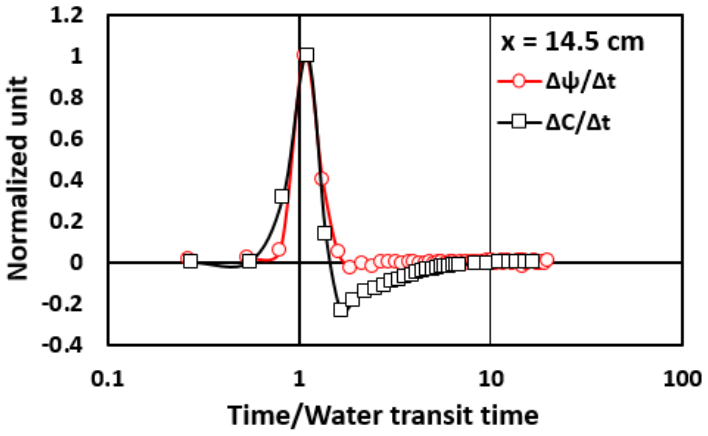

Figure 6. The maximum potential variation $(\Delta\Psi/\Delta t)_{max}$ and the change in tracer curve $(\Delta C/\Delta t)_{max}$ coincide in time and are close to the water transit time.

DOI:https//doi.org/10.22452/mjs.vol43no1.2
Malaysian Journal of Science 43(1): 11-21 (Mar 2024)

Due to the tracer dispersion effect by dilution at the input boundary, the travel time of water is earlier than the time to reach the maximum tracer concentration (Figure 5b). Experimental and simulation results demonstrate that the change in tracer curve $(\Delta C/\Delta t)_{max}$ agrees with the maximum potential variation $(\Delta \Psi/\Delta t)_{max}$ and is close to the water transit time, as illustrated in Figure 6.

Figure 7 shows the position of the tracer plume derived from ANSYS/CFX (ANSYS Student 2021 R2) (the plane z = 10 cm) relative to the location of the experimental electric potential anomalies at 4, 6, and 8 min. The electric potential signal anomalies were considered by analyzing the signal variation ($\Delta \Psi/\Delta t$, in mV/min). The results demonstrate that the location of the electric potential anomaly is relatively consistent with the position of the tracer plume. The centroid positions of the tracer plume are x = 11 cm, 19 cm, and 27 cm at 4, 6, and 8 min, respectively. The mean deviation of the peak potential anomaly location and the center of the tracer plume is 4 cm (about 10.5% of the total travel distance). The occurrence time of the signal anomaly at a location is close to the actual water travel time. Calculation results of pore water velocity were based on two approaches: (1) the location of the tracer plume determined from ANSYS/CFX, and (2) the location of the potential signal anomaly (Table 2). The calculated velocities show an error of about 10% if the water moving distance was measured from the center of the tracer plume, and an error of 6% if the water moving distance was measured from the position of the maximum potential anomaly.

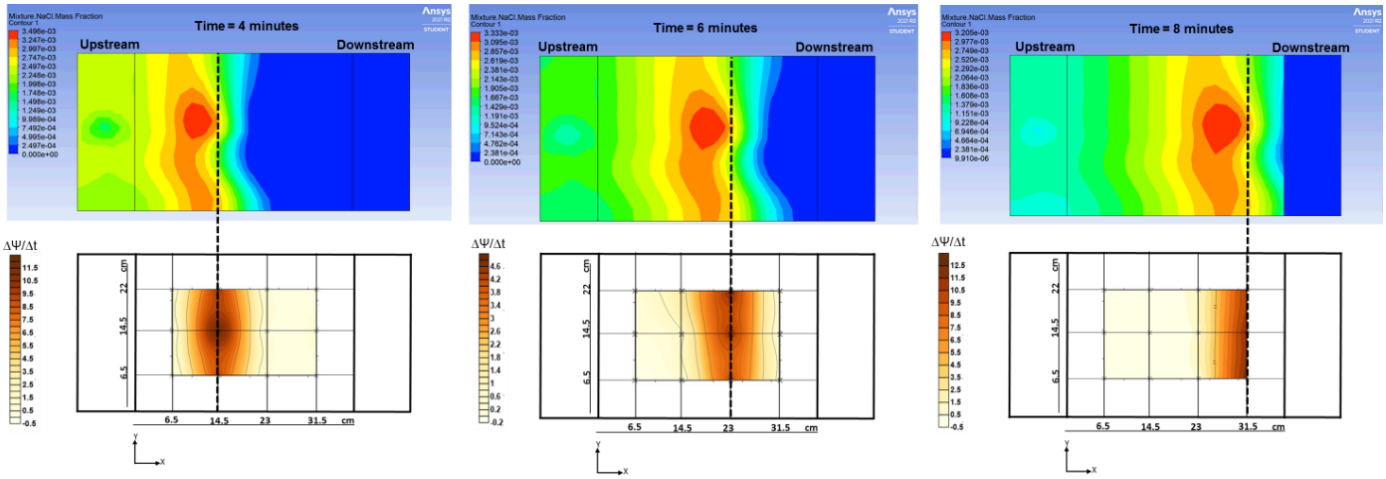

Figure 7. Positions of the tracer plume obtained from ANSYS/CFX (the plane z = 10 cm) compared to the self-potential anomalies. It is shown that tracer plumes are consistent with self-potential signal anomalies (courtesy of ANSYS, Inc.).

Table 2. Calculation results of pore water velocity of the model.

Observation time	4 min	6 min	8 min
Tracer travel distance			
Centroid position of the tracer plume	11 cm	19 cm	27 cm
Position of the maximum electric potential anomaly	14.5 cm	23 cm	31.5 cm
Pore water velocity			
Centroid position of the tracer plume	2.75 cm/min	3.17 cm/min	3.38 cm/min
Position of the maximum electric potential anomaly	3.63 cm/min	3.83 cm/min	3.93 cm/min

Field-Scale Experiment Results

The introduction of the NaCl tracer into the reservoir water at an elevation of 604.5 m allowed for precise monitoring and analysis of its dispersion and eventual seepage through the dam. The measurement of electrical conductivity and Cl^- concentration in the reservoir water at intervals of 0.8 hours, 1.8, 2.8, and 3.3 hours post-injection, as illustrated in Figure 8a, aimed to identify the seepage leakage inlet of the dam. The inlet is hypothesized to be the location where the concentration of the tracer peaks after a period of diffusion, indicating the most significant point of seepage.

The results from these measurements revealed that the peak conductivity and Cl^- concentration were observed approximately 42 meters from the point of tracer injection. This peak indicates the likely inlet of seepage through the dam, where the tracer concentration was highest. Following 3.3 hours after injection, the conductivity in the reservoir water approached the background levels again, suggesting the dispersion of the tracer away from the peak concentration point over time.

Figure 8b details the analysis of electrical conductivity and Cl^- concentration at the leak point itself, revealing the tracer's

DOI:https//doi.org/10.22452/mjs.vol43no1.2
Malaysian Journal of Science 43(1): 11-21 (Mar 2024)

response curve in the form of a single peak. Remarkably, the peak occurred 40 days after the tracer was introduced, with the highest recorded conductivity value at 118.70 µS/cm, which corresponds to a Cl^- concentration of 28.06 mg/L. This significant delay in reaching the peak concentration at the leak point underscores the slow movement of water through the dam's structure, providing critical insights into the dynamics of seepage and the efficacy of tracer tests in identifying and analyzing potential leakage paths within dam infrastructures.

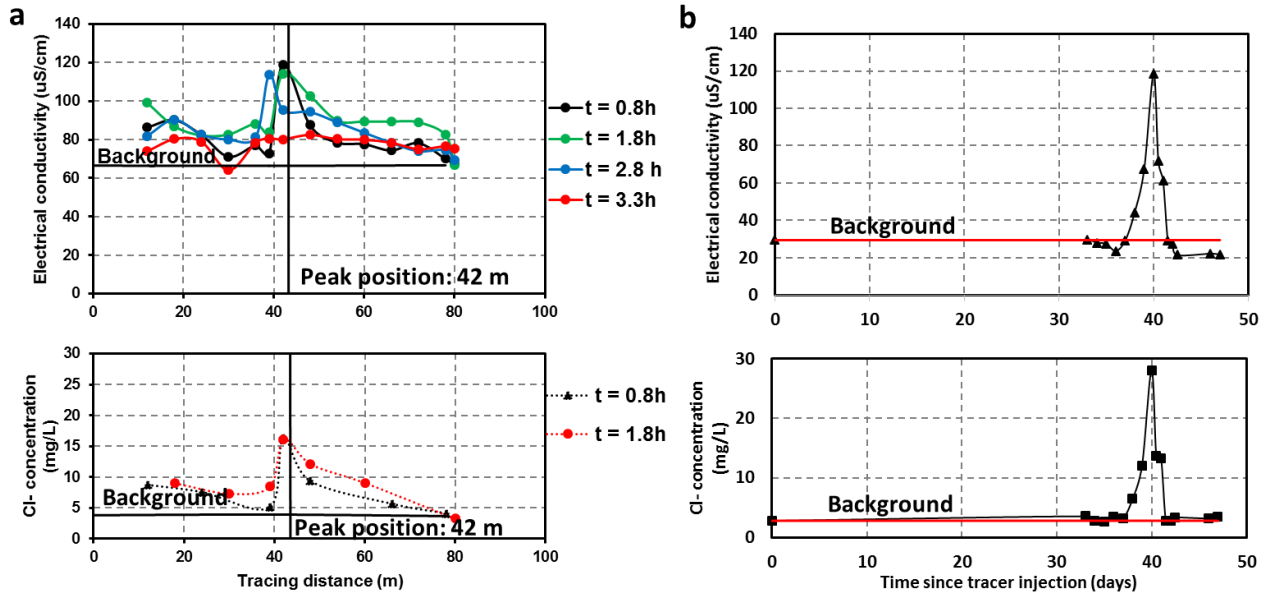

Figure 8. Results of salt tracer test at the study dam: (a) Measurement results of electrical conductivity and Cl^- concentration in reservoir water at 0.8, 1.8, 2.8, and 3.3 hrs after injection; (b) Electrical conductivity and Cl^- concentration in water at the leak point over time.

The potential anomaly is indicated by the signal variation ($\Delta\Psi/\Delta t$) quantity. By comparing the potential signal variation before and after under the same field-scale conditions, the distinctive region associated with the presence of salt ions can be easily identified. Figure 9 presents the results of electric potential anomalies at the dam after 18, 30, and 40 days since the injection. The location of the anomaly that indicates the direction of the tracer movement from upstream to the leak point has a horizontal V-shape. The travel time of the salt tracer from upstream (position 1) to Line 2 (position 2) is 18 days, from Line 2 (position 2) to Line 5 (position 3) is 12 days, and from Line 5 (position 3) to the leak point is ten days. Based on the distance of movement, the local pore water velocity is presented in Table 3.

The local pore water velocity ranges from $1.2\text{x}10^{-5}$ m/s to $7.0\text{x}10^{-5}$ m/s. The calculation results demonstrate that the velocity in the 2 - 3 position range is the greatest. Taking into account the tortuosity of the porous medium, the actual velocity of the water is proportional to the actual distance travelled $L_a = L\tau$, where τ is the tortuosity. The actual velocity results are presented in Table 2 with τ = 1.4 (Freeze & Cherry, 1979). The critical velocity, which causes internal erosion, was estimated using Equation (6) with the physical characteristics of the soil embankment (Table 1) as $2.5\text{x}10^{-5}$ m/s (υ = $0{,}8927\text{x}10^{-6}$ m^2/s at 25˚C and ρ_w = 997 kg/m^3 at 25˚C). It can be seen that the pore water velocity in the 2 - 3 position range is approximately four times greater than the critical value.

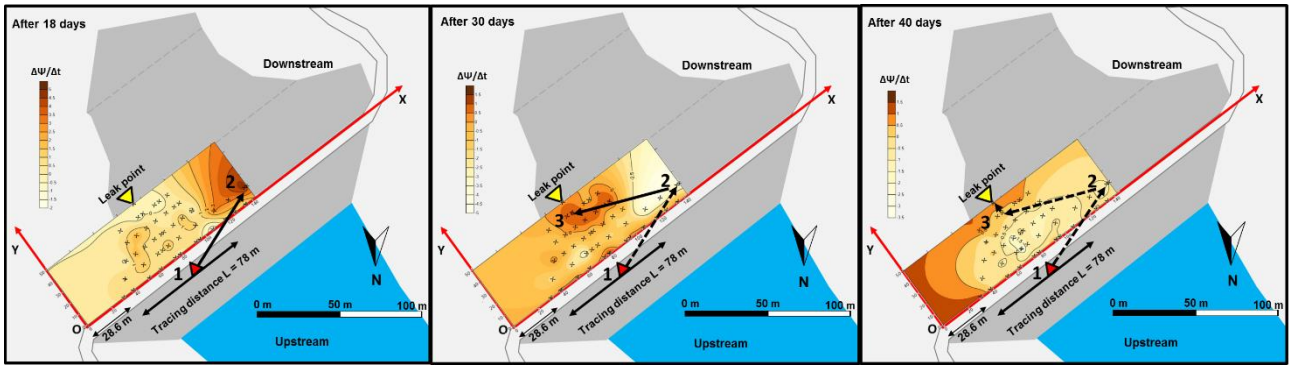

Figure 9. Location of electric potential anomalies at the study dam after injection: 18, 30, and 40 days. Position 1 is conventionally the leakage inlet, determined at the point where the conductivity/Cl^- concentration peaks after injection.

DOI:https//doi.org/10.22452/mjs.vol43no1.2
Malaysian Journal of Science 43(1): 11-21 (Mar 2024)

Table 3. Local pore water velocity along the preferential flow of the study dam.

Position	Travel distance (m)	Travel time (days)	Local pore water velocity (m/s)	Actual pore water velocity (m/s)
1-2	77.8	18	$5.0x10^{-5}$	$7.0x10^{-5}$
2-3	73.0	12	$7.0x10^{-5}$	$9.9x10^{-5}$
3-Leak point	10.4	10	$1.2x10^{-5}$	$1.7x10^{-5}$

6. Conclusion

This study introduced a novel approach to evaluating the local pore water velocity of preferential flow paths through porous media by monitoring the movement of a NaCl salt tracer and observing the associated electric potential anomalies on the ground. Experiments conducted on a physical model demonstrated a close correlation between the timing of signal variations and the movement of water to the measuring positions. Additionally, the distribution of the salt tracer plume, as determined from ANSYS/CFX simulations, aligned well with the observed positions of electric potential anomalies over time. The pore water velocity, inferred from the location exhibiting the maximum electric potential anomaly, showed consistency with the experimental values, boasting an error margin of less than 6%.

A field-scale salt tracer experiment conducted at a leaking earth dam in Vietnam further underscored the practicality of this method. The tracer response curve obtained from the leak site revealed that the seepage water's transport time was approximately 40 days. Following tracer injection, the electric potential anomalies provided insight into the preferential flow path from upstream to the leak point and enabled the estimation of local pore water velocities.

This methodological approach presents a significant advancement in assessing internal erosion caused by seepage within earthen dams, utilizing the criterion of pore water velocity. It offers substantial benefits over traditional methods, notably in terms of cost-effectiveness and the ability to overcome challenges associated with sample collection for tracer analysis at the field site. This technique not only aids in the precise identification of seepage paths and velocities but also enhances the capability to effectively manage and mitigate risks associated with dam integrity and safety.

7. Acknowledgement

This work was supported by the Vietnam Ministry of Science and Technology. The authors also show gratitude to ANSYS Inc. for introducing the free version for academic purposes.

6. References

Atkinson, T.C., Smith, D.I., Lavis, J.J., and Whitaker, R.J. (1973). Experiments in tracing underground waters in limestones. Journal of Hydrology, 19, 323–349.

Battaglia, D., Birindelli, F., Rinaldi, M., Vettraino, E., Bezzi, A. (2016). Fluorescent tracer tests for detection of dam leakages: The case of the Bumbuna dam - Sierra Leone. Engineering Geology, 205, 30–39.

Bedmar, A.P, Araguas, L. (2002), Detection and Prevention of Leaks from Dams. A.A. Balkema Publishers.

Bigman, D.P, Day, D.J. (2022). Ground penetrating radar inspection of a large concrete spillway: A case-study using SFCW GPR at a hydroelectric dam. Case Studies in Construction Materials, 16, e00975.

Birk, S., Liedl, R., and Sauter, M. (2004). Identification of localized recharge and conduit flow by combined analysis of hydraulic and physio-chemical spring responses (Urenbrunnen, SW Germany). Journal of Hydrology, 286, 179-193.

Bolève, A., Janod, F., et al. (2011). Localization and quantification of leakages in dams using time-lapse self-potential measurements associated with salt tracer injection. Journal of Hydrology, 403, 242–252.

Evans, G. V. (1983). Tracer Techniques in Hydrology. Int. J. Appl. Radiat. Lsot, 34(I), 451-475.

Foster, M., Fell, R., & Spannagle, M. (2000). The statistics of embankment dam failures and accidents. Canadian Geotechnical Journal, 37(5), 1000-1024.

Freeze, R. A, Cherry, J. A. (1979). Groundwater. Prentice-Hall, Englewood Clifs.

Goldscheider, N., Meiman, J., Pronk, M., & Smart, C. (2008). Tracer tests in karst hydrogeology and speleology. International Journal of Speleology, 37(1), 27-40.

Goltz, M., Etzer, T., Aufleger, M., & Muckenthaler, P. (2009, 12-23 October). Assessing the critical seepage velocity causing transport of fine particles in embankment dams and their foundation, Long term behaviour of dams proceeding of the 2nd international conference, Graz, Austria, (pp.479-484).

Hickey, C.J., Ekimov, A., Hanson, G., & Sabatier, J., (2010). Time-Lapse Seismic Measurements on a Small Earthen Embankment During an Internal Erosion Experiment. In SAGEEP 2009 Proceedings. Keystone, Colorado.

DOI:https//doi.org/10.22452/mjs.vol43no1.2
Malaysian Journal of Science 43(1): 11-21 (Mar 2024)

Hui, L., Haitao, M. (2011). Application of Ground Penetrating Radar in Dam Body Detection. Procedia Engineering, 26, 1820 – 1826.

Ikard, S. J., Revil, A., et al. (2012). Saline pulse test monitoring with the self-potential method to nonintrusively determine the velocity of the pore water in leaking areas of earth dams and embankments. Water Resource Research, 48(W04201).

Käss, W. (1998). Tracing Technique in Geohydrology. Rotterdam, Balkema, 581.

Kukemilks, K., Wagner, J.-F. (2021). Detection of Preferential Water Flow by Electrical Resistivity Tomography and Self-Potential Method. Appl. Sci, 11, 4224.

Maineult, A., Bernabé, Y. (2005). Detection of advected concentration and pH fronts from self-potential measurements. Journal of Geophysical Research, 110(B11205).

Noraee-Nejad, S., Sedghi-Asl, M., Parvizi, M., Shokrollahi, A. (2021). Salt tracer experiment through an embankment dam. Iranian Journal of Science and Technology, Transactions of Civil Engineering.

Qiu, H., Hu, R., Huang, Y., Gwenzi, W. (2022). Detection and Quantification of Dam Leakages Based on Tracer Tests: A Field Case Study. Water, 14, 1448.

Revil, A., Linde, N. (2006). Chemico-electromechanical coupling in microporous media. Journal of Colloid and Interface Science, 302, 682–694.

Revil, A., Naudet, V., Nouzaret, J., & Pessel, M. (2003). Principles of electrography applied to self-potential electrokineticsources and hydrogeological applications. Water resources research, 39(5), 1114.

Smart, C.C. (1988). Quantitative tracing of the Maligne karst system, Alberta, Canada. Journal of Hydrology, 98, 185–204.

Zhang, L., Peng, M., Chang, D., & Xu, Y. (2016). Dam Failure mechanisms and risk assessment. John Wiley & Sons Singapore Pte. Ltd.

Zumr, D., David, V., Jeřábek, J., Noreika, N & Krása, J. (2020). Monitoring of the soil moisture regime of an earth-filled dam by means of electrical resistance tomography, close range photogrammetry, and thermal imaging. Environ Earth Sci, 79, 299.

DOI:https//doi.org/10.22452/mjs.vol43no1.2
Malaysian Journal of Science 43(1): 11-21 (Mar 2024)

MALAYSIAN JOURNAL OF SCIENCE
MJS
ISSN 1394-3065

Regular Issue

Malaysian Journal of Science 43(1): 22-33 (Mar 2024) https://mjs.um.edu.my

BACTERIAL CELLULOSE INCORPORATED ZINC PHOSPHATE NANOCOMPOSITE FOR ANTIBACTERIAL AGENT AND AIR PARTICULATE MATTER FILTRATION

Nurhidayah Nurhidayah[1a], La Ode Ahmad Nur Ramadhan[2b]*, Abdul Haris Watoni[3b], Laode Abdul Kadir[4b], Muhammad Daffa Rahmatullah[5b], and Cindy Agriningsih Haruna[6b]

Abstract: This study investigates the synthesis and the antibacterial properties of bacterial cellulose (BC) incorporated zinc phosphate nanocomposite-mediated dragon fruit extract (BC-ZP-DF). The composite was prepared by a three-step process that involved bacterial cellulose (BC), zinc phosphate (ZP), and nanocomposite BC-ZP synthesis. BC was prepared by fermenting coconut water with the components of ammonium sulfate, acetic acid, and *Acetobacter xylinum* culture. Zinc phosphate was made through the green synthesis method by reacting zinc nitrate and diammonium hydrogen phosphate using a sensitizer agent from red dragon fruit peel extract (DF) with volume variations of 5, 10, 20, 30, 40, and 50 mL. The composite was prepared by immersing BC with zinc phosphate. Phase crystallinity, functional group, and morphology of the samples were characterized using XRD, FTIR, and SEM. It was found that the nanocomposite was constructed by the nano green of zinc phosphate in the form of a hopeite structure with antibacterial PO_4^{3-} and OH functional groups. Morphological analysis using SEM revealed that the nanocomposites contained various small powder grains. Based on the FTIR spectrum, XRD pattern, and surface morphology of composite film, the incorporation of zinc phosphate in the BC framework was confirmed. The antibacterial activity tests of nanocomposite films using *Staphylococcus aureus* and *Pseudomonas aeruginosa* bacteria revealed that the nanocomposite was highly effective in inhibiting both bacteria, and the nanocomposite BC-ZP-DF10 film had the strongest inhibition. The results of the air filter test exhibited that the composition was efficient on all films with the highest percent of efficiency (%E) of 90.10%.

Keywords: *Zinc phosphate, bacterial cellulose, antibacterial, particulate matter filtration, filtration*

1. Introduction

In recent years, rapid industrial growth has led to a rise in air pollution worldwide (Lippi et al., 2022). Air pollution containing particulate matter (PM) is an increasingly prevalent environmental issue that threatens human health, ecosystems, and the climate. The lethal effects of particulate pollutants vary mainly by their diameter. Typically, PM larger than 10 µm in diameter cannot penetrate the human lung and will instead be efficiently filtered and captured by the respiratory organs. Smaller PM with a diameter of 2.5 to 10 µm and less than 2.5 µm are called PM10 and PM2.5, respectively. These are harmful to humans because they can easily and unabatedly penetrate the lungs (Wu et al., 2022). Recent reports indicate that prolonged exposure to environmental particulates can elicit respiratory and cardiovascular illnesses, such as stroke, atherosclerosis, bronchitis, and asthma (Xing et al., 2016). In addition, atmospheric chemicals, bacteria, microorganisms, and viruses use PM as a carrier substance to penetrate the human body, resulting in the spread of various diseases among humans (Wu et al., 2022; Xing et al., 2016). Therefore, solutions to prevent the harmful effects of air particulates are urgently needed. One such solution is air quality control, both indoors and in car spaces so that particulates, dust, and bioaerosols containing harmful microorganisms can be filtered out of the air inhaled by humans. To overcome the problem of air pollution, researchers have developed functional advanced materials, such as the High-Efficiency Particulate Air (HEPA) Filter technology. Currently, HEPA technology, one component of which is a filter matrix, is effectively capable of filtering 99.97% of very fine particles up to 0.3 µm (Franchitti et al., 2020). This technology has been utilized for cleaning static air environments in various fields, such as isolation rooms in hospitals, biotechnology laboratory rooms, and portable air purifiers (Franchitti et al., 2020). However, the existing filter matrix material is not environmentally friendly because it is dominantly made of synthetic polymer raw materials. Therefore, alternative raw materials that are environmentally friendly and sustainable need to be identified. One potential option for using natural polymers as composite material is cellulose.

BC is a naturally biodegradable cellulose with fiber diameters ranging from 20 to 100 nm (Jonsirivilai et al., 2022). Due to its hydrophilic characteristics, BC has a high water-holding capacity. It also has high mechanical strength with a smaller fiber diameter measuring 3–4 nm thick, and it is relatively more affordable to produce. The fiber is biocompatible, non-toxic, and precisely

Authors information:
[a]Department of Chemistry, Postgraduate, Halu Oleo University, Kendari, INDONESIA. E-mail: nhayahidayah@gmail.com[1]
[b]Department of Chemistry, Faculty of Mathematics and Natural Science, Halu Oleo University, Kendari, INDONESIA. E-mail: laode.ramadhan@uho.ac.id[2]; ahwatoni@uho.ac.id[3]; laode.kadir90@uho.ac.id[4]; mdaffa2709@gmail.com[5]; cindyaharuna@gmail.com[6]
*Corresponding Author: laode.ramadhan@uho.ac.id

Received: December 9, 2022
Accepted: May 7, 2023
Published: March 31, 2024

DOI:https//doi.org/10.22452/mjs.vol43no1.3
Malaysian Journal of Science 43(1): 22-33 (March 2024)

structured with a large surface area (Manoukian et al., 2019). Due to its high surface area, nanofiber diameter, and high hydrophilicity, the use of BC as an air filter membrane produces a more potent and efficient filtration effect than commercial membranes (Manoukian et al., 2019). The production of air filters takes into consideration numerous characteristics. Good quality filters are characterized by a low-pressure drop, which is reflected through high permeability and a wide surface area that will support the absorption of more particles. Nowadays, BC is one of the most commonly used materials for air filtration, as it can capture aerosol particles from gas streams by their fibers via Brownian diffusion, direct interception, inertial impact, gravity regulation, and electrostatic deposition. The airflow velocity, particle characteristics, and shape of the air filtering material all directly influence this mechanism, which regulates the air filtration process (Lippi et al., 2022). The BC used in this research is Nata de Coco cellulose. Nata de Coco cellulose is a cellulose polymer sourced from abundant coconut water fermentation using the *Acetobacter xylinum* bacteria (Mulyasuryani & Mustaghfiroh, 2019). Furthermore, BC has unique physical and mechanical characteristics, such as high porosity, high crystallinity, exceptional mechanical strength, and a significant water-holding capacity (Nugroho & Aji, 2015). BC composited with zinc phosphate nanoparticles can potentially be used as an excellent antimicrobial matrix for high-efficiency particulate absorbing (HEPA) filters. Nanoparticles are well known for their excellent antimicrobial properties (Sabherwal et al., 2017). An essential, multipurpose inorganic substance known as zinc phosphate is also a type of often utilized luminous host material (Kimbonguila et al., 2019). Zinc phosphate can be synthesized from zinc nitrate and different phosphate compounds, including phosphoric acid (Kopel et al., 2018), sodium dihydrogen phosphate (Wang et al., 2011), disodium hydrogen phosphate (Horky et al., 2019), sodium pyrophosphate (Kopel et al., 2018; Onoda & Haruki, 2016), trisodium phosphate (Wang et al., 2011), or sodium triphosphate (Grzmil et al., 2007; Onoda & Haruki, 2016). However, zinc phosphate produced from these precursors exhibits a fairly low photocatalytic action (Grzmil et al., 2007; Kopel et al., 2018). Therefore, it is necessary to find alternative precursors to produce zinc phosphate that has a high photocatalytic action. One such precursor is diammonium hydrogen phosphate.

Zinc phosphate can be reacted with plant extracts containing dyes as sensitizing agents. In addition to reducing the particle size, this reaction is expected to increase antibacterial activity. The antimicrobial properties of nanoparticles are due to their ability to deface bacterial cell walls, disrupt cell metabolism, and inhibit microbial cell formation (Sabherwal et al., 2017). Synthesis of zinc phosphate nanoparticles was performed through an environmentally friendly green synthesis approach with a sensitizing agent from the waste extract of the red dragon fruit. Red dragon fruit peel extract has potential use as a sensitizing agent because it contains several active compounds including flavonoids, alkaloids, and terpenoids (Rahmayanti et al., 2019). Thus far, there has been no research exploring the use of red dragon fruit peel extract and diammonium hydrogen phosphate in the synthesis of zinc phosphate and its use in antibacterial composites on HEPA filter membranes. Hence, this research was conducted to evaluate the zinc phosphate nanoparticle material and its antibacterial characteristics under preparation with the addition of extract-sensitizing agents of the red dragon fruit peel plant. The findings of the study were assessed based on visual observation and characteristic determination of the material using UV-Vis (Ultraviolet-Visible) spectrophotometer, FTIR (Fourier Transform Infrared) spectrophotometer, XRD (X-ray diffraction), and SEM (Scanning Electron Microscope). The composite was then tested for its antibacterial activity and its efficiency as an air filter. The synthesized composite film has a greater advantage as an air particulate matter filter due to the presence of zinc phosphate and red dragon fruit peel extract, both of which have the good antibacterial activity. In comparison, previous studies conducted by Liu et al. (2017) only explored its use as particulate matter filters.

2. Materials and Methods

Materials

In this study, the materials used were dragon fruit peel, coconut water, aquades, ethanol p.a (Emsure Merck), sugar ($C_6H_{12}O_6$), ammonium sulfate (ZA), glacial acetic acid p.a (Emsure Merck), *Acetobacter xylinum* stater, nutrient agar (Emsure Merck), nutrient broth (Emsure Merck), *P. aeruginosa*, *S. aureus*, Whatman filter paper No. 40, $Zn(NO_3)_2.6H_2O$ p.a (Emsure Merck), $(NH_4)_2HPO_4$ p.a (Emsure Merck), NaOH p.a (Emsure Merck), and NaCl p.a (Emsure Merck).

The instruments used were XRD (Phillips), FTIR Spectrophotometer (Shimadzu), UV-Vis Spectrophotometer (Vernier), Scanning Electron Microscope (JEOL JSM-6360), PM Analyzer (Kailishen SYSC-BR8), Digital Optic Microscope (OEM), Rotary Evaporator (Buchi), Dessicator (Duran), oven (YNC-OV50L), Hydraulic Hot Press Machine (HTM 634), and Mini Aerosol Generator (Tasco).

Methods

Preparation of Red Dragon Fruit Peel Extract and Bacterial Cellulose

To extract the dragon fruit peel waste, we used a maceration method adapted from Manihuruk et al. (2017). First, 500 g of simplicia powder was added to a 1000 ml-Beaker glass, and 96% ethanol was added. Then, it was macerated for 3×24 hours by the filtering procedure every 24 hours, and the simplicia was soaked again with a new solvent. The filtration results were then evaporated for three hours using a rotary evaporator at 45 °C to obtain the red dragon fruit extract.

Next, BC preparation was adapted from Nugroho and Aji (2015) by fermenting coconut water with the ingredients of ammonium sulfate, acetic acid, and *Acetobacter xylinum* culture. This was done at 28 °C for 10 days until the BC sheet was obtained. This sheet was used as a matrix in the synthesis of filter composites.

DOI:https//doi.org/10.22452/mjs.vol43no1.3
Malaysian Journal of Science 43(1): 22-33 (March 2024)

Synthesis of Zinc Phosphate-Red Dragon Fruit Peel Extract

The synthesis method was adapted from Pavel et al. (2019). First, 4.46 g of $Zn(NO_3)_2.6H_2O$ was dissolved in distilled water and heated to 60 °C, followed by the addition of 1.32 g of $(NH_4)_2HPO_4$ in 20 ml of distilled water, and incorporation of the red dragon fruit extract solution. The mixture was stirred until a precipitate was formed. The suspension produced was stirred for two hours and cooled, and water was added to reach 100 ml. The suspension was then centrifuged and decanted (Horky et al., 2019). The composition ratio of the mixture of materials can be seen in Table 1. The outcome of the synthesis was characterized by observing their functional groups using an FTIR Spectrophotometer, their crystalline and oxide structures using an X-ray diffractometer, their morphology using SEM, and their nanoparticle stability using a UV-Vis Spectrophotometer. Antimicrobial actions were tested using the paper disc method.

Table 1. Synthetic composition zinc phosphate

Sample code*	$Zn(NO_3)_2.6H_2O$ (grams)	$(NH_4)_2HPO4$ (grams)	Extract of dragon fruit peel (ml)
ZP	4.46	1.32	0
ZP-DF5	4.46	1.32	5
ZP-DF10	4.46	1.32	10
ZP-DF20	4.46	1.32	20
ZP-DF30	4.46	1.32	30
ZP-DF40	4.46	1.32	40
ZP-DF50	4.46	1.32	50

*ZP is zinc phosphate, and ZP-DF5 to ZP-DF50 are zinc phosphate and extract.

Synthesis of BC-zinc Phosphate Composite Film-Mediated Red Dragon Fruit Peel Extract

The composite film of BC was neutralized with 1% w/v NaOH and then rinsed with distilled water until the pH was neutral. The composite was then modified into pieces of film sheets sized 4x9 cm. The film was pressed using a hot press to reduce its water content. Subsequently, the film was composited with synthesized nanoparticles (Table 1) by immersing it for 1x24 hours. The film was then pressed again using a hot press and dried in an oven at 150 °C for 10 minutes. The films were removed from the oven and cooled in a desiccator for ± 15 minutes to obtain a composite film with an average thickness of 0.20 mm; they were coded BC-ZP, BC-ZP-DF5, BC-ZP-DF10, BC-ZP-DF15, BC-ZP-DF20, BC-ZP-DF30, BC-ZP-DF40, and BC-ZP-DF50. The composites were then characterized using FTIR, XRD, and SEM.

Antibacterial Testing

Antibacterial testing was conducted using the paper disc method. The suspension of the test bacteria (*S. aureus* and *P. aeruginosa*) was poured into an Erlenmeyer containing NA media to be homogenized. The NA medium was poured into each petri dish, then gently shaken to form a figure eight to spread the bacterial culture evenly, and allowed to stand until the media solidified. The filter paper that had been cut into pieces utilizing a hole jab was then dipped into the test sample using sterile tweezers. The mixture was transferred to an NA medium containing *S. aureus* and *P. aeruginosa* bacteria cultures in the aseptically arranged distance, labeled according to the treatment group, and incubated for 24 hours at 37 °C (Massoud & Saffari, 2020). After 24 hours, a clearer area was observed around the sample area. The clearer area indicates the inhibition zone for the growth of *S. aureus* and *P. aeruginosa*. The inhibition zone formed was measured using a caliper. Antibacterial activity was measured or calculated using Equation 1 as follows:

$$Z = \frac{(D1-Dfc) + (D2-Dfc) + (D3-Dfc)}{3} \quad (1)$$

Where: Z = Zone clear (mm), D1= Vertical diameter (mm), D2 = Horizontal diameter (mm), D3 = Diagonal diameter (mm), and Dfc = Film diameter composite (mm). Based on the calculation of the inhibition zone diameter, the antibacterial activity of the composite can be categorized as follows: diameter > 20 mm = very strong, 11-20 mm = strong, 6-10 = moderate, and < 5 = weak (Massoud & Saffari, 2020).

Air Filter Test

The performance of the air filter system was analyzed by systems using NaCl aerosol as recommended by Konda et al. (2020). The test was carried out at 1 atm and 29 °C. The filter was tested for its ability to filter NaCl aerosol, where nano-sized particles were generated using a NaCl aerosol generator. The collection of NaCl aerosol particles was then pumped in through the test filter. The test filter used was a circular filter film with a diameter of 2.54 cm. The concentration of particles before they pass through the filter (C_i) and after they pass through the filter (C_f) was measured using the Particulate Matter (PM) Analyzer (SYSC BR-8). The performance of the air filter media is indicated by the results of the efficiency measurement, as expressed by Equation 2.

$$\%E = \frac{Ci-Cf}{Ci} x100 \quad (2)$$

where % E is the percent of efficiency, C_f and C_i are the number of particles after and before passing through the filter, respectively. The air filter test scheme is depicted in Figure 1.

DOI:https//doi.org/10.22452/mjs.vol43no1.3
Malaysian Journal of Science 43(1): 22-33 (March 2024)

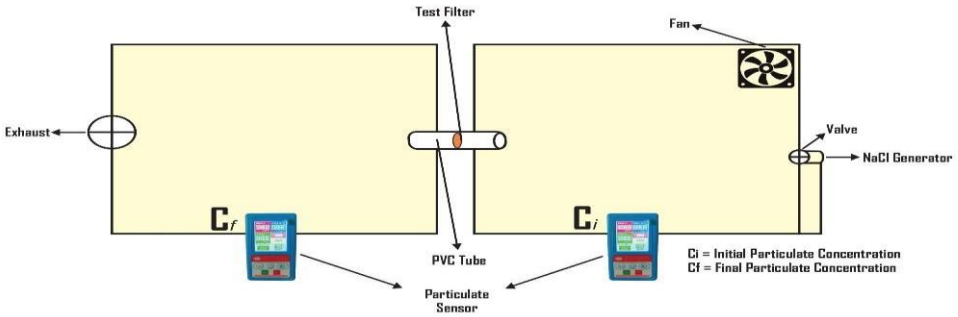

Figure 1. The illustration of the air filter test scheme

3. Results

Red Dragon Fruit Peel Extract

The extraction process of the red dragon fruit peel waste produced a concentrated extract of 160 ml with a yield of red dragon fruit peel extract of 10.6%.

Synthesis of Zinc Phosphate-Red Dragon Fruit Peel Extract

The resulting zinc phosphate was in the form of powder with various colors. The synthesized zinc phosphate yield can be seen in Table 2.

Table 2. Yield of zinc phosphate-red dragon fruit peel extract

Sample Code	Yield (%)
ZP	60.46
ZP-DF5	63.73
ZP-DF10	89.34
ZP-DF20	95.73
ZP-DF30	111.48
ZP-DF40	171.76
ZP-DF50	60.46

The yield of zinc phosphate increased when more extract was used. This can be observed in the yield obtained from ZP-DF5 to ZP-DF40, which increased periodically to reach a maximum limit at ZP-DF40 and decreased at ZP-DF50. This is because the penetration of the synthesizer agent into the material had decreased, so less zinc phosphate was formed in the material.

Mixing red dragon fruit peel extract with zinc phosphate produced a precipitate that varied from brown to yellowish brown (Figure 2). This color change indicates a reaction in the mixture caused by the sensitizing agent used in this study, the red dragon fruit peel extract. This extract contains dyes, namely anthocyanin compounds. The conjugated double bond with the chromophore moiety in the anthocyanin backbone allows for light energy to be absorbed with maximum absorbance in the visible light range. As the length and number of the double bonds conjugated to anthocyanins increase, the color becomes stronger (Nurtiana, 2019). The dye molecules are stimulated during this sensitization process by absorbing visible light, and electrons are then moved from the highest-occupied molecular orbital (HOMO) to the lowest-vacant molecular orbital (LUMO) (Dil et al., 2019).

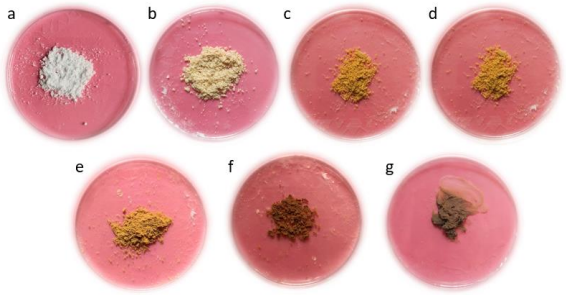

Figure 2. Products of the synthesis of zinc phosphate: (a) ZP, (b) ZP-DF5, (c) ZP-DF10, (d) ZP-DF20, (e) ZP-DF30, (f) ZP-DF40 and (g) ZP-DF50.

Stability Analysis of Zinc Phosphate-Red Dragon Fruit Peel Extract

The UV-Vis absorbance spectrum of transparent colloidal solution was observed using a UV-Vis spectrophotometer in the wave range of 200-800 nanometers. Measuring the zinc phosphate nanoparticles-red dragon fruit peel extract using a UV-Vis spectrophotometer caused an excitation phenomenon due to the interaction of light with precious metal nanoparticles called the surface plasmon resonance (SPR) phenomenon (Budi, 2017). The SPR phenomenon is related to the color of the zinc phosphate nanoparticle solution (Haiss et al., 2008; Zakir & Budi, 2016).

The SPR absorption band is a collection of electron oscillations (Haiss et al., 2008). The collection of electron oscillations that can be observed from the change of color of the solution from yellow to dark brown shows the distribution of zinc nanoparticles in the solution (Budi, 2017). Based on UV-Vis analysis results, the stability of the complex compound of zinc phosphate nanoparticles from the Red Dragon fruit peel extract was reasonably good. Based on the interaction of the solution with UV-Vis light, the zinc phosphate was stable for 30 minutes as seen from the stability of the curve of zinc phosphate nanoparticles-red dragon fruit peel extract (Figure 3). Due to the visible light being absorbed during this sensitization process, dye molecules from dragon fruit peel extract are stimulated, and electrons are then moved from the highest occupied molecular orbital (HOMO)

DOI:https//doi.org/10.22452/mjs.vol43no1.3
Malaysian Journal of Science 43(1): 22-33 (March 2024)

to the lowest vacant molecular orbital (LUMO). These excited electrons are eventually transferred to the conduction band of the photocatalyst molecule semiconductor, resulting in the formation of highly reactive superoxide anions (O_2^-) and/or hydroxyl radicals (•OH) (Ghosh et al., 2020). The maximum wavelength shifts to a lower value as the concentration of $Zn(NO_3)_2$ increases, which means that the interaction energy between organic compounds in the extract and Zn increases.

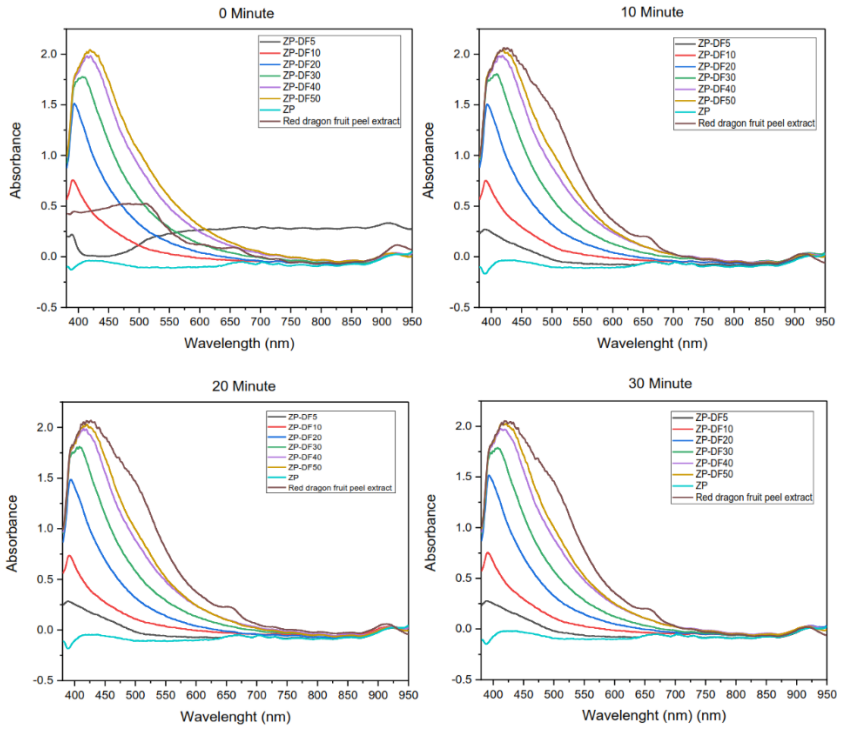

Figure 3. UV-Vis absorbance spectrum of zinc phosphate nanoparticles-red dragon fruit peel extract at intervals of (a) 0 minutes, (b) 10 minutes, (c) 20 minutes, and (d) 30 minutes.

Functional Group Analysis of Zinc Phosphate Nanoparticles-Red Dragon Fruit Peel Extract Using an Ftir Spectrophotometer

Based on the FTIR data in Figure 4, there is a wide band data centered on 3334–3353 cm^{-1} for all samples (extract, ZP-DF5, ZP-DF10, ZP-DF20, ZP-DF30, ZP-DF40, and ZP-DF50), which identifies the –OH stretching vibration (Ghosh et al., 2020; Zhang et al., 2019). In addition, a strong vibrational band at 1618–1643 cm^{-1} is associated with H_2O bonds. The FTIR spectrum exhibits characteristic bands associated with PO_4^{3-} and H_2O. Bandwidths are exhibited at 500 ~ 700 cm^{-1} (peak at 632 cm^{-1}) and 900 ~ 1300 cm^{-1} (ref: 900 ~ 1200 cm^{-1}) for ZP-DF5, ZP-DF10, ZP-DF20, ZP-DF30, ZP-DF40, and ZP-DF50 nanoparticles, respectively. Each spectrum is associated with the presence of PO_4^{3-} flexible and Zn strain vibration groups. Therefore, this peak is not visible in the extracted spectrum because it does not contain zinc. From the synthesized zinc phosphate, a very strong, recognizable peak at 1010 cm^{-1} was caused by the antisymmetric stretching of PO_4^{3-} (Wang et al., 2011).

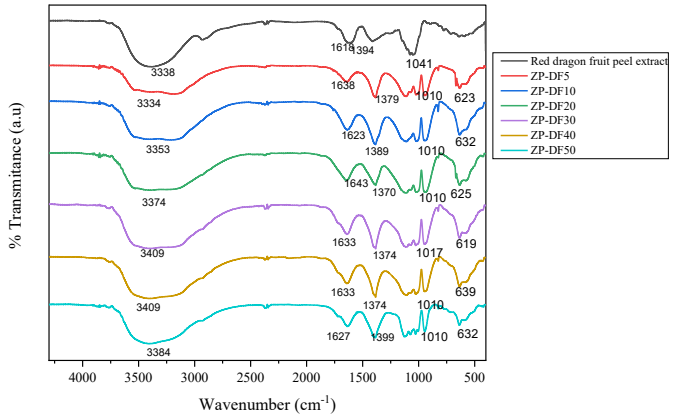

Figure 4. FTIR spectrum of zinc phosphate nanoparticles-red dragon fruit peel extract

Crystallite Size Analysis of Zinc Phosphate Nanoparticles

The results of zinc phosphate synthesis are supported by an X-ray diffractogram, which is compared to the standard diffraction pattern from the Crystallography Open Database (COD) zinc phosphate with an entry number of 95-900-0523. The existing peak 2θ data are 9,54º, 16,55º, 17,31º, 18,09º, 19,23º, 19,93º, 22,23º, 22,82º, 25,57º, 26,14º, 31,26º, 34,21º, 39,26º, 46,82º, and 49,89º. From the diffractograms of ZP-DF20 to ZP-DF50, some narrow and small intensity peaks of 2θ over the range 16,70º-18,28º are evident. This is thought to be derived from

DOI:https//doi.org/10.22452/mjs.vol43no1.3
Malaysian Journal of Science 43(1): 22-33 (March 2024)

diammonium hydrogen phosphate residues and extracts. However, the overall results of the analysis prove that $Zn_3(PO_4)_2$ has a good match with the Hopeite structure. The XRD pattern of zinc phosphate-red dragon fruit extract powder is shown in Figure 5.

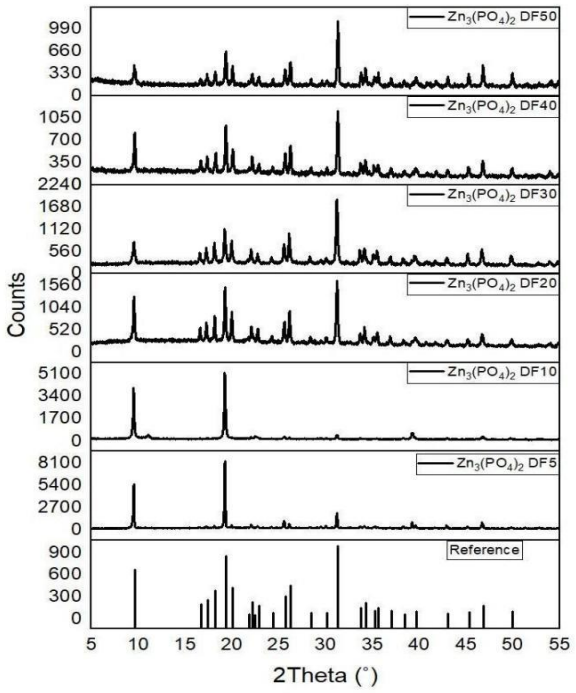

Figure 5. XRD spectrum of zinc phosphate nanoparticles-red dragon fruit peel extract

From the XRD characterization data, the size of the crystal could be estimated by using the Scherrer formula

$$D = \frac{K\lambda}{\beta cos(\theta)} \quad (4)$$

where length wave X-rays are used, and = angle diffraction, K = is large constant - depends on factors from the crystal, diffraction (hkl) plane and definition quantity β used, whether - as Full Width at Half Maximum (FWHM) or Integral Breadth of a peak. True K value varied from 0.62 to 2.08. The typical value used for K is 0.94 if β is FWHM and 0.89 for Integral Breadth (Franchitti et al., 2020; Wu et al., 2022). The equation observed that the wide peak varied with angle 2θ in the form of cos (θ). A defined quantity β was FWHM and the constant K was chosen to be 0.94. With the thereby obtained number of N sizes crystals under field, the measured hkl are presented in Table 3. ZP-DF10 shows the average size crystal, the smallest of which is 37.48 nm. The existence of an additional extract peel fruit dragon could influence the size of the resulting crystals. This has been proven with a comparison with pure zinc phosphate, which was researched previously by Grzmil et al. who produced an average crystallite size of 43 nm (Grzmil et al., 2007).

Table 3. Crystallite size of zinc phosphate nanoparticles

Sample Code	Crystallite Size (nm)
ZP-DF5	38.96
ZP-DF10	37.48
ZP-DF20	40.32
ZP-DF30	42.99
ZP-DF40	44.19
ZP-DF50	37.98

2.3. Morphological Analysis of Zinc Phosphate Nanoparticles

SEM analysis of the synthesized zinc phosphate showed the morphology of each test sample. It is apparent from the analysis that some samples have aggregate forms. The ZP-DF10 sample shows a morphology with small grains and is randomly distributed at 1000× magnification of observation (Figure 6).

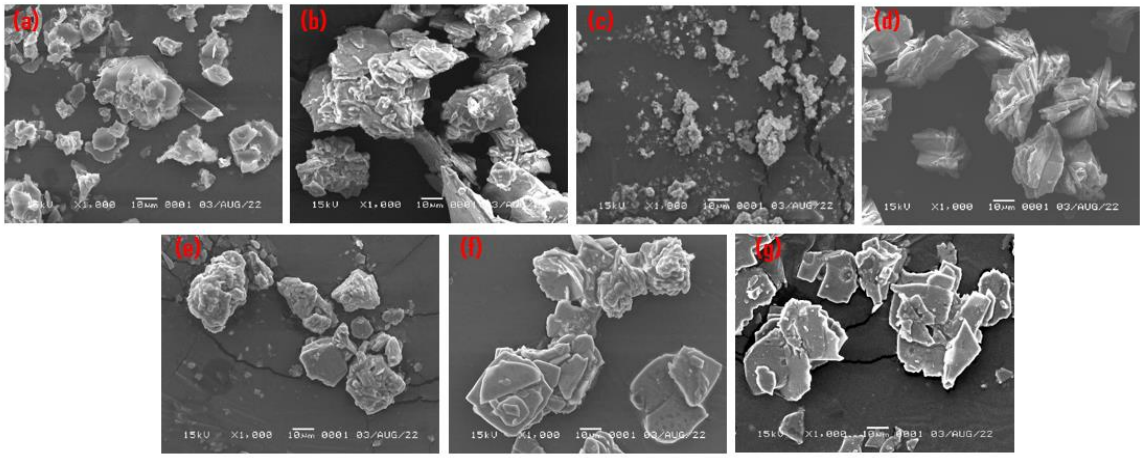

Figure 6. The results of the analysis of ZP-dragon fruit peel nanoparticles: (a) ZP, (b) ZP-DF5, (c) ZP-DF10, (d) ZP-DF20, (e) ZP-DF30, (f) ZP-DF40, (g) ZP-DF50.

DOI:https//doi.org/10.22452/mjs.vol43no1.3
Malaysian Journal of Science 43(1): 22-33 (March 2024)

Synthesis of Bacterial Cellulose-Zinc Phosphate Composite Film

BC is a layer of cellulose, which is a secondary metabolite formed by *Acetobacter xylinum* microorganisms through the fermentation process. Cellulose is a polysaccharide consisting of (1-4)-glucoside chains. BC can be produced from the activity of bacteria from the Acetobacter, Rhizobium, Agrobacterium, and Sarcina groups (Lippi et al., 2022).

The color of nata produced after soaking is yellowish-white with a slippery surface. Soaking with NaOH aims to create an alkaline atmosphere and raise the pH so that the *Acetobacter xylinum* bacteria are eliminated. Additionally, it aims to get rid of bacteria and non-cellulose elements that could interfere with the cellulose molecular chains' ability to form membrane bonds.

A BC membrane that has been composited forms a color that varies according to the color of the nanoparticle sample used in immersion. It ranges from white to yellow and orange to brown, which visually shows that the BC membrane has been distributed with zinc phosphate nanoparticles.

BC acts as a membrane that will stabilize the size of nanoparticles. In addition, BC has been used as a stabilizing agent that plays a role in the formation of nano-sized particles. The BC-ZP-red dragon fruit peel extract composite film was pressed with a hot press to form a film as shown in Figure 7.

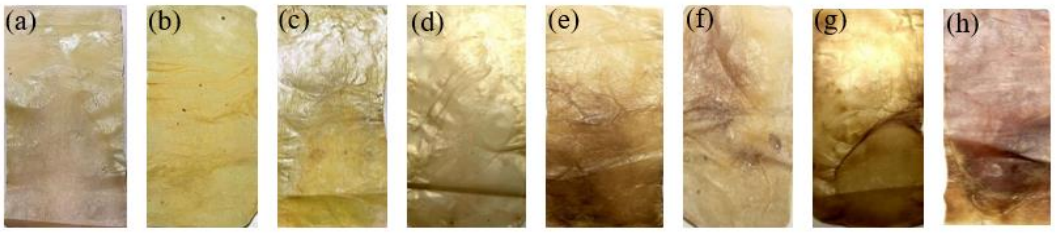

Figure 7. BC-zinc phosphate-red dragon fruit peel extract composite films: (a) BC-ZP, (b) BC-ZP-DF5, (c) BC-ZP-DF10, (d) BC-ZP-DF20, (e) BC-ZP-DF30, (f) BC-ZP-DF40, (g) BC-ZP-DF50, (h) BC-Extract.

Furthermore, the success of composite film synthesis is proven by FTIR Spectroscopy (Figure 8). The spectrum of pure BC film was compared with the spectrum of the composite film BC-ZP-DF10; the most significant peak change was seen between the FTIR spectrum of the pure BC film and the composite film BC-ZP-DF10. For pure BC spectrum at wavenumbers of 3345 cm^{-1} to 2902 cm^{-1}, it shows the presence of –OH stretching. However, in the FTIR spectrum for BC-ZP-DF10 composite, the OH peak is not as wide as exhibited in the pure BC spectrum because some of the –OH has interacted with zinc phosphate. In the BC spectrum, it is also clear that there are wide peaks at 2800 cm^{-1} to 2900 cm^{-1} indicating C-H stretching, 1160 cm^{-1} indicating C-O-C stretching, and 1035 cm^{-1} to 1060 cm^{-1} indicating C=O stretching. In the BC-ZP-DF10 spectrum, it is clear that there is a sharp peak at a wavenumber of 1391 cm^{-1} which is the characteristic peak of PO_4^{3-}. The wide band is exhibited at 500 ~ 700 cm^{-1} indicating the presence of PO_4^{3-} flexural and Zn strain vibration groups. Therefore, the composite film that was synthesized exhibits the successful integration of zinc phosphate nanoparticles into the BC Film.

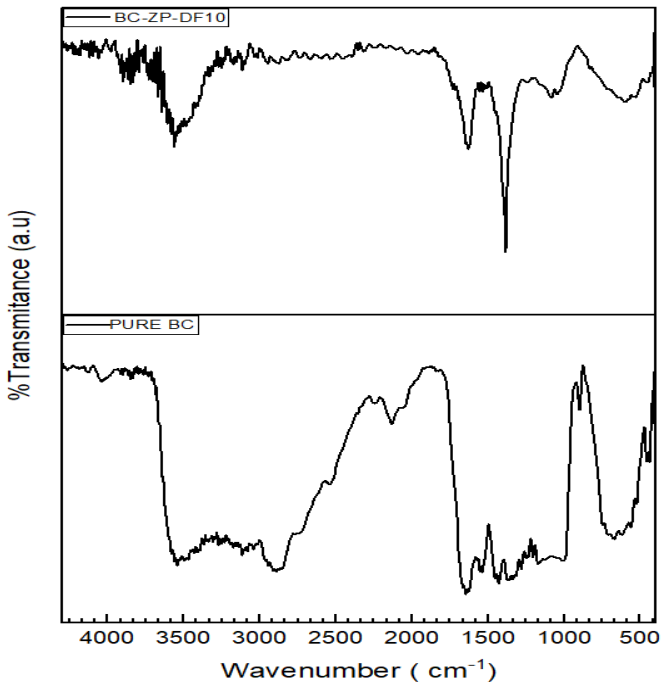

Figure 8. FTIR spectrum of composite films: (A) BC-ZP-DF10,

DOI:https//doi.org/10.22452/mjs.vol43no1.3
Malaysian Journal of Science 43(1): 22-33 (March 2024)

(B) Pure BC Film.

Morphological analysis was conducted to determine the morphology of the composite film in the form of pores and particle size on the BC-ZP-DF10, which greatly influences the effectual properties of the membrane that role as a filter and composite as an antibacterial. The pore size of the membrane significantly affects the number of metal nanoparticles deposited in it (Ottenhall et al., 2018). The results of the morphological analysis using a Digital Optic Microscope are shown in Figure 9.

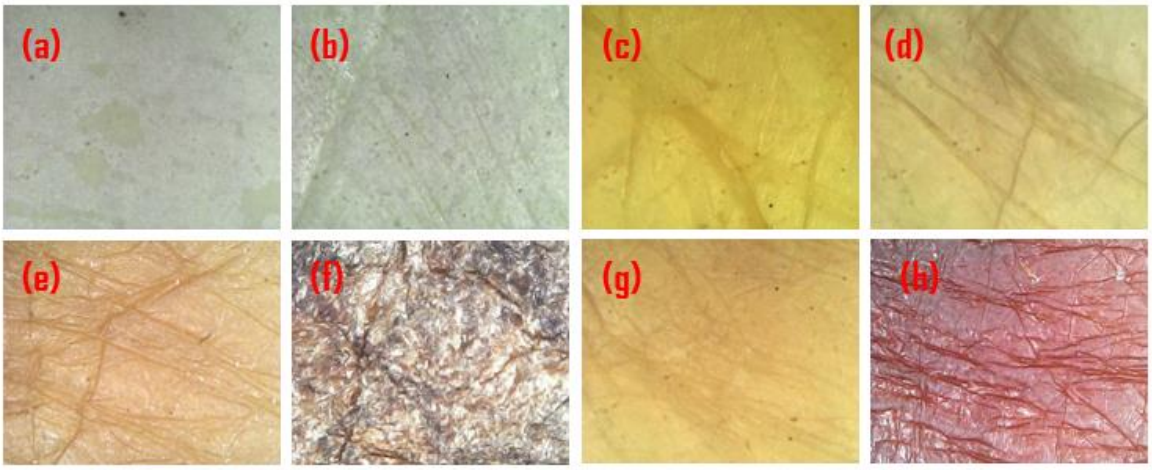

Figure 9. Digital microscope analysis results of BC-ZP-red dragon fruit peel extract composite films: (a) BC-ZP, (b) BC-ZP-DF5, (c) BC-ZP-DF10, (d) BC-ZP-DF20, (e) BC-ZP-DF30, (f) BC-ZP-DF40, (g) BC-ZP-DF50, (h) BC-Extract.

This analysis shows an even distribution of zinc phosphate nanoparticles on the surface of BC. A very good distribution pattern is also shown in the film BC-ZP-DF10. The ZP-DF10 nanoparticles, which have the smallest size, were strengthened from the morphological analysis of ZP-DF10 nanoparticles using SEM (Figure 6), allowing them to be easily distributed into the pores of the BC membrane. Therefore, to further prove the formation of the composite film, the BC-ZP-DF10 composite film, and pure BC film were further tested for their morphology using SEM. Figure 10a displays the results of the SEM analysis of pure BC. From the morphology image of BC, it is evident that the pores are still empty. After being composited with nanoparticles, it is clear that the pores are evenly filled with ZP-DF10 nanoparticles (Figure 10b).

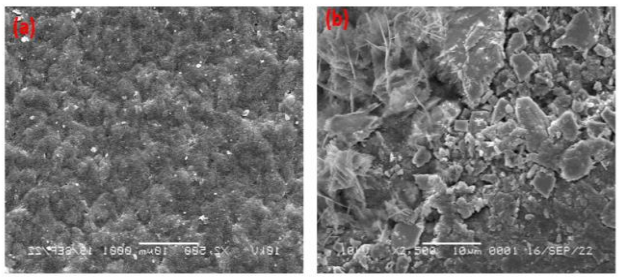

Figure 10. The results of the analysis of the morphology of the film: (A) Pure BC Film, (B) Composite film of BC-ZP-DF10.

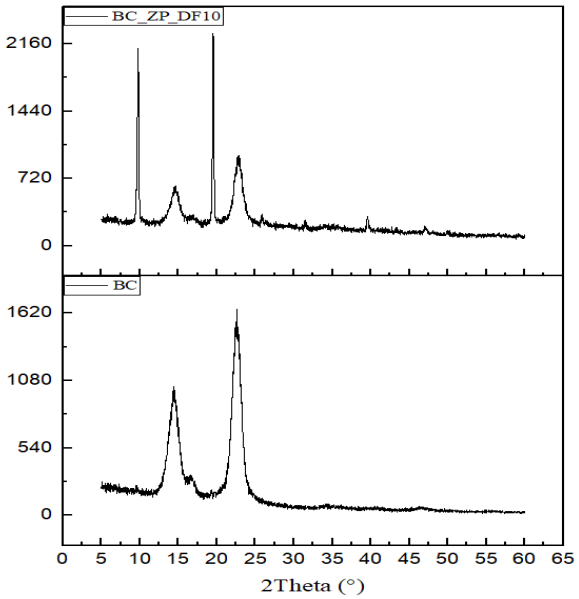

Figure 11. XRD spectrum of composite: (a) Composite film of BC-ZP-DF10, (b) Pure BC.

Figure 11 shows that there is a difference between peak two theta on BC and BC-ZP-DF10 composite. The XRD spectrum of the BC filter shows a semicrystalline phase with a little wide peak at two theta of 14.48º and 22.62º. After incorporation with zinc phosphate, the peak change that there is the additional peak of two theta of 9.78º, 19.48º, 39.63º, and 47.17º, while the peak intensity of the semicrystalline phase reduced. This finding clarifies the profile from FTIR data and SEM morphology. It also proves that zinc phosphate is incorporated in the cellulose BC framework as well.

DOI:https//doi.org/10.22452/mjs.vol43no1.3
Malaysian Journal of Science 43(1): 22-33 (March 2024)

Antimicrobial Activity Test

The synthesized zinc phosphate and composite samples were tested for their antibacterial activities against *S. aureus* (Figure 12) and *P. aeruginosa* (Figure 13).

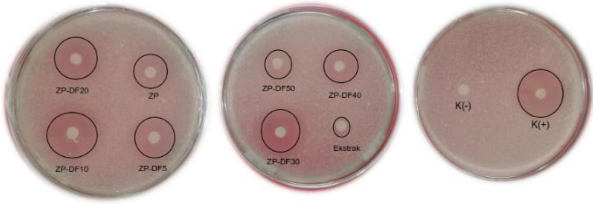

Figure 12. *S. aureus* antibacterial test results on samples ZP, ZP-DF5, ZP-DF10, ZP-DF20, ZP-DF30, ZP-DF40, ZP-DF50, and red dragon fruit peel extract.

Figure 13. *P. aeruginosa* antibacterial test results on samples ZP, ZP-DF5, ZP-DF10, ZP-DF20, ZP-DF30, ZP-DF40, ZP-DF50, and red dragon fruit peel extract.

The results of antibacterial activity tests of zinc phosphate nanoparticles are displayed in Table 4. Based on the results, all test samples noticeably inhibited the growth of *S. aureus* and *P. aeruginosa*, except for the negative control. The ZP-DF10 test sample had the most potent antibacterial activity of all samples. Based on this finding, further characterization for composite films only used two samples, namely BC and ZP-DF10.

Table 4. Average diameter of inhibition zone of zinc phosphate nanoparticle samples-red dragon fruit peel extract

Indicator Bacteria	**Test Sample**	Diameter of Inhibition Zone **(mm)**	**Indication**
S. aureus	ZP	14.02	Strong
	ZP-DF5	21.35	Very strong
	ZP-DF10	23.69	Very strong
	ZP-DF20	19.36	Strong
	ZP-DF30	17.00	Strong
	ZP-DF40	14.36	Strong
	ZP-DF50	10.69	Strong
	Extract	8.35	Moderate
	(+)Tetracycline	26.03	Very strong
	(-) Distillate Water	-	-
P. aeruginosa	ZP	10.68	Moderate
	ZP-DF5	13.37	Strong
	ZP-DF10	14.68	Strong
	ZP-DF20	11.69	Strong
	ZP-DF30	8.02	Moderate
	ZP-DF40	8.35	Moderate
	ZP-DF50	7.03	Moderate
	Extract	8.34	Moderate
	(+)Tetracycline	29.01	Very strong
	(-) Distillate Water	-	-

Based on the diameter of inhibition zone measurements, the results of the antimicrobial activity test of BC-ZP-dragon fruit extract nanocomposite film revealed that all test samples had excellent bacterial growth inhibition against *S. aureus* (Figure 14 and Table 5). ZP-DF10 had the widest inhibition zone among all test samples, which was equal to 21.35 mm. However, after testing the widest inhibitory zone for *P. aeruginosa*, the inhibition zone was classified as weak in each test sample (Figure 15 and Table 5).

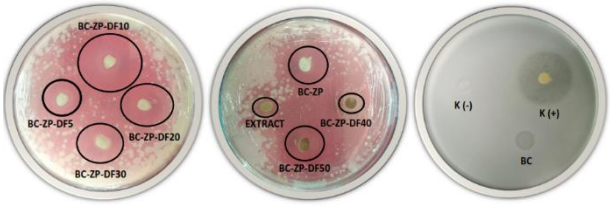

Figure 14. The results of the antibacterial activity test of film BC-ZP-DF5, BC-ZP-DF10, BC-ZP-DF20, BC-ZP-DF30, BC-ZP-DF40, BC-ZP-DF50, BC-ZP, and red dragon fruit peel extract to *S. aureus* bacteria.

DOI:https//doi.org/10.22452/mjs.vol43no1.3
Malaysian Journal of Science 43(1): 22-33 (March 2024)

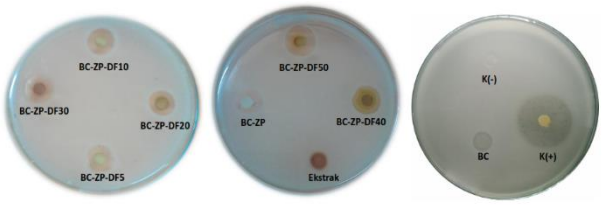

Figure 15. The results of the antibacterial activity test of film BC-ZP, BC-ZP-DF5, BC-ZP-DF10, BC-ZP-DF20, BC-ZP-DF30, BC-ZP-DF40, BC-ZP-DF50, and red dragon fruit peel extract to *P. aeruginosa* bacteria.

Table 5. Average diameter of inhibition zone of bacteria growth on the zinc phosphate nanoparticle composite film

Indicator bacteria	**Composite**	Diameter of Inhibition Zone **(mm)**	**Indication**
S. aureus	BC-ZP	14.02	Strong
	BC-ZP-DF5	17.50	Strong
	BC-ZP-DF10	21.35	Very strong
	BC-ZP-DF20	19.36	Strong
	BC-ZP-DF30	17.00	Strong
	BC-ZP-DF40	7.42	Strong
	BC-ZP-DF50	11.69	Strong
	Extract	8.35	Moderate
	(+)Tetracycline	26.13	Very strong
	(-) Distillate Water	-	-
P. aeruginosa	BC-ZP	3.51	Weak
	BC-ZP-DF5	4.26	Weak
	BC-ZP-DF10	3.84	Weak
	BC-ZP-DF20	3.53	Weak
	BC-ZP-DF30	2.73	Weak
	BC-ZP-DF40	2.83	Weak
	BC-ZP-DF50	2.34	Weak
	Extract	2.83	Weak
	(+)Tetracycline	29.28	Very strong
	(-) Distillate Water	-	-

Air Filter Efficiency Test

Performance analysis of the air filter of the BC-zinc phosphate composite film aimed to evaluate the separation of particulate materials based on their molecular size and shape. The composite film retains particulate components from the feed that are larger than the membrane pores and passes the smaller ones.

The performance of the air filter media is indicated by the results of the efficiency measurement. This is expressed by Equation (2), where %*E* is the percent of efficiency and *Cf* and *Ci* are the numbers of particles after and before passing through the filter, respectively. The results of the air filter performance test of the BC-zinc phosphate nanoparticles composite are presented in Figure 16.

Performance testing of the film filter samples for cellulose of nata de coco, BC-ZP, NC-Extract, BC-ZP-DF5, BC-ZP-DF10, BC-ZP-DF20, BC-ZP-DF30, BC-ZP-DF40, and BC-ZP-DF50 showed that the average efficiency of the composite film were 79.80%, 84.33%, 86.73%, 83.44%, 90.10%, 85.87%, 88.87%, 86.56%, and 88.26%, respectively (Figure 16). The incorporation of zinc phosphate on the cellulose filter increased the filtering efficiency until BC-ZP-DF10 and then decreased on BC-ZP-DF20. This is presumably because the crystal size of the zinc phosphate nanoparticles started to increase and aggregate on the surface of the BC cellulose filter (shown in Table 3 and Figure 6), resulting in a less even distribution on the composite film surface. The capability of the film as an antibacterial material was an additional advantage in particulate matter filter application.

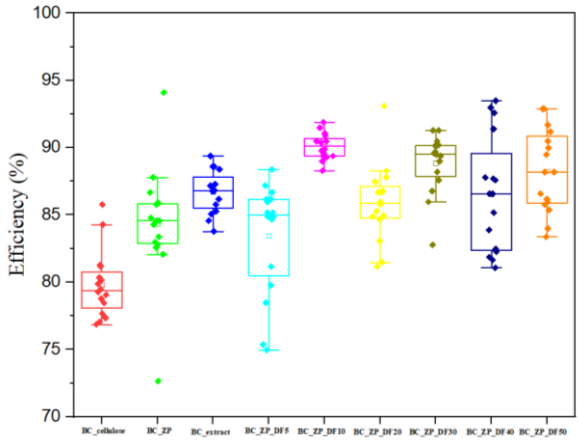

Figure 16. Air filter test of the composite film

4. Conclusion

In this study, the synthesis of zinc nanoparticles through a green chemistry approach was carried out by reacting a red dragon fruit peel extract with a zinc phosphate solution. The results of UV-Vis analysis showed that the absorbance values for 30 minutes tended to be stable. Functional group analysis using FTIR demonstrated the presence of functional group interactions between the compounds in the red dragon fruit peel extract and zinc phosphate. The results of XRD analysis showed that the peak of two thetas at 9.54º, 19,93º, and 31,26º indicate the typical presence of zinc phosphate. The estimated crystallite size analyzed from XRD shows that ZP-DF10 has an average-sized crystal with the smallest value of 37.48 nm. The red dragon fruit peel extract nanoparticles composited with BC film showed morphological differences with the pure BC film. The SEM test revealed that BC had empty pores. After being composited with nanoparticles, it was clear that the pores were evenly filled with ZP-DF10 nanoparticles. The XRD spectrum of the BC film showed a semicrystalline phase with a little wide peak at two theta of 14.48º and 22.62º. After incorporation with zinc phosphate, the peak change that there is the additional peak of two theta of

DOI:https//doi.org/10.22452/mjs.vol43no1.3
Malaysian Journal of Science 43(1): 22-33 (March 2024)

9.78º, 19.48º, 39.63º, and 47.17º, while the peak intensity of the semicrystalline phase reduced. This finding clarifies the profile from FTIR data and SEM morphology, and it also proves that zinc phosphate is incorporated in the cellulose BC framework. Antimicrobial activity tests of nanocomposite films using *S. aureus* and *P. aeruginosa* bacteria confirmed that all compositions had good inhibitory properties, and composite film NC-ZP-DF10 had the strongest inhibition. The results of the air filter test for particulate matter demonstrated that the best average efficiency of the BC-zinc phosphate nanoparticles composite is 90.10%.

5. Acknowledgements

The author would like to thank the Ministry of Education, Culture, Research and Technology of the Republic of Indonesia, especially the Directorate of Research and Community Service for the research grant in accordance with the Research Program Implementation Contract Number: 108/E5/PG. 02.00.PT/2022 dated 10 May 2022. We would also like to thank the Institute for Research and Community Service at Halu Oleo University.

6. References

Budi, P. (2017). Biosynthesis of Silver Nanoparticles Using Ketapang Leaf Extract, Modification With P- Coumaric Acid For Detecting Melamine. *Indonesian Journal of Chemical Science*, *4*(2), 367–372.

Dil, M. A., Haghighatzadeh, A., & Mazinani, B. (2019). Photocatalytic Activity of Aeroxide TiO2 Sensitized By Natural Dye Extracted From Mangosteen Peel. *Bulletin of Materials Science*, *42*(5). https://doi.org/10.1007/s12034-019-1927-9

Franchitti, E., Pascale, E., Fea, E., Anedda, E., & Traversi, D. (2020). Methods For Bioaerosol Characterization: Limits And Perspectives For Human Health Risk Assessment In Organicwaste Treatment. *Atmosphere*, *11*(5). https://doi.org/10.3390/ATMOS11050452

Ghosh, M., Chowdhury, P., & Ray, A. K. (2020). Photocatalytic Activity of Aeroxide TiO2 Sensitized By Natural Dye Extracted From Mangosteen Peel. *Catalysts*, *10*(8). https://doi.org/10.3390/catal10080917

Grzmil, B., Kic, B., & Lubkowski, K. (2007). Studies on Obtaining of Zinc Phosphate Nanomaterials. *Reviews on Advanced Materials Science*, *14*(1), 46–48.

Haiss, W., Thanh, N. T. ., Jenny, A., & Fernig, D. G. (2008). Determination of Size and Concentration of Gold Nanoparticles from UV-Vis Spectra. *Zidonghua Xuebao/ Acta Automatica Sinica*, *34*(9), 1040–1046. https://doi.org/10.3724/SP.J.1004.2008.01040

Horky, P., Skalickova, S., Urbankova, L., Baholet, D., Kociova, S., Bytesnikova, Z., Kabourkova, E., Lackova, Z., Cernei, N., Gagic, M., Milosavljevic, V., Smolikova, V., Vaclavkova, E., Nevrkla, P., Knot, P., Krystofova, O., Hynek, D., Kopel, P., Skladanka, J., … Smerkova, K. (2019). Zinc phosphate-based nanoparticles as a novel antibacterial agent: In vivo study on rats after dietary exposure. *Journal of Animal Science and Biotechnology*, *10*(1), 1–12. https://doi.org/10.1186/s40104-019-0319-8

Jonsirivilai, B., Torgbo, S., & Sukyai, P. (2022). Multifunctional filter membrane for face mask using bacterial cellulose for highly efficient particulate matter removal. *Cellulose*, *29*(11), 6205–6218. https://doi.org/10.1007/s10570-022-04641-3

Kimbonguila, A., Matos, L., Petit, J., Scher, J., & Nzikou, J.-M. (2019). Effect of Physical Treatment on the Physicochemical, Rheological and Functional Properties of Yam Meal of the Cultivar "Ngumvu" From Dioscorea Alata L. of Congo. *International Journal of Recent Scientific Research*, *10*(October), 30693–30695. https://doi.org/10.24327/IJRSR

Konda, A., Prakash, A., Moss, G. A., Schmoldt, M., Grant, G. D., & Guha, S. (2020). Aerosol Filtration Efficiency of Common Fabrics Used in Respiratory Cloth Masks. *ACS Nano*, *14*(5), 6339–6347. https://doi.org/10.1021/acsnano.0c03252

Kopel, P., Cernei, N., Gagic, M., Horky, P., Smerkova, K., & Adam, V. (2018). Zinc phosphate nanoparticles preparation and their antimicrobial activity. *Nanocorn 2018 Conference Proceedings*.

Lippi, M., Riva, L., Caruso, M., & Punta, C. (2022). Cellulose for the Production of Air-Filtering Systems: A Critical Review. *Materials*, *15*(3). https://doi.org/10.3390/ma15030976

Liu, X., Souzandeh, H., Zheng, Y., Xie, Y., Zhong, W. H., & Wang, C. (2017). Soy protein isolate/bacterial cellulose composite membranes for high efficiency particulate air filtration. *Composites Science and Technology*, *138*, 124–133. https://doi.org/10.1016/j.compscitech.2016.11.022

Manihuruk, F. M., Suryati, T., & Arief, I. I. (2017). Effectiveness of the red dragon fruit (Hylocereus polyrhizus) peel extract as the colorant, antioxidant, and antimicrobial on beef sausage. *Media Peternakan*, *40*(1), 47–54. https://doi.org/10.5398/medpet.2017.40.1.47

Manoukian, O. S., Sardashti, N., Stedman, T., Gailiunas, K., Ojha, A., Penalosa, A., Mancuso, C., Hobert, M., & Kumbar, S. G. (2019). Biomaterials for tissue engineering and regenerative medicine. In *Encyclopedia of Biomedical Engineering* (Vols. 1–3). Elsevier Inc. https://doi.org/10.1016/B978-0-12-801238-3.64098-9

DOI:https//doi.org/10.22452/mjs.vol43no1.3
Malaysian Journal of Science 43(1): 22-33 (March 2024)

Massoud, R., & Saffari, H. (2020). Screening methods for assessment of antibacterial activity in nature. *4th International Conference on Applied Researches in Science and Engineering*, *December*, 0–11.

Mulyasuryani, A., & Mustaghfiroh, A. M. (2019). Development of Potentiometric Phenol Sensors by Nata de Coco Membrane on Screen-Printed Carbon Electrode. *Journal of Analytical Methods in Chemistry*, *2019*. https://doi.org/10.1155/2019/4608135

Nugroho, D. A., & Aji, P. (2015). Characterization of Nata de Coco Produced by Fermentation of Immobilized Acetobacter xylinum. *Agriculture and Agricultural Science Procedia*, *3*, 278–282. https://doi.org/10.1016/j.aaspro.2015.01.053

Nurtiana, W. (2019). Anthocyanin As Natural Colorant: a Review. *Food ScienTech Journal*, *1*(1), 1. https://doi.org/10.33512/fsj.v1i1.6180

Onoda, H., & Haruki, M. (2016). Influence of phosphate source on preparation of zinc phosphate white pigments. *International Journal of Industrial Chemistry*, *7*(3), 309–314. https://doi.org/10.1007/s40090-015-0067-3

Ottenhall, A., Henschen, J., Illergård, J., & Ek, M. (2018). Cellulose-based water purification using paper filters modified with polyelectrolyte multilayers to remove bacteria from water through electrostatic interactions. *Environmental Science: Water Research and Technology*, *4*(12), 2070–2079. https://doi.org/10.1039/c8ew00514a

Rahmayanti, H. D., Amalia, N., Munir, R., Yuliza, E., Utami, F. D., Sustini, E., & Abdullah, M. (2019). A Study of Physical and Mechanical Properties of Nata de Coco in the Market. *IOP Conference Series: Materials Science and Engineering*, *599*(1). https://doi.org/10.1088/1757-899X/599/1/012031

Sabherwal, S., Chaku, D., Mathur, U., V, S., & A, M. (2017). Are high-efficiency particulate air (HEPA) filters and laminar air flow necessary in operating rooms to control acute post-operative endophthalmitis? *[1] 'Symposium Recent Advances and Challenges in the Management of Retinoblastoma Globe - Saving Treatments', BMC Ophthalmol., Vol. 17, No. 1, p. 1, 2017, Doi: 10.4103/ljo.IJO.BMC Ophthalmology*, *17*(1), 1. https://doi.org/10.4103/ijo.IJO

Wang, J. D., Li, D., Liu, J. K., Yang, X. H., He, J. L., & Lu, Y. (2011). One-Step Preparation and Characterization of Zinc Phosphate Nanocrystals with Modified Surface. *Soft Nanoscience Letters*, *01*(03), 81–85. https://doi.org/10.4236/snl.2011.13015

Wu, A., Hu, X., Ao, H., & Chen, Z. (2022). Rational design of bacterial cellulose-based air filter with antibacterial activity for highly efficient particulate matters removal. *Nano Select*, *3*(1), 201–211. https://doi.org/10.1002/nano.202100086

Xing, Y. F., Xu, Y. H., Shi, M. H., & Lian, Y. X. (2016). The impact of PM2.5 on the human respiratory system. *Journal of Thoracic Disease*, *8*(1), E69–E74. https://doi.org/10.3978/j.issn.2072-1439.2016.01.19

Zakir, M., & Budi, P. (2016). Effect of AgNO3 concentration and synthesis temperature on surface plasmon resonance (SPR) of silver nanoparticles. *J. Chem. Res*, *4*(1), 356–361.

Zhang, J., Wang, J., Xu, H., Lv, X., Zeng, Y. X., Duan, J., & Hou, B. (2019). The effective photocatalysis and antibacterial properties of AgBr/AgVO3 composites under visible-light. *RSC Advances*, *9*(63), 37109–37118. https://doi.org/10.1039/c9ra06810d

DOI:https//doi.org/10.22452/mjs.vol43no1.3
Malaysian Journal of Science 43(1): 22-33 (March 2024)

MALAYSIAN JOURNAL OF SCIENCE
MJS
ISSN 1394-3065

Regular Issue

Malaysian Journal of Science 43(1): 34-43 (Mar 2024) https://mjs.um.edu.my

GROUNDWATER QUALITY ASSESSMENT IN THE RIVER ATBARA ALLUVIAL SEDIMENTS, EASTERN SUDAN

Khalid Nayl[1a]*, Adill Elkrail[2b], Abdalla Elsheikh[3b] and Hago Ali[4b]

Abstract: According to the standard rates for water testing, 45 wells were sampled and analyzed to evaluate and assess the groundwater chemistry, classify the hydrochemical facies, and identify the sources of salinity in the study area. The main constituents determined included Sodium, Potassium, Chloride, Sulfate, Magnesium, Calcium, Nitrate, and Bicarbonate. Electrical conductivity, Total Dissolved Solids, Total and Excess Alkalinity, and pH were measured on-site during field trips. Using Piper's diagram, chemical information was utilized to identify the groundwater's chemical facies. Despite most chemical concentrations being within the Sudanese Standards and Metrology Organization (SSMO) and World Health Organization (WHO) standard limits, salinity hazards were observed in the middle part of the study area, such as in Shaoat Sherg, Almugatah Shreg, and Umm Oud villages, attributed to the concentration of sodium and chloride in basaltic rocks. The dissolved solids in the study area ranged between 200 to 800 mg/L. The values of calcium ranged between 6.4 to 90 mg/L. The magnesium ion concentration ranged between 4.8 and 90 mg/L. The sodium concentration ranged between 7 and 420 mg/L. The concentration of chloride ranged between 6 and 1098 mg/L. Potassium ranged between 1.2 and 46 mg/L. The concentration of bicarbonate ranged between 78 and 793 mg/L. The sulfate concentration ranged between 0.5 and 508 mg/L. The nitrate (NO_3^-) concentration was found to be very small. Based on Piper's diagram, the samples resulted in 60% being mixed groundwater type and 40% being Na-HCO_3, Na-Cl, and Ca-Mg-HCO_3 groundwater types. Most samples were deemed good for human and agricultural use. Only nine were found to be above the recommended values, with reference to SSMO (2002) and WHO (2008) standards.

Keywords: *Major constituents, water examination, total dissolved solids, groundwater types*

1. Introduction

Groundwater plays a critical role in maintaining river and stream flows during dry periods and in supporting wetland ecosystems. It is a vital source of drinking water globally (Brassington, 2007). Groundwater is considered the safest and cleanest form of water, with access to clean water recognized as a human right and a fundamental requirement for development (Reinhard, 2006). The suitability of groundwater for human consumption, agricultural, and industrial activities is determined by its water quality, which in turn depends on the chemical composition and concentration of elements within the Groundwater (Pebesma, 1996). Analyzing the chemical components of groundwater is an essential aspect of assessing groundwater resources. Various activities that rely heavily on water depend on the chemical characteristics of groundwater. The study of water chemistry offers crucial insights into the formations bearing water, and the occurrence, movement, recharge, and discharge possibilities of groundwater. Additionally, unusual chemical constituents in groundwater may provide important hints about the presence of hidden ore deposits (Technical Committee Reports, 1996). The investigation of water chemistry in the current research is significant for understanding the chemical evolution of groundwater, aiming to grasp spatial and temporal variations in groundwater chemistry better, thereby enabling the efficient management of groundwater resources for domestic, industrial, and agricultural purposes. Some borehole samples reflected water quality that was unfit for domestic use. The current study involves determining and describing the main dissolved chemical components in groundwater and relating these constituents to water usage. Water samples from the study area were collected and analyzed. Therefore, identifying elements that exceed acceptable ranges and understanding the reasons behind high concentrations play a central role in this research. Investigating water chemistry and hydro-geochemical processes related to hydro-geologic settings is crucial for the sustainable utilization of groundwater resources in the study area.

2. Study Area

The area under study is located in the eastern part of Sudan, specifically within the Gedaref and Kassala states, positioned between the towns of Wad Elhelew and Khashm El Girba. It is bounded by latitudes 14.134171° N to 14.961005° N and longitudes 35.536335° E to 35.962209° E, covering an area of 3100 square kilometers (Figure 1). The region is traversed by the

Authors information:
[a]Groundwater and Wadies Directorate, Ministry of Water Resources, Kassala State, SUDAN. E-mail: nail62964@yahoo.com[1]
[b]Department of Hydrogeology, Faculty of Petroleum & Minerals, Al Neelain University, Khartoum, SUDAN. E-mail: adilmagboul321@yahoo.com[2]; abdalla.elsheikh@gmail.com[3]; hagoali@gmail.com[4]
*Corresponding Author: nail62964@yahoo.com

Received: February 26, 2022
Accepted: March 15, 2023
Published: March 31, 2024

DOI:https//doi.org/10.22452/mjs.vol43no1.4
Malaysian Journal of Science 43(1): 34-43 (Mar 2024)

seasonal River Setit and Upper Atbara River, which originate in the Ethiopian highlands and converge at Eltomat village, south of Showak city.

The climate of the study area is characterized by long, hot summers and short, cold winters (Saeed, 1969). Winter temperatures (January) range from a maximum average of 37.5°C to a minimum average of 15.2°C, while summer temperatures (April) can reach up to 43.5°C, with minimum averages around 27°C. Annual rainfall varies between 420 – 1170 mm. The highest evaporation rate occurs in April, reaching 22.3 mm/day, while the lowest is in August, at approximately 3.1 mm/day.

Vegetation in Kassala State is largely influenced by rainfall and the flooding of the River Gash, with common crops including bananas, citrus, and vegetables. Natural vegetation, comprising bushes and trees like Acacia species alongside short-lived grasses during the rainy season, covers the remaining alluvial strips. Currently, large areas in Gash are dominated by Miscats trees (Zeinelabdein et al., 2017). In contrast, Gedaref state has seen its natural vegetation altered by mechanized farming, growing crops such as sesame, sorghum, and millet (Mirghani, 2002). Rain-fed plantations represent the primary land use and human activity in the area.

In semi-arid regions, estimating water resources is challenging due to limited hydrological information and scarce topographic data (Edmund et al., 1992). The study area is split into two distinct parts; the first is near the Rivers Atbara and Setit, marked by rugged topography and a unique land feature known as the Karab (Kerib) formation. The second part encompasses the plain areas, gently sloping westward on the eastern bank and eastward on the western bank of Rivers Atbara and Setit, with a general slope across the plain from southeast to northwest.

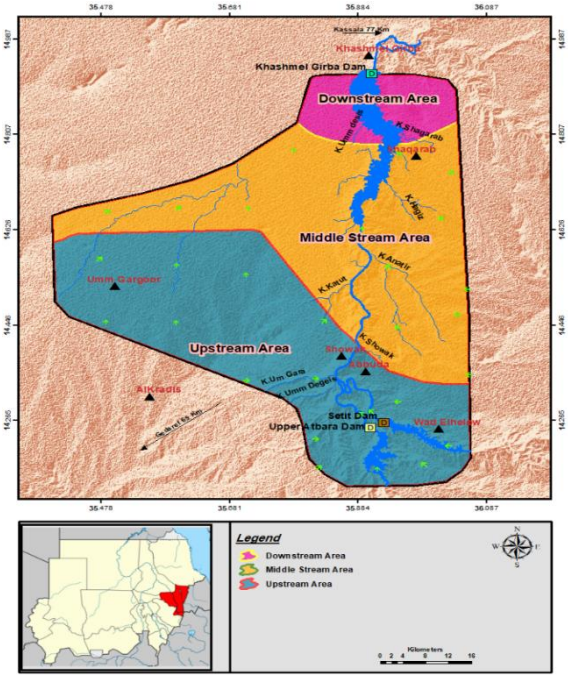

Figure 1. Location and sectors of the study area showing the study area is divided into three sectors; Upstream area, Middle area and Downstream area.

3. Geology and Hydrogeology

Hussien et al. (1989), Ibrahem et al. (1992), Hussein and Adam (1995), and Fadull et al. (1999) conducted geological surveys in the study area. The hydrogeological units of the area are represented by Basement rocks (Pre-Cambrian), Sedimentary rocks (Cretaceous), Basalts (Cenozoic), River Atbara and Setit sediments (Late Tertiary to Early Quaternary), Karab formation (Pleistocene), and the superficial layer at the top (Figure 2). The Basement Complex is composed of granitic gneiss, schist, slates, quartzite, and pegmatitic rocks. The Cretaceous sedimentary rocks consist of sandstone, siltstone, conglomerate, and mudstone, which constitute the major aquifers in the upstream zone. The Cenozoic basalt occurs as thin layers intruded within the loose formations and sometimes overlie the basement rocks. The deposits from the Setit and River Atbara primarily consist of sands, silt, clay, and gravelly clay layers that dominate this sequence. These sediments characterize the main aquifer in the middle and downstream areas. The superficial deposits, occurring as the top layer, are represented by alluvial deposits of Pleistocene to Recent age.

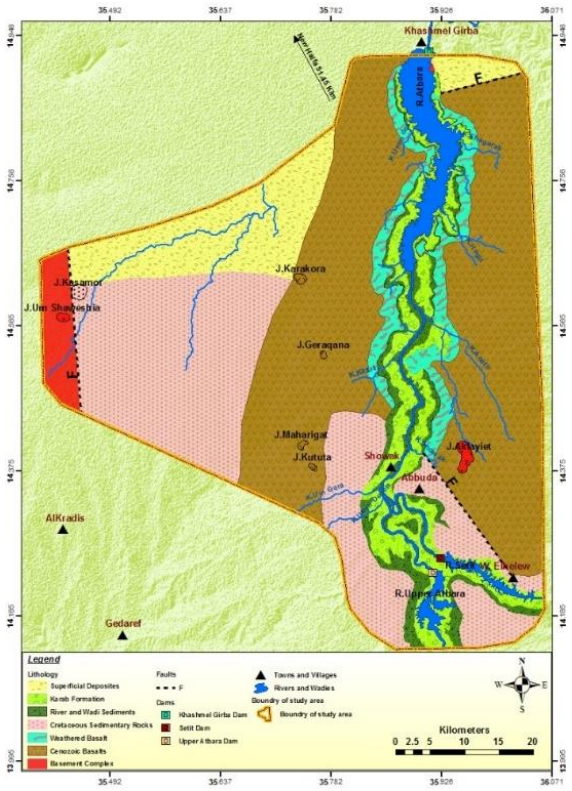

Figure 2. The Geological map of the study area showing six geological sequences.

4. Methodology

Several methods were employed during this research. These methods encompassed both fieldwork and office work to achieve the research objectives. Water samples were collected from forty-five boreholes located throughout the study area (see

DOI:https//doi.org/10.22452/mjs.vol43no1.4
Malaysian Journal of Science 43(1): 34-43 (Mar 2024)

Figure 3). Parameters such as Total Dissolved Solids (TDS), Electrical Conductivity (EC), and pH were measured in the field using a TDS-meter and EC-pH meter. Bottles were used to collect water samples for subsequent chemical analysis in the laboratory. The concentration of anions and cations was determined at the Laboratories of the Groundwater and Wadies Directorate in Gedaref and Kassala towns, as well as the Laboratory of Kassala State Water Corporation, following standard analytical procedures that involved Titrimetric, Spectrophotometric, ultraviolet, flame photometric, and titration methods.

Geographical Information System (Arc-GIS) version 10.2 (2013) was employed to display the locations of water sampling sites and the distribution of chemical constituents as spatial maps. Microsoft Excel and Word software version 14.0.6023.1000 (2010) were used for data entry and diagram preparation. Surfer program version 9.8.669 (2009) and Digital Elevation Model Acquisition (DEM) version (2011) were utilized to create the TDS map. Piper's diagram was adopted to classify the groundwater types.

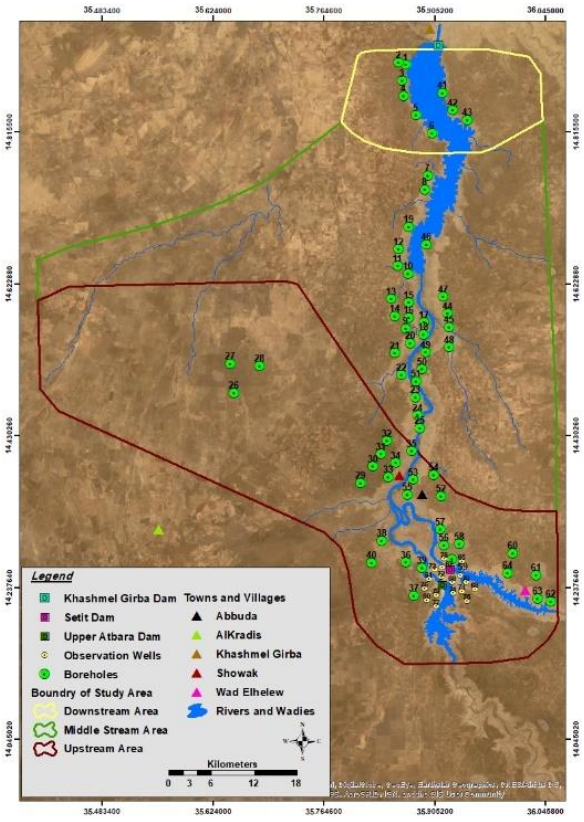

Figure 3. Location of the boreholes in the study area, water samples were taken from forty-five boreholes.

5. Results and Discussion

The groundwater characteristics in the study area are explained in the following sections (Table 1). The electrical conductivity (EC) in the study area varies between 287 and 3580 µS/cm. The high EC values in the study area are primarily concentrated in the fractured basaltic aquifers in the downstream area (Eldeweh well) (Figure 4), the middle area (Umm Oud, Mabroukah, and Shaoat Sharg wells) (Figure 5), and the upstream area (Karkora 1 well) (Figure 6). With regard to the concentration of EC in the study area, it complies with WHO and SSMO standards, except for nine sites that exceed the established standards (Table 1).

The hydrogen ion concentration (pH) of the solution indicates the effective hydrogen concentration H+ (Mazor, 2004) and is mathematically expressed as follows:

$$pH = - \log H^{+} \quad (1)$$

The pH values in the study area range from 6.2 to 8.5, which falls within the normal range for water quality (Hem, 2005). However, there are four exceptions where samples from Magat Abd Elnabe2, Magate Shoot Shamal, Umm Oud, and Mellagah1 villages exhibit high sodium content, leading to elevated pH values. In general, the pH values in the study area conform to the established standards of both WHO and SSMO, except for these four sites (Table 1).

DOI:https//doi.org/10.22452/mjs.vol43no1.4
Malaysian Journal of Science 43(1): 34-43 (Mar 2024)

Table 1. Statistic overview of chemical and physicochemical analysis of wells in the study area (Data in mg\l unless otherwise indicated)

\Downstream				
Parameter	MAX	MIN	AVERAGE	STANDARD DEVIATION
Hardness	204	28	138	58.77414
pH	8.4	7.2	7.9	0.517687
EC(µS/cm)	2050	287	1048.667	744.133
TDS	1333	201	695.1667	463.8467
Ca	56	6.4	24.4	19.6204
Mg	39.4	1.92	18.48667	15.59632
Na	420	250	319.4167	61.43648
K	4.3	1.5	2.583333	0.978604
HCO^3	427	97.6	270.3333	123.905
Cl	404	6.39	134.6483	159.7418
SO^4	250	0.5	100.5833	110.7495
No^3	7.8	0.44	5.253333	3.062644
Midstream				
Parameter	MAX	MIN	AVERAGE	STANDARD DEVIATION
Hardness	960	150	316.1471	191.1748
pH	8.8	6.2	7.976471	0.620009
EC(µS/cm)	3139	582	1234.941	792.3401
TDS	2040	378	803.1176	516.5334
Ca	71.3	6.88	33.49882	19.16756
Mg	190	4.5	56.34706	39.69301
Na	400	93.52	281.4171	80.9951
K	31	1.3	4.475	0.830662
HCO^3	1411	174.3	387.2353	285.6081
Cl	1098	10.7	156.2706	263.8523
SO^4	508	12	93.73529	122.162
No^3	18.48	0	2.826235	4.493662
Upstream				
Parameter	MAX	MIN	AVERAGE	STANDARD DEVIATION
Hardness	514	28	215.9545	116.3363
pH	8.6	6.6	7.654545	0.509647
EC(µS/cm)	3340	287	992	576.5388
TDS	1670	200	600.0909	308.7955
Ca	90	6.4	36.19091	22.58415
Mg	110	1.92	31.28	25.85884
Na	360	7.04	171.5859	98.02315
K	46	1.2	5.217727	9.263125
HCO^3	793	78	383.15	161.4407
Cl	670	21.1	93.77091	136.2717
SO^4	175	0	73.02273	51.60714
No^3	44	0	10.99545	9.910983

DOI:https//doi.org/10.22452/mjs.vol43no1.4
Malaysian Journal of Science 43(1): 34-43 (Mar 2024)

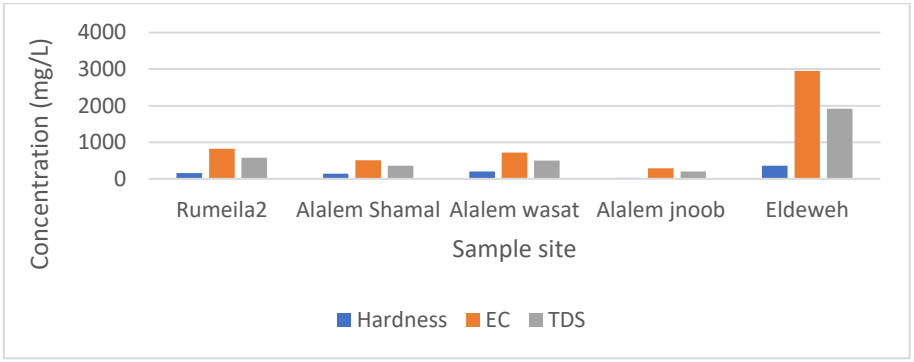

Figure 4. Comparison between TDS and Total Hardness (mg/L) and EC (µS/cm) in groundwater in downstream sector.

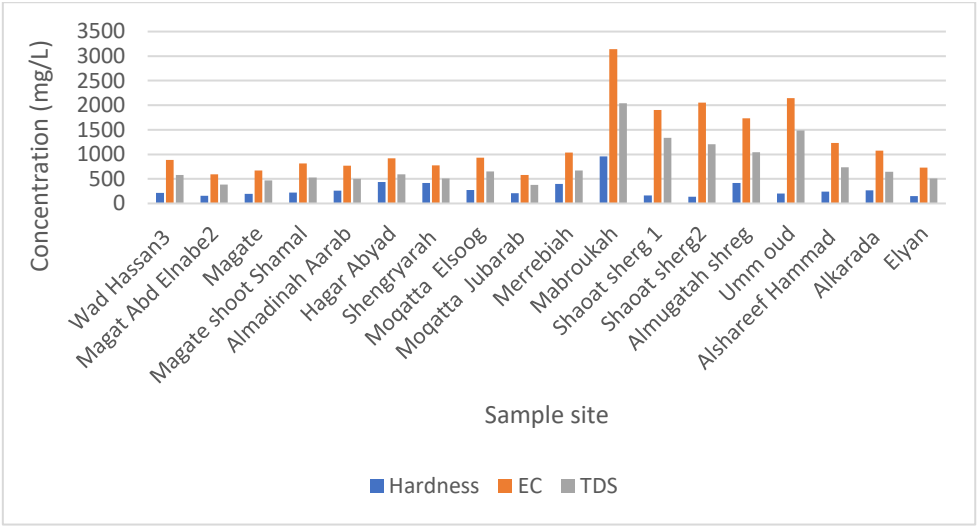

Figure 5. Comparison between TDS ,Total Hardness (mg/L) and EC (µS/cm) in groundwater in middle sector.

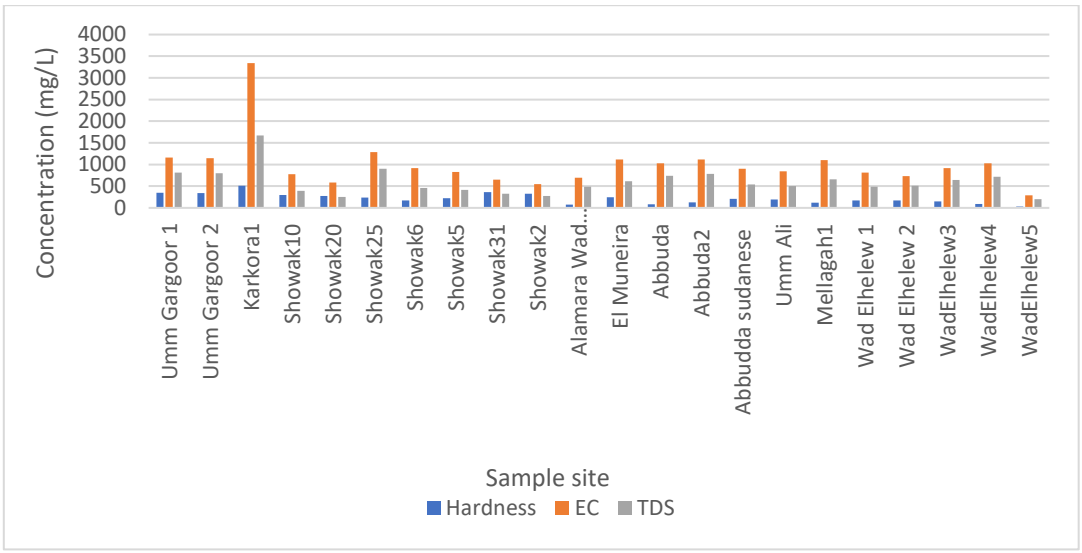

Figure 6. Comparison between TDS and Total Hardness (mg/L) and EC (µS/cm) in groundwater in upstream sector.

DOI:https//doi.org/10.22452/mjs.vol43no1.4
Malaysian Journal of Science 43(1): 34-43 (Mar 2024)

There are conflicting definitions and difficulties in characterizing hardness, as noted by Hem et al. (1982). TH is primarily attributed to the concentration of magnesium and calcium salts. In the specific study area, total hardness ranges from 28 to 960 (see Figure 7). According to the classifications by Sawyer & McCarly (1967), the groundwater in this area can be categorized from soft water to hard water.

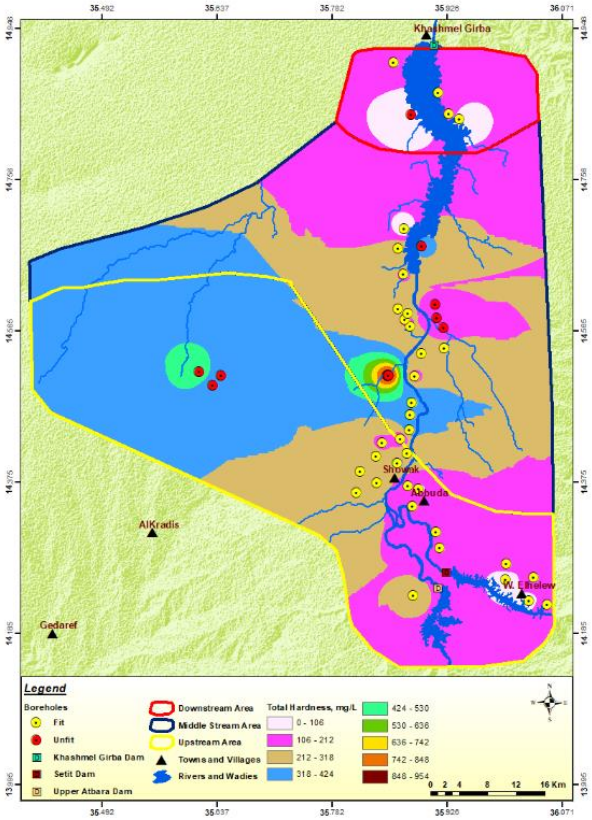

Figure 7. Spatial identification of Total Hardness showing the study area is classified from soft water to very hard water.

TDS in water consists of inorganic salts, including calcium, sulfates, chlorides, magnesium, potassium, sodium, and bicarbonates, as mentioned by Hago (2014). In the study area, TDS values range from 200 to 2040 mg/L (see Table 1). The salinity levels vary from slightly saline to moderately saline, with the exception of seven samples that are highly saline and exceed the established standards (see Figures 3, 4, and 5). In general, the TDS levels in the study area meet the standards, except for nine specific sites (see Figure 8).

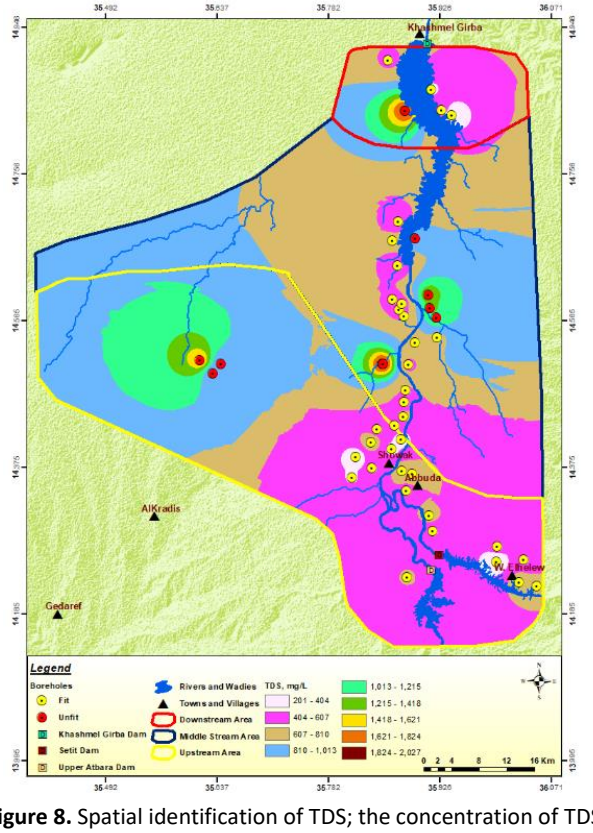

Figure 8. Spatial identification of TDS; the concentration of TDS at the study area within the WHO and SSMO standards except nine sites are above the standards.

DOI:https//doi.org/10.22452/mjs.vol43no1.4
Malaysian Journal of Science 43(1): 34-43 (Mar 2024)

The major dissolved solids of water in downstream, middle and upstream areas are presented in the following Figures.

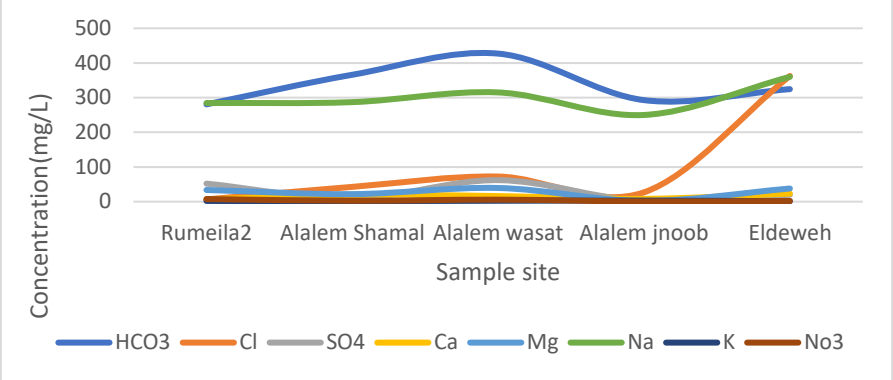

Figure 9. Major dissolved solids in groundwater in downstream sector (mg/L).

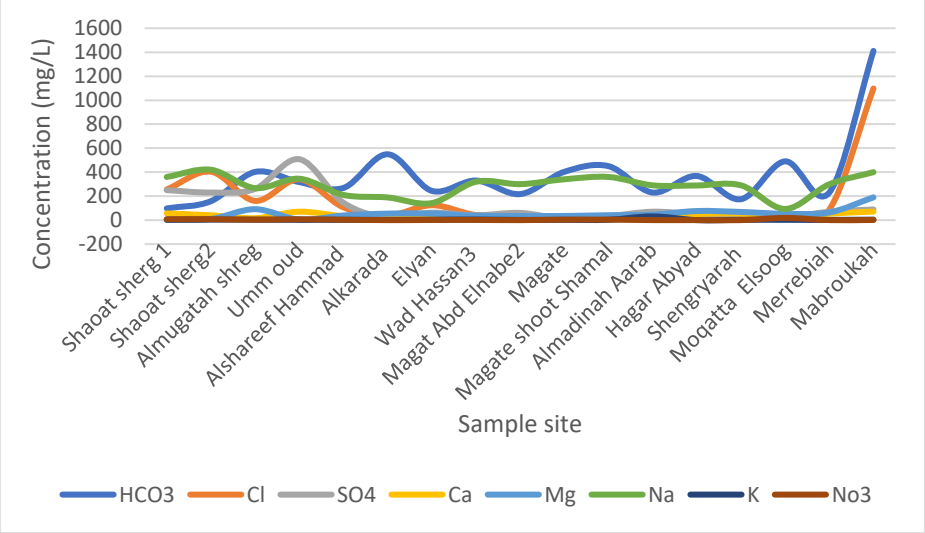

Figure 10. Major dissolved solids in groundwater in midstream sector (mg/L).

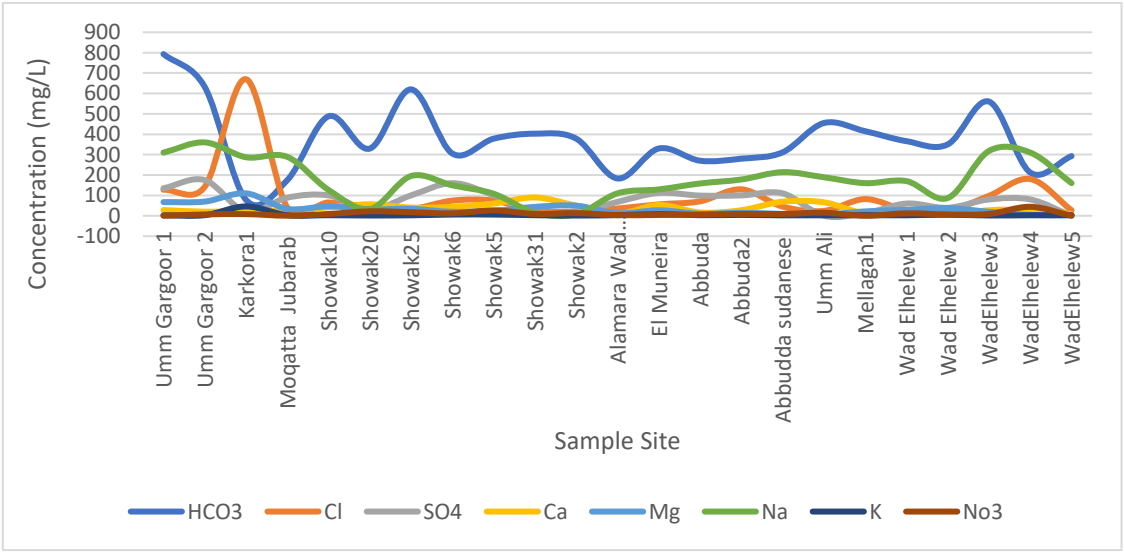

Figure 11. Major dissolved solids in groundwater in upstream sector (mg/L).

DOI:https//doi.org/10.22452/mjs.vol43no1.4
Malaysian Journal of Science 43(1): 34-43 (Mar 2024)

Calcium (Ca^{2+}) ions are abundant in the Earth and mobile in the hydrosphere. Calcium is one of the most common ions in subsurface water (Davis & Dewiest, 1966). However, the minimum value of calcium in the study area is 6.4 mg/L, while the maximum value is about 90 mg/L (see Table 1). Generally, high concentrations of calcium are found in the middle area (Mabroukah wells) (see Figure 10) and in the upstream area (Showak and Abbuda wells) (see Figure 11), which may be attributed to the dissolution of carbonate minerals in the country rock.

The primary source of Magnesium (Mg^{2+}) in groundwater in the study area involves basic volcanic rocks rich in ferro-magnesian minerals (Olivine, pyroxene, and amphiboles). In water chemistry, the geochemical behavior of Mg^{2+} is similar to that of Ca^{2+} (Davis & Dewiest, 1966). The concentration of magnesium in the study area ranges between 1.92 and 190 mg/L (see Table 1). It increases towards the boundary of the recharge area, where volcanic rock is concentrated, such as Mabroukah well in the middle area (see Figure 10) and Karkora1 and Umm Gargoor wells in the upstream area (see Figure 11). Generally, magnesium levels in the study area meet the WHO and SSMO standards, except for four specific sites.

The Sodium ion concentration (Na^{+}) in the study area generally ranges between 10 and 415 mg/L (see Table 1). High sodium values are observed in the downstream area (Eldeweh well) (see Figure 9) and in the middle area (Shaoat Sherg 1&2, Almugatah Shareg, and Mabroukah wells) (see Figure 10). This may be a result of Aegirine Pyroxene in the granitic rocks. More than 50% of the sites have high sodium concentrations, exceeding the WHO and SSMO standards.

The Potassium concentration (K^{+}) in the study area is lower than sodium. In the middle area (Almadinah Aarab well) and in the upstream area (Karkora1 well), the K^{+} concentration reaches relatively high values (31 and 46 mg/L, respectively) (see Figures 10 and 11). The variation in potassium levels in groundwater is related to leaching processes along the groundwater regime, especially from southwest to northeast (higher values upstream and lower values downstream). The Potassium concentration in the study area generally meets the WHO and SSMO standards, except for the Karkora site (upstream area), which exceeds the standards.

The sulfate concentration (SO_4^{2-}) displays significant spatial variation. The increase in sulfate concentration does not entirely coincide with the direction of groundwater flow. Sulfate concentrations in the study area range between 0.7 and 500 mg/L (see Table 1). High sulfate values are observed in wells located in volcanic zones in the middle of the study area, such as Shaoat sherg (1) and (2), Almugatah sherg, and Um Oud (see Figure 10). This may be attributed to volcanic intrusions, which can impact groundwater quality in the mentioned boreholes. Sulfate concentrations in the study area generally meet the WHO and SSMO standards, except for four specific sites.

The dissociation of Bicarbonate (HCO_3^{-}) to carbonate is influenced by the pH value. The dissolution of carbonate rocks and the presence of carbon dioxide in the soil and atmosphere are considered the main sources of bicarbonate and carbonate in water. Bicarbonate concentrations in the study area range between 78 and 1411 mg/L (see Table 1). High bicarbonate values are found in Mabroukah (middle area) and Umm Gargoor 1 (upstream area) boreholes (see Figures 10 and 11), possibly due to evaporite deposits in the calcareous sandstone, thick mudstones, and upper soil layer. Generally, bicarbonate concentrations meet the standards, except for fourteen specific sites.

Chloride (Cl^{-}) is the main element in water exposed to the atmosphere (Hem, 1992). Chloride concentrations in the study area range between 6 and 1098 mg/L (see Table 1). High chloride concentrations are observed in the middle zone (Mabroukah well) and the upstream zone (Karkora1 well) (see Figures 10 and 11), possibly due to the dissolution of chloride minerals in the basaltic or granitic rocks (Kuarod & Sandell, 1963). Generally, chloride levels in the study area meet the WHO and SSMO standards, except for six specific sites located in basaltic zones.

Nitrate concentration (NO_3^{-}) in the study area is very low. Nitrate may have originated from organic matter contamination within the aquifer. During this study, other sources of contamination, such as fertilizers, were not reported, especially those located away from horticultural zones (see Table 1).

The primary ions' composition in groundwater is used to identify groundwater facies, classified based on the cations and anions. Such classification can be graphically represented using various methods (Hem, 1992). Collins (1923), Piper (1944), Raji & Alagbe (1997), and Domenico & Schwartz (1998) have proposed and modified chemical analysis methods.

Based on Piper's diagram, the majority of well samples collected from the study area (60%) belong to the mixed groundwater type, while (40%) fall into Na-HCO_3, Na-Cl, and Ca-Mg-HCO_3 groundwater types (see Figure 12).

DOI:https//doi.org/10.22452/mjs.vol43no1.4
Malaysian Journal of Science 43(1): 34-43 (Mar 2024)

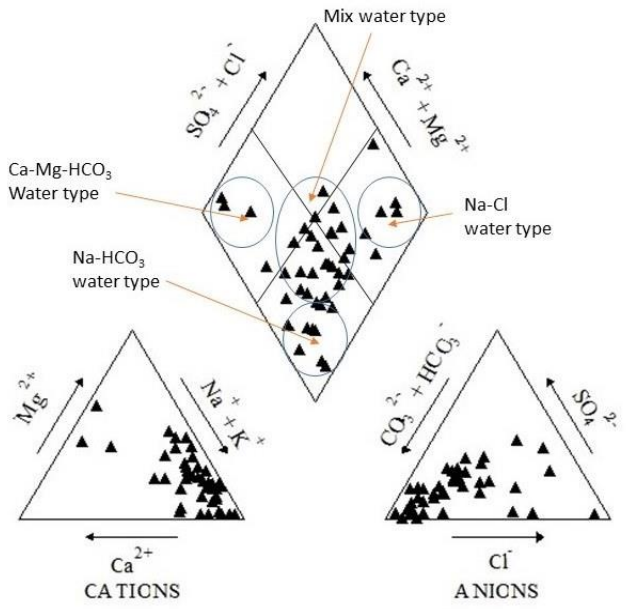

Figure 12. The diagram shows groundwater facies in the study area.

In terms of water quality analysis for the 45 groundwater samples collected from the study area, the TDS values range from 201 to 801 mg/L, which falls within the acceptable range for human consumption. However, nine samples exhibit TDS values ranging from 1201 to 2040 mg/L, exceeding the standards set by WHO and SSMO, making them unsuitable for human consumption. This higher TDS content is attributed to elevated levels of sodium (Na^+), magnesium (Mg^{2+}), and chloride (Cl^-) in the basaltic rocks. The majority of the samples (60%) belong to mixed groundwater types, while the remaining samples are classified as Na-HCO_3, Na-Cl, and Ca-Mg-HCO_3 groundwater types.

The primary land use and human activity in the study area are rain-fed plantation. Irrigation in the region relies on either rainfall or direct extraction from surface water sources. Fortunately, most of the groundwater samples in the study area are suitable for irrigation purposes.

6. Conclusion

The TDS values in the study area range from 200 to 800 mg/L, making the water suitable for human use. However, nine samples have TDS values ranging from 1200 to 2040 mg/L, rendering them unsuitable for human consumption. These elevated TDS levels may be attributed to the concentrations of magnesium (Mg^{2+}), chloride (Cl^-), and sodium (Na^+) in the basaltic rocks.

Based on the findings from the investigations mentioned above, it is strongly recommended to employ isotopic techniques using O18 to identify the source of salinity in the nine sites that exceed the established standards. Additionally, due to population growth and horticultural expansion within the study area, it is advisable to conduct chemical and bacteriological analyses annually to monitor changes in the water quality of the study area.

7. Acknowledgments

The authors sincerely thank the Groundwater Research Offices in Gedaref and Kassala states. Moreover, they wish to thank the State Water Corporation and WES Project in Kassala Town.

6. References

Brassington, R. (2007). Field Hydrogeology. 3th ed. London: John Wiley and Sons, 265 pp.

Collins, W. D. (1923). Graphic Representation of Water Analyses. Indus and Eng. Chem. 15 (4), 394-394.

Davis, S. N. and Dewiest, R. J. M. (1966). Hydrogeology. New York: John Wiley and Sons, 463 pp.Deer, W. A., Howie, R. A., and Zussman, J. (1978). Rock Forming Minerals. Second ed. New York: John Wiley and Sons, vol. 2A.

Domenico, P. and Schwartz, F. (1998). Physical and Chemical Hydrology. Second ed. New York: John Wiley & Sons.

Edmunds, W.M., Darling, W.G., Kinniburgh, D.G. & Mallgoub, S. (1992). Sources of recharge at Abu Delaig, Sudan. J. hydrol.131, p.1-24.

Fadull, H.M., Salih, A. A., Ali, I. A and Lnanagaz, S. (1999). Use of Remote Sensing to Map Gully Erosion along the Atbara River, Sudan. JAG, Volume 1-issue 3/4 -1999, pp.175-180.

Hago, Ali. Hago. (2014). Hydrochemical characteristics of groundwater, midstream area–Gash River basin, Eastern Sudan .pub .Ph.D. Thesis. TU Berlin, Germany.144pp.

Hem J. D., Roberson C. E., and Fournier R. B. (1982). Stability of -MnOOH and manganese oxide deposition from spring water. Water. Resour. Res., 18:563–570.

Hem, J.D. (1992): Study and interpretation of the chemical characteristics of natural water. US. Geological Survey Water Supply Paper 2254, 263p.

Hem, J. D. (2005). Study and interpretation of the chemical characteristics of natural water. University Press of the Pacific, Hawaii.

Hussein, M.T & Adam, E.G. (1995). Water quality of the Gedaref basin, Sudan. Hydrological Science Journal, Vol.40. No2, pp.205-216.

DOI:https//doi.org/10.22452/mjs.vol43no1.4
Malaysian Journal of Science 43(1): 34-43 (Mar 2024)

Hussein, T. Mula, A.G & Schneider. (1989). Geological and Seismic investigations with regard to shallow groundwater explorations in eastern Sudan Republic. Journal of African earth Sciences ,Vol,8.No.1, pp.75-78.

Ibrahim, K. E., Hussein, M. T. & Gidoo, I.M. (1992). Application of combined geophysical and hydrogeological technique to groundwater exploration. A case study of Showak – Wad Elhelew area, eastern Sudan. Journal of Africa Earth Science, Vol.15, No.1, pp.1-10.

Kuarod, P.K. & Sandell, E.B. (1963). Chlorine in Igneous rocks, some Aspect of the Geochemistry of Chlorine. Bullet in Geological society of America.Vol64.pp.879-898.

Mazor, Emanuel. (2004). Isotopic Groundwater Hydrology. 3rd ed. New York: Marcel Dekker, 453pp.

Mirgani, M. (2002). Concepts and models for the characterization of the West Gedaref Hydrogeologic System, Sudan. Ph.D. Thesis, Berlin.117pp.

Pebesma, Jan. Edzer (1996). Mapping Groundwater Quality in the Netherlands, pub .Ph.D. Thesis. Universiteit Utrecht, Netherlands.105 pp.

Piper, A. M. (1944). A graphical procedure in the geochemical interpretation of water analysis. Am. Geophys. Union Trans 25, 914-928.

Raji, B. and Alagbe, S. (1997). Hydrochemical facies in parts of the Nigerian basement complex. Environ. Geol. 29, pp 46– 49.

Reinhard, Kirsch. (2006). Groundwater geophysics, A tool for hydrology. Springer-Verlag Berlin Heidelberg,493pp.

Saeed, E.M. (1969). Groundwater appraisal of the Gash River basin at Kassala, Kassala province, Democratic Republic of Sudan. Ministry of Industry and Mining, Geological and Mineral Resources Dept.Bull.17.88.pp.

Sawyer. C. N. and McCarty, P. L. (1967). Chemistry for sanitary engineers, 2nd ed. McGraw – Hill, New York, 518 pp.

SSMO.(2002). Sudanese Standards and Metrology Organization, Drinking Water Standard, ICS 13.060.00.

Technical committee – Kassala, Reports, (1996): Hydrochemical investigations on the eastern bank of River Atbara (Adr Habib area), G.W.A., Kassala. Unpublished report.

W.H.O. (2009). Guidelines for Drinking-water Quality, Geneva, Switzerland.

Zeinelabdein, K. A. E., Bireir, F. A., Abdelraheem, M. A. (2017). Hydrogeological, IWRM, EIA and Geophysical Investigations in Algadaref, Hamadaeit and Algoz, Areas of Kassala State and Elmafaza and Elgalabat, Areas of Gedaref State, Eastern Sudan. (Unpublished report).

DOI:https//doi.org/10.22452/mjs.vol43no1.4
Malaysian Journal of Science 43(1): 34-43 (Mar 2024)

MALAYSIAN JOURNAL OF SCIENCE
MJS
ISSN 1394-3065

Regular Issue

Malaysian Journal of Science 43(1): 44-58 (March 2024) https://mjs.um.edu.my

AN EFFECTIVE COMPUTATIONAL SCHEME FOR SOLVING VARIOUS MATHEMATICAL FRACTIONAL DIFFERENTIAL MODELS VIA NON-DYADIC HAAR WAVELETS

Ratesh Kumar[1a] and Jaya Gupta[2a]*

Abstract: The non-dyadic Haar wavelet (Haar scale-3) collocation approach is used in this article to generate numerical solutions for fractional differential equations. The non-linear fractional ordinary differential equations are linearised using the Quasilinearisation technique. The Haar scale-3 wavelet approach works by transforming a set of differential calculations into a set of linear algebraic equations. The reliability of the numerical solution can be improved by raising the degree of resolution, and error analysis can be performed. The numerical examples were solved to test the simplicity and flexibility of the method. The outcomes of the numerical examples are compatible with the exact solution and provide better results than previous results existing in the literature. This means that the procedure used here is consistent, reliable, and convenient to use.

Keywords: *Non-dyadic Haar wavelet (HS3WM), Quasilinearisation technique, fractional differential equation, non-linear ordinary differential equation, Riccati fractional equation*

1. Introduction

In recent years, the usage of fractional-order derivatives has exploded in engineering and biological sciences, as well as other fields of study. Modelling and controlling numerous dynamic systems is one of the biggest advantages of using fractional differential equations. Fractional derivatives and integrals are more useful and cost-effective than conventional derivatives in formulating specific electrochemical applications (Oldham & Spanier, 1974). This discovery stimulated their curiosity not only in the applications of the concepts of arbitrary order integrals and derivatives but also in the fundamental mathematical features of these interesting operators (Li & Zeng, 2015). Many physical phenomena, such as the behaviour of biological and mechatronic systems, rheology, complex viscoelasticity, anomalous diffusion, and so on, cannot be well defined and justified based on partial calculus. This has led researchers to explore alternative approaches, as highlighted by Baleanu and Shiri (2015), Miller and Ross (1993), and Podlubny (1993). In distinct fields such as science and engineering, fractional differential equations have many practical applications. Numerous substantial and technical structures, such as dielectric polarisation methods, viscoelastic systems, and electrode-electrolyte polarisation, are modelled using fractional derivatives (Almeida & Bastos, 2016; Gowrisankar & Uthayakumar, 2016). As a result of the expanding applications, many numerical approaches for solving these equations have been developed, including the wavelet method (Chen et al., 2012), the generalised differential transform method, the modified homotopy method (Odibat & Momani, 2008), the finite difference method (Sun et al., 2012), and so on. Non-linear phenomena can be seen in several scientific fields, including fluid dynamics, plasma physics, solid-state physics, chemical kinetics, engineering, and other fields. The mathematical technique of wavelet analysis is well-known and extensively applied. Wavelets are a set of expressions that have been combined to generate a sum of basic functions, and to generate these basic functions, a mother wavelet is translated and compressed. Therefore, it produces locality and smoothness properties. The use of wavelets has aroused researchers' interest in solving conventional ordinary and partial differential equations numerically. Numerous traditional wavelet techniques for solving these equations have recently been expanded by researchers. Numerical solutions and numerical integration of fractional ordinary and partial differential equations are two further wavelet applications in practical mathematics. For the time being, wavelets such as the B-spline, Legendre wavelet, Haar wavelet, Daubechies wavelet and Boubaker wavelet are used (Kobra & Mohsen, 2021). Many studies have employed the Haar scale wavelet, a wavelet that is orthonormal with compact support (Saeed & Rehman, 2013; Shah et al., 2017). A fractional differential equation is converted into an algebraic structure with a finite number of variables by using Haar wavelets (Amin et al., 2021). In 2018, HS3WM was used by Mittal and Pandit to solve a variety of differential equations and expressed that many various types of mathematical models controlled by differential equations, such as dispersive equations (Kumar & Gupta, 2022) and second-order linear integrodifferential equations (Kumar & Bakhtawar, 2022), can be equally capable of solving these wavelet bases (Mittal et al.,

Authors information:
[a]Department of Mathematics, Lovely Professional University, Punjab- 144411, INDIA. E-mail: rateshqadian@gmail.com.q[1]; jayagupta9295@gmail.com[2]
*Corresponding Author: jayagupta9295@gmail.com

Received: February 24, 2022
Accepted: September 18, 2023
Published: March 31, 2024

DOI:https//doi.org/10.22452/mjs.vol43no1.5
Malaysian Journal of Science 43(1): 44-58 (March 2024)

2018). They also depicted that, in terms of convergence, the HS3WM is more rapidly convergent than the Haar scale-2 wavelet. Furthermore, the attributes of the solution to the non-linear fractional differential equation are yet to be investigated using HS3WMs. This inspires us to introduce a new technique for analysing the behaviour of fractional equation-governed systems by employing the HS3WM.

The following types of differential equations are used to assess the applicability of modified HS3WM (Arora et al., 2020).

$$Du^{\alpha}(z) = G(z, u(z), u'(z), u"(z)) \quad (1)$$

With the given set of initial and boundary conditions,

Initial conditions: $u(0) = \mu_1$ and $u'(0) = \mu_2$ (2)

Dirichlet boundary conditions: $u(0) = \mu_3$ and $u(1) = \mu_4$ (3)

The manuscript is organised in the following sections: The fundamental definitions of fractional calculus are provided in Section 2. The HS3W and structure of its family in explicit forms, as well as the process for finding their integrals, were briefly discussed in Section 3. Section 4 explains the Quasilinearisation technique to solve a non-linear term in a differential equation. In Section 5, the present approach is used to solve five distinct models of fractional differential equations to evaluate their efficiency and performance. The conclusion drawn from the data, as well as future study ideas, is presented in Section 6.

2. Basic Definition of Fractional Calculus

In the given section, we discussed the basic definitions of fractional differentiation and integration.

Reimann Liouville Fractional differential operator of order α: For the positive real numbers α, t across the interval [m, n], the fractional differential operator established by Riemann-Liouville is given by Das (2011):

$$d^{\alpha}f(t) = \frac{1}{\Gamma(p-\alpha)}\left[\frac{d}{dt}\right]^{p}\int_{m}^{n} f(x)(t-x)^{p-\alpha-1}dx$$

where α denotes the order of the derivative and $t\epsilon$ [m, n].

Caputo fractional differential operator of order α: For positive real numbers α, t, the fractional differential operator developed by Caputo, an Italian mathematician, is (Shah et al., 2022):

$$d^{\alpha}f(t) = \frac{1}{\Gamma(p-\alpha)}\int_{m}^{n}\left[\frac{d}{dt}\right]^{p} f(x)(t-x)^{p}dx$$

where α denotes the order of the derivative and $t\epsilon$ [m, n].

3. Haar Scale-3 Wavelet

The main difference between Haar scale-2 wavelets is that the construction of the entire wavelet family can be done only by one mother wavelet, whereas in the HS3W, for the construction of the entire wavelet family, two distinct shapes of mother wavelets are responsible. Due to this, with the help of HS3W, the rate of convergence of the solution has increased. With dilation factor three, the family of HS3W with detailed information about Haar function, father wavelet, and symmetric and antisymmetric mother wavelets is provided below (Arora et al., 2020; Shiralashetti & Deshi, 2016).

$$f(z) \approx c_1\phi_1(z) + \sum_{even\ index\ i\geq 2}^{\infty} c_i\varphi_i^1(z) + \sum_{odd\ index\ i\geq 3}^{\infty} c_i\varphi_i^2(z)$$

Hence, the generalised form of the HS3-W family can be expressed in the form of:

$$h_i(t) = \phi(t) = \begin{cases} 1 & , \ a \leq t < b \\ 0 & , \ otherwise \end{cases} for\ i = 1$$

$$h_i(t) = \varphi_i^1(3^j - k) = \frac{1}{\sqrt{2}}\begin{cases} -1 & \chi_{11}(i) \leq t < \chi_{12}(i) \\ 2 & \chi_{12}(i) \leq t < \chi_{13}(i) \\ -1 & \chi_{13}(i) \leq t < \chi_{14}(i) \\ 0 & otherwise \end{cases} for\ i = 2,4,6\ldots\ldots,3p-1$$

DOI:https//doi.org/10.22452/mjs.vol43no1.5
Malaysian Journal of Science 43(1): 44-58 (March 2024)

$$h_i(t) = \varphi_i^2(3^j - k) = \sqrt{\frac{3}{2}} \begin{cases} 1 & \chi_{11}(i) \le t < \chi_{12}(i) \\ 0 & \chi_{12}(i) \le t < \chi_{13}(i) \\ -1 & \chi_{13}(i) \le t < \chi_{14}(i) \\ 0 & otherwise \end{cases} \quad for\ i = 1,3,5\ldots\ldots,3p$$

$\chi_{11}(i) = a + (b-a)\frac{k}{p}, \chi_{12}(i) = a + (b-a)\frac{3k+1}{3p}, \quad \chi_{13} = a + (b-a)\frac{3k+2}{3p}, \quad \chi_{14} = a + (b-a)\frac{k+1}{p}.$ Here, $p = 3^j, j = 0,1,2,3,\ldots\ldots, k = 0,1,2,\ldots\ldots, p-1.$

The translation characteristics, resolution level (dilation factor), and wavelet number of the wavelet family are represented by k, j, and i, respectively. We defined integrals for HS3W as follows:

$$\int_0^x \phi_{i,s}(r)dr = \phi_{i,s+1}(r) = \begin{cases} \frac{r^s}{\Gamma(s+1)} & , \quad a \le r < b \\ 0 & otherwise \end{cases}$$

$$\int_0^x \varphi_{i,s}{}^1(r)dr = \varphi_{i,s+1}{}^1(r) = \frac{1}{\sqrt{2}} \begin{cases} 0 & ; 0 \le r < \chi_{11}(i) \\ \frac{-[r-\chi_{11}(i)]^s}{\Gamma(s+1)} & ; \chi_{11}(i) \le r < \chi_{12}(i) \\ \frac{3[r-\chi_{12}(i)]^s - [r-\chi_{11}(i)]^s}{\Gamma(s+1)} & ; \chi_{12}(i) \le r < \chi_{13}(i) \\ \frac{3[r-\chi_{12}(i)]^s - 3[r-\chi_{13}(i)]^s - [r-\chi_{11}(i)]^s}{\Gamma(s+1)} & ; \chi_{13}(i) \le r < \chi_{14}(i) \\ \frac{3[r-\chi_{12}(i)]^s - 3[r-\chi_{13}(i)]^s - [r-\chi_{11}(i)]^s + [r-\chi_{14}(i)]^s}{\Gamma(s+1)} & ; \chi_{14}(i) \le r < 1 \end{cases}$$

$$\int_0^x \varphi_{i,s}{}^2(r)dr = \varphi_{i,s+1}{}^2(r) = \sqrt{\frac{3}{2}} \begin{cases} 0 & ; 0 \le r < \chi_{11}(i) \\ \frac{[r-\chi_{11}(i)]^s}{\Gamma(s+1)} & ; \chi_{11}(i) \le r < \chi_{12}(i) \\ \frac{[r-\chi_{11}(i)]^s - [r-\chi_{12}(i)]^s}{\Gamma(s+1)} & ; \chi_{12}(i) \le r < \chi_{13}(i) \\ \frac{[r-\chi_{11}(i)]^s - [r-\chi_{12}(i)]^s - [r-\chi_{13}(i)]^s}{\Gamma(s+1)} & ; \chi_{13}(i) \le r < \chi_{14}(i) \\ \frac{[r-\chi_{11}(i)]^s - 3[r-\chi_{12}(i)]^s - [r-\chi_{13}(i)]^s + [r-\chi_{14}(i)]^s}{\Gamma(s+1)} & ; \chi_{14}(i) \le r < 1 \end{cases}$$

4. Quasilinearisation Technique

Basically, the Quasilinearisation technique is a generalised form of the Newton-Raphson technique. It converges to a solution in its exact form. Quadratically, it must show monotone convergence (Saeed & Rehman, 2013). Here, consider a non-linear second-order differential equation:

$$\psi''(v) = k(v, \psi(v)) \qquad (4)$$

With boundary conditions:

$$\psi(a_1) = \theta_1, \psi(b_1) = \theta_2;\ a_1 \le v \le b_1$$

Here, k is in terms of $\psi(v)$. Let us choose an approximation at the initial step of solution $\psi(v)$. Let us say $\psi_0(v)$. k can be expanded around $\psi_0(v)$ and is written in the form

$$k(\psi(v), v) = k(\psi_0(v), v) + (\psi(v) - \psi_0(v))k_{\psi_0(v)}(\psi_0(v), v) \qquad (5)$$

$$\psi''(v) = k(\psi_0(v), v) + (\psi(v) - \psi_0(v))k_{\psi_0(v)}(\psi_0(v), v) \qquad (6)$$

$$\psi''(v) = k(\psi_1(v), v) + (\psi(v) - \psi_1(v))k_{\psi_1(v)}(\psi_1(v), v) \qquad (7)$$

The form of a recurrence relationship is:

$$\psi_{s+1}{}''(v) = k(\psi_s(v), v) + (\psi(v) - \psi_s(v))k_{\psi_s(v)}(\psi_s(v), v) \qquad (8)$$

for obtaining $\psi_{s+1}(v)$, here, use $\psi_s(v)$, whose value is already known. A non-linear differential equation with the required conditions is given as follows:

DOI:https//doi.org/10.22452/mjs.vol43no1.5
Malaysian Journal of Science 43(1): 44-58 (March 2024)

$$\psi_{s+1}(\upsilon) = \alpha, \psi_s(\upsilon) = \beta. \quad (9)$$

Now, consider the non-linear second-order differential equation of the form:

$$\psi''(\upsilon) = k(\psi'(\upsilon), \psi(\upsilon), \upsilon)$$

Here, the first derivative $q'(m)$ can be considered as another function

$$\psi_{s+1}{}''(\upsilon) = k(\psi'(\upsilon), \psi(\upsilon), \upsilon) + (\psi'_{s+1}(\upsilon) - \psi'_s(\upsilon))\, k_{\psi'_s(\upsilon)}(\psi'_s(\upsilon), \psi_s(\upsilon), \upsilon)) + (\psi_{s+1}(\upsilon) - \psi_s(\upsilon))\, \mathrm{k}\, (\psi'_s(\upsilon), \psi_s(\upsilon), \upsilon) \quad (10)$$

With boundary conditions $\psi_{s+1}(\upsilon) = \alpha, \psi_s(\upsilon) = \beta.$ (11)

Follow the same technique to establish the recurrence relation for higher-order non-linear differential equations.

$$L^j\psi_{s+1}(\upsilon) = k(\psi_s(\upsilon), \psi'_s(\upsilon).\ldots\ldots \psi_s^{j-1}(\upsilon), \upsilon) + \sum_{p=0}^{n-1}(\psi^p_{s+1}(\upsilon) - \psi^p_s(\upsilon))\, k_{\psi^p}(\psi'_s(\upsilon), \psi_s(\upsilon), \ldots., \psi_s^{j-1}(\upsilon), \upsilon) \quad (12)$$

The order of the differential equation is j; the above equation is linear, and it can be solved recursively, $\psi_s(\upsilon)$, if it has a known value and can be used to get the value of $\psi_{s+1}(\upsilon)$.

5. Applications of Fractional Differential Equations

In this part, the HS3WM is used to solve certain numerical problems for solving linear as well as non-linear fractional differential equations and compare the results with the results obtained by methods available in the literature to demonstrate the method's compatibility.

Numerical Experiment No. 1: Fractional Riccati Equation

$$D^\alpha y(x) = -y^2(x) + 1, for\ x \geq 0, 0 \leq \alpha \leq 1 \quad (13)$$

Subject to the initial condition y (0) = 0.

exact solution at $\alpha = 1$,

$$y(x) = \frac{e^{2x}-1}{e^{2x}+1} \quad (14)$$

Solution:

Applying the Quasilinearisation technique to the non-linear term of equation (13), we get

$$D^\alpha y_{s+1}(x) + 2\, y_s(x) y_{s+1}(x) = y_s^2 + 1, x \geq 0 \quad (15)$$

With the initial condition $y_{s+1}(0) = 0$, we applied HS3WM to equation (15), and we approximated the term containing the highest derivatives by Haar wavelet series as follows:

$$D^\alpha y_{s+1}(x) = \sum_{l=1}^{3M} c_l h_l(x) \quad (16)$$

On integrating the above equation (16), we obtained the lower derivatives, and by using the initial condition, we have,

$$y_{s+1}(x) = \sum_{l=1}^{3M} c_l P_{\alpha,l}(x) \quad (17)$$

Now, substituting equations (16) and (17) in equation (15), we get

$$\sum_{l=1}^{3M} c_l[h_l(x) + 2\, y_s(x) P_{\alpha,l}(x)] = y_s^2(x) + 1 \quad (18)$$

DOI:https//doi.org/10.22452/mjs.vol43no1.5
Malaysian Journal of Science 43(1): 44-58 (March 2024)

For α = 1, we assigned the differential order to equation (13) and at J = 2 resolution level. Tables 1 and 2 show the comparative study of the exact and approximate solutions as well as the values of errors, respectively, derived using the Haar scale-3 wavelet technique, and graphical results are shown in Figure 1. The absolute inaccuracy decreases as the number of iterations increases. Using the Quasilinearisation technique at a given level of resolution, the precise answer at α = 1 and the Haar wavelet resolution at various $\alpha's$ are demonstrated in Figure 2.

Table 1. Comparison of Exact Value and Approximate Value at Different Values of *x* and Result Comparison by Two Different Methods

x	Exact Value	Approx. value	Absolute Error by HS3WM	Kobra, 2021
0.1	0.01851640192288	0.018512172212923	2.8650e-05	6.11e-05
0.2	0.05549847010902	0.055485850362306	4.2584e-05	1.16e-04
0.3	0.092328886151755	0.092308082564065	5.9053e-05	1.12e-04
0.4	0.128908385222714	0.128879735027882	6.7831e-05	8.34e-04
0.5	0.165140412924629	0.165104375053012	6.9465e-05	6.69e-03
0.6	0.200932122324545	0.200889264899714	6.6312e-05	6.64e-03
0.7	0.236195287939167	0.236146273143560	5.7972e-05	6.24e-04
0.8	0.270847118516721	0.270792685450088	4.6444e-05	5.86e-03
0.9	0.304810954186844	0.304751900397517	3.7996e-05	1.48e-04

Table 2. Comparison of Value of Error of L_2 Error and L_∞ Errors at Different Levels of Resolution.

Level of resolution	J=2	J=3	J=4	J=5
HSWM3 $L_2 error$	1.0785e-04	1.1896e-05	1.3217e-06	1.5412e-07
HSWM3 $L_\infty error$	6.9465e-05	7.7184e-06	8.5760e-07	9.7023e-08

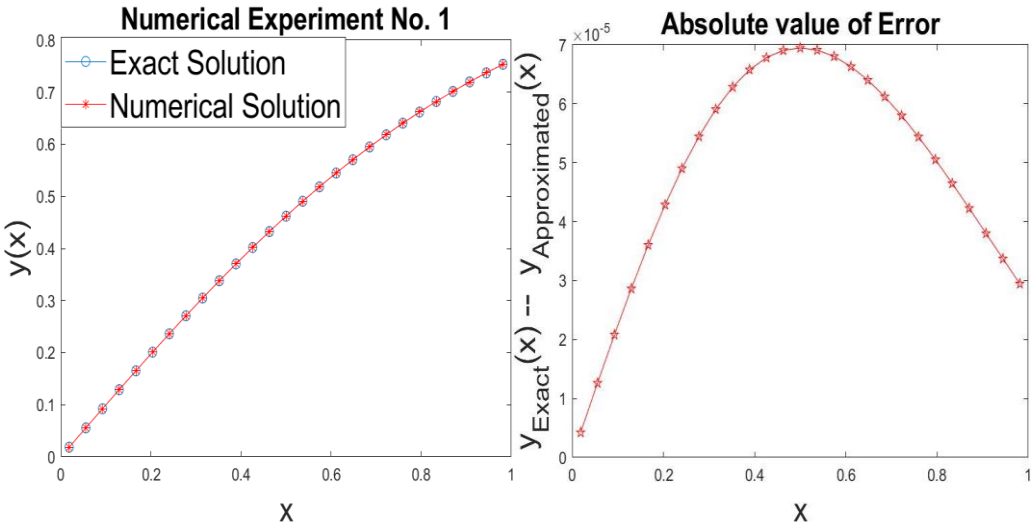

Figure 1. Graphical Representation of the Exact Solution and the Numerical Solution at $\alpha = 1$

DOI:https//doi.org/10.22452/mjs.vol43no1.5
Malaysian Journal of Science 43(1): 44-58 (March 2024)

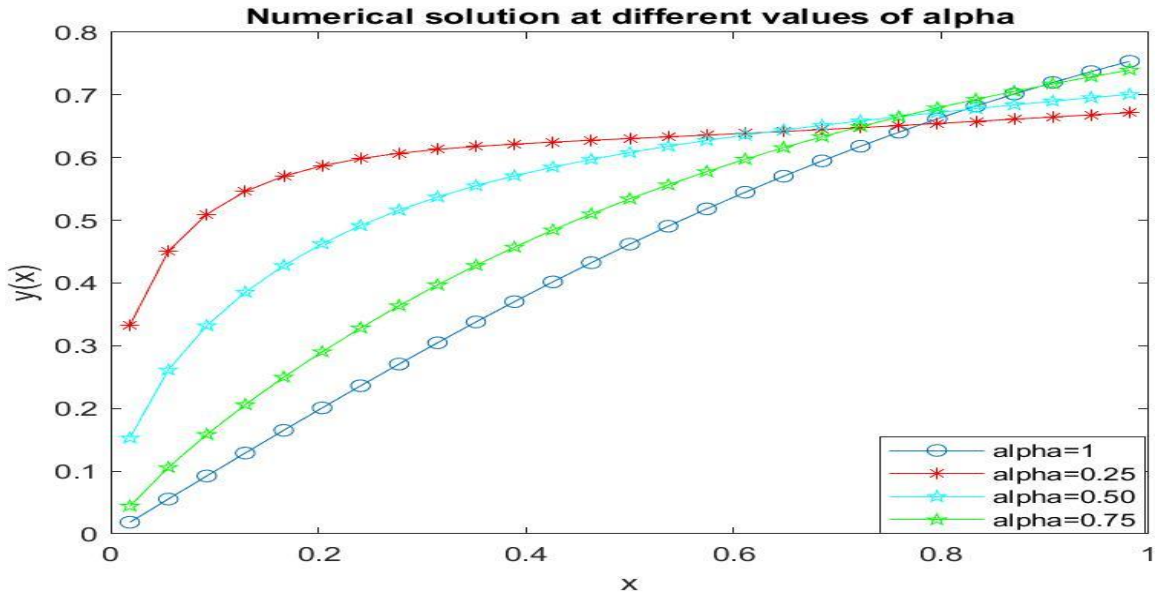

Figure 2. Graphical Representation of the Numerical Solution for Different Values of α Lies Between 0 and 1. At j = 2 Resolution Level.

Numerical Experiment No. 2: Fractional Vander-Pol Oscillator Problem

$$D^{\alpha}y(x) + \frac{dy(x)}{dx} + y(x) + y^2(x)\frac{dy(x)}{dx} = 2\,cos(x) - cos^3(x), \qquad 1 \le \alpha \le 2 \qquad (19)$$

Subject to early circumstances: y (0) = 0, $y'(0) = 1$
At $\alpha = 2$, the precise answer that exists in the literature (Odibat & Momani, 2008) is given by: y(x)= sin(x)
Solution: After applying the Quasilinearisation technique to equation (19), we get

$$D^{\alpha}y_{s+1}(x) + \big(1 + 2y_s(x){y_s}'(x)\big)y_{s+1}(x) + \big(1 + {y_s}^2(x)\big){y_{s+1}}'(x) = 2{y_s}'(x){y_s}^2(x) + 2cos(x) - cos^3(x), 1 \le \alpha \le 2 \qquad (20)$$

With the initial condition $y_{s+1}(0) = 0, {y_s}'(0) = 1$, we applied the Haar scale-3 method to (20), and we approximated the term with the highest derivatives by the Haar wavelet series as follows:

$$D^{\alpha}y_{s+1}(x) = \sum_{l=1}^{3M} c_l h_l(x) \qquad (21)$$

On integrating the above equation (21), we obtained the lower derivatives, and by using the initial condition, we have

$$y_{s+1}(x) = \sum_{l=1}^{3M} c_l P_{\alpha,l}(x) \qquad (22)$$

Now, substituting equations (21) and (22) in equation (20), we get

$$\sum_{l=1}^{3M} c_l[\,h_l(x) + (1 + 2y_s(x)\,{y_s}'(x))\,P_{\alpha,l}(x) + (1 + {y_s}^2(x))P_{\alpha-1,l}(x)] = 2{y_s}^2(x){y_s}'(x) - (1 + 2{y_s}'(x)y_s(x)\,)x - 1 - {y_s}^2(x) + 2cos(x) - cos^3(x) \qquad (23)$$

With initial approximations $y_0(x) = 0, {y_0}'(x) = 1$

We assigned the differential order to equation (20) for α = 2 and the level of resolution to J = 2. Tables 3 and 4 show the comparative study of the exact and approximate solutions as well as the values of errors, respectively, derived using the Haar scale-3 wavelet technique, and graphical results are shown in Figure 3. With more iterations, the absolute error decreases. The precise solution at α = 1 and the Haar wavelet solution at distinct $\alpha's$ are represented in Figure. 4 via the Quasilinearisation technique at a fixed level of resolution.

DOI:https//doi.org/10.22452/mjs.vol43no1.5
Malaysian Journal of Science 43(1): 44-58 (March 2024)

Table 3. Comparison of the Exact Value and the Approximate Value at Different Values of *x* and Discussion of Absolute Error by Scale-3 Haar Wavelets with Haar Scale Wavelets

x	Exact Value	Approx. value	Saeed, 2017	Absolute Error by HS3WM
0.1	0.0998334166	0.0998334056	0.0998333872	2.89934e-06
0.2	0.1986693308	0.1986693108	0.1986692768	8.67113e-06
0.3	0.2955202067	0.2955202012	0.2955201331	1.44070e-05
0.4	0.3894183423	0.3894182990	0.3894182543	2.01071e-05
0.5	0.4794255386	0.4794255100	0.4794254413	2.57714e-05
0.6	0.5646424734	0.5646423900	0.5646423719	3.13998e-05
0.7	0.6442176872	0.6442176329	0.6442175863	3.69924e-05
0.8	0.7173560909	0.7173560600	0.7173559950	4.25492e-05
0.9	0.7833269096	0.7833268874	0.7833268225	4.80701e-05

Table 4. Comparison of the Value of the Error of the Scale-3 Haar Wavelet at Different Levels of Resolution.

Level of resolution	J=2	J=3	J=4
HSWM3 $L_2 error$	6.33395260e-05	7.03695009e-06	7.81873793e-07
HSWM3 $L_\infty error$	4.12718973e-05	4.58592395e-06	5.09566047e-07

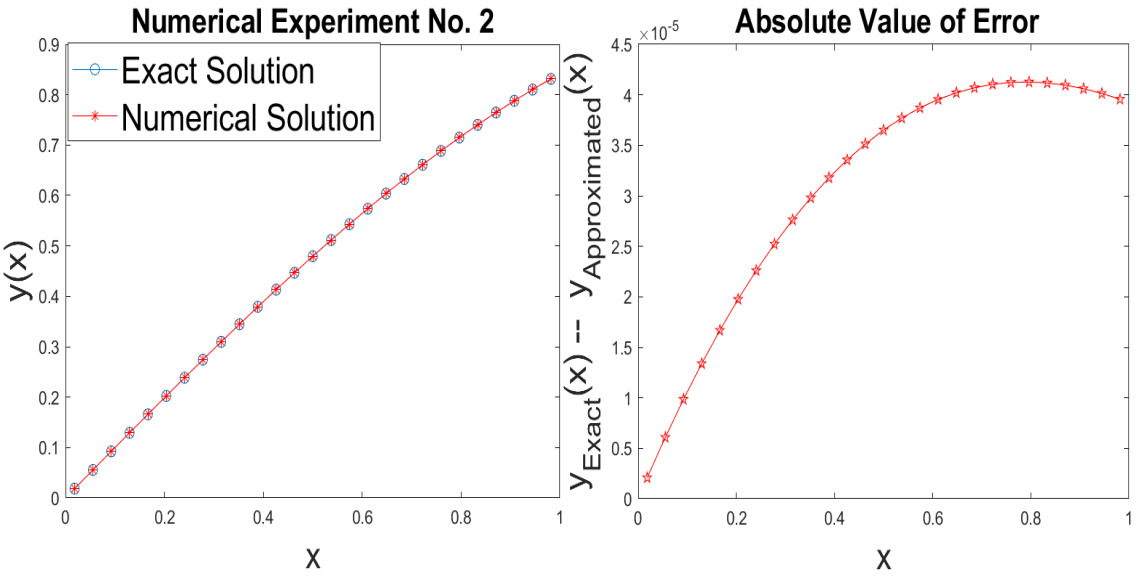

Figure 3. Graphical Representation of the Exact Solution and the Numerical Solution

DOI:https//doi.org/10.22452/mjs.vol43no1.5
Malaysian Journal of Science 43(1): 44-58 (March 2024)

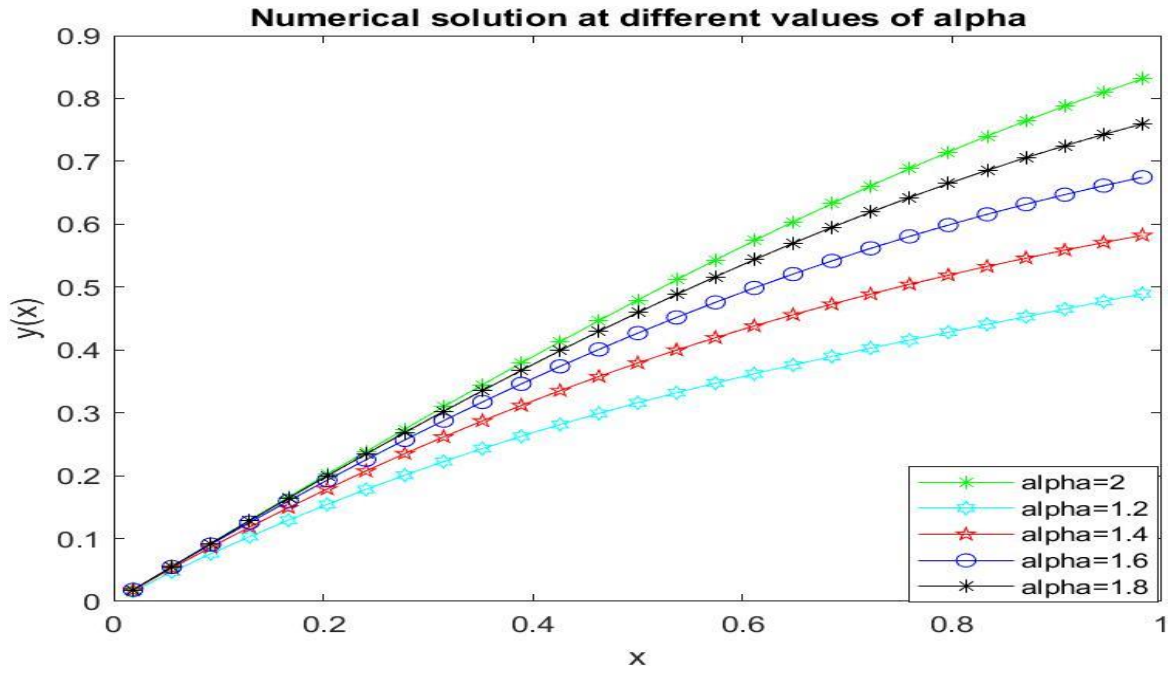

Figure 4. Graphical Representation of Numerical Solution for Different Values of α Lies Between 1 and 2. At *j = 2* Resolution Level

Numerical Experiment No. 3: Non-linear Oscillator Ordinary Differential Equation

$$D^{\alpha}y(x) + (y')^2(x) - y(x) + y^2(x) - 1 = 0, \quad 1 < \alpha \leq 2 \qquad (24)$$

With the initial condition y (0) = 2, $y'(0) = 0$
The value of the exact solution at $\alpha = 2$ given as,

y(x)=1+cos(x)

Solution:
Applying the Quasilinearisation technique to equation (24) and the equation becomes
$D^{\alpha}y_{s+1}(x) + 2y_s'(x)y_{s+1}'(x) - (1 - 2y_s(x))y_{s+1}(x) = y_s^2(x) + (y'_s)^2(x) + 1$ (25)
With the initial conditions $y_{s+1}(0) = 0, y_s'(0) = 0,$

We applied HS3WM to (24), and we approximated the term that contains the highest derivatives by Haar wavelet series as follows:

$$D^{\alpha}y_{s+1}(x) = \sum_{l=1}^{3M} c_l h_l(x) \qquad (26)$$

On integrating the above equation (26), we obtained the lower derivatives, and by using the initial condition, we have

$$y_{s+1}(x) = \sum_{l=1}^{3M} c_l P_{\alpha,l}(x) + 2 \qquad (27)$$

$$y'_{s+1}(x) = \sum_{l=1}^{3M} c_l P_{\alpha-1,l}(x) \qquad (28)$$

Now, substituting equations (26), (27), and (25) in equation (24), we get

$\sum_{l=1}^{3M} c_l[h_l(x) + 2y_s'(x)\, P_{\alpha-1,l}(x) - (1 - 2y_s'(x))\, P_{\alpha,l}(x)] =$ $y_s^2(x) + y_s'^2(x) + 2(1 - 2y_s(x)) + 1$ (29)

With initial conditions $y_0(x) = 0, y_0'(x) = 0$

DOI:https//doi.org/10.22452/mjs.vol43no1.5
Malaysian Journal of Science 43(1): 44-58 (March 2024)

For α = 2, we assigned the differential order to equation 25 and at J = 2 resolution level. Tables 5 and 6 show the comparative study of the exact and approximate solutions as well as the values of errors, respectively, derived using the Haar scale-3 wavelet technique, and graphical results are shown in Figure 5. The absolute inaccuracy decreases as the number of iterations increases. At a constant level of resolution, the exact solution at α = 1 and the Haar wavelet solutions at various $\alpha's$ are shown in Figure 6.

Table 5. Comparison of Exact Value and Approximate Value at Different Values of *x*. Discussion of Absolute Error by Scale-3 Haar Wavelets with Haar Scale Wavelets.

x	Exact Value	Approx Value	Saeed 2013	Absolute Error by HS3WM
0.1	1.995004165	1.995004166	1.995004166	3.734e-06
0.2	1.980066578	1.980066579	1.980066581	1.568e-05
0.3	1.955336489	1.955336492	1.955336496	3.958e-05
0.4	1.921060994	1.921060999	1.921061007	7.543e-05
0.5	1.877582562	1.877582576	1.877582583	1.232e-04
0.6	1.825335615	1.825335628	1.825335647	1.830e-04
0.7	1.764842187	1.764842204	1.764842233	2.547e-04
0.8	1.696706709	1.696706740	1.696706772	3.384e-04
0.9	1.621609968	1.621609998	1.621601051	4.341e-04

Table 6. Comparison of Values of the Error Scale-3 Haar Wavelet at Different Levels of Resolution.

Level of resolution	J=2	J=3	J=4
HSWM3 $L_2 error$	8.69048147e-06	9.66118381e-07	1.07352784e-07
HSWM3 $L_\infty error$	3.71196461e-05	4.25861607e-06	4.78242174e-07

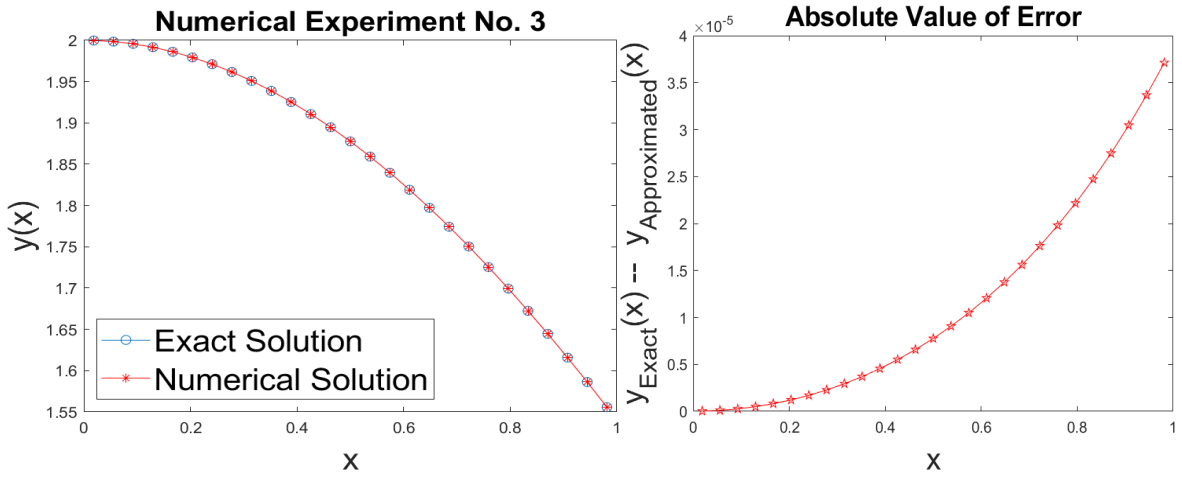

Figure 5. Graphical Representation of the Exact Solution and the Numerical Solution

DOI:https//doi.org/10.22452/mjs.vol43no1.5
Malaysian Journal of Science 43(1): 44-58 (March 2024)

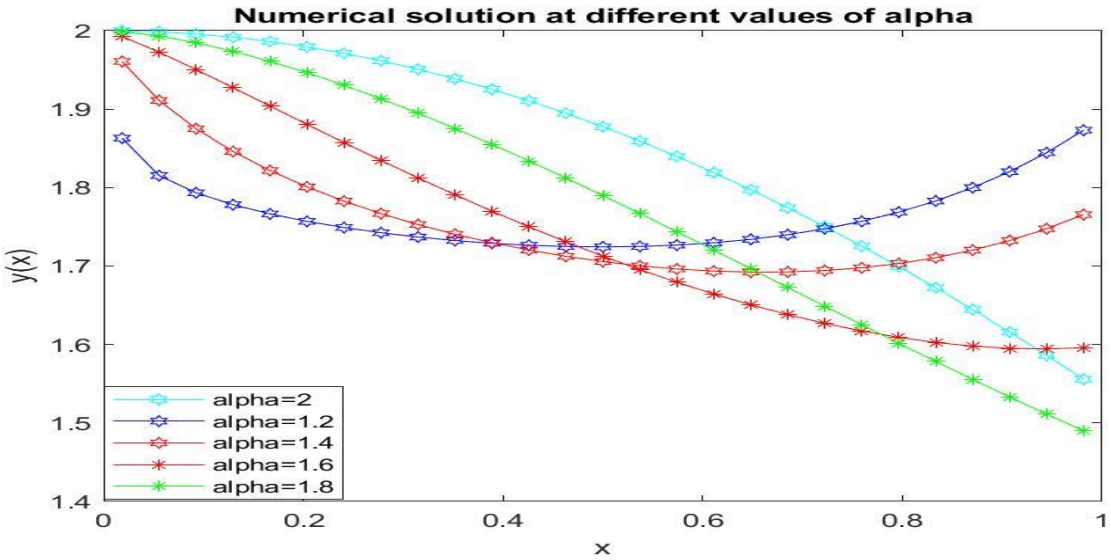

Figure 6. Graphical Representation of the Numerical Solution for Different Values of α Lies Between 1 and 2. At j = 2 Resolution Level.

Numerical Experiment No. 4: Composite Fractional Oscillation Equation

$$D^{\alpha}y(x) + y(x) = f(x), 0 < \alpha < 1 \qquad (30)$$

With initial condition $y(0) = 0$, where $f(x) = x^2 + \frac{2x^{2-\alpha}}{\Gamma(3-\alpha)}$ (31)

For $\alpha = 1$, the exact solution of the equation is y(x)=x^2

Solution:

We applied the Haar scale-3 method to (30), and we estimated the advanced derivatives term by Haar wavelet series as follows:

$$D^{\alpha}y(x) = \sum_{l=1}^{3M} c_l h_l(x) \qquad (32)$$

On integrating the above equation (32), we obtained the lower derivatives, and by using the initial condition, we have

$$y(x) = \sum_{l=1}^{3M} c_l P_{\alpha,l}(x) \qquad (33)$$

now using equations (33) and (32) in equation (30).

$$\sum_{l=1}^{3M} c_l[h_l(x) + P_{\alpha,l}(x)] = x^2 + \frac{2x^{2-\alpha}}{\Gamma(3-\alpha)} \qquad (34)$$

We assigned the differential order to equation 30 for α = 1 and the level of resolution to J = 2. Table 7 depicts the absolute error at α = 1 and other fractional values of alpha, and Table 8 presents the value of L_2 and L_∞ error at different values of J. Here, Figure 7 depicts the exact and approximate solutions obtained using the HS3WM approach. With more iterations, the absolute error decreases. The precise solution at α = 1 and the Haar wavelet solution at distinct $\alpha's$ are represented in Figure 8.

DOI:https//doi.org/10.22452/mjs.vol43no1.5
Malaysian Journal of Science 43(1): 44-58 (March 2024)

Table 7. Comparison of Exact Value and Approximate Value at Different Values of *x*. Discussion of Absolute Error by Scale-3 Haar Wavelet with Haar Scale Wavelets at Different Values of α

x	Exact Value $\alpha = 1$	Approx. Value $\alpha = 1$	Absolute error at $\alpha = 1$	Absolute Error by HS3WM $(\alpha = 0.25)$	Shah 2017	$(\alpha = 0.50)$	Shah 2017
0.1	0.01	0.0101	3.012e-04	4.225e-06	9.000e-03	4.1904e-06	4.000e-03
0.2	0.04	0.0414	2.797e-04	4.105e-06	8.000e-03	4.3903e-06	5.000e-03
0.3	0.09	0.0914	2.503e-04	4.004e-06	4.000e-03	4.0882e-06	1.000e-03
0.4	0.16	0.1609	2.224e-04	3.939e-06	2.800e-03	3.9885e-06	8.000e-03
0.5	0.25	0.2500	2.085e-04	3.875e-06	6.300e-03	3.9234e-06	2.300e-03
0.6	0.36	0.3634	1.816e-04	3.843e-06	3.200e-03	3.8435e-06	6.000e-03
0.7	0.49	0.4923	1.665e-04	3.812e-06	2.000e-03	1.6807e-06	7.000e-03
0.8	0.64	0.6406	1.490e-04	4.088e-06	9.000e-03	1.5997e-06	0.000
0.9	0.81	0.8159	1.384e-04	3.796e-06	5.200e-03	1.7160e-06	1.400e-03

Table 8. Comparison of the Value of Error of HS3WM at Different Levels of Resolution

Level of resolution	J=2	J=3	J=4
HS3WM $L_2 error$	5.0450146e-04	5.602634e-05	6.2247865e-06
HS3WM $L_\infty error$	3.3670033e-04	3.787018e-05	4.2250783e-06

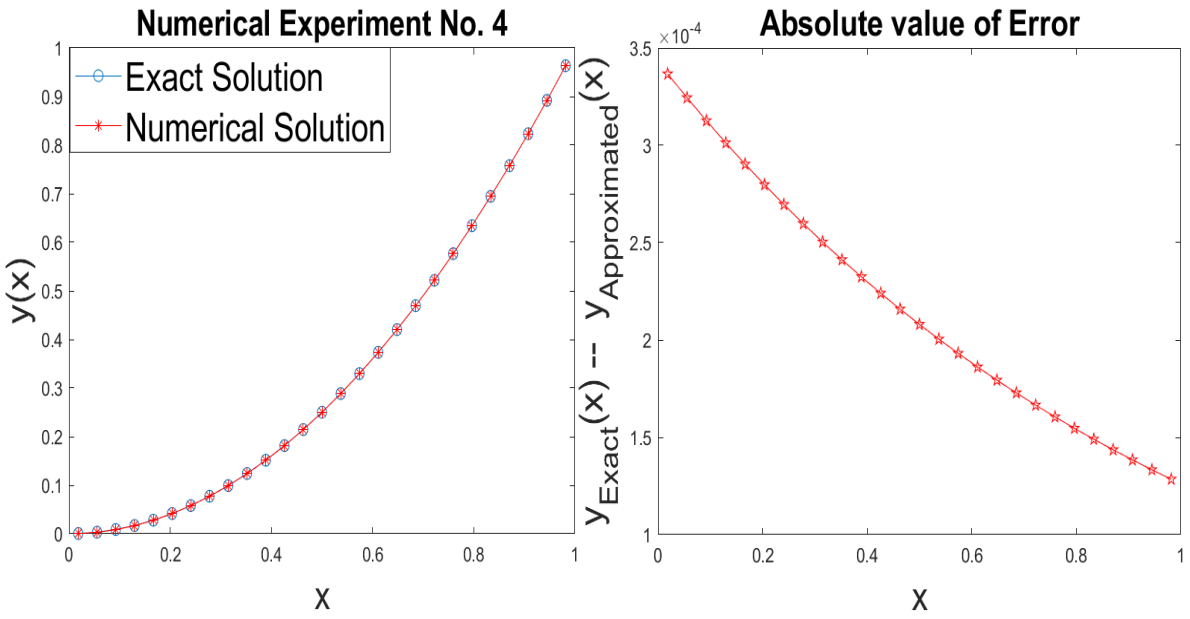

Figure 7. Graphical Representation of Exact Solutions and Numerical Solutions

DOI:https//doi.org/10.22452/mjs.vol43no1.5
Malaysian Journal of Science 43(1): 44-58 (March 2024)

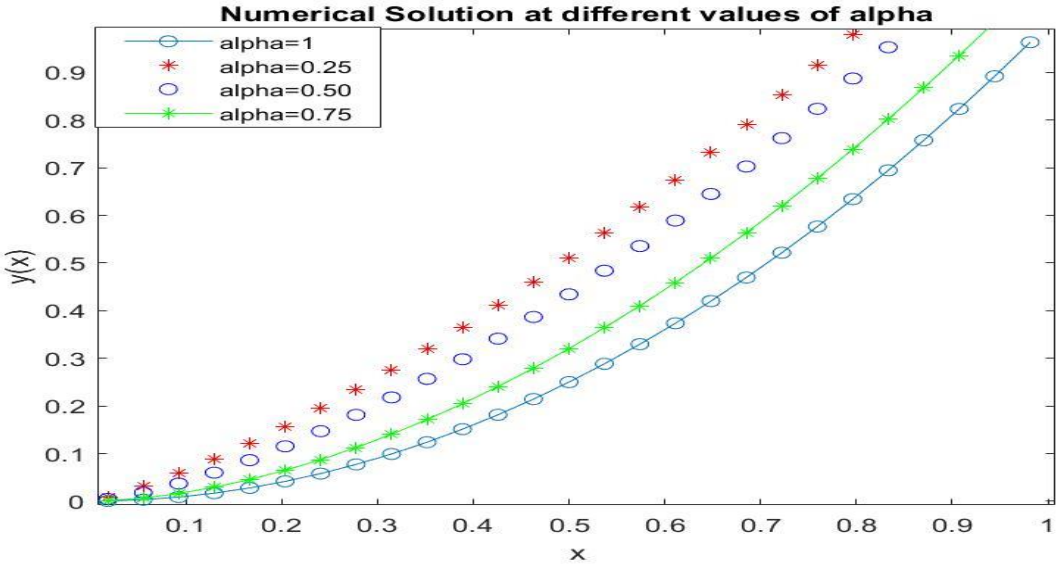

Figure 8. Graphical Representation of Numerical Solution for Different Values of α Lies Between 0 and 1. At *j = 2* Resolution Level.

Numerical Experiment No. 5: Fractional Relaxation-Oscillation Equation

$$\boldsymbol{D^{\alpha}y(x) + y(x) = f(x), 0 < \alpha < 1} \qquad (35)$$

With initial conditions y (0) = 0.

Here,

$$f(x)=1-4x+5x^2-\frac{4}{\Gamma(2-\alpha)}x^{1-2\alpha}+\frac{10}{\Gamma(3-\alpha)}x^{2-\alpha} \qquad (36)$$

for $\alpha = 1$, the exact solution of the given equation is $y(x) = 1-4x+5x^2$

Solution:
We applied HS3WM to (35) and approximated the term that has derivatives by Haar wavelet series as follows:

$$D^{\alpha}y(x) = \sum_{l=1}^{3M} c_l h_l(x) \qquad (37)$$

On integrating the above equation (37), we obtained the lower derivatives, and by using the initial condition, we have

$$y(x) = \sum_{l=1}^{3M} c_l P_{\alpha,l}(x) \qquad (38)$$

now using equations (37) and (38) in equation (35).

$$\sum_{l=1}^{3M} c_l[h_l(x) + P_{\alpha,l}(x)] = 1 - 4x + 5x^2 - \frac{4}{\Gamma(2-\alpha)}x^{1-2\alpha} + \frac{10}{\Gamma(3-\alpha)}x^{2-\alpha}$$

We assigned the differential order to equation 35 for α = 1 and the level of resolution to J = 2. Table 9 depicts the absolute error at α = 1 and other fractional values of alpha, and Table 10 presents the value of L_2 and L_∞ error at different values of J. Here, Figure 7 depicts the exact and approximate solutions obtained using the HS3WM approach. With more iterations, the absolute error decreases. The precise solution at α = 1 and the Haar wavelet solution at distinct $\alpha's$ are represented in Figure 8.

DOI:https//doi.org/10.22452/mjs.vol43no1.5
Malaysian Journal of Science 43(1): 44-58 (March 2024)

Table 9. Comparison of Exact Value and Approximate Value at Different Values of *x*. Discussion of Absolute Error by Scale-3 Haar Wavelet with Haar Scale Wavelets at Different Values of α.

x	Exact Value $\alpha = 1$	Approximate Value $\alpha = 1$	Absolute error at $\alpha = 1$	Absolute Error by HS3WM. $(\alpha = 0.25)$	Shah 2017	Absolute Error by HS3WM $(\alpha = 0.50)$	Shah 2017
0.1	0.6500	0.6475	1.506e-03	2.1038e-05	8.000e-03	2.0525e-05	2.300e-03
0.2	0.4000	0.4058	1.399e-03	2.0441e-05	1.700e-03	1.4646e-05	3.000e-03
0.3	0.2500	0.2500	1.252e-03	1.9942e-05	2.000e-03	1.3941e-05	1.000e-03
0.4	0.2000	0.2006	1.121e-03	1.9536e-05	3.100e-03	1.3601e-05	2.200e-03
0.5	0.2500	0.2542	1.040e-03	1.5579e-05	1.210e-03	1.1873e-05	6.800e-03
0.6	0.4000	0.4142	9.314e-04	1.5199e-05	8.400e-03	1.0238e-05	2.200e-03
0.7	0.6500	0.6599	8.333e-04	9.1999e-04	6.000e-03	1.0017e-05	2.600e-03
0.8	1.0000	1.0016	7.456e-04	8.9387e-04	2.700e-03	9.5078e-05	0.0000
0.9	1.4500	1.4665	6.678e-04	7.8681e-04	1.720e-03	1.9536e-05	5.300e-03

Table 10. Comparison of Value of Error of Scale-2 and Scale-3 Haar Wavelets at Different Levels of Resolution.

Level of resolution	J=2	J=3	J=4
HSWM3 $L_2 error$	1.382717e-03	1.53448107e-04	1.704744e-05
HSWM3 $L_\infty error$	1.683501e-03	1.89350905e-04	2.112539e-05

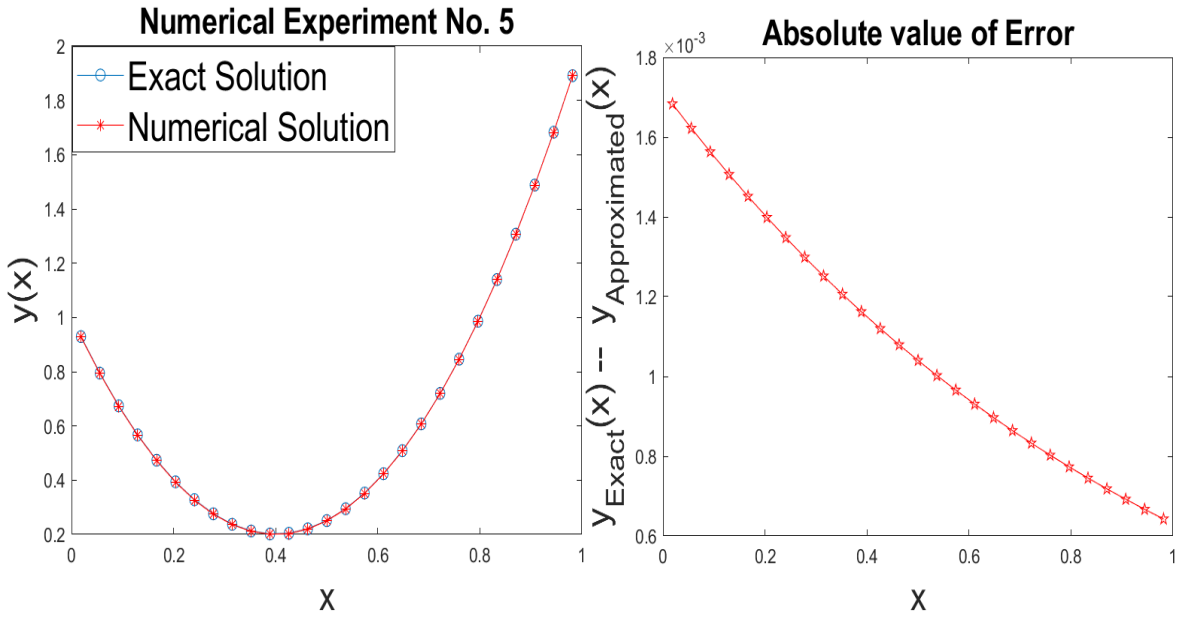

Figure 9. Graphical Representation of Exact Solutions and Numerical Solutions

DOI:https//doi.org/10.22452/mjs.vol43no1.5
Malaysian Journal of Science 43(1): 44-58 (March 2024)

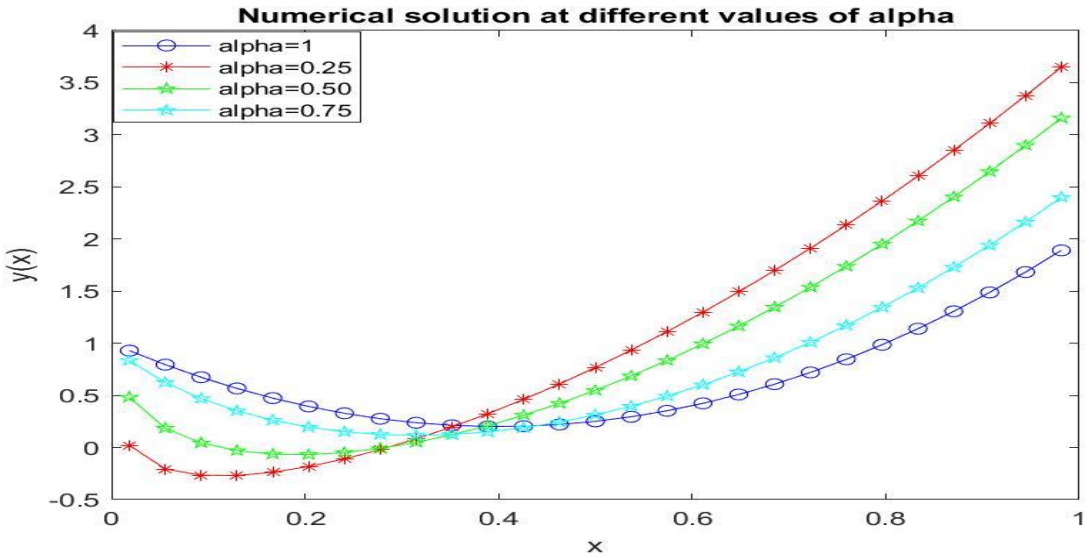

Figure 10. Graphical Representation of Numerical Solution for Different Values of α Lies Between 0 and 1. At $j = 2$ Resolution Level.

6. Conclusions and Results

The Haar scale-3 wavelet operational matrix of fractional order integration is used to solve fractional differential equations numerically in this article. This proposed method has been used to analyse both linear and non-linear problems with success. The study found that the applied technique is less complicated and more convergent than others. The proposed method is used to discuss numerical problems of this kind with reliability. Furthermore, the approaches for error analysis are thoroughly examined with the help of MATLAB, which shows good agreement of the numerical solution with the exact solution and other solutions existing in the literature. Through our study, we conclude that in the future, the proposed method could be applied to many fractional differential equations to generate more precise findings or to equations that have higher-order fractional derivatives.

7. Acknowledgement

The authors of this manuscript greatly appreciate the support provided by the Department of Mathematics, School of Chemical Engineering and Physical Sciences, Lovely Professional University, while writing this paper

8. Referencences

Almeida, R., & Bastos, N. R. O. (2016). A numerical method to solve higher-order fractional differential equations. *Mediterranean Journal of Mathematics*, *13*(3), 1339–1352.

Amin, R., Shah, K., Asif, M., Khan, I., & Ullah, F. (2021). An efficient algorithm for numerical solution of fractional integrodifferential equations via Haar wavelet. *Journal of Computational and Applied Mathematics*, *381*, 113028.

Arora, G., Kumar, R., & Kaur, H. (2020). Scale-3 Haar wavelet and Quasi-linearisation based hybrid technique for solution of coupled space-time fractional-Burgers' equation. *Pertanika Journal of Science & Technology*, *28*(2), 579–607.

Baleanu, D., & Shiri, B. (2018). Collocation methods for fractional differential equations involving non-singular kernel. *Chaos, Soliton & Fractals*, *116*, 136–145.

Chen, Y., Yi, M., & Yu, C. (2012). Error analysis for numerical solution of fractional differential equation by Haar wavelets method. *Journal of Computational Science*, *3*(5), 367–373.

Das, S. (2011). *Functional fractional calculus*. Springer.

Gowrisankar, A., & Uthayakumar, R. (2016). Fractional calculus on fractal interpolation for a sequence of data with countable iterated function system. *Mediterranean Journal of Mathematics*, *13*(6), 3887–3906.

Kobra, R., & Mohsen, R. (2021). Fractional-order Boubaker wavelets method for solving fractional Riccati differential equations. *Applied Numerical Mathematics*, *168*, 221–234.

Kumar, R., & Bakhtawar, S. (2022). An improved algorithm based on Haar scale 3 wavelets for the numerical solution of Integro-differential equations. *Mathematics in Engineering, Science & Aerospace (MESA)*, *13*(2), 617–633.

Kumar, R., & Gupta, J. (2022). Numerical analysis of linear and non-linear dispersive equation using Haar scale-3 wavelet. *Mathematics in Engineering, Science & Aerospace (MESA)*, *13*(4), 993–1006.

Li, C., & Zeng, F. (2015). *Numerical methods for fractional calculus*. Chapman & Hall/CRC.

DOI:https//doi.org/10.22452/mjs.vol43no1.5
Malaysian Journal of Science 43(1): 44-58 (March 2024)

Miller, K. S., & Ross, B. (1993). *An introduction to the fractional calculus and fractional differential equations*. Wiley.

Mittal, R. C., & Pandit, S. (2018a). New scale-3 Haar wavelets algorithm for numerical simulation of second order ordinary differential equations. *Proceedings of the National Academy of Sciences, India Section A: PhysicalSciences*, *89*(4), 799–808.

Mittal, R. C., & Pandit, S. (2018b). Quasi-linearized scale-3 Haar wavelets-based algorithm for numerical simulation of fractional dynamical systems. *Engineering Computations (Swansea, Wales)*, *35*(5), 1907–1931.

Odibat, Z., & Momani, S. (2008). Modified homotopy perturbation method: Application to quadratic Riccati differential equation of fractional order. *Chaos, Solitons & Fractals*, *36*(1), 167–174.

Oldham, K. B., & Spanier, J. (1974). *The fractional calculus: Theory and applications of differentiation and integration to arbitrary order*. Academic Press.

Podlubny, I. (1999). *Fractional differential equations*. Academic Press.

Saeed, U., & Rehman, M. U. (2013). Haar wavelet–Quasi-linearization technique for fractional nonlinear differential equations. *Applied Mathematics and Computation*, *220*, 630–648.

Shah, F. A., Abass, R., & Debnath, L. (2017). Numerical solution offractional differential equations using Haar wavelet operational matrix method. *International Journal of Applied and Computational Mathematics*, *3* (3), 2423–2445.

Shah, K., Khan, Z. A., Ali, A., Amin, R., Khan, H., and Khan, A. (2022). Haar wavelet collocation approach for the solution of fractional order COVID-19 model using Caputo derivative. *Alexandria Engineering Journal*, *59*(5), 3221–3231.

Shiralashetti, S. C., & Deshi, A. B. (2016). Haar wavelet collocation method for solving Riccati and fractional Riccati differential equations. *Bulletin of Mathematical Sciences and Applications*, *17*, 46–56.

Su, H., Chen, W., Li, C., & Chen, Y. (2012). Finite difference schemes for variable-order time fractional diffusion equation. *International Journal of Bifurcation and Chaos in Applied Sciences and Engineering*, *22*(04), 1250–1085.

DOI:https//doi.org/10.22452/mjs.vol43no1.5
Malaysian Journal of Science 43(1): 44-58 (March 2024)

MALAYSIAN JOURNAL OF SCIENCE
MJS
ISSN 1394-3065

Regular Issue

Malaysian Journal of Science 43(1): 59-71 (March 2024) https://mjs.um.edu.my

INVESTIGATE THE PROPERTIES OF DIFFERENT IRRADIATED STARCH BIOPLASTIC FOR PACKAGING APPLICATION

Nurin Najwa Rohidi[1a] and Siti Amira Othman[2a]*

Abstract: Plastics have become the preferred materials for use due to their barrier properties and strength. This study aimed to determine the wettability, contact angle, and polymer chemical properties by comparing pure and mixed starch bioplastics with different plasticizers. Gamma radiation and electron beams are used in industrial applications. Gamma radiation is used because it is extreme in penetration, and Cobalt-60 is often used for sterilization. Most bioplastics with citric acid as the plasticizer produced a high contact angle and achieved hydrophobicity. Materials used in constant amounts are distilled water and glycerol. Others manipulate variables based on the presence of starch, such as corn, potato, rice, or a mixture of the two starches. The Samples were characterized using tensile and elongation tests, water contact angle, Fourier Transform Infrared (FTIR) analysis, topography using Atomic Force Microscopy (AFM), moisture content tests, and biodegradability tests. Potato and corn-rice bioplastics have low moisture contents. Meanwhile, the corn bioplastic degraded faster at 80.17%. Potato rice with citric acid lead tensile test with 4.095 MPa. However, potatoes with sorbitol lead with 34.57% for the elongation case. FTIR analysis identified the functional groups of the normal polymeric OH and C-H stretching of the methylene group at wavenumbers of 3280–3300 cm^{-1} and 2920–2935 cm^{-1}, respectively. According to FTIR analysis, corn rice with the presence of citric acid bioplastic was chosen to undergo AFM to survey roughness in case to determine whether crosslinking might happen; the different average roughness between pre-irradiated and post-irradiated samples is 8.82 nm. Based on these findings, bioplastics may contribute tremendous benefits, especially in smart packaging applications.

Keywords: *Waterproof, irradiated, packaging, bioplastic, cobalt-60*

1. Introduction

Plastics are everywhere, including the market, ocean, streets, and in the body. None degrade well because the plastic compounds are hard to break down. Plastics have become popular due to their barrier properties and strengths. We can obtain them anywhere; they are cheap, resistant to water, and flexible. Currently, polymers can be molded into various shapes. Most people are obsessed with plastic, and the beloved planet becomes dirty and unorganized, negatively affecting lands, waterways, and the ocean. This is because plastics have been used for more than 50 years. It was created in the late 19th and early 20th centuries. Besides, plastic bombing occurred during World War II (Clunies-Ross, 2019).

Carbon emissions cause environmental issues during manufacturing because they cause harm rather than positive effects. An estimated 33 billion tons of plastic are produced annually due to the increasing rate of plastic production. Single-use plastics accounted for approximately one-third of the total plastic production in 2018, with an estimated 359 million tones. Many efforts have been made to reduce the amount of plastics, but they have not been successful, including the 3R program, reduction, reuse, and recycling. This affects but not on a large scale. Thus, bioplastics are created to educate people about making better choices to save the earth.

Many people are unfamiliar with bioplastic production, but only a few have used it in their lives. Bioplastics are now widely known in society and their awareness has occasionally increased. Therefore, biodegradable materials are preferred to overcome fossil fuel consumption and plastic accumulation (Tokiwa et al., 2009). Natural polymers are more environmentally friendly and easy to dispose of (Marichelvam et al., 2019). Their chemical and physical properties must meet the ideal characterization to construct a beautiful structure to evaluate the biodegradability of solid polymers. The term “bioplastic” can be confusing because some petroleum-based plastic also degrades or bio-based plastic, which is synthesized from biomass or renewable sources. Some bio-based plastics, like Nylon 11, has been produced as non-biodegradable. Unlike acetyl cellulose, biodegradability refers to the degree of acetylation.

However, fossil fuel is at an endangered level. Hence, plastics synthesized from biomass are preferable. Bioplastics have many kinds because the molecules can be carbohydrate-based or fat and oil-based polymers to reduce dependency on fossil fuels. However, carbohydrate-based polymers are the most popular because they are derived from starch, cellulose, lactic acid, lactide, polyhydroxyalkanoates, and chitosan, which are easier to obtain, especially starch-based polymers because they are the

Authors information:
[a]Department of Physics and Chemistry, Faculty of Applied Sciences and Technology, Universiti Tun Hussein Onn Malaysia, Pagoh, Johor, MALAYSIA. E-mail: sitiamira@uthm.edu.my[2]
*Corresponding Author: sitiamira@uthm.edu.my

Received: February 26, 2023
Accepted: March 15, 2023
Published: March 31, 2024

DOI:https//doi.org/ 10.22452/mjs.vol43no1.6
Malaysian Journal of Science 43(1): 59-71 (March 2024)

cheapest among others. Bioplastics are growing in market niches, such as packaging, agriculture, and automotive parts due to cost and trends (Aranda-Garcia et al., 2015).

Domestic and municipal composting are the preferred end-of-life disposal options for these materials (Mostafa et al., 2018) instead of landfills, which is the worst disposal option. Starch and water cannot compete with polyethylene (PE) or polypropylene (PP). Therefore, plasticizers must be added to enhance the water barrier and mechanical strength. Plasticizers, such as glycerol, sorbitol, citric acid, and beeswax (Byun et al., 2014), have been tested in several studies to reduce water permeability. However, not all studies will derive the same result because each plasticizer has weaknesses. Therefore, the wettability of bioplastics must be determined by studying their moisture content and water contact angle.

When it comes to radiation exposure to products, people make a fuss, and myths about the products emerge over time. People fear ionizing radiation because it involves radioactive substances or handling equipment. Most people believe that radiation exposure is equivalent to death. Many studies have been conducted on handling and using radiation as a progress to produce a product. A few incidents show how evil radiation can be, but scientists were more careful after that incident, and standard operations and policies were enhanced to ensure that workers faced less health risks. The incident became a story that served as a reminder to prioritize safety. "The benefits hidden behind a negative image are finally revealed."

Packaging material is widely used in markets, industries, and households. Over 67 million tons of packaging have been reported (Maulida et al., 2016), leading to severe environmental complications. In a landfill, the dumps of packaging material increase yearly as online shopping becomes a trend among shoppers. This results in a poor situation because most packaging is polymer-based and degrades poorly. Some studies have started to apply bioplastic in the packaging sector, but due to its short-term shelf-life nature, it does not spread well, especially when dealing with water resistance. Many studies have been conducted on handling and using radiation as a progress to produce a product. A few packaging materials are listed in Title 21 of the Code of Federal Regulations (CFR) (Paquette et al., 2004) and irradiated under regulation 179.45(d) with a maximum dose of 60 kGy. This shows that packaging material has already been introduced to radiation for years.

Bioplastics have many properties that must be enhanced to achieve a good packaging standard and can replace petroleum-based plastics in the future. Environmentally friendly materials have a shorter shelf life, as they degrade faster than petroleum-based plastics, removing carbon dioxide, methane, water, wood, humic matter, and other natural substances (Ibrahim et al., 2017). Starch-based bioplastics are mixtures of amylose/amylopectin ratios, depending on their botanic origin (Jiang et al., 2017). Starch may have many weaknesses, and plasticizers help maintain their chemical and physical robustness. Since bioplastic's biodegradability is faster than petroleum-based plastics, their lifelong has been questioned many times. They can be an excellent choice for degradation, but wearing them for a long time is not recommended.

Barrier properties have focused on providing an effective and cost-effective packaging system and maximizing the shelf life of packaged foods and beverages. Hydrophobicity mostly depends on the material used or the concentration of the material. Bioplastics must achieve a level where they can be picked as desired products. Bioplastics production must beat petroleum-based plastic standards because, through composition, all these biomaterials are hydrophilic but quite crystalline, messing things up, specifically regarding the packaging of wet products. For decades, many studies have experimented with radiation toward polymers. The radiation process is difficult because it can cause significant damage and may break the bonds of the plasticizer and other compounds as the polymer chains are broken and/or cross-linked, allowing the mechanical, thermal, and physicochemical properties to change if exposure over the limit of the substance can be handled (Zygoura et al., 2011).

In this study, mixed- and pure-starch bioplastics were compared. Rice, potato, and corn starches were used to produce the samples. Examples of mixed starches include potato rice, corn rice, and corn potato. Additional materials, including glycerol and distilled water, were used at a constant weight. Plasticizers such as sorbitol and citric acid were compared to analyze their wettability and mechanical properties. Then, bioplastic samples undergo a characterization test and irradiation treatment effect test.

The wettability of the samples under characterization can be determined by measuring the contact angle with a sessile drop and studying their moisture content. Fourier Transform Infrared (FTIR) spectroscopy was used to determine the polymer behavior and molecule concentration to compare pre- and post-irradiation bioplastic samples. Pure and mixed starch morphology were compared to common plastic using atomic force microscopy (AFM). Gamma radiation was used to irradiate samples at doses ranging from 0.5 kGy to 2.5 kGy.

2. Methodology

Chemicals

In this study, 5 g of corn flour, 5 g of rice flour, and 5 g of potato flour were combined to prepare a bioplastic. However, 1.5 g of glycerol, 1 g of sorbitol, 0.3 g of starch, 0.5 g of citric acid, and 1 mL of distilled water were mixed with each type of bioplastics. Low-density polyethylene (LDPE) plastic was used for comparison. All the chemicals were purchased from Emory.

DOI:https//doi.org/ 10.22452/mjs.vol43no1.6
Malaysian Journal of Science 43(1): 59-71 (March 2024)

Table 1. Abbreviations used for Bioplastics with Different Types of Plasticizers

Types of Bioplastics	Types of Plasticizers	Sorbitol	Citric acid (CA)
Starch (S)	Corn (C)	CS	CCA
	Rice (R)	RS	RCA
	Potato (P)	PS	PCA
	Corn-Potato (CP)	CPS	CPCA
	Corn-Rice (CR)	CRS	CRCA
	Potato-Rice (PR)	PRS	PRCA

Sample Preparations

Different solution mixtures were stirred until the starches achieved the gelatinization phase, and the solution's liquid consistency turned from watery to a thick gel. The temperature was regularly checked to prevent overheating of the molecular mixtures, as it might decrease the function or properties of the bioplastics. When the solutions thickened, it was poured into the proper mold. The solution was dried for three–four days before turning into the solid phase. Bioplastic films were made in several pieces for characterization tests. LDPE and bioplastic pieces were produced for tensile strength testing. All plastics were exposed to five doses of gamma radiation: 0.5, 1.0, 1.5, 2.0, and 2.5 kGy. Afterward, all the post-irradiated sample conditions were compared to the pre-irradiated sample conditions with water contact angle reading and Fourier-Transform Infrared (FTIR) spectroscopy.

Sample Characterizations Water Contact Angle

Hydrophilicity has become a problem for bioplastic production. The bioplastic hydrophilicity was determined by measuring the wettability of the bioplastic surface. The contact angle is the most sensitive surface analytical technique because wettability is influenced by the top of the surface nanometer. The contact angle was determined by checking the intersection angle. The test was run in a temperature- and humidity-controlled room to reduce random errors when reading was performed. Moreover, sessile droplets were used to interact with polymer molecules. The contact angle test was performed using Video Contact Angle (VCA) optima.

Moisture Content Test

This test has a similar goal to the water contact angle test. However, in this case, glycerol played a significant role in determining the moisture content percentage, which was obtained using the following equation:

$$\text{Moisture Content} = \frac{(W_1 - W_2)}{W_1} \text{x} 100 \quad (1)$$

with W_1 = initial weight before drying, W_2 = final weight after drying

W_2 can be obtained by drying the bioplastic sample at 100C - 110 ^{o}C in an oven to obtain a fixed reading as the final weight.

Biodegradability Test

The soil burial method was chosen to consider landfill conditions for at least 15 days, and the time could be lengthened if necessary. The weight loss percentage was calculated using the following formula:

$$\text{Weight loss percentage} = \frac{(W_0 - W)}{W_0} \text{x} 100 \quad (2)$$

with W_0 = weight of the sample before burial , W = weight of sample after burial.

The samples were buried for 15 days before being weighed. The biodegradability test was conducted in a plastic bag to avoid confusion with other foreign materials. Each bag was filled with approximately 300 g of soil, and the sample was buried deeply to ensure that the soil covered the sample. Each sample had its bag and was labeled with stickers.

Tensile Strength Test

All samples were set to the same length and height. All samples were placed vertically, with a tensile grip probe gripping both ends and measuring 1 cm wide and 7 cm long. A texture analyzer (Stable Micro System machine) was used for the assisted tensile strength test. Fixed parameters for the test were chosen under the packaging film standard test, with a test speed of 60 mm/min and tension mode.

FTIR Spectroscopy

FTIR spectroscopy is an analytical machine to ease the research journey. FTIR is well known for characterization analysis due to its accuracy and sensitivity by affecting atomic vibration with infrared radiations. There are several wavenumber divisions: far, mid, and near spectra. However, the mid-region of the wavenumber was used to analyze the samples because this spectrum region was divided into four more categories: single bond ranging from 2500 to 4000 cm^{-1}, triple bond ranging from 2000 to 2500 cm^{-1}, double bond labeled ranging from 1500 cm^{-1} to 2000 cm^{-1}, and fingerprint ranging from 600 cm^{-1} to 1500 cm^{-1}. Approximately 1 g of different types of bioplastics were prepared for FTIR characterization.

AFM

AFM was used to determine the roughness of sample surfaces. A laser beam was produced to light behind the cantilever and was reflected towards the photodiode. There are three modes: contact, tapping, and lateral. This experiment was performed in tapping mode, where the contact between the tip and samples is discontinuous due to the sensitive sample surface. Moreover, tip contamination may result in a convex fold related to the contaminant size relative to the surface size features to be measured.

DOI:https//doi.org/ 10.22452/mjs.vol43no1.6
Malaysian Journal of Science 43(1): 59-71 (March 2024)

Gamma Irradiation Treatment

In this study, gamma and ultraviolet (UV) irradiation treatments were used to apply to the samples. However, a photosensitizer was required to complete the UV irradiation treatment process because it was feared that increasing the barrier properties would cause the sample to become completely hydrophobic. Therefore, gamma radiation was used in this study. The samples were treated with five doses of 0.5, 1.0, 1.5, 2.0, and 2.5 kGy.

3. Results and Discussion

Water Contact Angle

LDPE is the control sample, showing 97.70° for the contact angle and 99.60° for the right after irradiation; it decreased to 96.40° for the left and 95.30° for the right. Irradiation treatment can degrade and reduce the contact angle in the presence of free radicals (Gorna *et al*., 2003). Crosslinking may occur in some samples as the contact angle values increase. However, it maintained a hydrophobic state after losing 1°. For sorbitol in pure starch, the contact angle for the pre-irradiated potato bioplastic was 0°; however, after irradiation treatment, it increased to 49.40° for the left and 56.10° for the right. The same applies to the corn bioplastic case, where the contact angle increased. After treatment, the rice bioplastics experienced much lower contact angles of 13.30° on the left and 17.60° on the right. Unlike when citric acid is involved, all pure starch bioplastics do not experience a significant difference after treatment. Corn-potato bioplastic reading angles were unique in the mixed bioplastic cases because when sorbitol was present, the contact angle decreased, whereas citric acid produced the opposite result. It increases from approximately 30° to 60°. Simultaneously, the corn-rice bioplastic contact angle differed significantly before and after irradiation, starting at approximately 30° and becoming hydrophobic at approximately 106°.

Plasticizers in bioplastics help reduce brittleness/fragility and increase flexibility in films, making them simpler to handle and prevent cracks and pores. Plasticizers are classified into two types, hydrophilic and hydrophobic, based on their chemical properties. When hydrophilic plasticizers are applied to bioplastics at greater concentrations, they can lead to increased water diffusion in the plastic. Hydrophobic plasticizers can reduce water uptake by plugging the micro-voids into the films (Varee and Bhaswati, 2019). These factors influence the wettability of bioplastics. Different bioplastics exhibit varying degrees of wettability.

Table 2. Contact Angle of Bioplastic with Presence of Sorbitol or Citric Acid

Contact Angle (°) (Left, Right) Types of Bioplastic	Types of Plasticizers			
	Sorbitol		Citric Acid	
	Before Radiation	After Radiation	Before Radiation	After Radiation
Corn	41.10, 37.60	67.10, 67.90	103.90,100.60	99.70, 98.90
Rice	22.10, 23.80	13.30, 17.60	101.90, 99.80	109.10, 106.70
Potato	0.00, 0.00	49.40, 56.10	33.10, 25.70	33.70, 37.90
Corn-Rice	96.70, 94.50	85.50, 89.50	28.70, 29.00	106.70, 105.20
Corn-Potato	43.40, 44.20	27.40, 28.70	34.10, 39.70	61.90, 60.90
Potato-Rice	29.10, 12.80	20.80, 19.30	100.10, 98.60	103.80, 100.90
	Before		After	
LDPE	97.70, 99.60		96.40, 95.30	

DOI:https//doi.org/ 10.22452/mjs.vol43no1.6
Malaysian Journal of Science 43(1): 59-71 (March 2024)

i 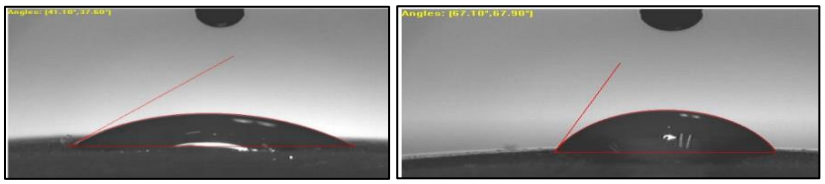

ii 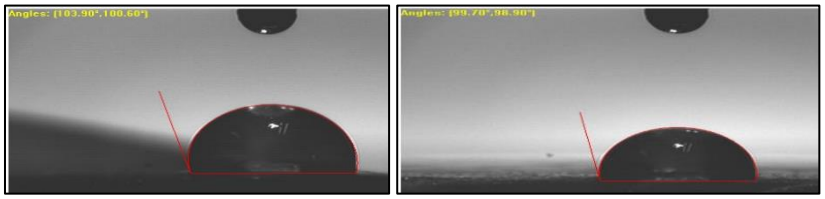

iii 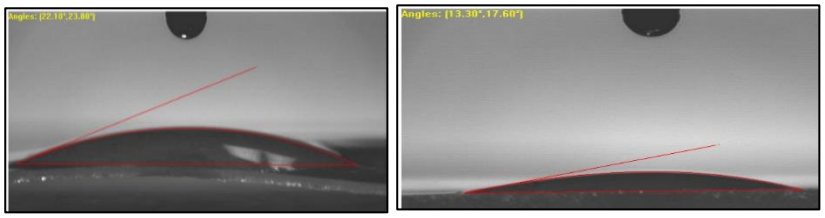

iv 

v No image for this because the angle is 0.00° making it unreadable by the system.

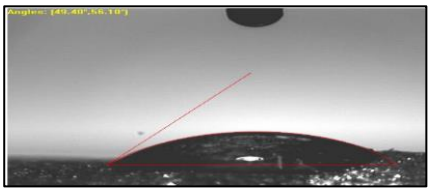

vi 

vii 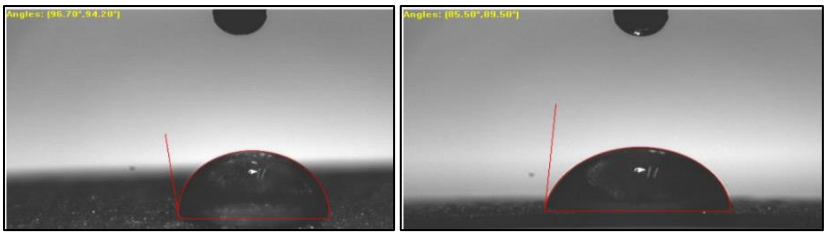

DOI:https//doi.org/ 10.22452/mjs.vol43no1.6
Malaysian Journal of Science 43(1): 59-71 (March 2024)

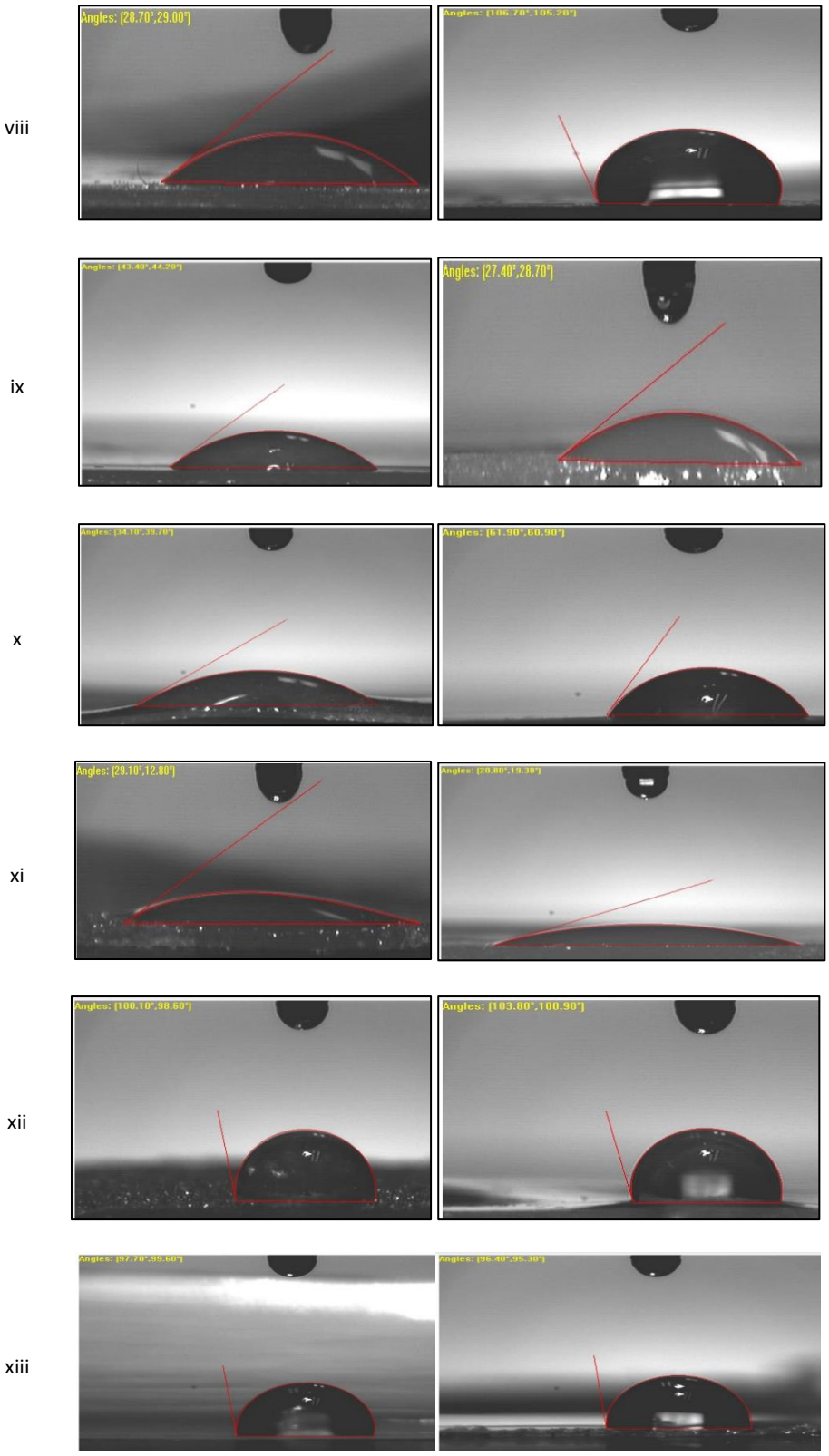

Figure 1. Contact angle of bioplastic with presence of sorbitol or citric acid (a) Pre-irradiation (b) Post-irradiation for (i) CS (ii) CCA (iii) RS (iv) RCA (v) PS (vi) PCA (vii) CRS (viii) CRCA (ix) CPS (x) CPCA (xi) PRS (xii) PRCA (xiii) LDPE samples

DOI:https//doi.org/ 10.22452/mjs.vol43no1.6
Malaysian Journal of Science 43(1): 59-71 (March 2024)

Content of Moisture Test

When all the bioplastics were dried in an oven from 100 °C to 110 °C for the first 30 min, their weights did not differ considerably. Thus, several samples showed weight changes for the second time, but all samples had a difference in weight for the third time. All the samples were placed in an oven for the fourth time to ensure a fixed weight of the dried samples. Some remained at the same weight as before, while others decreased and reached a fixed weight after the fifth 30 min. The duration of this test was approximately 2 h and 30 min. Table 3 shows that rice-sorbitol bioplastic has a high moisture content of 18.49% in the pure starch category, whereas corn has 21.21% in the citric acid category. Regarding the mixed starch category, potato-rice bioplastics had a high moisture content of 16.68%. However, when citric acid replaced sorbitol, the corn-potato bioplastic had the highest moisture content (22.11%). The moisture content of the bioplastics is related to their wettability. It is defined as the tendency of a fluid to spread or adhere to a material surface (Tarek Ahmed, 2019). Therefore, it alters the three-dimensional network of the polymer chains, resulting in increased mobility by increasing the free volume. Plasticizers aid in bioplastic resistance to migration and extraction in water or solvents (Sothornvit and Krochta, 2005).

Table 3. Weight of Samples for Moisture Content of Bioplastic with Presence of Sorbitol or Citric Acid

Type of Bioplastic	Weight	Types of Plasticizers					
		Sorbitol			Citric Acid		
	Initial Weight (g)	Final Weight (g)	Moisture Content (%)	Initial Weight (g)	Final Weight (g)	Moisture Content (%)
Corn	0.3654	0.3114	17.34	0.2372	0.1957	21.21
Rice	0.3582	0.3023	18.49	0.2005	0.1714	16.98
Potato	0.5586	0.4750	17.60	0.1481	0.1287	15.07
Corn-Rice	0.4704	0.4105	14.59	0.2844	0.2455	15.85
Corn-Potato	0.9380	0.8558	9.60	0.3407	0.2790	22.11
Potato-Rice	0.2203	0.1888	16.68	1.4673	1.2555	16.87

Biodegradability Test

Degradation is required to dispose of waste without negatively affecting environmental conditions, and bioplastics should pass this test. Consequently, the duration of degradation varies depending on the mixture of molecules. When hydrophobicity increases, the chance of degradability may decrease; however, all bioplastics beat the challenge. The lowest weight loss percentage was 9.9% for the corn-potato bioplastic (Table 4). Moreover, all bioplastics involving sorbitol as a plasticizer experience a great weight loss percentage, from 47.36% to 80.17%. Unlike when citric acid played the role of sorbitol, only rice bioplastics had a high weight loss of 53.15%, while the others only achieved a range of 11.34% to 21.28%. The primary process generated by irradiation is degradation, which is accompanied by cross-linking. Irradiation-induced changes in film characteristics can be attributed to changes in the film surface properties (particularly surface oxidation) and structures. The chain scission process causes degradation to reduce the molecular weight of all irradiated samples (IAEA, 2019). Adding plasticizers to pure starch may increase its workability and reduce film brittleness. Plasticizers aim to improve starch flexibility and processibility by lowering the strong intermolecular interactions between starch molecules. Therefore, the polymeric chain mobility increases, improving the flexibility, extensibility, and ductility of plasticized films (Sanyang *et al.,* 2015).

Table 4. Weight of Samples for Biodegradability of Bioplastic with Presence of Sorbitol or Citric Acid

Types of Starch	Weight of Samples (g)	Types of Plasticizers					
		Sorbitol Biodegradability			Citric Acid Biodegradability		
	Initial Weight (g)	Final Weight (g)	Weight Loss (%)	Initial Weight (g)	Final Weight (g)	Weight Loss (%)
Corn	0.7840	0.1555	80.17	0.2918	0.2587	11.34
Rice	0.5109	0.2102	58.86	0.8972	0.4203	53.15
Potato	1.0268	0.5045	47.36	0.7229	0.6311	12.69
Corn-Rice	1.2442	0.5920	52.42	2.3591	1.8570	21.28
Corn-Potato	1.8327	1.6512	9.90	1.5723	1.2878	18.09
Potato-Rice	1.0188	0.3980	60.93	1.9409	1.5718	19.02

DOI:https//doi.org/ 10.22452/mjs.vol43no1.6
Malaysian Journal of Science 43(1): 59-71 (March 2024)

Figure 2. Images of Bioplastic with Presence of Sorbitol or Citric Acid During Soil Burial Process (a) before (b) after for (i) CS (ii) CCA (iii) RS (iv) RCA (v) PS (vi) PCA (vii) CRS (viii) CRCA (ix) CPS (x) CPCA (xi) PRS (xii) PRCA samples.

i

ii

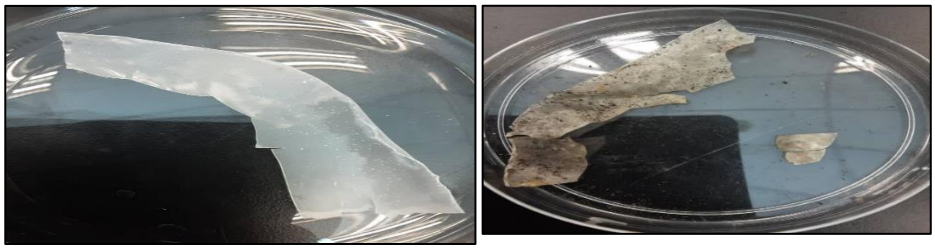

iii

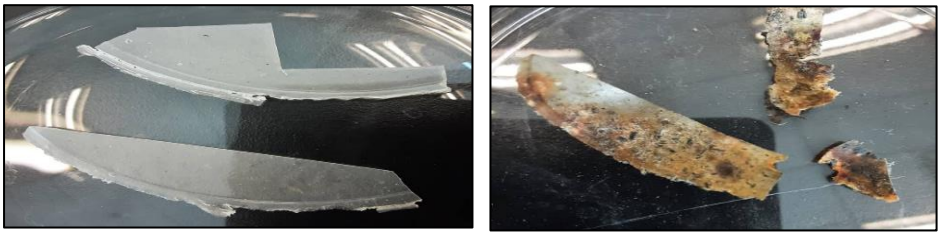

iv

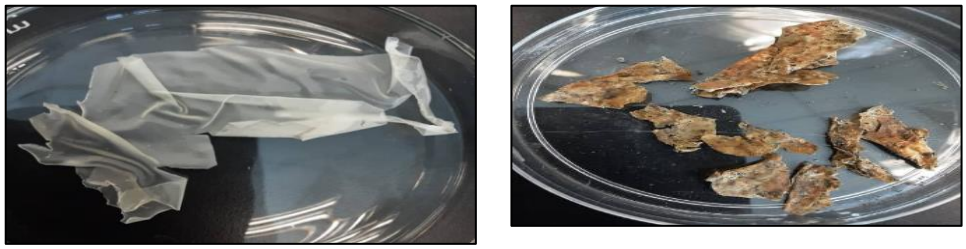

v

vi

DOI:https//doi.org/ 10.22452/mjs.vol43no1.6
Malaysian Journal of Science 43(1): 59-71 (March 2024)

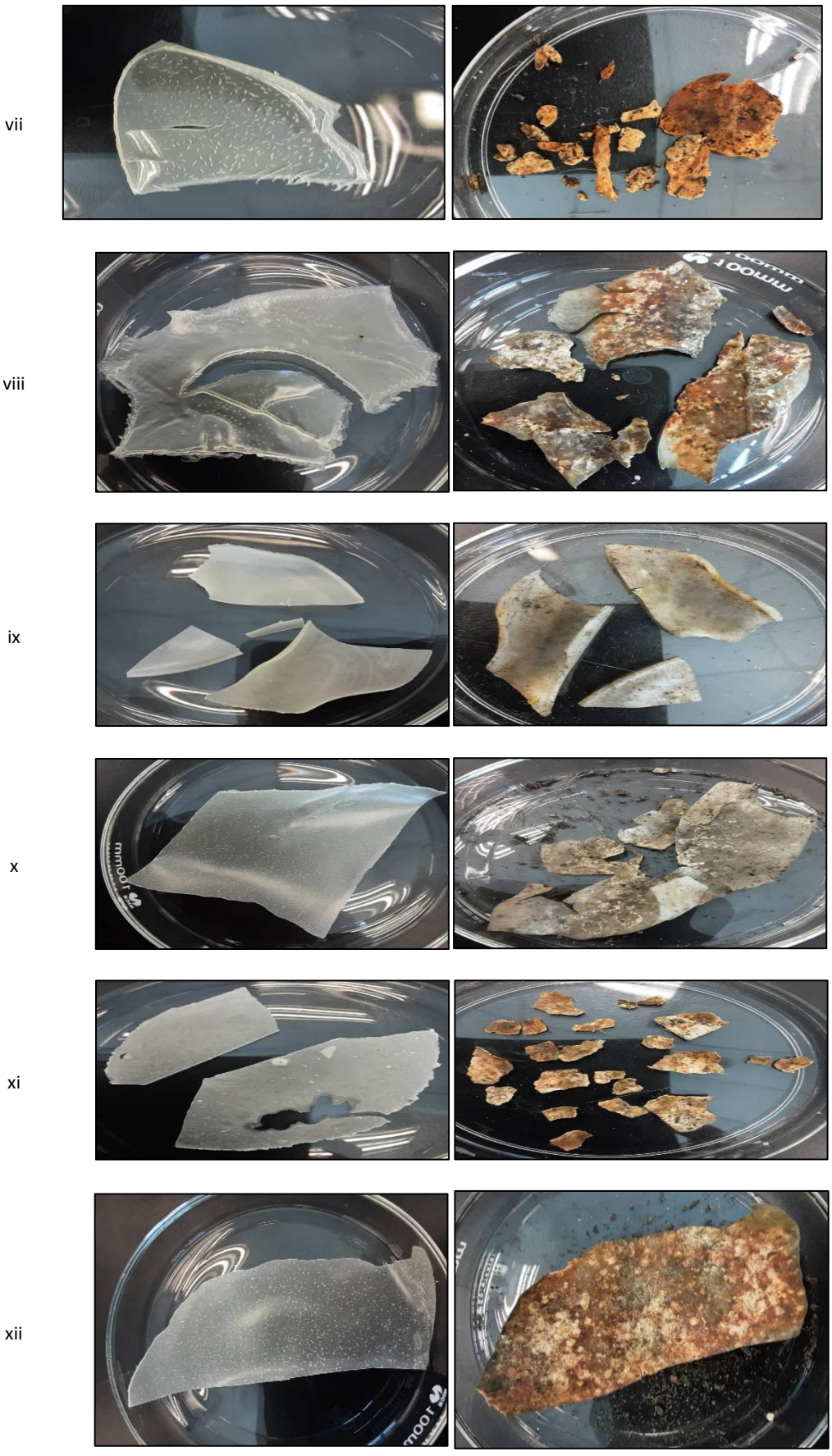

DOI:https//doi.org/ 10.22452/mjs.vol43no1.6
Malaysian Journal of Science 43(1): 59-71 (March 2024)

Tensile Strength and Elongation Test

From the maximum force, F_{max} (kg), the tensile strength of the bioplastics was calculated using the equation for the force per initial area of the samples. Simultaneously, the elongation percentage was estimated from the difference between the initial and elongated length of the samples. Table 5 shows that for bioplastics with sorbitol as a plasticizer, the highest tensile strength would be the corn-rice bioplastic with 2.916 MPa, but the potato bioplastic had the highest percentage (34.57%). Meanwhile, when citric acid replaced the sorbitol, potatoes experienced 3.189 MPa. However, corn bioplastics had a high elongation percentage (28.98%). Bioplastics containing citric acid experience higher tensile strength due to their crosslinking characteristic, resulting in high rigidity in the polymer. The covalent intermolecular interactions between the hydroxyl and carboxyl groups may strengthen the bonds between the plasticizer and starch compounds (Azeredo *et al*., 2016). However, the samples' tensile strength is inconsistent with the elongation percentage reading.

Table 5. Tensile (MPa) and Elongation (%) of Bioplastics with Presence of Sorbitol or Citric Acid

Tensile and Elongation	Types of Plasticizer Involved					
	Sorbitol			Citric Acid		
Types of Bioplastic	F_{max} (kg)	Tensile strength (MPa)	Elongation (%)	F_{max} (kg)	Tensile strength (MPa)	Elongation (%)
Corn	1.0300	1.4430	31.150	1.058	1.4820	28.980
Rice	0.5970	0.8364	16.120	0.538	0.7537	14.410
Potato	1.1930	1.6710	34.570	2.276	3.1890	18.980
Corn-Rice	2.0810	2.9160	10.350	1.198	1.6780	23.150
Corn-Potato	1.2160	1.7040	13.780	1.592	2.2300	16.980
Potato-Rice	0.6350	0.8896	6.240	2.923	4.0950	8.297
Type of Plastic	F_{max} (kg)		Tensile strength (MPa)		Elongation (%)	
LDPE	1.558		2.183		84.31	

FTIR Spectroscopy

FTIR spectroscopy was used to investigate the molecules that appeared with a certain transmittance percentage. Figure 3(a) indicates that each bioplastic experienced a curve ranging between 2800 and 2930 cm^{-1} and at wavenumbers of 3200–3400 cm^{-1} in the pre-irradiated samples. However, PRCA achieved the highest transmittance (73.62%) with a wavenumber of 3287 cm^{-1}. In contrast, RPS exhibited the lowest transmittance (50.78%) at 3292.96 cm^{-1}. The LDPE graph narrowed down to 2916 cm^{-1} and 2848 cm^{-1} with transmittances of 69.97% and 72.35%, respectively. The CS curve exhibits a transmittance of 77.95% at 2929 cm^{-1}. This shows that LDPE and CS have a highly functional group of methylene C-H asymmetric/symmetric stretching, whereas RPS has a highly normal polymeric OH stretching.

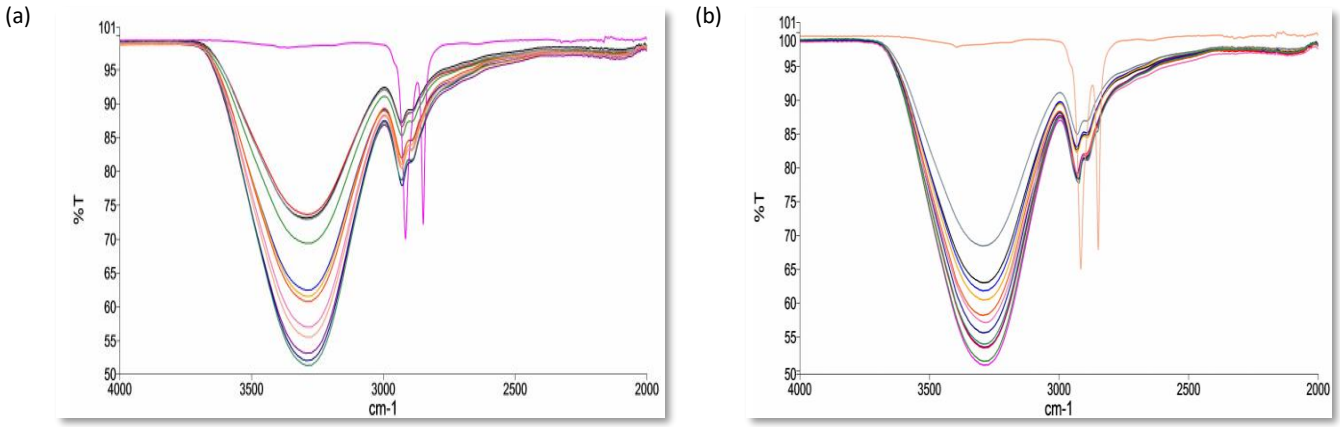

Figure 3. Graph of FTIR Analysis of (a) Pre-Irradiated samples (b) 0.5kGy Irradiated Samples

DOI:https//doi.org/ 10.22452/mjs.vol43no1.6
Malaysian Journal of Science 43(1): 59-71 (March 2024)

Figure 3(b) shows that the PRS has a low transmittance percentage at 3292 cm^{-1} (50.78 %), followed by RS (51.36 %). However, in the range of 2800 cm^{-1} to 3000 cm^{-1}, RS had the lowest transmittance percentage of 78.56% at 2931.39 cm^{-1}, although there was not much difference with the PRS transmittance percentage at 78.63%. LDPE maintained the same wavenumber but decreased the transmittance percentage by 65.81% and 71.765%, respectively. Figure 4(a) shows that almost all bioplastics have a similar transmittance percentage, but the lowest is PRS, with 51.20% at 3293 cm^{-1}, followed by CS at wavenumber 3291 with 53.07%, and the lowest is bioplastic at 2923 cm^{-1} with 77.34%. The LDPE curves in three different regions, 3393 cm^{-1} with 95.93%, at 2916 cm^{-1} with 66.098%, and 2848 cm^{-1} with 67.99%. The result exposed 1.5 kGy gamma radiation, which resulted in a slightly lower transmittance percentage than the 1.0 kGy (Figure 4b). PS had the lowest 50.77% at 3285 cm^{-1}, followed by CS with 50.89% at 3283.9 cm^{-1}. At wavenumber 2931 cm^{-1}, it has an equal transmittance percentage with CRCA at 2930 cm^{-1} with 78.59%.

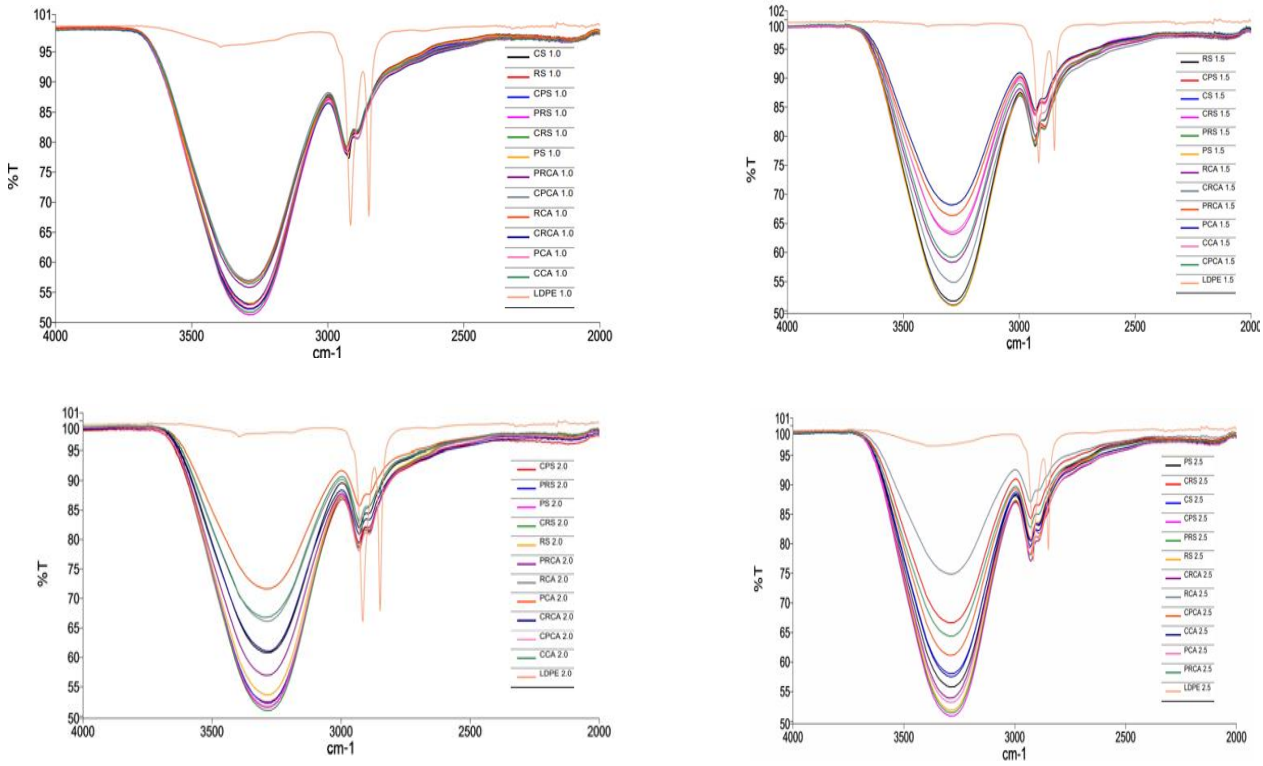

Figure 4. Graph of FTIR Analysis of (a) 1.0 kGy Irradiated Samples (b) 1.5 kGy Irradiated Samples (c) 2.0 kGy Irradiated Samples (d) 2.5 kGy Irradiated Samples

Figure 4(c) shows the results of the sample treated under gamma radiation at a dose of 2.0 kGy. CRS achieved the lowest transmittance of 50.89% at a wavenumber of 3285 cm^{-1}. The LDPE remained at the same wavenumber, but the transmittance percentage changed to 66.03% at 2916 cm^{-1} and 68.18% at 2848 cm^{-1}. PS achieved low transmittance percentages of 51.68% at 3266 cm^{-1} and 78.62% at 2931 cm^{-1}. Figure 4(d) shows that the CPS percentage was 50.75%, making it have the lowest transmittance at 3293 cm^{-1}, followed by CRCA at 3294 cm^{-1} with 53.81%. However, CRCA leads with 77.17% at 2928 cm^{-1} than CPS with 79.38% at 2933 cm^{-1}. LDPE again obtained three readings at wavenumbers of 3361 cm^{-1} with 96.73%, 2915 cm^{-1} with 77.29%, and 2848 cm^{-1} with 79.03%.

Most bioplastics experienced decreasing transmittance percentages as exposure radiation doses increased due to interactions via the hydroxyl group of bioplastics. Furthermore, bonding significantly enhances the mechanical strength and degradation of bioplastics for polymeric materials (Wang *et al.,* 2017). In contrast, RCA had the highest percentage when exposed to a dose of 2.5 kGy for the pure starch bioplastic. However, CRCA had the lowest percentage of mixed-starch bioplastics. All bioplastics show two huge curves, with the first curve at wavenumbers in the range of 3280–3300 cm^{-1}, followed by the second curve at wavenumbers in the range of 2920–2935 cm^{-1} from all six graphs of FTIR analysis due to similarities of functional groups (Hindi *et al*., 2017). The first curve shows the normal polymeric OH stretch group and the second curve defines the asymmetric C-H stretch of the methylene group (Coates, 2006).

DOI:https//doi.org/ 10.22452/mjs.vol43no1.6
Malaysian Journal of Science 43(1): 59-71 (March 2024)

Table 6. Functional Groups from FTIR Analysis Spectrum

Functional group	Wavenumbers (cm^{-1})
OH stretch group	3280- 3300
C-H stretch of methylene group	2920- 2935

AFM

To analyze the roughness, an image of the sample topography in the tapping mode was used to reduce contact between the tip and the samples, as shown in Figure 6.

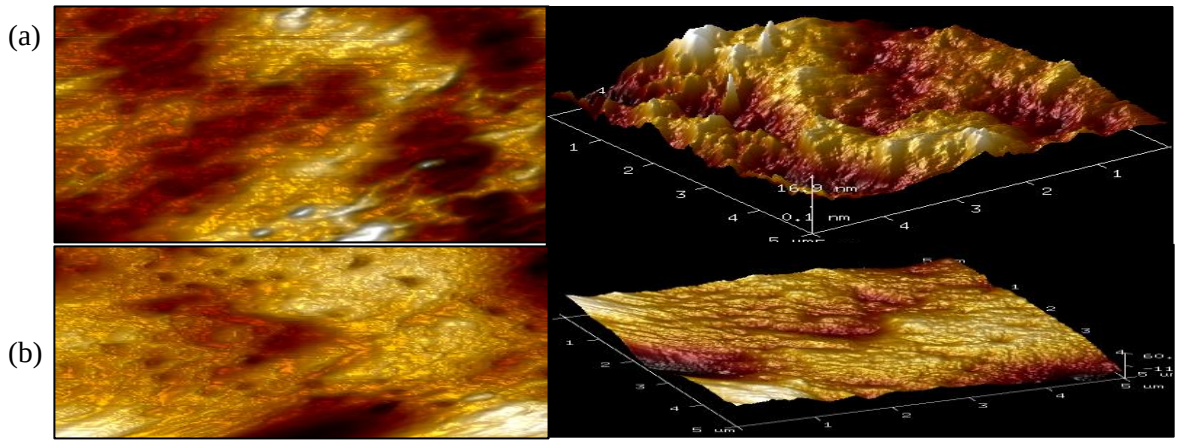

Figure 5. CRCA roughness conditions (a) before and (b) after irradiation exposure

The pre-irradiation sample had a peak-to-peak distance of 2.14011 nm. The minimum peak depth was 17.7510 nm and the maximum peak depth was 19.9 nm. The maximum depth at the histogram was 19.8911 nm, with 157 peaks. The difference in the image surface area was 0.0647%. The root means square image was 4.64 nm with an average roughness of 3.68 nm. The maximum image roughness was detected at 34.7 nm. When the samples underwent irradiation treatment, the peak-to-peak distance became 2.74845 nm, with a minimum peak depth of 44.1834 nm. The maximum peak depth was recorded at 46.9 nm, with 162 peaks and a maximum histogram depth of 46.9318 nm. The roughness result was described with an image surface area difference of 0.738%, with a root mean square of 17.1 nm, average roughness equal to 12.5 nm, and maximum image roughness was detected at 122 nm. According to Oleyaeia *et al*. (2016), surface roughness is related to water permeability. However, irradiation treatment might indicate surface etching, leading to increased roughness.

4. Conclusions

Regarding wettability, mixed starches were confirmed to deal with hydrophilicity, but pure starch could handle it with citric acid as a plasticizer. However, CRS was the highest for sorbitol, while PRCA was the best angle for citric acid as a plasticizer, with readings of 100.10 ˚and 103.8˚, respectively. The water contact angle test revealed that many bioplastics containing citric acid act as plasticizers to achieve hydrophobicity. Regarding moisture content, RS (21.21%) led to pure starch, but corn potato with citric acid (22.11%) was present in the mixed starches. The highest biodegradability percentages were for CS (80.17%), PRS (60.93%), and RCA (53.13%). The tensile strength cases were enclosed by the CRS (2.916 MPa) and PRCA (4.095 MPa) results. Meanwhile, for elongation, PS (34.57%), and CCA (28.98%). CRCA was subjected to AFM topography to survey its surface roughness because it has a high transmittance percentage from FTIR analysis under dose radiation-exposed 2.5 kGy. The hydrophobicity levels for bioplastics can achieve LDPE standards, but other physical properties are far from the target. However, only the C-H stretch methylene group could achieve the same transmittance percentage for chemical bonding. Therefore, this study meets the objectives and can serve as a reference to other researchers to enhance the properties of existing and future bioplastics, especially in smart packaging applications.

5. Acknowledgement

The authors would like to thank Universiti Tun Hussein Onn Malaysia for the facilities provided that make the research possible.

6. References

Aranda-García, F. J., González-Núñez, R., Jasso-Gastinel, C. F., & Mendizábal, E. (2015). Water absorption and thermomechanical characterization of extruded starch/poly (lactic acid)/agave bagasse fiber bioplastic composites. International Journal of Polymer Science, 2015.

Azeredo, H. M., Morrugares-Carmona, R., Wellner, N., Cross, K., Bajka, B., & Waldron, K. W. (2016). Development of pectin films with pomegranate juice and citric acid. Food Chemistry, 198: 101-106.

Byun, Y., Zhang, Y., & Geng, X. (2014). Plasticization and Polymer Morphology. In Innovations in Food Packaging (pp. 87-108). Academic Press.

DOI:https//doi.org/ 10.22452/mjs.vol43no1.6
Malaysian Journal of Science 43(1): 59-71 (March 2024)

Clunies-Ross, P. (2019). Plastics in the Environment: Te Ao Hurihuri–The Changing World Evidence Summary.

Coates, J. (2006). Interpretation of infrared spectra, a practical approach. Encyclopedia of analytical chemistry: applications, theory and instrumentation.

Gorna, K., & Gogolewski, S. (2003). The effect of gamma radiation on molecular stability and mechanical properties of biodegradable polyurethanes for medical applications. Polymer degradation and stability, 79(3): 465-474.

Hindi, S. S. Z., Albureikan, M. O., Al-Ghamdi, A. A., Alhummiany, H., & Ansari, M. S. (2017). Synthesis, characterization and biodegradation of gum arabic-based bioplastic membranes. Nanosci Nanotechnol, 4(2): 32-42.

Ibrahim Muhammad Shamsuddin, Jafar Ahmad Jafar, Abubakar Sadiq Abdulrahman Shawai, Saleh Yusuf, Mahmud Lateefah & Ibrahim Aminu. (2017). Bioplastics as Better Alternative to Petroplastics and Their Role in National Sustainability: A Review. Advances in Bioscience and Bioengineering. 5(4): 63-70

International Atomic Energy Agency (IAEA). (2019). Use of Radiation Technologies in the Development of Active Packaging Materials. Report of the Technical Meeting, Budapest, Hungary. 1-32.

Jiang, L., & Zhang, J. (2017). Biodegradable and biobased polymers. In Applied plastics engineering handbook (pp. 127-143). William Andrew Publishing

Marichelvam, M. K., Jawaid, M., & Asim, M. (2019). Corn and rice starch-based bio-plastics as alternative packaging materials. Fibers, 7(4): 32.

Maulida, S. M., & Tarigan, P. (2016). Production of starch based bioplastic from cassava peel reinforced with microcrystalline celllulose avicel PH101 using sorbitol as plasticizer. In J. Phys. Conf. Ser. 710: 12012.

Mostafa, N. A., Farag, A. A., Abo-dief, H. M., & Tayeb, A. M. (2018). Production of biodegradable plastic from agricultural wastes. Arabian journal of chemistry, 11(4): 546-553.

Oleyaei, S. A., Zahedi, Y., Ghanbarzadeh, B., & Moayedi, A. A. (2016). Modification of physicochemical and thermal properties of starch films by incorporation of TiO2 nanoparticles. International Journal of Biological Macromolecules, 89: 256-264.

Paquette, K. E. (2004). Irradiation of Prepackaged Food: Evolution of the U.S. Food and Drug Administration's Regulation of the Packaging Materials. Irradiation of Food and Packaging, 182–202. doi:10.1021/bk-2004-0875.ch012

Rochman, C. M., Browne, M. A., Halpern, B. S., Hentschel, B. T., Hoh, E., Karapanagioti, H. K., & Thompson, R. C. (2013). Classify plastic waste as hazardous. Nature, 494 (7436): 169-171.

Sanyang, Muhammed L., Salit M. Sapuan, Mohammad Jawaid, Mohamad R. Ishak, & Japar Sahari. 2015. Effect of Plasticizer Type and Concentration on Tensile, Thermal and Barrier Properties of Biodegradable Films Based on Sugar Palm (*Arenga pinnata*) Starch. *Polymers* 7, no. 6: 1106-1124. https://doi.org/10.3390/polym7061106.

Sothornvit R. & Krochta J.M. 2005. Chapter 23- Plasticizers in edible films and coatings. Editor(s): Jung H. Han, In Food Science and Technology, Innovations in Food Packaging, Academic Press, 403-433, https://doi.org/10.1016/B978-012311632-1/50055-3.

Tarek Ahmed. 2019. Chapter 4 - Fundamentals of Rock Properties, Editor(s): Tarek Ahmed, Reservoir Engineering Handbook (Fifth Edition), Gulf Professional Publishing,167-281, https://doi.org/10.1016/B978-0-12-813649-2.00004-9.

Tokiwa, Y., Calabia, B., Ugwu, U., & Aiba, S. (2009). Biodegradability of Plastics. *International Journal of Molecular Sciences*, *10*: 3722–3742. https://doi.org/10.3390/ijms10093722

Varee Tyagi & Bhaswati Bhattacharya. (2019). Role of plasticizers in bioplastics. MOJ Food Processing and Technology. 7(4): 128- 130.

Wang J., Shenhua S., Shang G., Ravi M., Renchen L., & Qing M. (2017). Mg-ion conducting gel polymerelectrolyte membranes containing biodegradable chitosan: Preparation, structural, electrical andelectrochemical properties. Polymer Testing 62 278–286. https://doi.org/https://doi.org/10.1016/j.polymertesting.2017.07.016.

Zygoura, P. D., Paleologos, E. K., & Kontominas, M. G. (2011). Effect of ionising radiation treatment on the specific migration characteristics of packaging–food simulant combinations: effect of type and dose of radiation. Food Additives and Contaminants, 28(5): 686-694.

DOI:https//doi.org/ 10.22452/mjs.vol43no1.6
Malaysian Journal of Science 43(1): 59-71 (March 2024)

MALAYSIAN JOURNAL OF SCIENCE
MJS
ISSN 1394-3065

Regular Issue

Malaysian Journal of Science 43(1): 72-85 (March 2024) https://mjs.um.edu.my

APPLICATION OF BENTHIC MACROINVERTEBRATES AS POTENTIAL BIO-INDICATORS IN MALAYSIAN'S RIVERS: GAP AND BIBLIOMETRIC ANALYSES

Nadeesha Dilani Hettige[1c], Rohasliney Hashim[2a]*, and Ahmad Abas Kutty[3b]

Abstract: The literature on reliable indices, suitable bio-indicators, taxonomic level, frequency of measurements, and replications on benthic macroinvertebrates remains scarce in Malaysia. In addition, no review study was conducted using bibliometric analysis related to this discipline. Thus, this review aimed at gap and bibliometric analysis of publications on benthic macroinvertebrates as potential biological indicators. Sixty-six relevant scientific research papers from 2011 to 2022 were selected from the different databases. Then, descriptive and inferential statistical analyses were performed to assess the most reliable potential bio-indicators for river assessment and monitoring. Visualized statistics regarding bibliographic coupling analysis of authors, journal proceedings, and organizations were analyzed. The findings revealed that publications on invertebrates had no significant relationship in the last ten years ($r = 0.241$; $p > 0.05$). Most publications on macroinvertebrates in Malaysian rivers were found in the Scopus database (53.57%). Therefore, research articles must be published in journals included in the Journal Citation Report (JCR) to improve their quality further. Besides, benthic macroinvertebrates are commonly identified only up to the family level (47%) due to incomplete tropical benthic macroinvertebrates identification keys. As such, using environmental DNA methods with the power of next-generation sequencing has come in handy in bio-indicator species identification. Among the potential bio-indicators found in Malaysian rivers are Chironomidae (9.11%), Baetidae (8.87%), and Hydropsychidae (8.62%). Based on the approaches utilized in analyzing benthic macroinvertebrates as bio-indicators, in-depth research such as bioassay and toxicology tests is necessary to realize the potential bio-indicators fully. Many studies focused on recreational rivers in Peninsular Malaysia. Therefore, research studies would be expanded to urban rivers and rivers in Sabah and Sarawak. Also, to overcome the limitation of the single biotic index, developing a multimetric index to evaluate the water quality by selecting many river basins is essential. Bibliographic analysis showed that the Institute for Tropical Biology and Conservation, Universiti Malaysia Sabah, made the greatest total link strength. The Serangga Journal published the highest number of research articles. Finally, utilizing advanced technologies is recommended to address Malaysia's lack of potential bio-indicator studies.

Keywords: *Bio-indicators, bio-indices, biomonitoring, freshwater pollution, and macroinvertebrate*

1. Introduction

Streams and rivers are among the most endangered ecosystems globally due to anthropogenic activities, which can directly or indirectly harm river environments (Ekka et al., 2020). Traditionally, physicochemical parameters are used to evaluate the quality of running water in streams worldwide (Aazami et al., 2015), including in Malaysia. However, this method is cost-intensive, time-consuming, and dependent on particular instruments. Similarly, physicochemical parameters fluctuate over time and only show environmental conditions at the moment of measurement (Aazami et al., 2015; Dorji, 2016). Hence, if no long-term physicochemical parameters with good spatial coverage are available, it does not accurately signify a clear picture of the health of the river ecosystem.

Biological monitoring is imperative in evaluating the environmental health of aquatic ecosystems (Parmar et al., 2016; Yusop et al., 2017). Algae, fish, aquatic plants, and invertebrates serve as bio-indicators in bioassessment (Barbour et al., 1999). In brief, bio-indicators are living organisms generally utilized to assess the health of natural ecosystems (Parmar et al., 2016) due to their capacity to respond to pollutants present in the ambient environment (Kumari & Paul, 2020). Also, they can act as an index of measure or a model that categorizes aquatic ecosystem health (Manickavasam et al., 2019). In particular, benthic macroinvertebrates are considered useful bio-indicators for environmental changes in many aquatic ecosystems (Belal et al., 2016) due to their high biodiversity, minimal mobility, relatively long life cycle, bottom-dwelling nature, and immense sensitivity to environmental changes (Flores & Zafaralla, 2012; Jun et al., 2012; Tampus et al., 2012; Dacayana et al., 2013; Sharma et al., 2013; Selvanayagam & Abril, 2016). To date, the utilization of

Authors information:
[a]Department of Environment, Faculty of Forestry and Environment, Universiti Putra Malaysia, 43400 UPM Serdang, Selangor, MALAYSIA. E-mail: rohasliney@upm.edu.my[2]
[b]Department of Earth Science and Environment, Faculty of Science and Technology, Universiti Kebangsaan Malaysia, Bangi Selangor, MALAYSIA. E-mail: abas@ukm.edu.my[3]
[c]Department Environmental Studies Division, National Aquatic Resource Research and Development Agency (NARA), Crow Island, Colombo 15, SRI LANKA. E-mail: nadeeshahettige83@gmail.com[1]
*Corresponding Author: rohasliney@upm.edu.my

Received: August 22, 2022
Accepted: April 5, 2023
Published: March 31, 2024

DOI:https//doi.org/10.22452/mjs.vol43no1.7
Malaysian Journal of Science 43(1): 72-85 (March 2024)

benthic macroinvertebrates as bio-indicators has garnered significant attention in global river monitoring programs, including those in Malaysia (Gallacher, 2001; Resh, 2007; Narangarvuu et al., 2014; Tan & Beh, 2015).

Initially, stream biomonitoring studies predominantly employed single indices, such as ecological indices, to assess water quality status. These included the Shannon diversity index (Shannon, 1948), Margaleaf diversity index (Margalef, 1958), Simpson's diversity index (Simpson, 1949), Biological Monitoring Working Party (BMWP) in 1976 (Armitage et al., 1983), and Family Biotic Index (Hilsenhoff, 1988). However, this concept is an inadequate measure of overall ecological integrity because the cause-effect relationships of indicator organisms are not fully established and are often confusing (Barbour et al., 1999). Hence, multimetric indices have been developed as an alternative bio-assessment approach to reflect all types of degradation and cumulative impacts at the ecosystem level (Barbour et al., 1999). This approach held the potential for wide-ranging application in the assessment of stream ecosystems, as it involved various types of measurement and provided comprehensive comparative information relative to pre-determined criteria derived from non-impacted reference conditions (Klemm et al., 2002).

Toxicity testing is one of the methods that can be used to select bio-indicators. The main goal of toxicity testing is to monitor or predict the effects of single compounds, elements, or mixtures on the long-term health of individual organisms, populations, communities, and ecosystems. Researchers have found plants, plankton, and benthic macroinvertebrates as bio-indicators of water pollution in the aquatic environment. For example, Mazur et al. (2016) identified *Lymnaea stagnalis* as a highly sensitive bio-indicator capable of detecting even minimal levels of environmental stressors. Esposito et al. (2018) found *Leptodictyum riparium* to be a bio-indicator of toxic metal pollution. The significance of toxicity testing lies in its efficiency, which eliminates the need to conduct tests on numerous available pollutants (Peyravi *et al*., 2020).

A total of 189 river basins are found in Malaysia: 89 are located in Peninsular Malaysia, 78 in Sabah, and 22 in Sarawak (Diya et al., 2015). One of the earliest publications about biomonitoring in Malaysian rivers was reported by Bishop in 1973. This study comprehensively analyzed physical, chemical, and biological features, including algae, benthic invertebrates, and some vertebrates like fishes in the Gombak River, Selangor. Subsequently, the interest in river water quality monitoring using benthic macroinvertebrates has grown since 2010. The trend is a result of the limited prior studies and available data in Malaysian ecosystems, specifically the absence of physicochemical data. This scarcity has heightened the interest in utilizing benthic invertebrates (Arsad et al., 2012). However, most studies mainly focused on diversity, biotic indices application, water quality monitoring, and land use patterns to conduct biomonitoring (Al-Shami et al., 2011a; Md Rawi et al., 2014; Al-Shami et al., 2017; Shafie et al., 2017). In contrast, few studies have explored the role of benthic macroinvertebrates as bio-indicators to assess the water quality of rivers and streams (Azrina et al., 2006). Presumably, the river classifications are related to water quality levels based on the species composition of macroinvertebrates. Hence, some studies have developed river classification using macroinvertebrates for the Malaysia River (Arsad et al., 2012; Ghani, 2016). Also, few papers have reviewed this topic, and no systemic review has been done on benthic macroinvertebrates in Malaysia's rivers.

Bibliometric analysis is a statistical method used to assess the characteristics and significant development trends of a given research subject based on published research (Guo et al., 2019). This analytical approach has been applied to evaluate various aquatic organisms for water quality monitoring (Zyoud et al., 2014) and is applicable to quantify and characterize the global scientific production of Taxus-related research (Zyoud et al., 2014). Therefore, this study extends the application of bibliometric analysis to systematically review scientific publications on benthic macroinvertebrates as potential bio-indicators in Malaysian rivers. A novel aspect of this research involves integrating the science mappings approach, including bibliographic coupling analysis for authors, journal proceedings, and organizations, to visualize information related to benthic macroinvertebrates as bio-indicators in Malaysian rivers.

2. Materials and Methods

Statistical Analysis for Literature Approach

This review was conducted in January 2023 using resources extracted from journals and conferences from 2011 to 2022 in Scopus's primary scientific database and several other databases based on Universiti Putra Malaysia (UPM) subscription (Emerald Insights, Nature Journal, Oxford Journal, and Science Direct) for 12 years. The keywords used were "benthic macroinvertebrates, benthos, aquatic insects, and bio-indicators" in rivers, Malaysia. Since this study analyzed selected potential bio-indicator groups, only articles discussing potential bio-indicators in streams and rivers were included. Furthermore, articles published in Malay where bio-indicators are discussed were also included. Meanwhile, articles that did not mention benthic macroinvertebrates as bio-indicators were removed from the study scope. Abstracts and other documents (reviews, books, and book chapters) were also excluded because these are not primary literature. Moreover, the thesis was also excluded due to its unavailability in the selected databases. Out of the 205 papers, only 66 were evaluated for this review.

First, descriptive statistics were used to assess the trends and approaches, such as published journals, taxonomic identification, and study area. Then, the Pearson correlation was carried out to determine the time series trends in publications related to benthic macroinvertebrates and potential bio-indicators only for benthic macroinvertebrates. Also, selected research papers were searched via Journal Citation Report (JCR) to determine whether the journal's name is recorded as Q ranking based on JCR (Q1, Q2, Q3, and Q4).

The geographical locations of the studies, the frequency of measurements (i.e., number of sampling during the study period)

DOI:https//doi.org/10.22452/mjs.vol43no1.7
Malaysian Journal of Science 43(1): 72-85 (March 2024)

conducted by the researchers, replication variables used in their studies, taxonomic identification of identified potential bio-indicators, and methodological information used by the authors were summarized in this review paper. The dominant potential bio-indicators were determined based on the number of papers reported using the benthic macroinvertebrates families. The study areas for rivers, namely recreational, forested streams, urban or polluted rivers, and different land use areas, were categorized based on the information provided in the research paper.

Visualized Analysis

VOSviewer (Leiden University, Leiden, The Netherlands) was used to visualize and analyze the literature. The software was used for bibliographic coupling analysis for authors, journals, proceedings, and organizations. The total link strength of the authors was determined through the bibliographic coupling analysis of the authors. The total link strength represents the frequency of simultaneous appearances of two items in publications. Also, the bibliographic coupling analysis for journals and proceedings established the minimum threshold value of 155 and the total link strength for both journals and proceedings. Moreover, the total link strength of organizations was determined through bibliographic coupling analysis. In cases where the VOSviewer database contained duplicate author names and similar terms, a thesaurus file was created and used to combine the identical information.

3. Results and Discussion

Results

Research Trends

Figure 1 illustrates the percentage of publications related to benthic macroinvertebrates and potential bio-indicators of benthic macroinvertebrates in Malaysian streams for 12 years. There has been a surge in the use of benthic macroinvertebrates to evaluate Malaysia's river quality since 2011, with several peaks in 2013 and 2020. Meanwhile, benthic macroinvertebrates as potential bio-indicators started trending in 2011, recording the highest percentage in 2020. However, there is no significant relationship between the number of publications on benthic macroinvertebrates and the last 12 years (2011 to 2022) ($r = 0.241$: $p > 0.05$).

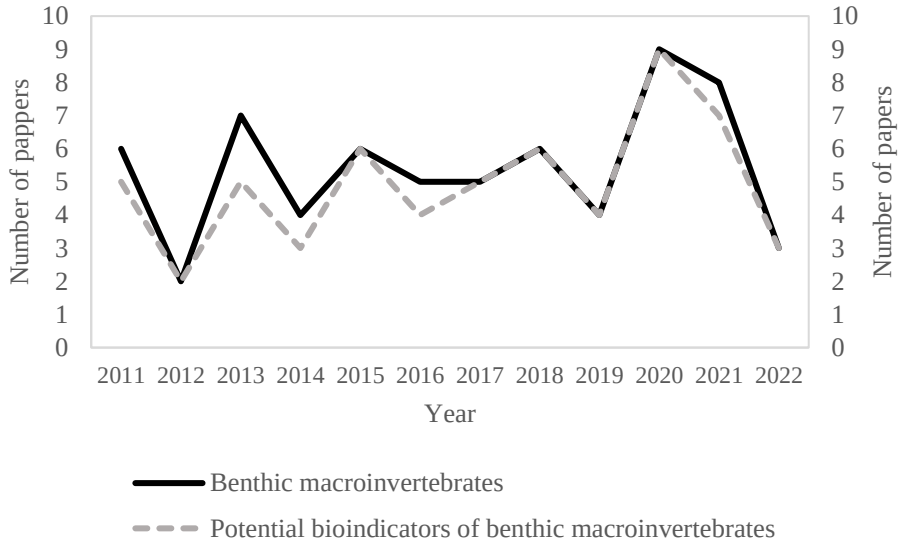

Figure 1. Time series plot for overall published papers on benthic macroinvertebrates and potential bio-indicators of benthic macroinvertebrates from 2010 to 2022.

Published Journals and Proceedings (Bibliographic Information)

Based on Figure 2, the Serangga Journal (Scopus indexed) published the highest number of papers. The second-highest papers were published in Sains Malaysiana (Journal Citation index: Q4), IOP Conference Series: Earth and Environmental Science, Sains Malaysiana, and Journal of Sustainability Science and Management. A total of five journals published in these databases were authored by researchers from Malaysian universities, namely Universiti Putra Malaysia (Pertanika Journal of Tropical Agricultural Science, and Pertanika Journal Science and Technology), Universiti Kebangsaan Malaysia (Serangga), and Universiti Sains Malaysia (Sains Malaysiana, and Tropical Life

DOI:https//doi.org/10.22452/mjs.vol43no1.7
Malaysian Journal of Science 43(1): 72-85 (March 2024)

Sciences Research). In addition, Jurnal Teknologi published two research papers on aquatic ecology. Many previous studies that identified potential benthic macroinvertebrates as biological indicators were published in high-impact journals, with the highest percentage (53.57%) recorded in Scopus index journals, followed by Journal Citation Report (JCR) index journals (25.00%), including Q1 and Q2. Moreover, approximately 14.29% of papers on this research area were published in other indexed journals, and about 7.14% of papers included proceedings. Meanwhile, only eight research papers related to potential bio-indicators were published in conference proceedings, notably the IOP Conference Series: Earth and Environmental Science Proceedings.

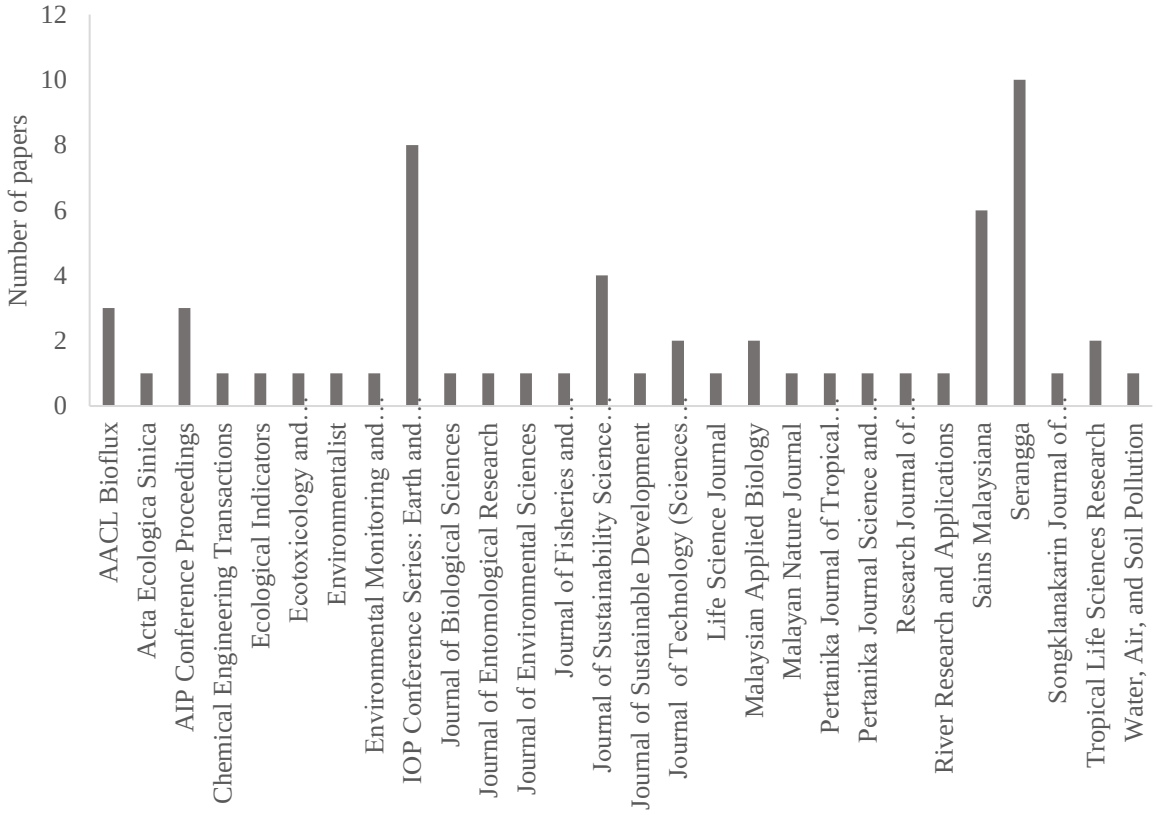

Figure 2. The number of published papers on benthic macroinvertebrates as potential bio-indicators.

There are two languages used by Malaysian researchers when they published their research: Malay and English. The Malay language was used in local journals, with 8.47% of publications related to potential bio-indicators. However, most research articles (91.53%) were published in English.

Geographical Locations of The Studies, Frequency of Measurement, and Replication

Most studies related to this discipline were conducted in Peninsular Malaysia (Table 1), and few were carried out in Sabah (five studies), while none were found in Sarawak.

Table 1. Geographical locations of the studies in Peninsular Malaysia with the year

State	River	River type	Year
Kedah	Tupah River	Forested	2012
	Selama River	Forested	2013
	Rivers of Gunung Jerai Forest Reserve	Forested	2017, 2019
	Rivers at various elevations of Gunung Jerai forest reserve	Forested	2019
	Perangin River	Recreational	2020
	Urian Perangin River		2020
Terengganu	Two freshwater streams of Hulu Terengganu	Recreational	2011
	Ikan River	Recreational	2015
	Three streams of Terengganu	Forested	2018
	Mendak River	Recreational	2019

DOI:https//doi.org/10.22452/mjs.vol43no1.7
Malaysian Journal of Science 43(1): 72-85 (March 2024)

Kelantan	Dawai and Dekong rivers	Forested	2014
	Recreational rivers	Recreational	2018
	Lata Janggut Recreational Area	Recreational	2020, 2021
Perak	Rivers in the Bukit Merah catchment area	Forested	2017
	Air terjun Lata Kinjang	Recreational	2018
Penang	Juru River Basin	Urban	2011, 2012
	Pauh River, Cameron Highlands	Forested	2015
	Air Terjun River	Recreational	2018
	Sayong River	Recreational	2021
	Jeriau River	Recreational	2022
Selangor	Semenyih River	Urban	2011
	Penchala River	Urban	2013
	Congkak River	Recreational	2013
	Langat River	Urban	2014
	Selangor River	Urban	2020, 2022
Johor	Berasau River	Forested	2015
	Tropical forest streams in Gunung Pulai	Recreational	2015
	Johor River		2017
	Asah River in Pulau Tioman	Recreational	2018
	Pontian Besar, Ulu Sedili Besar, Endau, and Skudai rivers	Recreational and Urban	2019
	Bantang River	Recreational	2019
	Kawal River	Recreational	2021
Negeri Sembilan	Kongkoi River	Different land use area	2013
Pahang	Lata Meraung Waterfall	Recreational	2015
	Janda Baik River	Recreational	2018
	Jeriau River, Bukit Fraser		2022
Melaka	Asahan Waterfall	Recreational	2016

The highest percentage of studies focused on recreational rivers (36%), followed by forested streams (24%) and urban or polluted rivers (20%) in Malaysia (Figure 3).

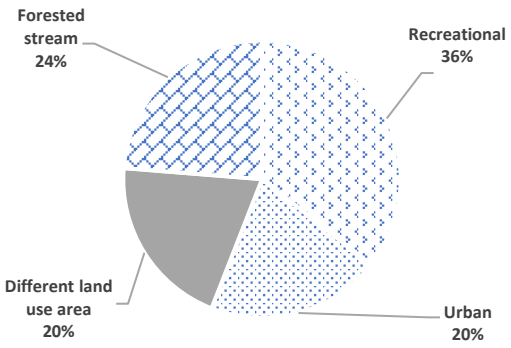

Figure 3. Study areas for potential bio-indicators research in Malaysian rivers.

Regarding the frequency of measurements (i.e., number of sampling during the study period), several researchers conducted (30.19%) only one sampling for biomonitoring of a particular river, while the other 18.87% did not state the frequency of measurements for their study. However, these researchers included the duration of their study. Meanwhile, approximately 22.64% of researchers conducted six samplings within a one-year study period. On the other hand, most studies did not mention the number of replicates used for their sampling (52.63%). However, several studies specified three (42.11%), five (3.51%), and six replicates (1.75%) of sampling to increase the precision of the study.

3.1.4 Taxonomic Identification of Identified Potential Bio-Indicators and Methodological Information

Most studies on Malaysian rivers used benthic macroinvertebrates at the family level (47%) due to incomplete identification of tropical benthic macroinvertebrates, especially in Southeast Asia. However, some studies achieved identification up to the genus level (29%), and a smaller proportion managed to identify them down to the species level (10%), as depicted in Figure 4.

DOI:https//doi.org/10.22452/mjs.vol43no1.7
Malaysian Journal of Science 43(1): 72-85 (March 2024)

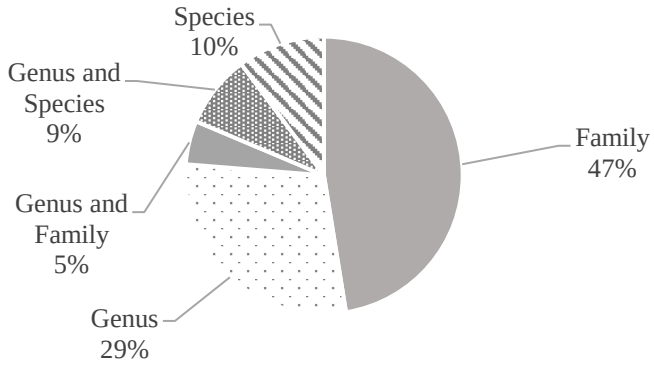

Figure 4. Resolution of taxonomic identification of benthic macroinvertebrates in reviewed studies.

According to Figure 5, a total of 22 families, namely Atyidae, Baetidae, Caenidae, Coenagrionidae, Chironomidae, Elmidae, Ephemerellidae, Euphaeidae, Gomphidae, Heptageniidae, Hydrophilidae, Hydropsychidae, Leptophlebiidae, Libellulidae, Perlidae, Potamanthidae, Simuliidae (Arthropoda), Hirudinidae, Lumbriculidae, Naididae, Turbificidae (Annelida), and Physidae (Mollusca) were identified as potential bio-indicators in Malaysian rivers. Chironomidae (9.11%) was identified as the dominant potential bio-indicator, followed by Baetidae (8.87%) and Hydropsychidae (8.62%). The examples of bio-indicators and relevant pollution identified from the previous studies are presented in Table 2.

Table 2. The bio-indicators identified with particular reference to the type of pollution

Common group	Bio-indicators	Type of pollution	Reference
Arthropoda	Atyidae	Clean water	(Kutty et al., 2017)
	Baetidae	Clean water	(Farah Safiah et al., 2020)
	Caenidae	Clean water	(Aweng et al., 2012)
	Coenagrionidae	Moderate pollution	(Al-Shami et al., 2014)
	Chironomidae	Urban pollution	(Al-Shami et al., 2013)
	Elmidae	Clean water	(Ahmad et al., 2013)
	Ephemerellidae	Clean water	(Azmi et al., 2018)
	Euphaeidae	Clean water	(Md Rawi et al., 2014)
	Gomphidae	Sensitive to pollution	(Suhaila et al., 2016)
	Heptageniidae	Clean water	(Hamid et al., 2016)
	Hydrophilidae	Clean water	(Mustaqim-Alias & Ahmad, 2013)
	Hydropsychidae	Clean water	(Nurhafizah-Azwa & Ahmad, 2018)
	Leptophlebiidae	Clean water	(Hettige et al., 2020)
	Libellulidae	Moderate pollution	(Al-Shami et al., 2011a)
	Perlidae	Clean water	(Mustaqim-Alias & Ahmad, 2013)
	Potamanthidae	Clean water	(Azmi et al., 2018)
	Simuliidae	Clean water	(Mohd Rasdi et al., 2012)
Annelida	Hirudinidae	Urban pollution	(Rak et al., 2011)
	Lumbriculidae	Urban pollution	(Hettige et al., 2020)
	Naididae (*Nais elinguis*)	Heavy metal pollution	(Othman et al., 2012).
		Urban pollution	(Rak et al., 2011)
	Turbificidae	Urban pollution	(Hettige et al., 2020)
Mollusca	Physidae	Urban pollution	(Mahazar et al., 2013)

DOI:https//doi.org/10.22452/mjs.vol43no1.7
Malaysian Journal of Science 43(1): 72-85 (March 2024)

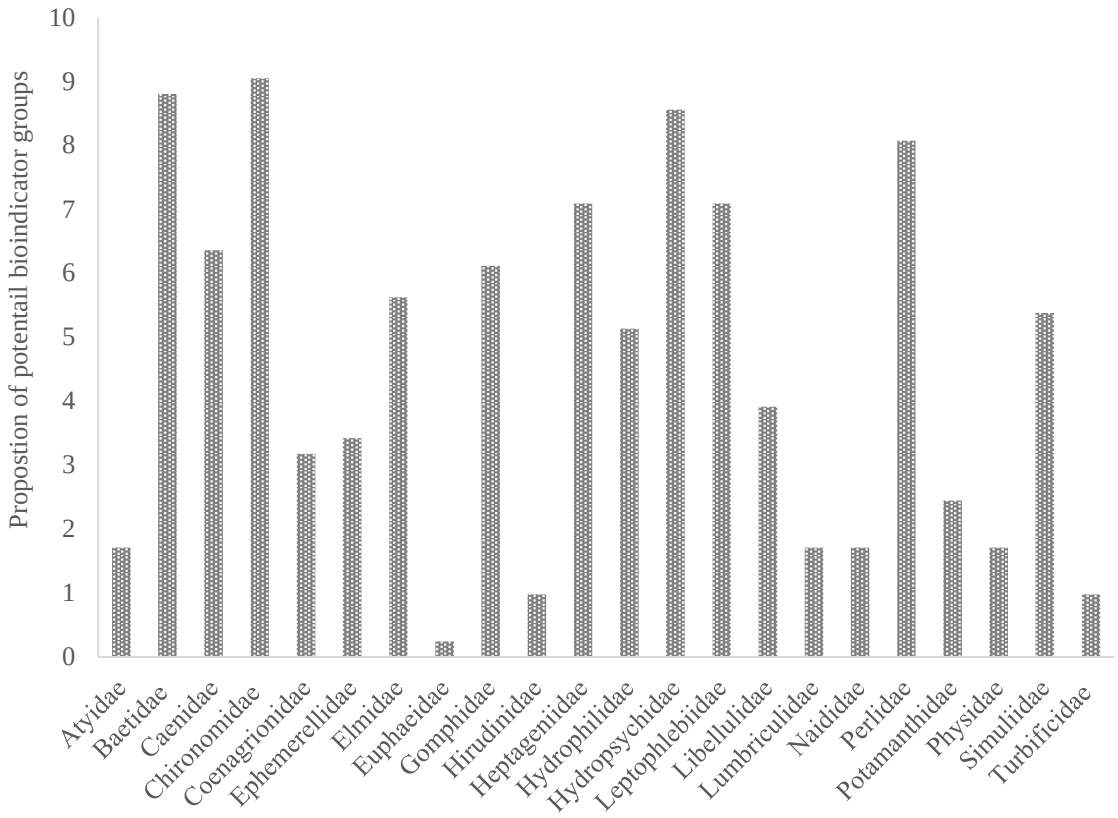

Figure 5. Benthic macroinvertebrate families were identified as potential bio-indicators.

Authors utilized many approaches in the analysis of benthic macroinvertebrates as bio-indicators. Based on Figure 6, the multivariate statistical analysis (28.99%) is currently the most popular option for these studies, followed by ecological indices (21.79%), biotic indices (20.29%), diversity indices (14.49%), diversity (8.70%), and genotoxicity (5.80%). Biotic and diversity indices (ecological indices) are commonly used in analyzing benthic macroinvertebrates. Out of all the reliable bio-indices, the biological monitoring working party (BMWP) (33.3%) is the most frequently used bio-indices, besides the Family Biotic Index (FBI) (17.33%) and Average Score Per Taxon (ASPT) (16.00%). Meanwhile, the Shannon-Weiner diversity index (29.49%) and the Margalef index (16.67%) are the most frequently used when considering diversity indices.

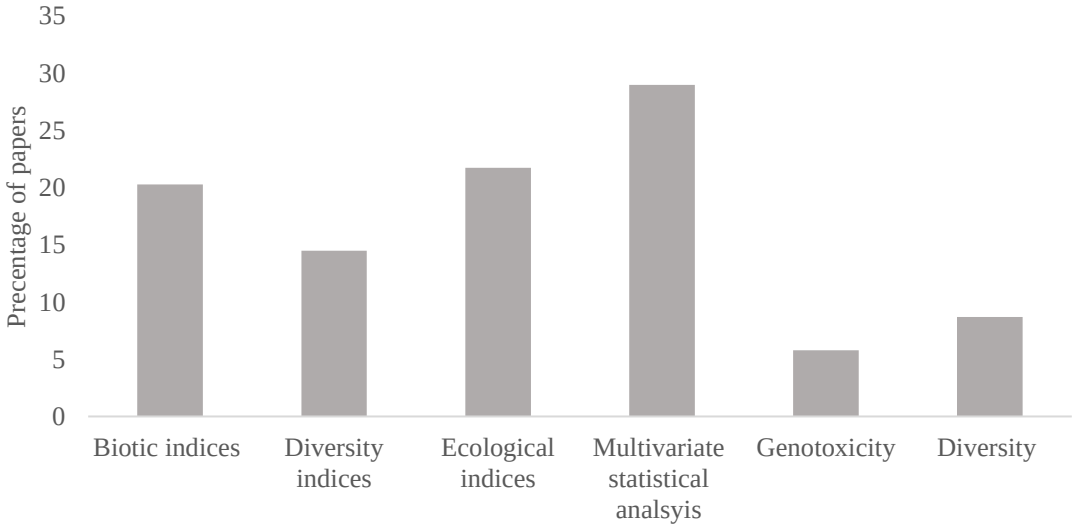

Figure 6. Approaches used in potential bio-indicators studies.

DOI:https//doi.org/10.22452/mjs.vol43no1.7
Malaysian Journal of Science 43(1): 72-85 (March 2024)

Visualized Analysis

Bibliographic Coupling Analysis

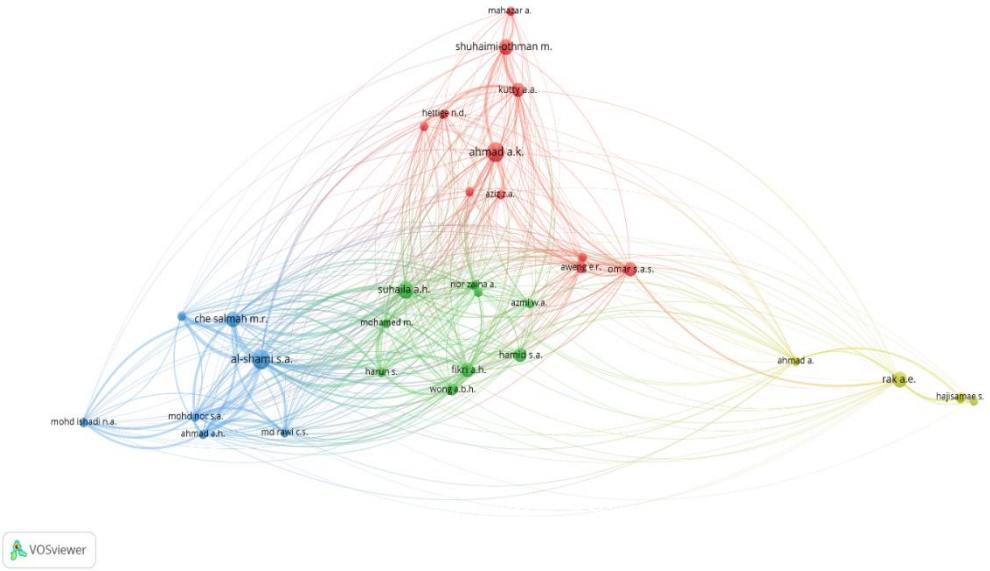

Figure 7. Bibliographic coupling analysis of authors.

Thirty-three authors were identified with a minimum threshold of two publications from a single author (Figure 7). The top three authors with the greatest total link strength were Al-Shami, S. A. (n = 1880), Suhaila, A. H. (n = 655), and Ahmad, A.K. (n = 461).

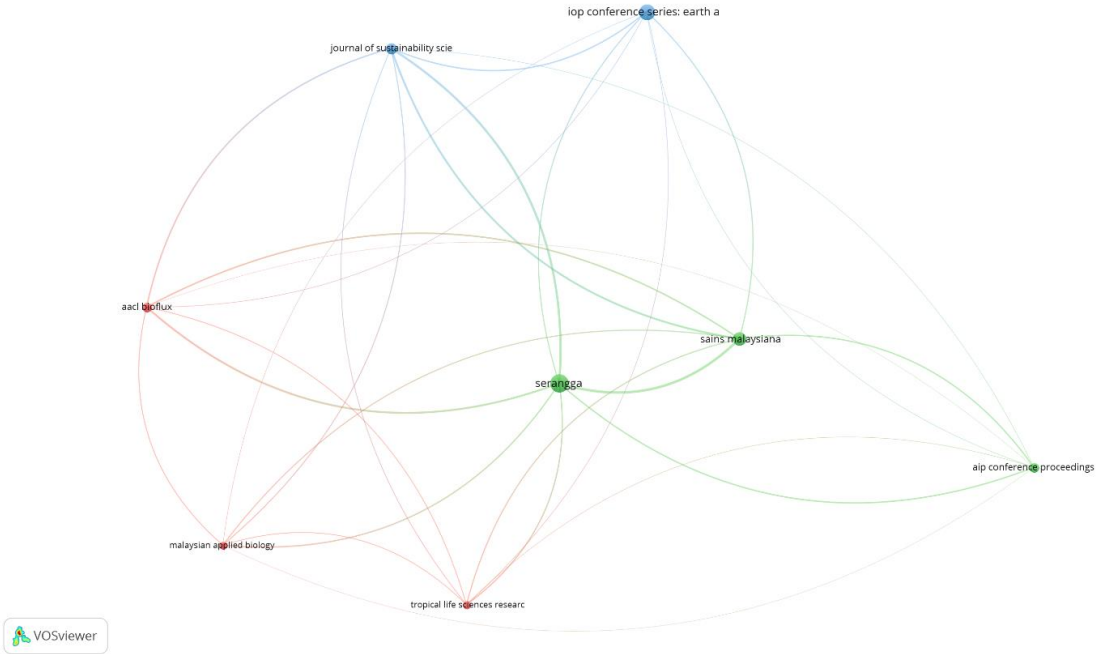

Figure 8. Bibliographic coupling analysis of journals and proceedings.

Of the 30 journals, 8 meet the minimum threshold of two (Figure 8). The top three journals with the greatest total link strength were Serangga Journal (n = 173), Sains Malaysiana (n = 145), and IOP Proceeding Conference Series: Earth and Environmental Science (n = 44).

DOI:https//doi.org/10.22452/mjs.vol43no1.7
Malaysian Journal of Science 43(1): 72-85 (March 2024)

Figure 9. Bibliographic coupling analysis of organizations.

The top three organizations with the greatest total link strength were the Institute for Tropical Biology and Conservation, Universiti Malaysia Sabah (n = 143), the School of Biological Science, Universiti Sains Malaysia (n = 71), and the Department of Technology and Natural Resources, Faculty of Applied Sciences and Technology, Universiti Tun Hussein Onn Malaysia (39) (Figure 9).

Discussion

The application of benthic macroinvertebrates as bio-indicators has received much scientific attention for continuous pollution monitoring due to the limitation posed by physicochemical parameters as a monitoring tool in freshwater ecosystems. An assessment of the literature on macroinvertebrates as bio-indicators in Malaysian rivers reveals a consistent upward trend over the years. As a result, many studies now concentrate on the health assessment of streams and rivers using benthic macroinvertebrates as bio-indicators in Malaysia, albeit many research gaps remain in this discipline. The papers were mainly published in leading periodicals with relevant scopes, including research on freshwater ecology. In addition, many papers with different studies were published in journals, e.g., Serangga and Sains Malaysiana.

Moreover, the reviewed findings also showed that the identification of macroinvertebrates primarily relies on morphological characteristics. Based on descriptive statistics, most studies in Malaysian rivers use benthic macroinvertebrates at the family level due to incomplete identification of tropical benthic macroinvertebrates, especially in Southeast Asia. Therefore, identifying up to the species level is vital to separate benthic macroinvertebrates based on their sensitivity to pollution. However, no studies have reported the use of molecular methods, such as Environmental DNA sequencing, to support or facilitate the identification of benthic macroinvertebrates in Malaysian rivers. Therefore, gaps still exist in the identification of benthic macroinvertebrates.

Many bio-indicator studies focused on microscopic identifications, along with biotechnology and toxicology analysis. Toxicity testing was also used to identify suitable organisms as bio-indicators, such as Oligochaeta. Only one toxicity test has been reported with Naididae (aquatic Oligochaeta) in Malaysia (Othman et al., 2012). This study identified *Nais elinguis* as a bio-indicator for heavy metal pollution, but this research did not conduct biomonitoring. Thus, in-depth research such as bioassay and toxicology tests are needed to realize the potential of Naididae as bioindicators fully. Besides, a genotoxicity study was conducted on *Chironomus kiiensis* in the Juru River (Al-Shami et al., 2013). The study revealed that sediments polluted by industrial wastes exhibit a more pronounced and immediate adverse genetic impact compared to urban pollution. As such, including molecular and genetic techniques is imperative in benthic macroinvertebrate studies in Malaysian rivers.

Biomonitoring is mainly categorized into four main approaches: single metrics, multimetric, multivariate, and models. Biological indices primarily consider the tolerance score of specific benthic macroinvertebrates (Blakely et al., 2014), which provides a clear idea about the bio-indicator taxa. However, in some southeast countries, taxa like Protoneuridae do not have tolerance values in the Family Biotic Index (FBI) due to the adaptation of the FBI by researchers from other countries to suit the context of their geographical regions. Hence, the development of a multimetric index using benthic macroinvertebrates is essential. For instance, Arman et al. (2019) developed a Malaysian water quality index based on aquatic

DOI:https//doi.org/10.22452/mjs.vol43no1.7
Malaysian Journal of Science 43(1): 72-85 (March 2024)

invertebrates specific to four different catchments in Johor State, Malaysia. Therefore, developing a multimetric index based on the benthic macroinvertebrates with an extensive nationwide database is also necessary. This initiative would benefit many bio-indicator studies within the local context, with a comprehensive collection of taxa throughout Malaysia.

Many studies conducted in Peninsular Malaysia were based on the geographical extent of studies. However, there were limited studies in Perak, Melaka, and Negeri Sembilan. On top of that, biomonitoring studies in rivers and streams of Sabah and Sarawak are still lacking; thus, species richness and ecology of aquatic invertebrates remain unknown in these regions. Yong & Yule (2004) stated similar findings. Also, many studies have been conducted on Peninsular Malaysia recreational rivers. Benthic macroinvertebrates' distribution varies based on geological location, elevation, and habitat condition (Mohd Rasdi et al., 2012; Min & Kong, 2020). Researchers in Peninsular Malaysia often select a mostly polluted river (e.g., Juru River, Penang) (Al-Shami et al., 2011a; Al-Shami et al., 2011b). Thus, there is a crucial need to direct future research towards urban rivers, given the limited understanding of the diverse impacts on the conditions of benthic macroinvertebrates in this specific river type.

In addition, most studies have focused on a one-time frequency of occurrence. Consequently, much sampling is required to obtain accurate data on invertebrates' life cycles and better represent benthic macroinvertebrates. Furthermore, multiple replicates substantially improve the data's precision and allow more minor changes to be detected. Therefore, conducting a minimum of three replicates is recommended to obtain reliable measures for ecological monitoring (Mavrič et al., 2013).

Bibliographic maps provide a valuable aid in the investigation of bibliographic coupling. To ensure a thorough analysis, focusing on the top three authors and journals of significance is recommended. This approach helps to analyze the relationships among each author, the journals, and the impact of their research in this field. The bibliographic coupling also highlights the most productive journals and their connections in this study area. This study is the first to present the primary paths of bibliographic coupling research besides examining the bibliographies of authors, journals, and organizations. The results of the primary path analysis indicate a future research trend, which involves consolidated analysis based on diverse citation structures and textual similarity.

4. Conclusions

This review has revealed the bias and gaps in scientific publications for future research needs in bio-indicators studies. The Atyidae, Baetidae, Caenidae, Coenagrionidae, Chironomidae, Elmidae, Ephemerellidae, Euphaeidae, Gomphidae, Heptageniidae, Hydrophilidae, Hydropsychidae, Leptophlebiidae, Libellulidae, Perlidae, Potamanthidae, Simuliidae (Athropoda), Hirudinidae, Lumbriculidae, Naididae, Turbificidae (Annelida), and Physidae (Mollusca) were identified as the most popular potential biological indicator species in Malaysian streams and rivers due to their presence in the most favorable environmental conditions in aquatic ecosystems. Several recommendations were given to overcome the research gaps in studies on benthic macroinvertebrates as potential bio-indicators, such as modeling and developing the multimeric index. Besides, species identification is scarce in Malaysia compared with other Asian countries. Identifying taxa up to the species level is difficult due to the lack of taxonomic expertise; hence, the eDNA barcoding method with the power of the next-generation sequencing technique can be applied to overcome this limitation.

Also, there is an urgent need for new studies to address the limited bioassay and toxicology tests in identifying certain benthic macroinvertebrates as potential bio-indicators. Moreover, since little attention is given to benthic macroinvertebrate studies in Sabah and Sarawak, studies in these geological locations are most pertinent. Lastly, proper coordination among government agencies and private organizations is crucial in developing benthic macroinvertebrate studies, especially in preparing a database that includes all publications related to benthic macroinvertebrates. Furthermore, this science mapping approach appears to be the first bibliographic analysis of Malaysian research on potential bio-indicators of benthic macroinvertebrates in streams and rivers.

5. Recommendations for Wayforward

- In order to disseminate their research widely and reach a diverse audience, researchers worldwide rely on publishing their findings in a variety of high-impact journals, both locally and internationally. To effectively communicate their knowledge to a global audience, they must use English as the primary language while publishing their research.
- Bibliographic analysis is a highly effective method for evaluating the status and trends of current research. Through bibliographic coupling analysis of journals and proceedings, we have discovered that the two Malaysian journals with the greatest total link strength were also the top two with the highest total link strength. Further analysis of authors and organizations revealed that the three authors with the most publications were affiliated with the three institutions that made the most significant contributions. This research highlights the value of bibliographic analysis for understanding research trends and identifying key players in a given field.
- It is imperative to enhance the accessibility of the macroinvertebrate database to facilitate its utilization by other researchers. Such an action will unlock new avenues for research and application in freshwater management and conservation.
- Developing a multimetric index is an effective method to classify the various impacts of pollution. Such indices can encompass a wide range of information and data, which are then condensed into a single figure, making it easier to understand and compare the different pollution levels.

DOI:https//doi.org/10.22452/mjs.vol43no1.7
Malaysian Journal of Science 43(1): 72-85 (March 2024)

The resulting index can provide valuable insights into pollution's severity and help guide efforts to mitigate its adverse effects.

7. Acknowledgments

The authors would like to acknowledge Universiti Putra Malaysia for providing permission to submit this review paper. Finally, the authors would like to thank the Sri Lanka Council for Agricultural Research Policy (SLCARP) and National Aquatic Resource Research and Development Agency (NARA), Crow Island, Colombo 15, Sri Lanka, for Nadeesha's postgraduate scholarship grant and study leave, respectively.

6. References

Aazami J., Esmaili-Sari A., Abdoli A., Sohrabi H., & Brink PJVD. (2015). Monitoring and assessment of water health quality in the Tajan River, Iran using physicochemical, fish and macroinvertebrates indices. Journal of Environmental Health Science & Engineering 13(1): 1–12. https://doi.org/org/10.1186/s40201-015-0186-y.

Ahmad A. K., Aziz ZA., Fun HY., Ling TM., & Othman M.S. (2013). Makroinvertebrat bentik sebagai penunjuk biologi di Sungai Kongkoi, Negeri Sembilan, Malaysia. Sains Malaysiana 42(5): 605–614.

Al-Shami SA., Hishamuddin SN., Md Rawi CS., Abdul NH., & Ahmad AH. (2014). Developmental instability in Odonata larvae in relation to water quality of Serdang River, Kedah, Malaysia. Life Science Journal 11(7): 152–159.

Al-Shami SA., Md Rawai CS., Hassan AA., Hamid SA., & Azizah MNS. (2011a). Influence of agricultural, industrial, and anthropogenic stresses on the distribution and diversity of macroinvertebrates in Juru River Basin, Penang, Malaysia. Environmental Monitoring and Assessment 177(5): 233–244. https://doi.org/10.1007/s10661-010-1630-1

Al-Shami, S. A., Md Rawi, C. S., Hassan, A. A., & Azizah, M. N. S. (2011b). Fluctuating Asymmetry of Chironomus spp . (Diptera : Chironomidae) Larvae in Association with Water Quality and Metal Pollution in Permatang Rawa River in the Juru River Basin , Penang, Malaysia. Water Air and Soil Pollution 216: 203–216. https://doi.org/10.1007/s11270-010-0528-4

Al-Shami SA., Md Rawi CS., Ahmad AH., Madrus MR., Hamid SA., Ghani WMHWA., Al-Harbi NA., & AlMutairi KA. (2017). Biodiversity patterns of aquatic macroinvertebrates in tropical forests streams as a response to logging activities and deforestation. Acta Ecologica Sinica 37(5): 332–339. https://doi.org/10.1016/j.chnaes.2017.03.004

Al-Shami SA., Md Rawi CS., Nor SZM., Ahmad AH., Adibah NUR., & Dieng H. (2013). Genotoxicity in Chironomus kiiensis (Chironomidae: Diptera) after exposure to polluted sediments from Rivers of North Peninsular Malaysia: Implication for ecotoxicological monitoring. River Research and Applications 29(1): 1195–1204. https://doi.org/https://doi.org/10.1002/rra.2594

Arman NZ., Salmiati S., Said MIM., & Aris A. (2019). Development of macroinvertebrate-based multimetric index and establishment of biocriteria for river health assessment in Malaysia. Ecological Indicators 104(1): 449–458. https://doi.org/10.1016/j.ecolind.2019.04.060

Armitage PD., Moss D., Wright JF., & Furse MT. (1983). The performance of a new biological water quality score system based on macroinvertebrates over a wide range of unpolluted running-water sites. Water Research 17(3), 333–347. https://doi.org/10.1016/0043-1354(83)90188-4

Arsad A., Abustan I., Md Rawi CS., & Syafalni S. (2012). Integrating biological aspects into river water quality research in Malaysia: An opinion. OIDA International Journal of Sustainable Development 4(2): 107–122.

Aweng ER., Suhaimi O., Nur Izzati S., Suhaimi E., & Nur Izzati O. (2012). Benthic macroinvertebrate community structure and distribution in Sungai Pichong, Gunung Chamah, Kelantan, Malaysia. American International Journal of Contemporary Research 2(1): 163–167. www.aijcrnet.com

Azmi WA., Hussin NH., & Amin NM. (2018). Monitoring of water quality using aquatic insect as biological indicators in three streams of Terengganu. Journal of Sustainability Science and Management 13(1): 67–76. http://jssm.umt.edu.my/wp-content/uploads/sites/51/2018/06/bab-6.pdf

Azrina MZ., Yap CK., Rahim Ismail A., Ismail A., & Tan SG. (2006). Anthropogenic impacts on the distribution and biodiversity of benthic macroinvertebrates and water quality of the Langat River, Peninsular Malaysia. Ecotoxicology and Environmental Safety 64(3): 337–347. https://doi.org/10.1016/j.ecoenv.2005.04.003

DOI:https//doi.org/10.22452/mjs.vol43no1.7
Malaysian Journal of Science 43(1): 72-85 (March 2024)

Barbour MT., Gerritsen J., Snyder BD., Stribling JB. (1999). Rapid bioassessment protocols for use in streams and wadeable rivers: periphyton, benthic macroinvertebrates and fish. US Environmental Protection Agency Office, Washington DC. 399 pp.

Belal AAM., El-Sawy MA., & Dar MA. (2016). The effect of water quality on the distribution of macro-benthic fauna in Western Lagoon and Timsah Lake, Egypt. Egyptian Journal of Aquatic Research 42(4): 437–448. https://doi.org/10.1016/j.ejar.2016.12.003.

Bishop J. (1973). Limnology of a small Malayan River Sungai Gombak, pp. 1-491, (J. Illies (Eds.); 22nd Ed. Dr. W. Junnk B.V., Publishers, Hague.

Blakely TJ., Eikaas HS., & Harding JS. (2014). The Singscore: A macroinvertebrate biotic index for assessing the health of Singapore's streams and canals Raffles. Bulletin of Zoology 62(1): 540–548.

Dacayana CML., Hingco JT., Socorro MMLD. (2013). Benthic macroinvertebrate assemblage in Bulod River, Lanao del Norte, Philippines. Journal of Multidisciplinary Studies 2(1): 2350–7020. https://doi.org/10.7828/jmds.v2i1.398.

Diya SG., Gasim MB., Toriman ME., & Abdullahi MG. (2015). Floods in Malaysia historical reviews, causes, effects and mitigations approach. International Journal of Interdisciplinary Research and Innovations *2*(4): 59–65.

Dorji K. (2016). Utility of an existing biotic score method in assessing the stream health in Bhutan (Ph.D). Queensland University of Technology, Australia.

Ekka A., Pande S., Jiang Y., & Zaag P. (2020). Anthropogenic modifications and river ecosystem services: A landscape perspective. Water (Switzerland) 12(10): 1–21. https://doi.org/10.3390/w12102706.

Esposito S., Loppi S., Monaci F., Paoli L., Vannini A., Sorbo S., Maresca V., Fusaro L., Karam E. A., Lentini M., De Lillo A., Conte B., Cianciullo P., & Basile A. (2018). In-field and in-vitro study of the moss *Leptodictyum riparium* as bioindicator of toxic metal pollution in the aquatic environment: Ultrastructural damage, oxidative stress and HSP70 induction. PLoS ONE 13(4), 1–16. https://doi.org/10.1371/journal.pone.0195717

Farah Safiah AN., Ahmad AK., Nurhafizah-Azwa S. (2020). Kualiti air dan kepelbagaian makroinvertebrat bentik, di Sungai Durian Perangin, Pulau Langkawi, Kedah, Malaysia. Serangga 25(2):10–23.

Flores MJL., Zafaralla MT. (2012). Macroinvertebrate composition, diversity and richness in relation to the water quality status of Mananga River, Cebu, Philippines. Philippine Science Letter 5(2): 103–113.

Gallacher D. (2001). The application of rapid bioassessment techniques based on benthic macroinvertebrates in East Asian rivers (a review). Internationale Vereinigung Für Theoretische Und Angewandte Limnologie: Verhandlungen 27(6): 3503–3509. https://doi.org/10.1080/03680770.1998.11902480.

Ghani WHWA., Md Rawi CS., Hamid SA. (2016). Variation in environmental conditions influences diversity and abundance of Ephemeroptera in forest streams of northern Peninsular Malaysia. Tropical Ecology 57(3): 489–501.

Guo YM., Huang ZL., Guo J., Li H., Guo XR., & Nkeli MJ. (2019). Bibliometric analysis on smart cities research. Sustainability (Switzerland) 11(13): 1–18. https://doi.org/10.3390/su11133606

Hamid SA., Rawi, CSM., & Ahmad AH. (2016). Life history of Thalerosphyrus (Ephemeroptera : Heptageniidae) in tropical rivers with reference to the varying altitude. Tropical Life Sciences Research 27(1): 43–62.

Hettige ND., Hashim RB., Kutty, ABA., Jamil NRB., & Ash'aari ZHB. (2020). Application of ecological indices using macroinvertebrate assemblages in relation to aquaculture activities in Rawang Sub-basin, Selangor River, Malaysia. Pertanika Journal Science & Technology 28(S2), 25–45.

Hilsenhoff WL. (1988). Rapid field assessment of organic pollution with a family-level biotic index. Journal of the North American Benthological Society *7*(1): 65–68. https://doi.org/10.2307/1467832

Jun YC., Won DH., Lee SHH., Kong DS., & Hwang SJ. (2012). A multimetric benthic macroinvertebrate index for the assessment of stream biotic integrity in Korea. International Journal of Environmental Research and Public Health 9(10): 3599–3628. https://doi.org/10.3390/ijerph9103599

Klemm DJ., Blocksom KA., Thoeny WT., Fulk, FA., Herlihy AT., Kaufmann PR., & Cormier SM. (2002). Methods development and use of macroinvertebrates as indicators of ecological conditions for streams in the Mid-Atlantic Highlands Region. Environmental Monitoring and Assessment 78(1), 169–212. https://doi.org/10.1023/A:1016363718037

Kumari D., & Paul DK. (2020). Assessing the role of bioindicators in freshwater ecosystem. Journal of Interdisciplinary Cycle Research 7(9): 58–74.

DOI:https//doi.org/10.22452/mjs.vol43no1.7
Malaysian Journal of Science 43(1): 72-85 (March 2024)

Kutty AA., Fauzi NMS., Nurhafizah-Azwa, Rak AE, & Oma SAS. (2017). Potential of benthic macroinvetebrates as biological indicator in recreational river ecosystem. Serangga 24(1): 42–57.

Mahazar A., Othman MS., Kutty AA., & Desa MNM. (2013). Monitoring urban river water quality using macroinvertebrate and physico-chemical parameters: Case study of Penchala River, Malaysia. Journal of Biological Sciences 13(6): 474–482. https://doi.org/10.3923/jbs.2013.474.482

Manickavasam S., Sudhan C., Bharathi & Aanand S. (2019). Bioindicators in aquatic environment and their significance. Journal of Aquaculture In The Tropics 34(1–2): 73–79. https://doi.org/10.32381/jat.2019.34.1-2.6

Margalef, R. (1958). Information theory in ecology. General Systems 3(1911): 36–37.

Mavrič B., Urbanič G., Lipej L., & Simboura N. (2013). Influence of sample size on ecological status assessment using marine benthic invertebrate-based indices. Marine Ecology 34(1): 72–79. https://doi.org/10.1111/j.1439-0485.2012.00526.x

Md Rawi CS., Al-Shami SA., Madrus MR., & Ahmad AH. (2014). Biological and ecological diversity of aquatic macroinvertebrates in response to hydrological and physicochemical parameters in tropical forest streams of Gunung Tebu, Malaysia : implications for ecohydrological assessment. Ecohydrology 7(2): 496–507. https://doi.org/10.1002/eco.1368

Min JK., & Kong DS. (2020). Distribution patterns of benthic macroinvertebrate communities based on multispatial-scale environmental variables in the river systems of Republic of Korea. Journal of Freshwater Ecology 35(1): 323–347.

Mohd Rasdi Z., Fauziah I., Ismail R., Mohd Hafezan S., Fairuz K., Hazmi AD., & Md Rawi CS. (2012). Diversity of aquatic insects in Keniam River, National Park, Pahang, Malaysia. Asian Journal of Agriculture and Rural Development *2*(3): 312–328. https://doi.org/DOI: 10.22004/ag.econ.197977.

Mazur R., Shubiao W., Szoszkiewicz K., Bedla D., & Nowak A. (2016). A Lymnaea stagnalis embryo test for toxicity bioindication of acidification and ammonia pollution in water. Water 8(1): 1–15. https://doi.org/10.3390/W8070295

Mustaqim-Alias M., & Ahmad AK. (2013). Benthic macroinvertebrates diversity and water quality assessment at Sungai Congkak recreational area, Hulu Langat, Selangor. In Murad AMA., Yen CC., Ismail ES., Maskat MY., Noorani MSM., Ibrahim N., Karim NHA., Yahya R., Khalid RM., Ismail WR., Ling, WS., & Ibrahim, Z. (eds.), AIP Conference Proceedings (Vol. 1571, pp. 608–613). https://doi.org/10.1063/1.4858721

Narangarvuu D., Hsu C., Shieh S., Wu F., & Yang P. (2014). Macroinvertebrate assemblage patterns as indicators of water quality in the Xindian watershed, Taiwan. Journal of Asia-Pacific Entomology 17(3): 505–513. https://doi.org/10.1016/j.aspen.2014.04.011

Nurhafizah-Azwa S. & Ahmad AK. (2018). Biodiversity of benthic macroinvertebrates in Sungai Kisap, Langkawi, Kedah, Malaysia. Journal of Tropical Resources and Sustainable Science 6(1): 36–40. http://www.jtrss.org/JTRSS/volume6/JTRSS-07-02-18-KT8/6-1-36-40.pdf

Othman MS., Nadzifah Y., Umirah NS., & Ahmad AK. (2012). Toxicity of metals to an aquatic worm, Nais elinguis (Oligochaeta, Naididae). Research Journal of Environmental Toxicology 6(4): 122–132. https://doi.org/10.3923/rjet.2012.122.132

Parmar TK., Rawtani D., & Agrawal YK. (2016). Bioindicators: the natural indicator of environmental pollution. Frontiers in Life Science 9(2): 110–118. https://doi.org/10.1080/21553769.2016.1162753

Peyravi, M., Jahanshahi, M., & Houshmand, T. (2020). Priority and emerging pollutants in water. In P. Devi, P. Singh, & S. K. Kansal (Eds.), Inorganic pollutants in water (pp. 97–103). Elsevier Academic Press.

Rak A., Said I., & Mohamed M. (2011). Effects of land use on benthic macroinvertebrate assemblages at three rivers in Endau catchment area , Kluang ,Johor, Malaysia. Journal of Applied Sciences in Envrionmental Sanitation 6(2): 97–103. http://civil.utm.my/ismid/files/2013/01/Effects-of-land-use-on-Benthic-Macroinvertebrate-assemblages-at-three-rivers-in-Endau-Catchment-Area.pdf

Resh VH. (2007). Multinational, freshwater biomonitoring programs in the developing world: lessons learned from African and Southeast Asian River surveys. Environmental Management 39: 737–748. https://doi.org/10.1007/s00267-006-0151-8

Selvanayagam M., & Abril R. (2016). Use of benthic macroinvertebrates as a biological indicator in assessing water quality of River Puyo, Puyo, Pastaza, Ecuador Mariadoss. American Journal of Life Sciences 4(1): 1–12. https://doi.org/10.11648/j.ajls.20160401.11

Shafie MSI., Wong ABH., Harun S., & Fikri AH. (2017). Land use influence on the aquatic insect communities on tropical forest streams of Liwagu River, Sabah, Malaysia. AACL Bioflux 10(2), 341–352.

DOI:https//doi.org/10.22452/mjs.vol43no1.7
Malaysian Journal of Science 43(1): 72-85 (March 2024)

Shannon C E. (1948). A mathematical theory of communication. Bell System Technical Journal 27(3): 379–423.

Sharma S., Dubey S., Chaurasia R., & Dave V. (2013). Macro-invertebrate community diversity in relation to water quality status of Kunda River (M.P.), India. Discovery 3(9): 40–46.

Simpson, E. H. (1949). Measurement of diversity. Nature, 163(1), 688.

Suhaila, A. H., Che Salmah, M. R., & Nurul Huda, A. (2016). Composition and distribution of odonata larvae and its relationship with physicochemical water quality in Northern Peninsular Malaysia. Malaysian Journal of Science 35(2): 213–225.

Tampus AD., Tobias EG., Amparado RF, Bajo L., & Sinco AL. (2012). Water quality assessment using macroinvertebrates and physico-chemical parameters in the riverine system of Iligan City, Philippines. Advances in Environmental Sciences Bioflux 4(2): 59–68. http://www.aes.bioflux.com.ro

Tan KW., & Beh WC. (2015). Water quality monitoring using biological indicators in Cameron Highlands Malaysia. Journal of Sustainable Development 8(3): 28–42. https://doi.org/10.5539/jsd.v8n3p28

Yong S. H., Yule C M. (2004). Freshwater invertebrates of the Malaysian region. pp. 1–337, Malaysia: Akademi Sains Malaysia.

Yusop Z., Kadir A A., Noor Z Z. (2017). Benthic macroinvertebrate composition and water quality status in Sungai Johor, Johor, Malaysia Chemical Engineering Transactions. 56(1): 187–192. https://doi.org/10.3303/CET1756032.

Zyoud S H., Al-Jabi S W., Sweileh W M., Awang R. (2014). A bibliometric analysis of research productivity of Malaysian publications in leading toxicology journals during a 10-year period (2003-2012). Human and Experimental Toxicology 33(12): 1284–1293. https://doi.org/10.1177/0960327113514101.

DOI:https//doi.org/10.22452/mjs.vol43no1.7
Malaysian Journal of Science 43(1): 72-85 (March 2024)

MALAYSIAN JOURNAL OF SCIENCE
MJS
ISSN 1394-3065

Regular Issue

Malaysian Journal of Science 43(1): 86-112 (March 2024) https://mjs.um.edu.my

SYNTHESIS AND BIOLOGICAL ACTIVITIES OF ACETAMINOPHEN AND IBUPROFEN METAL COMPLEXES OR DERIVATIVES: A REVIEW

Azni Izwati Hamdan[1a], Dike Dandari Sukmana[2a] and Norsyafikah Asyilla Nordin[3a]*

Abstract: We reviewed scientific literature on the synthesis of acetaminophen and ibuprofen, as well as their derivatives and biological properties. The synthesis of acetaminophen involves the acetylation of 4-aminophenol and acetic anhydride, while ibuprofen is synthesised by reacting isobutyl benzene and acetic anhydride in four continuous reaction stages, which are Friedel-Crafts acylation, carbonyl reduction, chloride substitution, and Grignard reaction. To obtain their derivatives, modifications have been made either by complexing the main structure of the drug compound with metal elements or adding certain desired moieties, such as thiourea, amide, ammonium, halogen, silicon, and 1,3,4-oxadiazole. Ibuprofen and acetaminophen have been recognised as effective painkillers and anti-inflammatories. Recently, their derivatives have been implicated in a variety of biological effects. The biological activities of acetaminophen and ibuprofen derivatives have been reported to exhibit urease inhibition and inflammatory inhibition, as well as inhibit the proliferation of breast cancer cells MCF-7. Overall, this review article describes the synthesis of acetaminophen and ibuprofen derivatives, complete with their biological activities such as antimicrobial, antifungal, anti-inflammatory, urease inhibitors, and anticancer.

Keywords: *Acetaminophen, ibuprofen, biological activity, chemical modification, comparative study*

1. Introduction

Human and diseases are inseparable. It is not an exaggeration to say that the plagues that happened over centuries are actually the humans' fault (Kiriiri et al., 2020). On the bright side, due to these phenomena, researchers have identified several ailments and listed a large range of herbal and other treatments. For instance, anaesthetic was one of the first synthetic chemicals ever made. This led to the development of synthetic organic chemistry, which led to the growth of the pharmaceutical industry (Hill & Rang, 2013). Pharmaceutical chemists are employed by the sector to design pharmaceuticals, perform drug research, and oversee quality assurance procedures. Nevertheless, issues with the efficacy and toxicity of medicinal drugs have impeded their success in clinical use, leading to the introduction of molecular/chemical modification. There exists a range of chemical modifications that can enhance various biological properties, including stability, cellular uptake, and potency (Corey, 2007). Drug designing can alter the chemical structure of the established drugs and integrate the principle of organic compounds, producing a tailored drug (Hughes et al., 2011). This approach establishes new research avenues and also introduces a novel compound with demonstrable therapeutic effect (Akhondzadeh, 2016).

There are many reasons on why therapeutic effect is important to the human body. For example, inflammation is common as it is adaptive immune response to infection. If left unchecked for a certain time, it may result in neurodegenerative disease or cancer (Dinarello, 2010). Therefore, anti-inflammatory drug is required. On the other hand, antimicrobial resistance is rapidly increasing, making infections from Gram-positive and Gram-negative pathogens difficult to almost impossible to treat (Collignon et al., 2016). Unsurprisingly, inappropriate prescription and poor antimicrobial control have also contributed to massive resistance issues (Reygaert, 2018). Another therapeutic effect is antiproliferative, which is used to inhibit cell growth on cells, especially tumours. This is an alternative approach in finding safe, effective, and stable drug modifications to treat or prevent cancer (AlKhalil et al., 2020).

Acetaminophen is known to have a mild antimicrobial activity due to the absence of enzyme that contributes to the mechanism of pain alleviation in microorganisms (Verma et al., 2020). Meanwhile, ibuprofen has low anticancer effects against several cancer cell lines (He et al., 2021; Pedro-Hernández et al., 2017) and does not inhibit urease by itself (Seraj et al., 2021). It is necessary to make structural modifications to increase drug potency and selectivity (Guo, 2012). Therefore, this review article documents, discusses, and compares the biological activities of the derivatives or metal complexes of acetaminophen and ibuprofen with their parent drugs, which can help researchers identify chemical modification variables. It also provides the understanding of the current state of knowledge in this area and identifies potential future explorations by understanding the factors (ligands, type and position of halogen, etc.) that affect biological activity.

Authors information:
[a]Faculty of Pharmacy, Universiti Sultan Zainal Abidin, Besut Campus, 22200, Besut, Terengganu, MALAYSIA. E-mail: azni64@gmail.com[1]; dikedandari1996@gmail.com[2]; asyillanordin@unisza.edu.my[3]
*Corresponding Author: asyillanordin@unisza.edu.my

Received: January 1, 2023
Accepted: May 12, 2023
Published: March 31, 2024

DOI:https//doi.org/10.22452/mjs.vol43no1.8
Malaysian Journal of Science 43(1): 86-112 (March 2024)

2. Acetaminophen

Acetaminophen (Figure 1), which is also known by the name paracetamol, is the non-prescription analgesic and antipyretic medication that is purchased in the greatest quantity worldwide. It has attracted interest as the first line of pharmacological therapy because it is more promising in terms of its safety profile compared to other treatment alternatives. A diverse variety of acute and chronic, severe symptoms are treated with acetaminophen (Ennis et al., 2016; Roberts et al., 2016).

Unlike non-steroidal anti-inflammatory drugs (NSAIDs) like aspirin and ibuprofen, it has no anti-inflammatory properties due to weak inhibition of cyclooxygenase (COX) enzyme in the peripheral tissues (Ohashi & Kohno, 2020). Acetaminophen does not bind to the active site of COX-1 or COX-2 enzyme, but it rather reduces the activity pathway of COX that inhibits the synthesis of prostaglandin in the central nervous system, making it a prominent analgesic and antipyretic agent (Gerriets et al., 2023). However, due to its availability, acetaminophen may lead to overdose, which can cause hepatotoxic (Bateman et al., 2014; Caparrotta et al., 2018; Ramachandran & Jaeschke, 2019). As it is eradicated through various metabolic pathways, acetaminophen is metabolised by several cytochrome P450 enzymes to the potentially toxic, chemically reactive metabolite N-acetyl-p-benzoquinone imine (NAPQI), and a small portion of it is excreted through urine as unchanged drug (Mian et al., 2020). NAPQI causes toxic metabolites as it is covalently bonded to protein, thus contributing to liver failure (Ozawa et al., 2019).

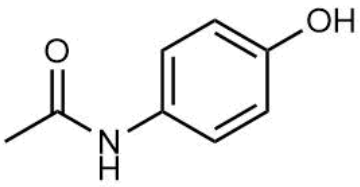

Figure 1. Structure of acetaminophen

Acetaminophen contains hydroxyl and amide functional groups. The incorporation of a hydroxyl group can make a molecule more lipophilic (Syahri et al., 2017), hence influencing its pharmacokinetic, pharmacodynamic, and toxicological profiles (Lobo, 2020).

Acetaminophen is synthesised in three stages, beginning with phenol with the addition of diluted sulphuric acid and sodium nitrate ($NaNO_3$), producing nitrophenol. Following that, sodium borohydride ($NaBH_4$) reduction is used to convert the nitro group on the para-substituted nitrophenol to an amine. Finally, acetic anhydride is reacted with the obtained para-aminophenol to produce acetaminophen via acetylation (Scheme 1) (Khosroshahi et al., 2016; Kingsley Ogemdi, 2019).

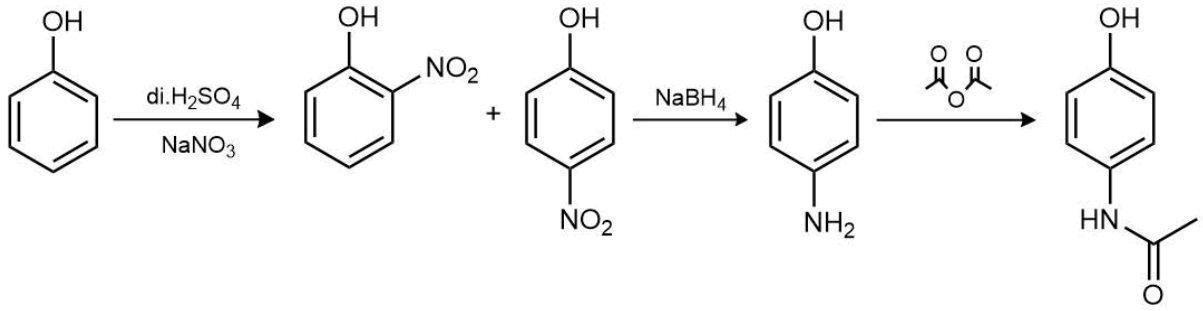

Scheme 1. Synthesis of acetaminophen

Acetaminophen with Metal Complexes

Metal complexes are important in drug design for coordination with metals (Amin et al., 2017), which are potent against cancer cells and can act as drug-resistant bacteria (Malik et al., 2018; Nandanwar & Kim, 2019). Metals seem to target a variety of different cellular processes, which results in the pleiotropic effect on bacterial cells (Turner, 2017). Complex metal (II) such as cobalt, nickel, copper, and zinc are potent against certain species of microorganisms, such as *Escherichia coli*, *Bacillus cereus*, and *Pseudomonas aeruginosa* (Damilola et al., 2019). These complex metals in the form of metal-based drugs possess modified pharmacological and toxicological potential. They form low molecular weight complexes which are more advantageous against numerous diseases (Rizzotto, 2012). There is a wide variety of modes of action for metal complexes, including ligand exchange or release, reactive oxygen species (ROS) production, coordination spheres, and redox activation, which can influence the kinetic and thermodynamic aspects of biological receptors (Malik et al., 2018; Zuegg et al., 2020). Metal complexes exert their effect by inhibition of cell membrane functions, arresting cell cycle, inhibiting enzymes, enhancing lipophilicity, etc. (Malik et al., 2018).

Antimicrobial Activity of Novel Metal Complexes of Piperaquine-Acetaminophen

Piperaquine (Figure 2) is a bisquinoline used in conjunction with dihydroartemisinin as a potential antimalarial agent (Assefa et al., 2021). It belongs to the 4-aminoquinoline group, a derivative of quinine (Ayipo et al., 2016), and is a highly lipophilic base that increases the oral bioavailability of drug when administered together with fat (Annerberg et al., 2011; Iseh et al., 2017). Although piperaquine derivatives are well-known for their antimalarial properties (Ma et al., 2019; Permala et al., 2017; Rasmussen et al., 2017), other derivatives also showed potential

DOI:https//doi.org/10.22452/mjs.vol43no1.8
Malaysian Journal of Science 43(1): 86-112 (March 2024)

in antibacterial (Ayipo et al., 2021) and antimicrobial studies (Ayipo et al., 2016).

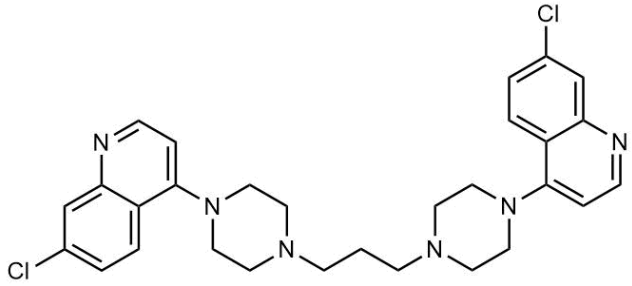

Figure 2. Structure of piperaquine

Although NSAIDs, like acetaminophen, have no antibiotic activity when used alone at therapeutic concentrations, they can enhance the inhibitory potential of antibiotics when co-administered with them. This joint administration can either impede bacterial growth or modify resistance mechanisms, resulting in more effective treatment (Singh et al., 2021). As metal complexes and piperaquine derivatives showed high potential in antimicrobial drugs, a metal-piperaquine-acetaminophen drug was investigated (Ayipo et al., 2016; Malik et al., 2018).

The procedure involved the combination of metal salt, piperaquine phosphate, and acetaminophen in a 1:1:1 mole ratio. The resulting mixed ligands were dissolved in a solution of 5% lactic acid and added to the previously prepared metal salt solutions in ethanol. 10% methanolic ammoniacal solution was added to maintain the pH of the mixture solution. The mixture was then refluxed for several hours and cooled in a refrigerator to facilitate the crystallisation of the metal. The resulting crystals were filtered, and the unwanted reactants and products were removed by washing them with diluted lactic acid and distilled water. The final products were then dried in a desiccator for several days. The same procedure was applied for all metal salts. The synthesised metal complexes piperaquine-acetaminophen (Figure 3) were evaluated for biological activity against *E. coli* and *S. aureus* (Ayipo et al., 2016).

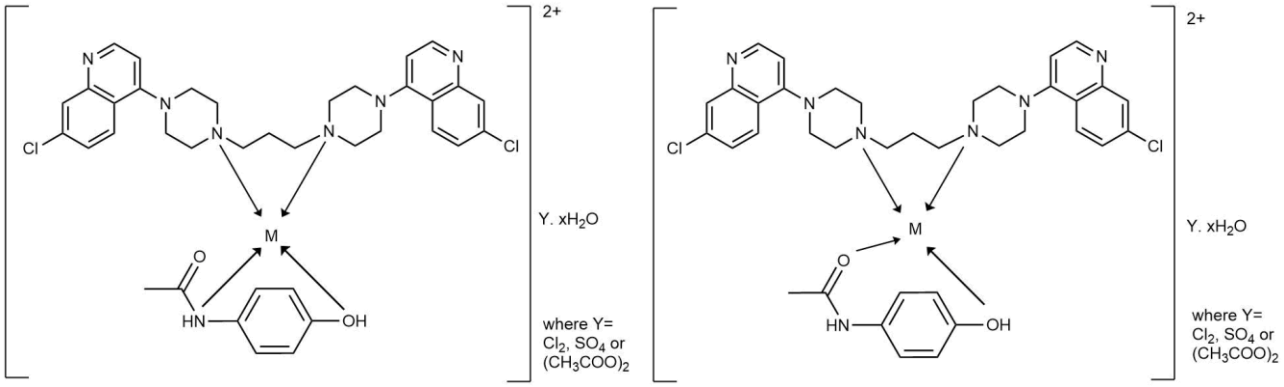

Figure 3. Proposed structures of metal complexes piperaquine-acetaminophen, where M = Fe(II), Cu(II), Zn(II), and Co(II)

Antimicrobial activities signify that piperaquine-acetaminophen metal complexes are stronger against Gram-positive bacteria (*S. aureus*) compared to the parent drug, acetaminophen. The result of the antimicrobial activities can be seen in Table 1.

Table 1. Antibacterial Activity of Acetaminophen, Piperaquine, and Their Metal Complexes

Compound / Complexes	Inhibition Zone (mm)
	S. aureus
$Cu(PQ)(Ac)Cl_2$	5.00
$Co(PQ)(Ac)(OAc)_2$	4.20
$Zn(PQ)(Ac)SO_4$	4.80
$Fe(PQ)(Ac)Cl_2$	5.20
Piperaquine (PQ)	3.55
Acetaminophen (Ac)	2.50

Among the piperaquine-acetaminophen metal complexes tested, Fe(II) showed the highest inhibition against *S. aureus* (5.20 mm), followed by Cu(II) (5.00 mm), Zn(II) (4.80 mm), and Co(II) (4.20 mm). The inhibition zone of piperaquine-acetaminophen against *S. aureus* increased significantly compared to the parent drug (Ayipo et al., 2016).

Chelation is effective in reducing the polarity of metal (II) complexes by sharing the metal's positive charge with ligand donor groups and delocalising the electron across aromatic rings. As a result, the metal atom's polarity weakens. It has increased the lipophilicity of the bacterial cell membrane, making it easier for it to get through the lipid layers of the bacterial membrane (Osowole et al., 2014). This shows that metal complexes of piperaquine and acetaminophen perform better against microorganisms than acetaminophen alone (Ayipo et al., 2016). Besides, heavy metals are known to be able to form secondary metabolites that can inhibit the growth of bacteria and are also toxic to organisms (Chudobova et al., 2015; Garza-Cervantes et al., 2017).

Antibacterial and Antifungal Activity of Cu(II) and Co(II) of Prednisolone-Acetaminophen

Prednisolone (Figure 4) is a synthetic cortisol glucocorticoid that works as analogue cortisol, a natural hormone that is produced by adrenal gland and used for many disease treatments

DOI:https//doi.org/10.22452/mjs.vol43no1.8
Malaysian Journal of Science 43(1): 86-112 (March 2024)

to suppress inflammations and various allergies (Straub & Cutolo, 2016). Prednisolone is also potentially a good anti-inflammatory agent as it can inhibit prostaglandin and leukotriene (Kumria et al., 2016; Santis & Saad, 2016; Motwani et al., 2018).

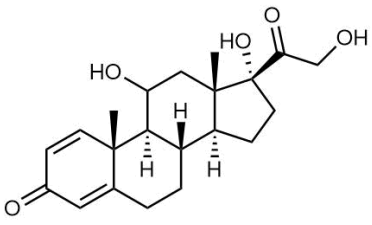

Figure 4. Structure of prednisolone

The synthesis of Co(II) and Cu(II) of prednisolone-acetaminophen used the same method (i.e., direct mixing). Prednisolone solution was prepared in distilled water-isopropyl alcohol medium and mixed in Cu(II) sulphate pentahydrate. The mixture was stirred for 1 h and then mixed with acetaminophen solution. The stirring continued for several hours. The mole ratio for metal salt, prednisolone, and acetaminophen was 1:1:1. The mixture was filtered and then washed using distilled water-isopropyl alcohol. The residue obtained was left to dry in a desiccator for several days and weighed. The process was repeated for Co(II) chloride (Damilola et al., 2019).

Gram-negative bacteria like *Xanthomonas axonopodis (A)*, *Streptococcus faecalis (B)*, *Pseudomonas aeruginosa (C)*, *Chromobacterium liusdium (D)*, and *Erwinia carotovora (E)* were used for antibacterial activity determination. The results showed that the inhibition zones of the synthesised drugs were higher compared to the parent paracetamol (Damilola et al., 2019). The results of the antibacterial activity are tabulated in Table 2.

Table 2. Antibacterial Activity of Acetaminophen, Prednisolone, Their Metal Complexes, and Streptomycin Sulphate

Compound/ Complexes	Zone of Inhibition (mm)				
	A	*B*	*C*	*D*	*E*
Cu(Pd)(Ac)(H_2O)	15.00	15.00	13.00	10.00	3.50
Co(Pd)(Ac)(H_2O)	20.00	19.00	17.00	17.50	18.50
Prednisolone (Pd)	10.00	1.00	6.00	3.50	0.00
Acetaminophen (Ac)	12.00	10.00	5.50	5.00	2.00
Streptomycin sulphate	27.00	31.00	31.00	33.00	22.00

The results showed that the metal complexes acetaminophen-prednisolone demonstrated higher inhibition against microbials, especially Co(Pd)(Ac)(H_2O). It gives an almost comparable value with the control when used against *E*. Although the results of the metal complexes of acetaminophen-prednisolone may not be as robust as the standard control (i.e., streptomycin sulphate), they still demonstrate satisfactory performance when compared with acetaminophen and prednisolone. The Co(II) and Cu(II) of prednisolone-acetaminophen showed more inhibition due to the antimicrobial mode of action. Different properties of metal ions gave higher activity of metal complexes due to chelation. This caused a decrease in the polarity of the metal ions by the overlapping of ligand orbitals and the partial sharing of the metal ion's positive charge with the donor group. Therefore, chelation facilitates complexes' penetration of lipid membranes and is more effective in inhibiting metal binding sites in bacterial enzymes (Al-Amiery et al., 2012).

Antimicrobial Activity of Mg(II) Complex of Acetaminophen

Mg(II) acetaminophen (Figure 5) was synthesised by the addition of $MgCl_2 \cdot 6H_2O$ to acetaminophen in distilled water and then heated for a few hours. It was left overnight to allow precipitation. The precipitate was filtered, washed, and allowed to dry for a few days. The final product was taken for the antimicrobial activity study by oral administration in rats (Paul et al., 2018). The microorganisms tested were *S. aureus*, *Bacillus subtilis*, *E. coli*, *Salmonella typhi*, *P. aeruginosa*, *Candida albicans*, and *Aspergillus niger* (Table 3).

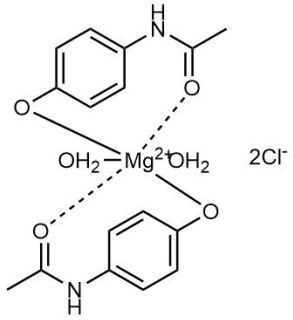

Figure 5. The proposed structure of Mg(II) acetaminophen

DOI:https//doi.org/10.22452/mjs.vol43no1.8
Malaysian Journal of Science 43(1): 86-112 (March 2024)

Table 3. Antimicrobial Activity of Acetaminophen, Mg(II) Acetaminophen Complex, and Control

Organism Tested	Zone of Inhibition (mm) at Varying Concentrations (mg/mL)				
	Compound/ Complex	6.25	12.5	25	50
S. aureus	Ac	0.0	0.0	0.0	0.0
	Mg(II)Ac	0.0	13.0	15.0	19.0
	Cp	20.0	25.0	30.0	38.0
B. subtilis	Ac	0.0	0.0	0.0	0.0
	Mg(II)Ac	0.0	0.0	0.0	0.0
	Cp	25.0	28.0	32.0	39.0
E. coli	Ac	0.0	0.0	0.0	0.0
	Mg(II)Ac	0.0	0.0	0.0	0.0
	Cp	19.0	22.0	25.0	30.0
S. typhi	Ac	0.0	0.0	0.0	0.0
	Mg(II)Ac	0.0	0.0	12.0	15.0
	Cp	25.0	28.0	32.0	37.0
P. aeruginosa	Ac	0.0	0.0	15.0	18.0
	Mg(II)Ac	0.0	13.0	18.0	27.0
	Cp	16.0	18.0	21.0	25.0
C. albicans	Ac	0.0	0.0	0.0	0.0
	Mg(II)Ac	0.0	0.0	0.0	0.0
	Fl	25.0	28.0	32.0	36.0
A. niger	Ac	0.0	0.0	0.0	0.0
	Mg(II)Ac	0.0	0.0	0.0	0.0
	Fl	13.0	15.0	20.0	25.0

Note:- Ac: Acetaminophen, Mg(II)Ac: Magnesium complex of acetaminophen, Cp: Ciprofloxacin, Fl: Fluconazole

The results showed that the parent drug (acetaminophen) did not inhibit bacterial growth at any concentration (6.25, 12.5, 25, and 50 mg/mL) except *P. aeruginosa* at 25 and 50 mg/mL (Paul et al., 2018). The antibacterial effects of acetaminophen have been reported to be negligible (Singh et al., 2021). However, the inhibition zones of *S. aureus*, *S. typhi*, and *P. aeruginosa* increased proportionally to the concentration of Mg(II) acetaminophen being administered (Paul et al., 2018). Although Mg(II) acetaminophen exhibits less potency than the standard control, it shows a noteworthy improvement in comparison to the isolated effects of acetaminophen. Tweedy's chelation hypothesis predicted that the polarity of the metal atom would decrease with chelation, mostly as a result of the metal's positive charge being partially shared with donor groups and perhaps resulting in electron delocalisation over the whole ring. This increased the lipophilic nature of the chelates, which made it more possible for them to penetrate through the lipid layers of the bacterial membrane (Al-Amiery et al., 2012).

Antimicrobial Activity of Metal Complexes of Acetaminophen-Ascorbic Acid

Ascorbic acid (Figure 6), commonly known as vitamin C or ascorbate, is made up of an enediol that is conjugated to the carbonyl group in the lactone ring. This enediol provides an electron for ascorbic acid's function as an antioxidant (Barba et al., 2014). It is a renowned water-soluble antioxidant that plays an essential part in several physiological processes in the human body (Attia et al., 2020). It can control the gastrointestinal absorption of iron ions and stabilise iron-binding protein, as well as post-translational hydroxylation of collagen, carnitine biosynthesis, and tyrosine metabolism (Golonka et al., 2017). Ascorbic acid is widely recognised as a strong antioxidant and free radical scavenger (Njus et al., 2020), but people do not seem aware of its other biological activities, such as anticancer (Shenoy et al., 2018), antitumor (Mata et al., 2016), antiviral (Biancatelli et al., 2020), and antimicrobial properties (Hernandez-Patlan et al., 2017; Sangcharoen et al., 2017; Verghese et al., 2018). As metal ions like cobalt, nickel, and zinc are known for their effectiveness against several diseases, the combination of analgesic-antioxidant drug metal complexes is being studied.

DOI:https//doi.org/10.22452/mjs.vol43no1.8
Malaysian Journal of Science 43(1): 86-112 (March 2024)

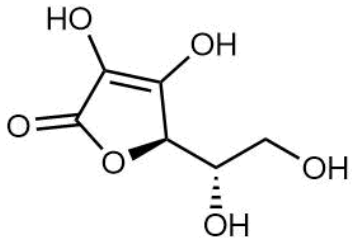

Figure 6. Structure of ascorbic acid

Acetaminophen-ascorbic acid metal complexes (Figure 7) are synthesised by the preparation of metal chlorides (Ni, Co, Fe, Cu) and metal sulphate (Zn) in aqueous solution. Then, acetaminophen and ascorbic acid were mixed in their appropriate solvent. The mixture was refluxed, and the resulting precipitate was filtered, solvent-washed, air-dried, and stored. The experiment was conducted in 3.0 and 5.0 mmol concentrations. The antimicrobial activity of acetaminophen, ascorbic acid, and acetaminophen-ascorbic acid metal complexes can be seen in Table 4.

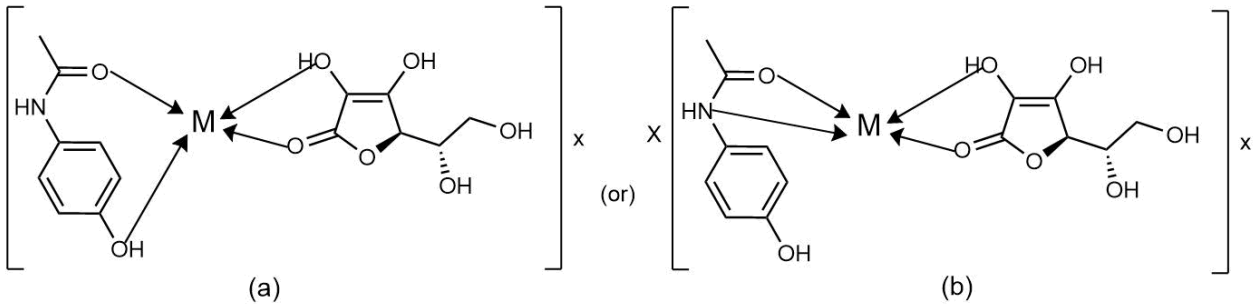

Figure 7. Proposed structures of acetaminophen-ascorbic acid metal complexes

Table 4. Antimicrobial Activity of Acetaminophen, Ascorbic Acid, and Acetaminophen-Ascorbic Acid Metal Complexes

Compound/ Complex	Inhibition Zones (mm)					
	Conc. (mmol)	A	B	C	D	E
$Co(Ac)(Asc)Cl_2$	3.0	5.0	0.0	2.0	3.0	2.0
	5.0	6.0	0.0	6.0	6.0	0.0
$Ni(Ac)(Asc)Cl_2$	3.0	14.0	9.0	5.0	10.0	2.0
	5.0	0.0	4.0	1.0	3.0	11.0
$Cu(Ac)(Asc)Cl_2$	3.0	2.0	6.0	4.0	0.0	0.0
	5.0	31.0	32.0	15.0	0.0	0.0
$Fe(Ac)(Asc)Cl_2$	3.0	1.0	0.0	3.0	0.0	0.0
	5.0	-	-	-	-	-
$Zn(Ac)(Asc)Cl_2$	3.0	7.0	0.0	10.0	0.0	0.0
	5.0	0.0	0.0	0.0	0.0	0.0
Acetaminophen (Ac)	3.0	2.0	4.0	5.0	3.0	9.0
	5.0	-	-	-	-	-
Ascorbic acid (Asc)	3.0	5.0	0.0	5.0	9.9	2.0
	5.0	-	-	-	-	-

Biological assays of the complexes were experimented on for 3 days against *Enterococcus faecalis (A)*, *S. aureus (B)*, *Clostridium difficile (C)*, *Klebsiella spp. (D)*, and *Helicobacter pylori (E)*. Different concentrations of complexes were found to give different results.

At 3.0 mmol, the acetaminophen-ascorbic acid metal complexes did not exhibit antimicrobial activity on the first day. Meanwhile, at a concentration of 5.0 mmol, acetaminophen-ascorbic acid with copper complex, $Cu(Par)(Asc)SO_4$ against *S. aureus* (32 mm) and acetaminophen-ascorbic acid with cobalt complex, $Co(Par)(Asc)SO_4$ against *H. pylori* (31 mm) showed the best antimicrobial activity. Both complexes showed higher inhibition compared to the parent acetaminophen itself. However, the complexes' inhibition decreased on the third day due to the reduction in the concentration of the drug (Babamale et al., 2016). This is due to the population of bacteria exposed to

DOI:https//doi.org/10.22452/mjs.vol43no1.8
Malaysian Journal of Science 43(1): 86-112 (March 2024)

an inadequate concentration of a specific drug as they can develop resistance to the drug (Kowalska-Krochmal & Dudek-Wicher, 2021).

3. Ibuprofen

Ibuprofen (2-(4-isobutylphenyl) propionic acid) (Figure 8) is a common over-the-counter drug used as an analgesic and antipyretic agent. It is consumed to inhibit COX, thus reducing the level of prostaglandin in the human body, which is used to treat inflammation or pain and can also be used as a fever reliever. It is usually used to treat headaches, menstrual cramps, minor injury, toothaches, and blood clotting, and to control blood pressure. The adverse effect of ibuprofen is likely due to frequent and widespread usage (Gomaa, 2018). Ibuprofen exerts its anti-inflammatory effect based on the inhibition of COXs in prostaglandin synthesis (Amir et al., 2016). It also has an antibacterial effect, especially on *E. coli*, which is a major pathogen causing urinary tract infection (Ahmed et al., 2016). The presence of carboxyl and aromatic groups in the molecular structure of ibuprofen has been reported to contribute to its biological properties (Martínez et al., 2017).

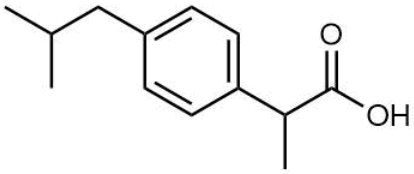

Figure 8. Structure of ibuprofen

The synthesis of ibuprofen can be accomplished using isobutyl benzene and acetic anhydride with four continuous reactions, which are Friedel-Craft acylation, carbonyl reduction, chloride substitution, and Grignard reaction (Kilburg & Tyler, 2017) (Scheme 2).

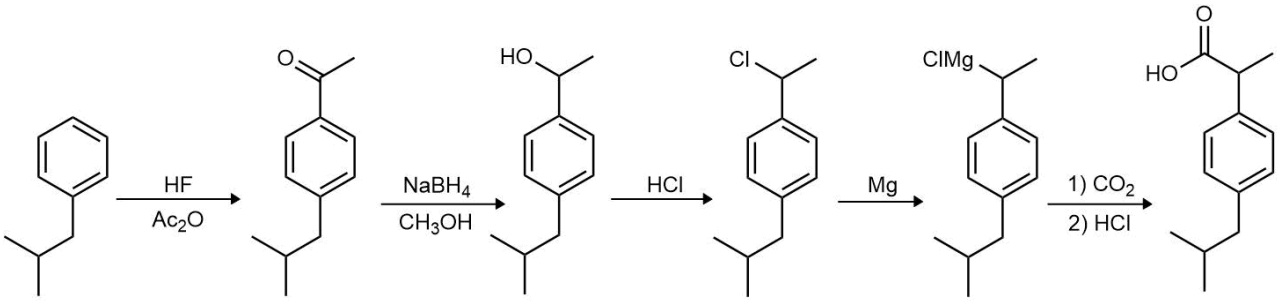

Scheme 2. Synthesis of ibuprofen

Urease Inhibition of Co(II) Complex of Ibuprofen-Thiourea Derivatives

Thiourea derivative is known for its biological activities, such as antimicrobial (Stratan et al., 2018; Vedavathi et al., 2017), antituberculosis (Stratan et al., 2018), and analgesic (Shoaib et al., 2017). It has a variety of uses outside of pharmaceuticals, including as a fungicide and herbicide, a growth inhibitor for plants, and as a substance used to control insect and insect-related growth (Shakeel, 2016). It has also been considered as a particularly good chelating agent for transition metal complexes by inhibiting enzymes due to their specific molecular architecture (Mumtaz et al., 2018). Urease is a nickel-based metalloenzyme that is present throughout the human body (Seraj et al., 2021). It catalysed the hydrolysis of urea to produce ammonia and carbon dioxide, which were subsequently protonated to produce ammonium (Rizvi et al., 2019). This assists in an increase of pH in the stomach. Urease enzyme can promote the growth of *H. pylori* that caused many pathological conditions including peptic ulcer, hepatic encephalopathy, and urinary stone formation, which answered the growing interest of urease inhibitor in the medicinal field in recent years (Kafarski & Talma, 2018; Mumtaz et al., 2018; Seraj et al., 2021).

Mumtaz et al. (2018) studied urease inhibition by introducing metal ligands into ibuprofen-thiourea. Ibuprofen-thiourea with halogen substitutes obtained were characterised and underwent reaction with metal complex (Figure 9) (Mumtaz et al., 2018). The synthesis of Co(II) complex of ibuprofen-thiourea is represented below (Scheme 3).

DOI:https//doi.org/10.22452/mjs.vol43no1.8
Malaysian Journal of Science 43(1): 86-112 (March 2024)

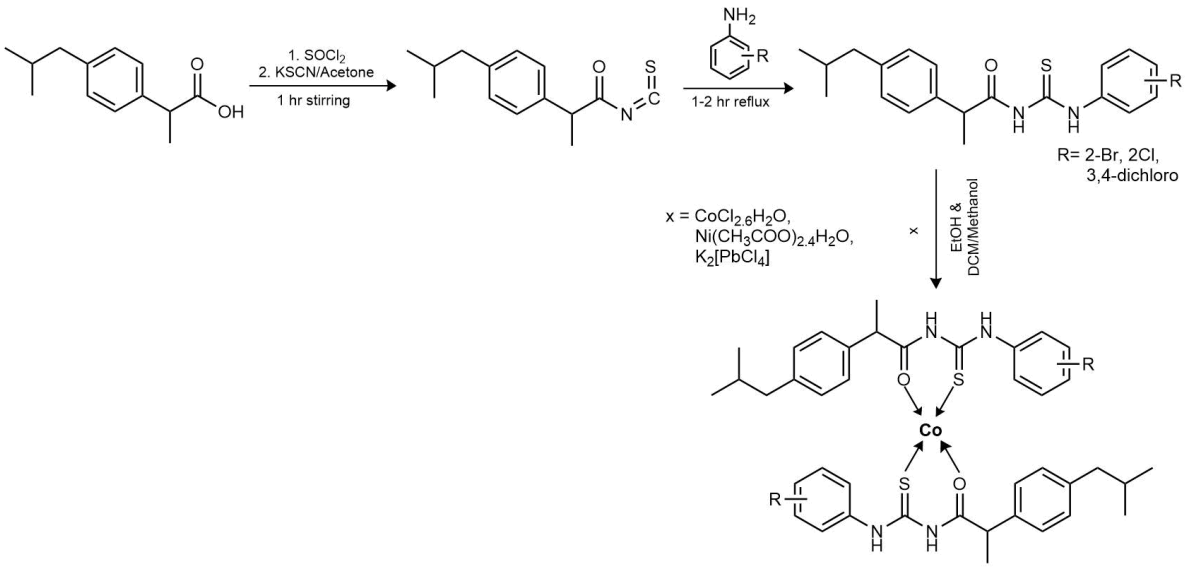

Scheme 3. Synthesis of Co(II) complex of ibuprofen-thiourea

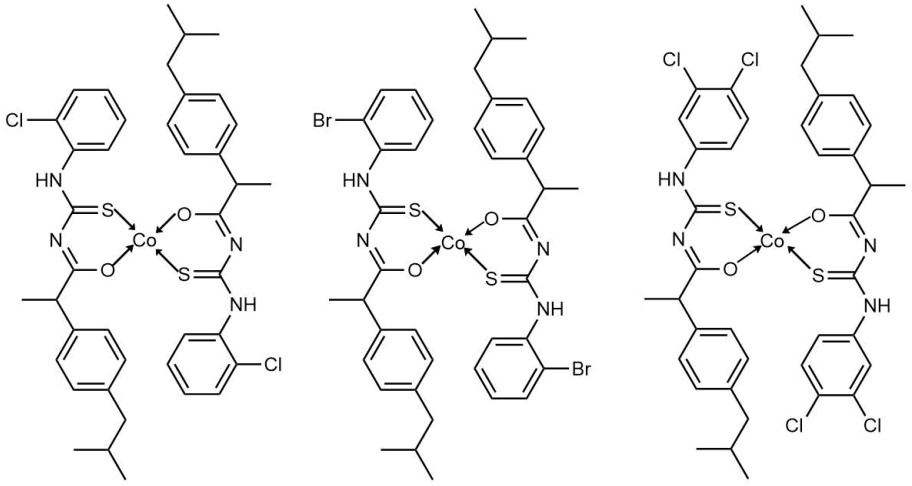

Figure 9. Proposed structure of Co(II) complex of ibuprofen-thiourea: (a) chloro substituent, (b) bromo substituent, and (c) dichloro substituent

Urease inhibition of ibuprofen-thiourea derivatives were compared with jack bean urease. The enzyme activity was determined by the amount of ammonia produced measured by the indophenol method and the absorbance was recorded (Mumtaz et al., 2018). The collected data indicated that ibuprofen was unable to inhibit urease enzyme. However, the incorporation of thiourea moiety into ibuprofen has increased the inhibition potency of enzyme activity (Seraj et al., 2021). Therefore, thiourea has been used as a standard for urease inhibition. Table 5 shows the results for urease inhibition of Co(II) complex of ibuprofen-thiourea.

Table 4. Urease Inhibition Activity of Co(II) Complex of Ibuprofen-Thiourea Derivatives

Compound	IC_{50} (µM) ± SEM
(a)	14.6 ± 3.3
(b)	32.9 ± 14.1
(c)	24.6 ± 7.45
Standard (thiourea)	21.1 ± 1.23
Ibuprofen	-

Ibuprofen-thiourea derivative with metal ligand bearing -Cl exhibited the most potent inhibition against urease enzyme. Ibuprofen-thiourea metal-containing bromine atom showed lower urease inhibition than -Cl (Mumtaz et al., 2018). Although both -Cl and -Br belong to the electron-withdrawing group (EWG),

DOI:https//doi.org/10.22452/mjs.vol43no1.8
Malaysian Journal of Science 43(1): 86-112 (March 2024)

-Cl is more electronegative and has smaller atomic size than -Br, which may affect the urease inhibitory activity (Rashid et al., 2020). Moreover, -Br exhibits inadequate inhibition of enzyme due to extended bulkiness of the compound, which resulted in longer and more labile bonds (metal ligand easily broken), thus unsuitable for drug candidates, whereas the presence of -Cl has altered the volume and shape of the compound, allowing for positioning in deep cavities of enzyme (Fejzagić et al., 2019). Compound (c) containing two -Cl at meta-para position showed a moderate result compared to the standard and compound (b). This shows that the position of halogens determines the inhibitory activity instead of the number of halogen present (Ashraf et al., 2019).

Antibacterial Activity of Metal Complexes with Isoniazid-Ibuprofen

Formerly, metal has been used as an antimicrobial agent that is highly beneficial in the medical field. Normal cell metabolism requires many metals, but higher concentrations may cause health risks. According to the oligodynamic effect, heavy metal can bind to thiol or amine moiety of cellular protein, leading to deactivation and precipitation of proteins. As proteins are strongly attracted to metal ions, it results in cellular concentration growth and cell death (Mittapally et al., 2018). As antibiotics are developed, the use of metals as antimicrobials is gradually being phased out. However, the emergence of several reports related to antibiotic resistance became a reason for the development of metals used as antibiotic conjugates (Hegde et al., 2021; Mittapally et al., 2018).

Isoniazid (Figure 10), also called isonicotinyl hydrazide (INH), is an antibiotic consisting of a pyridine ring with hydrazine moiety that has a narrow spectrum antimicrobial against *Mycobacterium tuberculosis* (Hegde et al., 2021).

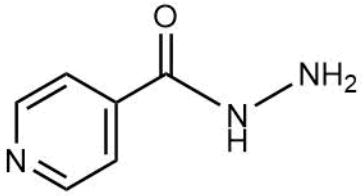

Figure 10. Structure of isoniazid

It is a pro-drug activated by KatG (a biological enzyme presents in mycobacteria) to generate isonicotinoyl radical. Nicotinamide adenine dinucleotide (NAD+) and this free radical interact to form a complex called NAD-INH, which functions as a competitive inhibitor of InhA. The inhibition interrupts the entire process of mycolic acid synthesis, which is responsible for the formation of mycobacterial cell wall. Furthermore, the inhibition process resulting in NADH accumulation and ATP burst that is toxic to the mycobacterial itself (Shetty & Dick, 2018; Hegde et al., 2021).

Isoniazid has been used as an antituberculosis agent for more than 6 decades until the emergence of resistance cases. Numerous researchers have established isoniazid derivatives to combat INH resistance using newly discovered mycobacterial targets and host-directed treatment (Torfs et al., 2019). The combination of isoniazid-pyrrole hybrid LL-3858 resulting in a promising compound for tuberculosis treatment (Hu et al., 2017). Isoniazid embedded with triazole moiety induces antitubercular and antimicrobial activities. Mixed isoniazid-ibuprofen metal complexes also showed antibacterial activities (Bamigboye et al., 2019).

The synthesis of isoniazid-ibuprofen metal complexes (Figure 11) started with isoniazid in methanol and ibuprofen in ethanol, which were mixed in metal chloride salts (Cu^{2+}, Zn^{2+}, Ni^{2+}, and Cd^{2+}) and dissolved in solvents. After being refluxed for a short period of time at a certain temperature, the mixture was cooled to room temperature, allowed to precipitate, filtered, and washed with a mixture of solvents. The product was dried in a desiccator and used in antibacterial screening against *E. coli*, *S. aureus*, and *P. aeruginosa* (Bamigboye et al., 2019).

DOI:https//doi.org/10.22452/mjs.vol43no1.8
Malaysian Journal of Science 43(1): 86-112 (March 2024)

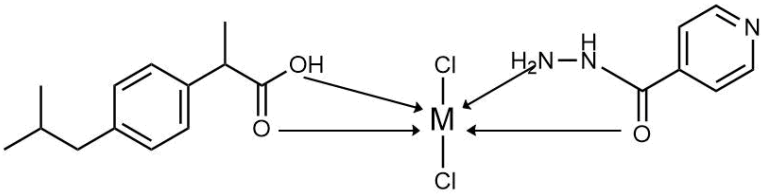

Figure 11. Proposed structure of isoniazid-ibuprofen metal

The antibacterial activity of metal complexes (Ni, Cu, Cd, and Co) isoniazid-ibuprofen compounds resulted in higher inhibition zones against *E. coli*, *S. aureus*, and *P. aeruginosa* compared to the parent ibuprofen. The results (Table 6) indicated that ibuprofen and isoniazid themselves did not inhibit bacteria at 20 and 40 µL/mL (except for isoniazid against *S. aureus* at 40 µL/mL) (Bamigboye et al., 2019).

Table 5. Antibacterial Activity of Complexes, Ibuprofen, and Isoniazid

Compound/Complexes	Inhibition Activity at 20 and 40 µL/mL Concentration					
	E. coli		*S. aureus*		*P. aeruginosa*	
	20.0	40.0	20.	40.0	20.0	40.0
Ni(Iso)(Ibu)Cl_2	11.0	14.0	8.0	12.0	8.0	13.0
Cu(Iso)(Ibu)Cl_2	4.0	16.0	5.0	24.0	14.0	19.0
Cd(Iso)(Ibu)Cl_2	22.0	29.0	13.0	14.0	13.0	16.0
Co(Iso)(Ibu)Cl_2	9.0	12.0	11.0	11.0	17.0	18.0
Isoniazid (Iso)	-	-	-	11	-	-
Ibuprofen (Ibu)	-	-	-	-	-	-

Meanwhile, the existence of metals in the complex enhanced the effectiveness of ligand to inhibit bacterial growth. This increasing antimicrobial activity can be linked to the chelation theory. Chelation usually results in ligand acting as a more effective bactericidal agent (Damilola et al., 2019). The donor atoms in the ligands partially share some of the positive charge of the metal, as in the complex, and may contribute to electron delocalisation in the chelate ring. This factor contributes to the lipophilicity of the central metal atom, which improves its hydrophobicity and solubility in lipids, allowing it to permeate through the lipid layer of bacterial membrane (Abd El-Halim et al., 2018).

Anti-Inflammatory and Ulcerogenic Activity of Ibuprofen Bearing Ammonium Moieties

Drugs containing carboxylic acid have an essential function in the medical treatment of pain and diseases. One of the roles is acting as a solubiliser to modulate lipophilicity and cell permeation (Badea & Radu, 2018). However, some claim that the damage caused by NSAIDs containing a carboxylic group (ibuprofen, aspirin) is more potent (Mehta et al., 2010). It has been questioned whether NSAIDs require the presence of carboxylic acid group. One of the test drugs is ibuprofen. The carboxylic acid-free group of ibuprofen can cause gastrointestinal (GI) toxicity (erosion or bleeding) due to its pharmacological mechanism that inhibits COX-1 and COX-2, thus decreasing the formation of prostaglandin and thromboxane systematically (Bhandari et al., 2008; Ullah et al., 2016).

The synthesis of ibuprofen bearing ammonium moieties is depicted below (Scheme 4).

DOI:https//doi.org/10.22452/mjs.vol43no1.8
Malaysian Journal of Science 43(1): 86-112 (March 2024)

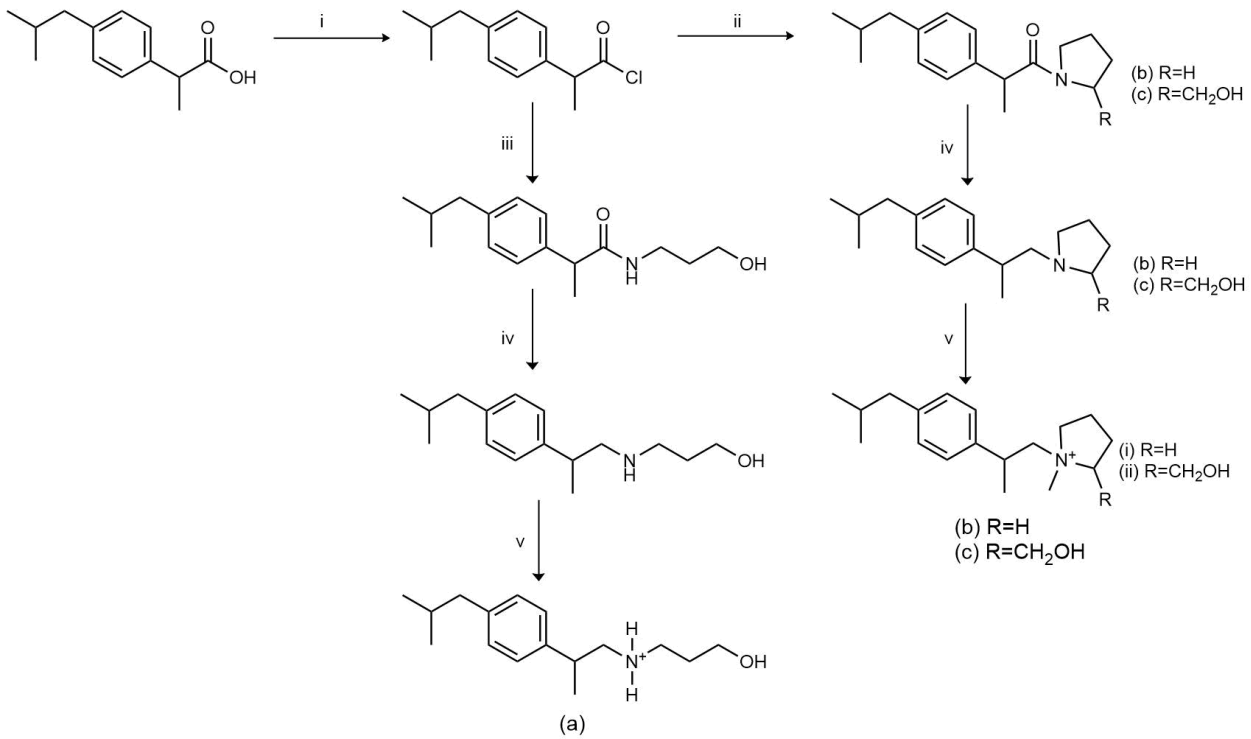

Scheme 4. Synthesis of ibuprofen bearing ammonium derivatives. Reagents and conditions: (i) oxalyl chloride, DCM, 25 °C, 3–12 h; (ii) pyrrolidine or L-proline, DCM, 25 °C, 3 h; (iii) 2-hydroxyethylamine, DCM, 25 °C, 3 h; (iv) $LiAlH_4$, THF, 25 °C for 3d, reflux (a) for 3 h; and (v) dry HCl, ether, N_2, 25 °C

The subsequent ammonium salt was taken for anti-inflammatory and ulcerogenic assay. Based on the in vitro results, compounds 2e, 3e(i), and 3e(ii) (Figure 12) gave the half-maximal inhibitory concentration (IC_{50}) values of 28.1, 22.2, and 20.7 µM, respectively, whereas celecoxib gave 0.02 µM. This indicates that these drug modifications are not as potent as celecoxib as the selective COX-2 inhibitor.

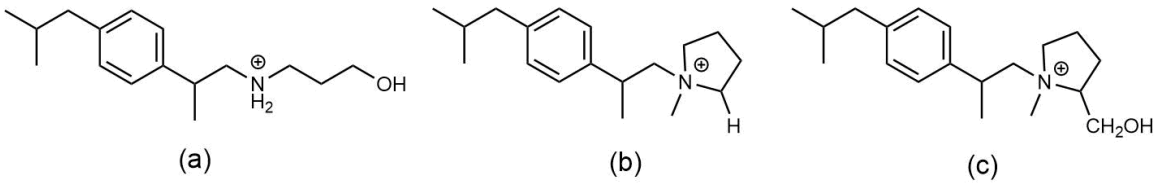

Figure 12. Structure of ibuprofen-ammonium derivatives

Meanwhile, in the findings of in vivo anti-inflammatory activity (Table 7), the compounds (a) and (b) had a statistically relevant anti-inflammatory impact in comparison to the control group, whereas compound (c) had no effect (Ullah et al., 2016). Drugs containing ammonium salts could improve solubility in body fluids (Ouellette & Rawn, 2018). The ammonium salts made from ibuprofen have shown that NSAIDs are not required to include carboxylic acid groups (Ullah et al., 2016). Nevertheless, further study needs to be done to increase the potency.

Table 6. COX-1 and COX-2 Inhibition of Ibuprofen Derivatives without Carboxylic Acid Group

Compounds	IC_{50} (µM)	
	COX-1	COX-2
(a)	>100	28.1
(b)	>100	22.2
(c)	>100	20.7
Celecoxib	>100	0.02

DOI:https//doi.org/10.22452/mjs.vol43no1.8
Malaysian Journal of Science 43(1): 86-112 (March 2024)

Anti-Inflammatory and Anticancer Activity of Ibuprofen-Amide Derivatives

Studies found that amide derivatives of NSAIDs contributed to antitumor activity (Zhang et al., 2021). Compared to the parent NSAIDs itself, amide derivatives are said to be potent inhibitors of cell proliferation. A compound comprises amide linkage is said to be anticancer, antimicrobial, antinociceptive, and anti-inflammatory (Haider et al., 2018). It is well-known that heterocyclic compounds containing nitrogen are a valuable source of therapeutic agents (Figure 13) (Ansari et al., 2017).

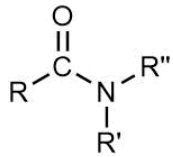

Figure 13. Structure of amide

Anti-Inflammatory Activity of with 1,3,4-Thiadiazolyl–Propanamide Ibuprofen Derivatives

Alkabodi et al. (2016) aimed to derive a potential ibuprofen-amide derivatives drug with selective COX-2 inhibition having a low ulcerogenic effect. The synthesis of the ibuprofen-amide derivatives is shown below (Scheme 5):

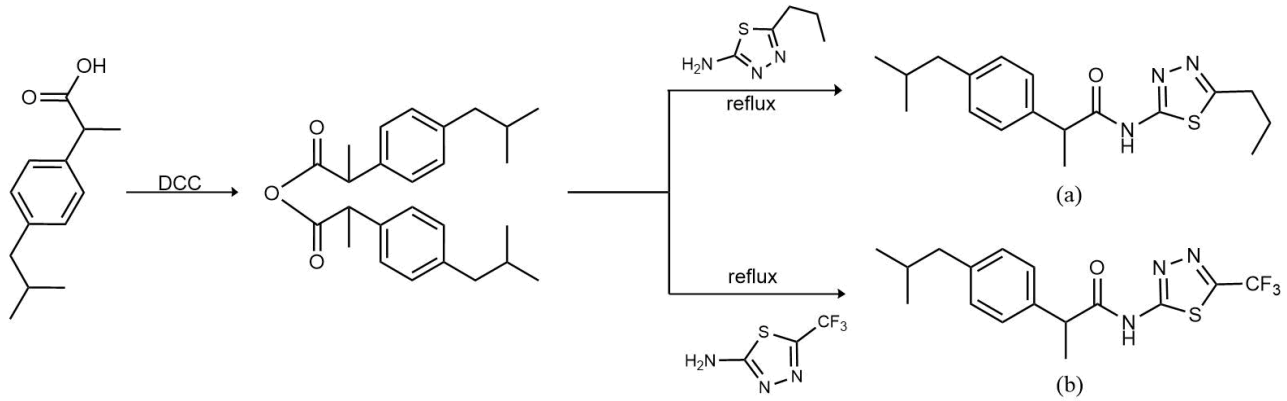

Scheme 5. Synthesis of ibuprofen-amide derivatives

The experiment continued with the anti-inflammatory activity test using the ovalbumin paw edema method of albino rats and ulcerogenic index screening, and the results obtained are as shown in Table 8 (Alkabodi et al., 2016).

Table 8. Percentage Inhibition of Paw Edema and Ulcer Index to Determine the Anti-Inflammatory Activity of Ibuprofen with 1,3,4-Thiadiazol Amide Derivatives

Compound	% Inhibition of Paw Edema	Ulcer Index
(a)	45.0	5.8
(b)	44.0	8.3
Diclofenac	41.0	-
Celecoxib	-	6.0
Indomethacin	-	17.0

The inhibition of compounds (a) and (b) resulted in a decent anti-inflammatory activity (45% and 44%, respectively) compared to the standard drug, diclofenac (41%) (Alkabodi et al., 2016). Meanwhile, the ulcerogenic screening showed that compounds (a) and (b) gave 5.8 and 8.3 ulcer index while celecoxib produced an ulcer index of 6.0. The activity of ibuprofen-amide derivatives was compared to diclofenac and celecoxib (selective COX-2 inhibitors). Overall, it was discovered that compound (a) gave better results in comparison to celecoxib. The difference between compound (a) and celecoxib is the presence of amide functional group (Alkabodi et al., 2016). Several studies found that the amide derivatives have increased the anti-inflammatory activity (Ahmadi et al., 2017; Narsinghani & Sharma, 2017).

Compounds (a) and (b) also consist of thiadiazol, which may contribute to COX-2 inhibition. Several studies on thiadiazol derivatives showed promising scaffolds for potent selective COX-2 inhibitors (Maddila et al., 2016; Ragab et al., 2017; Murahari et al., 2019).

The difference between these two compounds is the presence of ethyl in compound (a) and trifluoromethyl in compound (b). A study found that trifluoromethyl may affect the electrical properties of the target chemicals, and its lipophilicity can

DOI:https//doi.org/10.22452/mjs.vol43no1.8
Malaysian Journal of Science 43(1): 86-112 (March 2024)

promote membrane permeability (Cong et al., 2021). However, comparing compound (b) to non-selective COX inhibitor indomethacin, the GI side effects for compound (b) are less severe but not as efficient as a COX-2 inhibitor, celecoxib.

Hence, the presence of amide and 1,3,4-thiadiazol in ibuprofen-amide derivatives (compound (a)) has improved the anti-inflammatory effect on the edema paw of albino rats and gives better tolerance against the ulcerogenic of albino rats compared to celecoxib.

Anti-inflammatory Activity of Ibuprofen-Amide Derivatives as Dual FAAH/COX Inhibitor

Ibuprofen can initiate gastrointestinal toxicity after a long time of usage, and the pharmaceutical industry will design a new drug candidate with improved therapeutic properties compared to the parent drug (Mehta et al., 2010). The suppression of both COX-1 and COX-2 caused gastrointestinal damage. In order to overcome this phenomenon, the inhibition of fatty acid amide hydrolase (FAAH) alongside COX inhibitors is introduced (Deplano et al., 2019; Goodman et al., 2018). FAAH is a serine hydrolase that is important in controlling the endogenous level of anandamide, an endocannabinoid mediator with analgesic and tissue protective function, and works as a pain and inflammation reliever (Dainese et al., 2020; Deplano et al., 2019; Sasso et al., 2015; Scarpelli et al., 2016). A dual-action FAAH-COX inhibitor is reported to give useful therapeutic properties. The synthesis of ibuprofen-amide derivatives is shown below (Scheme 6).

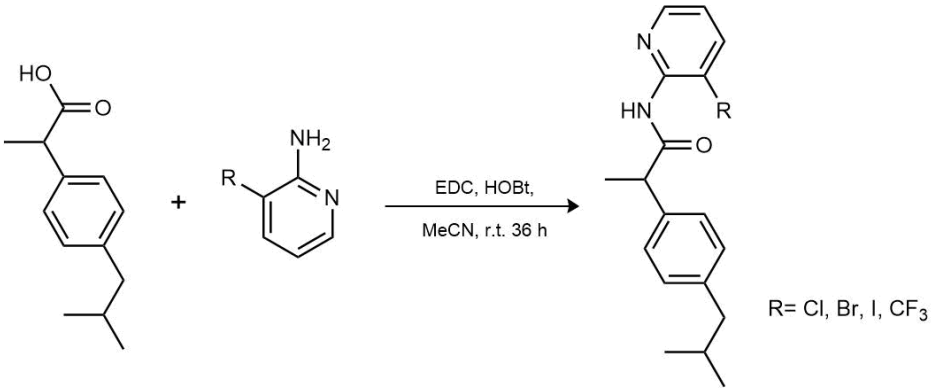

Scheme 6. Synthesis of ibuprofen-amide derivatives

Figure 14 shows the proposed structure of ibuprofen-amide derivatives with different substituents (halogen and trifluoromethyl). The first endogenous ligand discovered to interact with cannabinoid receptors is *N*-arachidonoylethanolamine (AEA). FAAH enzyme breaks down AEA to arachidonic acid and ethanolamine in most rat tissues (Ahn et al., 2009; Marrs & Stella, 2009). The ibuprofen-amide derivatives were tested towards rat brain FAAH-catalysed hydrolysis of AEA. The inhibition of the ibuprofen-amide derivatives at IC_{50} was analysed (Table 9) (Deplano et al., 2020).

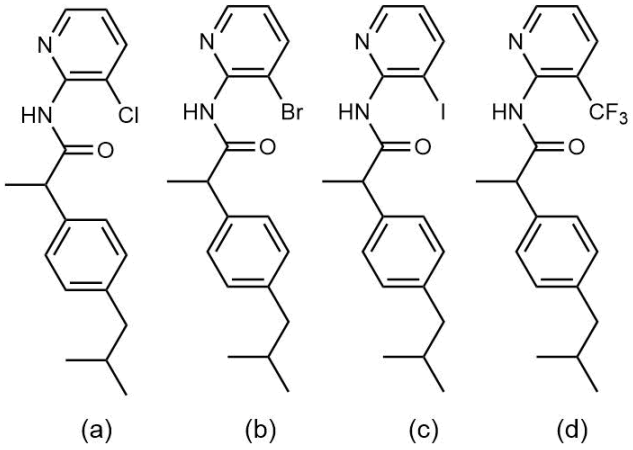

Figure 14. Structure of ibuprofen-amide derivatives (Cl, Br, I, CF_3)

DOI:https//doi.org/10.22452/mjs.vol43no1.8
Malaysian Journal of Science 43(1): 86-112 (March 2024)

Table 9. IC_{50} Values for the Inhibition of Rat Brain FAAH Catalysed Hydrolysis of AEA by Ibuprofen-Amide Derivatives

Compound	IC_{50} (µM)
(a)	0.910
(b)	0.083
(c)	0.120
(d)	0.360
Ibuprofen	-

The presence of -Cl, -Br, and -I resulted in bulky compounds, which blocked the active sites or affected the permeability of cell membranes. Even though brominated compounds were said to be longer with a more labile bond, it allowed for easier incorporation into molecules (Fejzagić et al., 2019). This explains the highest potency of ibuprofen-amide derivatives starting with (b), which has -Br at 0.083 µM, followed by (c) with -I at 0.120 µM, (d) with $-CF_3$ at 0.360 µM, and lastly (a) with -Cl at 0.910 µM (Deplano et al., 2020). These results indicated the presence of halogen, which increased the potency of ibuprofen-amide derivatives as FAAH inhibitors but still retained its ability as a selective COX-2 inhibitor. The presence of EWG such as halogen and trifluoromethyl gives higher activity compared to ibuprofen itself.

Anticancer Activity of Dexibuprofen-Amide Derivatives

Anhydrous benzene is present when a reaction took place between thionyl chloride and dexibuprofen, producing the corresponding acid chloride. In the second stage, the dexibuprofen acid chloride underwent condensation with substituted amines in the presence of dry acetone to obtain the required dexibuprofen-amides (a–d). After being synthesised, each dexibuprofen-amide derivative was subjected to flash chromatography to achieve purity and their structures were validated using spectroscopic data.

The dexibuprofen amides with halogen substituted on aromatic moieties improved the antitumor activities. These compounds (Figure 15) were evaluated against breast carcinoma cells (MCF-7).

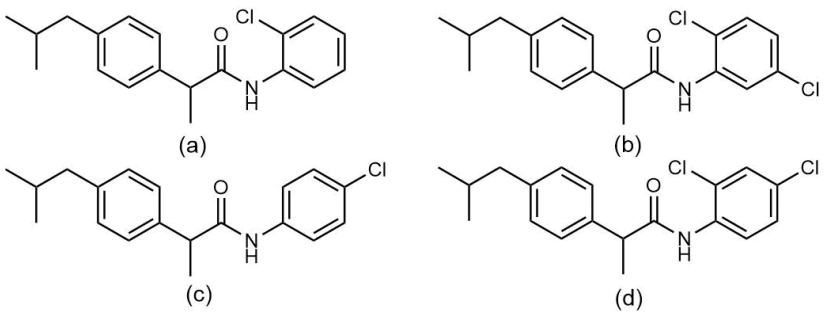

Figure 15. Structure of dexibuprofen-amide derivatives with different positions of chloro-halogen: (a) 2-Cl, (b) 2,5-dichloro, (c) 4-choro, and (d) 2,4-dichloro

Compound (a) with 2-chloro, (b) with 2,5-dichloro, (c) 4-chloro, and (d) 2,4-dichloro substituted gave excellent IC_{50} results for MCF-7 (Table 10). Both compounds (a) and (b) exhibited excellent outcomes against the cancer cells, but neither compound was cytotoxic to normal breast cells.

Table 10. Cytotoxic Activity against MCF-7 Cell Line by the Synthesised Dexibuprofen Amides, Erlotinib, and Doxorubicin

Compounds	IC_{50} (µM/mL)
	MCF-7
(a)	0.03 ± 0.004
(b)	0.01 ± 0.002
(c)	6.57 ± 1.54
(d)	1.02 ± 0.15
Erlotinib	0.02 ± 0.003
Doxorubicin	0.04 ± 0.006

For compounds (a) and (b), the chloro substituent at the ortho-position of the phenyl ring is crucial to the anticancer activity of these derivatives. Under these circumstances, the chlorine substituents' steric and/or electronic actions caused localised electronic attraction or repulsion, as well as steric interference with any nearby amino acids of the target proteins. (Fang et al., 2019). Compound (c) with a para-chloro substituent has reduced the cytotoxicity. Due to the increasing number of chloro-substituents, compound (d) demonstrated the least inhibition. It can be concluded that the location of the halogens, not their quantity, is the determining factor of inhibitory action (Ashraf et al., 2019).

Even though ibuprofen was not evaluated in this study, previous research has shown that it provides limited inhibitory effect against MCF-7 (Pedro-Hernández et al., 2017). Several amide derivatives of ibuprofen have shown enhanced antiproliferative effects when compared to the parent drug (Abourehab et al., 2021). This supports that dexibuprofen-amide derivatives are more effective in inhibiting MCF-7 than the parent drug, ibuprofen (He et al., 2021).

Anti-Inflammatory Activity of Ibuprofen Conjugated with Silicon

In 2017, novel silicon-containing amides derived from ibuprofen were successfully synthesised and investigated for their anti-inflammatory efficacy against nuclear transcription factor kB

DOI:https//doi.org/10.22452/mjs.vol43no1.8
Malaysian Journal of Science 43(1): 86-112 (March 2024)

(NF-kB). There were four potential derivative compounds of silicon-containing amide derivatives that offered better activities for inhibiting NF-kB when compared to ibuprofen as the parent drug. The presence of better biological activity coordinated with the increase in the derivative compound's lipophilicity supports its ability to pass through the cell membrane, making it easier to reach cytosol as the target area of NF-kB activation. From these results, it appeared that the conversion of ibuprofen to the form of amides can affect their anti-inflammatory activity (Pérez et al., 2017).

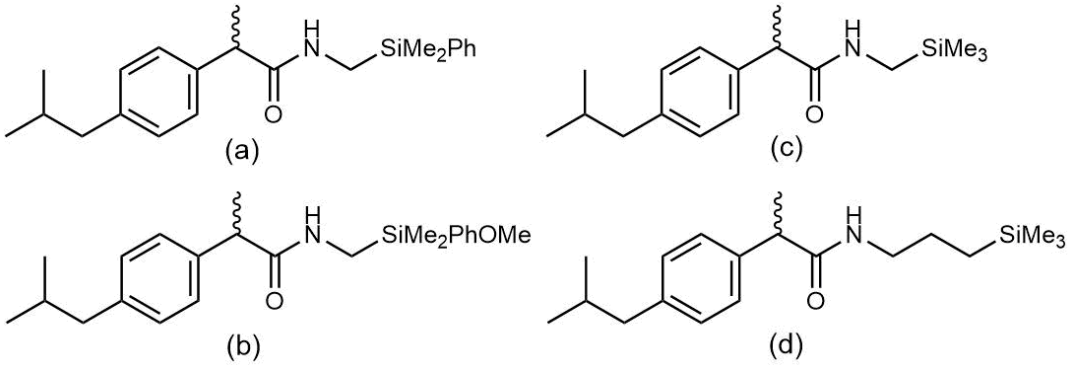

Figure 16. Chemical structure of silicon-containing amide derivatives of ibuprofen

Other studies conducted a modification at the alkyl side chain of ibuprofen by substituting silicon. The synthesis of silicon ibuprofen conjugate, which was later named sila-ibuprofen, was done by reacting 2-[(4-bromo-methyl) phenyl] propionic acid and dimethylchlorosilane (Me_2SiClH) in a one-pot reaction (Scheme 7) (Kleemiss et al., 2020).

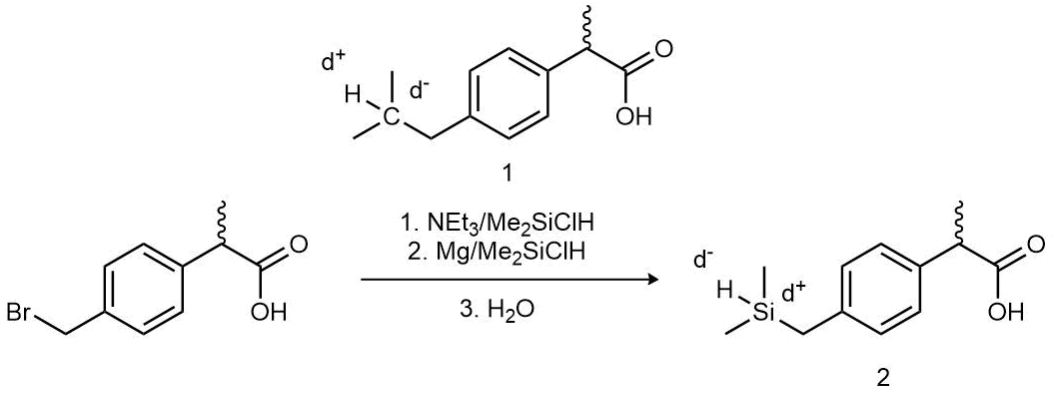

Scheme 7. Synthesis of silicon ibuprofen conjugate

Although there was no significant enhancement in its anti-inflammatory activity as a COX inhibitor, the substitution of silicon onto ibuprofen's structure showed the improvement of physical properties, especially in its solubility. Sila-ibuprofen has four times higher solubility in physiological media than ibuprofen and this property can be useful for further development (Kleemiss et al., 2020).

Anticancer Activity of Ibuprofen with N-Acyl-1,3,4-Oxadiazole Derivatives

Researchers in the field of medical and pharmaceutical chemistry are interested in heterocyclic compounds with nitrogen atoms. Examples of these types of molecules include oxadiazole moieties. Due to its versatility in terms of its effects on living things, the 1,3,4-oxadiazole heterocyclic ring is regarded as one of the most important heterocyclic moieties (Ahsan, 2018; Siwach & Verma, 2020). 1,3,4-oxadiazole derivatives have been reported to exhibit therapeutic activities, such as antibacterial (Glomb & Świątek, 2021), anti-inflammatory (Chawla et al., 2018), antioxidant (Mihailović et al., 2017), and antitumor (Nayak et al., 2021). The compounds have different mechanisms of action that are significant in perceiving the resistance of tumours to standard drug treatment (Glomb et al., 2018).

It was discovered that ibuprofen that is associated with 1,3,4-oxadiazole derivatives with halogen, methoxy, and nitro-substituents exhibited promising results in anticancer studies (Alderawy et al., 2020). The synthesis of the compounds can be summarised as below (Scheme 8).

DOI:https//doi.org/10.22452/mjs.vol43no1.8
Malaysian Journal of Science 43(1): 86-112 (March 2024)

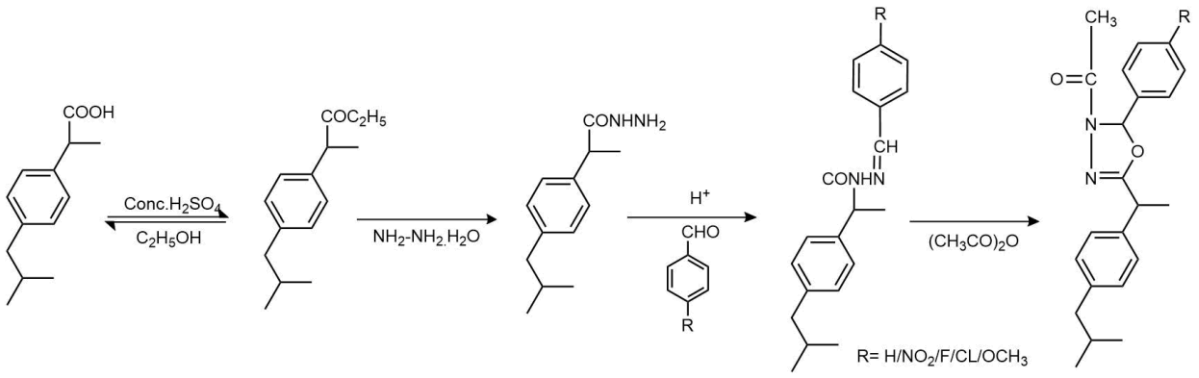

Scheme 8. Synthesis of ibuprofen-N-acyl-1,3,4-oxadiazole

Compounds (a)–(d) (Figure 17) were studied against MCF-7, and it was found that most of the compounds gave high percentage inhibition (Table 11) (Alderawy et al., 2020).

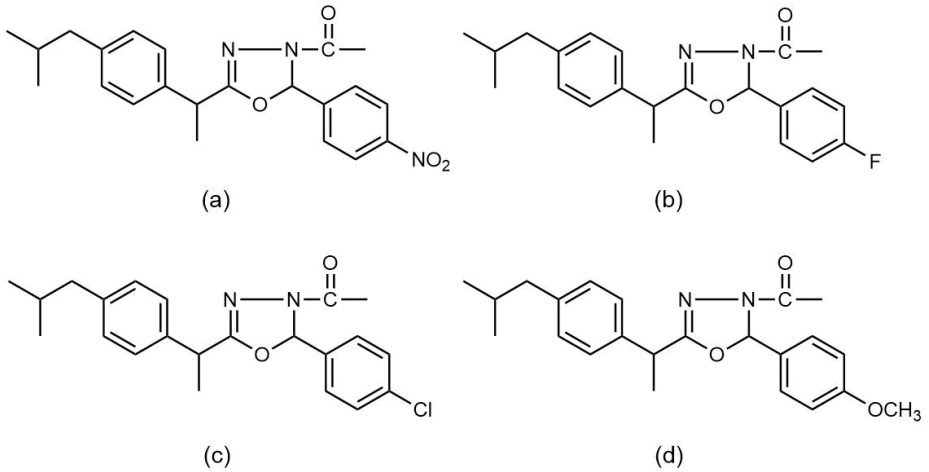

Figure 17. Structure of ibuprofen-N-acyl-1,3,4-oxadiazole with (a) 4-NO_2, (b) 4-Fl, (c) 4-Cl, and (d) 4-OCH_3

Table 11. Percentage Inhibition of MCF-7 by Ibuprofen-N-acyl-1,3,4-Oxadiazole Derivatives

Compound	% Inhibition of MCF-7
(a)	84.9
(b)	85.1
(c)	74.7
(d)	83.8
Control	0

Among all the tested compounds, compound (b) containing 4-fluoro gave the highest inhibition against MCF-7 cell line (85.1%) (Alderawy et al., 2020). The presence of 4-fluoro on 1,3,4-oxadiazole derivatives exhibited great focal adhesion kinase (FAK), which is a common intracellular kinase that regulates signalling pathways related with cellular migration, proliferation, and survival, making it a significant aim in developing anticancer drugs (Liew et al., 2020).

As presumed, NO_2 and 1,3,4-oxadiazole gave one of the highest inhibitions among derivatives, up to 84.9%. These moiety and substitute are quite common in compound derivatives to study the anticancer and antiproliferation activities and were found to be successful in several studies, especially against MCF-7 cell line (Alghamdi & Nazreen, 2020; Hassanzadeh et al., 2020; Khanam et al., 2017; Yadav et al., 2020). It has been demonstrated that derivatives containing aromatic rings and nitro groups exhibit significant cytotoxicity, especially when used against MCF-7 cancer cells.

As 4-methoxy is introduced as a substitute, there was a slight decrease in antitumor activity to 83.8% (Alderawy et al., 2020). Studies found that the methoxy group can contribute to positive results in anticancer activity (Bonakdar et al., 2017; El-Sayed et al., 2017). The number and positioning of the methoxy substituent are also crucial in cytotoxicity (Novilla et al., 2019).

Previous research demonstrated that ibuprofen has limited effectiveness (<20%) against MCF-7 (Pedro-Hernández et al., 2017), but this was not evaluated in the current study. However, the result indicates that the presence of N-acyl-1,3,4-oxadiazole contributes to the anticancer effect against breast cancer cells.

DOI:https//doi.org/10.22452/mjs.vol43no1.8
Malaysian Journal of Science 43(1): 86-112 (March 2024)

Anticancer Activity of Organoselenides-Ibuprofen Derivatives

Compounds containing organoselenium are becoming more significant in the fields of enzymology, medicine, and bio-organic chemistry (Mugesh et al., 2001). Organoselenium-based molecular probes allow accurate detection of physiologically relevant analytes, such as ROS. Production of ROS is linked to Alzheimer, Parkinson, and cancer, where excess production is a key cause (Kumawat et al., 2021; Madibone et al., 2020). The organoselenides-ibuprofen derivatives are synthesised according to Scheme 9.

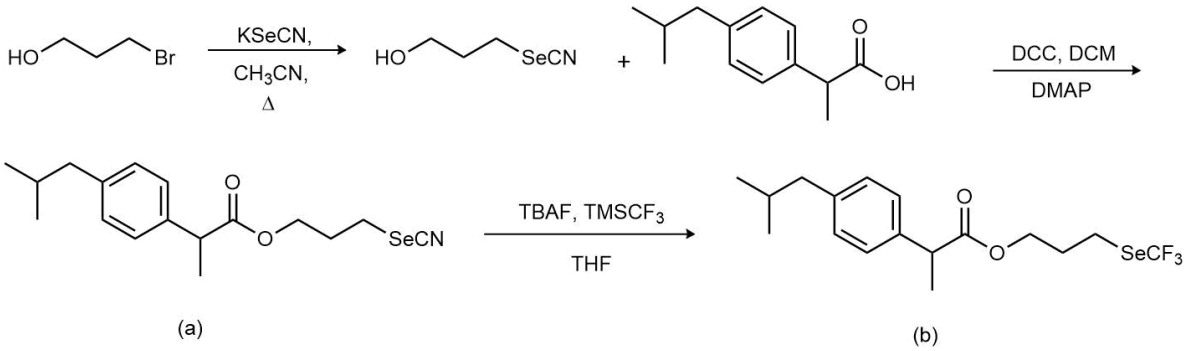

Scheme 9. Synthesis of organoselenides-ibuprofen derivatives. Compound (a) cyano substituted and compound (b) trifluoromethyl substituted

The capability of organoselenides-ibuprofen derivatives to suppress the development of human tumour cell lines, such as $CaCO_2$ (human epithelial colorectal adenocarcinoma cell line), BGC-823 (human gastric cancer cell line), MCF-7, and PC-3 (human prostate cancer cell line) was examined, and the results are presented in Table 12. MTT assay was used to evaluate anticancer activities in vitro while the positive control used was 5-fluorouracil as it is often used in cancer treatment, both adjuvant and palliative.

Table 7. Cytotoxic Activity against $CaCO_2$, BGC-823, MCF-7, and PC-3 by Organoselenides-Ibuprofen Derivatives, Ibuprofen, and 5-Fluorouracil

Compounds	IC_{50} (μM)			
	$CaCO_2$	BGC-823	MCF-7	PC-3
(a)	14.5 ± 1.8	17.3 ± 2.3	8.9 ± 0.8	11.2 ± 2.3
(b)	11.3 ± 1.5	8.2 ± 0.7	7.7 ± 0.6	10.4 ± 0.9
Ibuprofen	>50	>50	>50	>50
5-Fluorouracil	7.8 ± 3.1	15.4 ± 1.8	12.3 ± 2.2	9.5 ± 1.1

Although compound (a) was effective in inhibiting $CaCO_2$, BGC-823, and PC-3 cancer cells, it could not surpass the performance of 5-fluorouracil. However, it was still superior to standard ibuprofen.

Compound (b) was discovered to have higher inhibitory efficacy against $CaCO_2$, BGC-823, MCF-7, and PC-3 cells when the derivatives were compared to ibuprofen. The drug showed lower IC_{50} values against BGC-823 and MCF-7 cells in comparison to the standard anticancer drug, 5-fluorouacil. Compound (b) contains trifluoromethyl ($-CF_3$), which is known to have anticancer effects. It is possible that this factor contributed to the suppression of cancer cells (Lanquist et al., 2021; Olszewska et al., 2020; Scattolin et al., 2020; Wang et al., 2019). Fluorine-containing groups, notably perfluorinated fragments, can drastically modify pharmacological characteristics (Scattolin et al., 2020).

Anticancer Activity of Ibuprofen-Organotin Complexes

Figure 18 illustrates an example of an organotin compound, which is defined as bearing at least one covalent connection between a carbon (C) atom and a tin (Sn) atom. They are usually denoted by the formula $RaSnX_{4-a}$ (a = 1–3, R = aryl or alkyl, X = halogen ion or carboxylate, etc.) (Ghani & Yousif, 2021).

Figure 18. Chemical structure of organotin

Organotin compounds have two stable states, which are (II) and (IV) (Ghani & Yousif, 2021). Since the past few years, organic tin(IV) complexes have been used in the field of cancer treatment and have proven their effectiveness to treat lung cancer (A-549), cervical cancer (HeLa), and breast adenocarcinoma (MDA-MB-231) (Hazra et al., 2016). Lately, the cytotoxicity effect of organotin(IV) has been reported to have great complex synergy with NSAIDs (Antonenko et al., 2022). Complexes of ibuprofen with triorganotin(IV), IBF-dimethyltin(IV), and IBF-dibutyltin(IV) were successfully synthesised by Kumari et al. in 2020. In the same year, Farooqi et al. (2020) also reported on the synthesis of triphenyltin(IV) ibuprofen. The synthesis was done through a single-step reaction by reacting the mixture of triphenyltin

DOI:https//doi.org/10.22452/mjs.vol43no1.8
Malaysian Journal of Science 43(1): 86-112 (March 2024)

hydroxide and ibuprofen in dry ethanol under 7 h reflux. The yield of the product was favourable and it was characterised spectroscopically (Farooqi et al., 2020).

The synthesised compounds (Figure 19) were tested against human cancer cell lines viz. prostate cancer (DU145), colon adenocarcinoma (HCT-15), colorectal cancer ($CaCO_2$), breast cancer (MCF-7), androgen-sensitive prostate adenocarcinoma (LNCaP), and HeLa (Kumari et al., 2020).

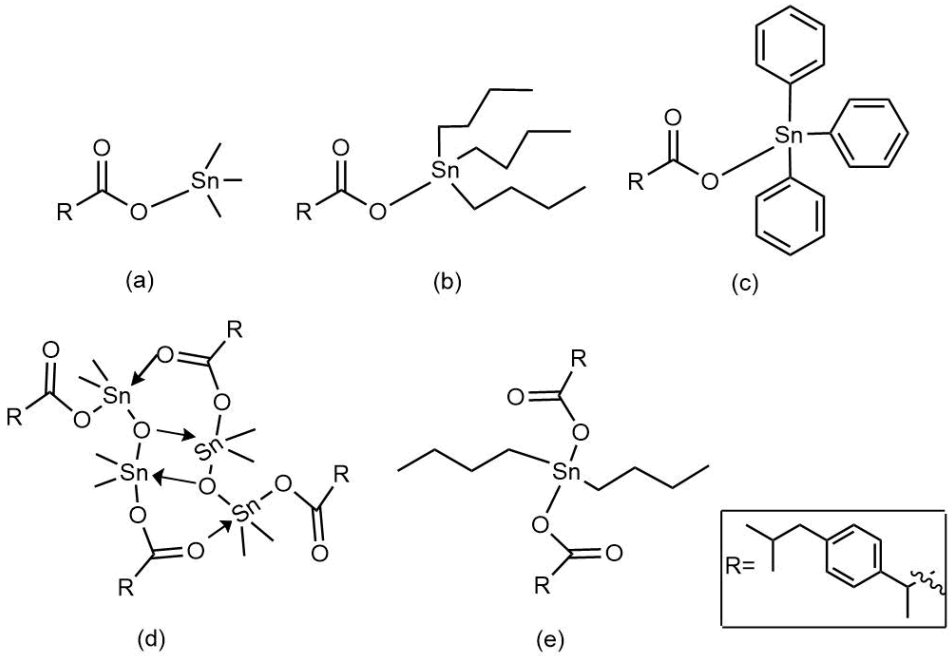

Figure 19. Chemical structure of organotin(IV) complexes with ibuprofen

According to the results (Table 13), the complexes exhibited several activities against various cell lines. Except for compound (a) [$Me_3Sn(IBF)$], all the compounds (b, c, d, and e) induced the cytotoxicity in the researched cancer cell lines. Compound (c) [$Ph_3Sn(IBF)$] exhibited the greatest cytotoxicity against colorectal cancer ($CaCO_2$), with an IC_{50} value of 1.21 µM, which was superior compared to cisplatin, followed by compound (b) [$Bu_3Sn(IBF)$] (IC_{50} = 2.48 µM) and compound (d) [$[Me_2Sn(IBF)]_2O_2$] (IC_{50} = 13.38 µM). Furthermore, IBF demonstrated potent cytotoxicity only against prostate cancer cells (DU145) (IC_{50} = 1.65 µM) while being non-cytotoxic (IC_{50} 100 µM) against HCT-15 and $CaCO_2$ cell lines. In terms of IC_{50} value against DU145, compound (d) and (e) [$Bu_2Sn(IBF)_2$] demonstrated approximately 2.6–4.0 times higher activity than 5-fluorouracil. Compound (c) was moderately cytotoxic to DU145. Compound (d) (IC_{50} = 2.188 µM) also demonstrated the greatest cytotoxicity against colon cancer cells (HCT-15), which was approximately 6 and 2 times greater than 5-fluorouracil and cisplatin, respectively. As a result, compound (d) was highly cytotoxic, with the greatest cytotoxicity against prostate and colon cancer cell lines among compound (a)–(e), whereas compound (c) was very cytotoxic to colorectal cancer cell lines (Kumari et al., 2020).

Table 8. Cytotoxicity of Synthesised Compounds against Tested Cancer Cell Lines

Compounds	IC_{50} (µM)		
	DU145	HCT-15	$CaCO_2$
(a)	100	100	100
(b)	100	100	2.48 ± 0.1
(c)	19.22 ± 0.8	100	1.21 ± 0.84
(d)	3.97 ± 0.81	2.188 ± 0.67	13.38 ± 1.5
(e)	5.92 ± 1.54	32.32 ± 2.1	100
Ibuprofen	1.65 ± 0.2	100	100
5-Fluorouracil	15.4 ± 0.8	12.2 ± 0.5	-
Cisplatin	-	5.04 ± 1.4	96.38 ± 32.03

DOI:https//doi.org/10.22452/mjs.vol43no1.8
Malaysian Journal of Science 43(1): 86-112 (March 2024)

4. Conclusions

The modification of drugs to find other or better biological activities that can benefit humankind has become increasingly common. This review article offers a comprehensive synthesis and analysis of common drugs, including their modifications and effects on potential biological activities. The introduction of metal complexes (Cu, Co, Mg, etc.) in over-the-counter drug modification, especially acetaminophen and ibuprofen, enhanced the effectiveness of ligands to inhibit bacterial growth. The antimicrobial activities of M-piperaquine-acetaminophen, M-prednisolone-acetaminophen, Mg(II)acetaminophen, and M-acetaminophen-ascorbic acid against Gram-positive and Gram-negative bacteria are higher compared to standard acetaminophen. The metal complex of ibuprofen-thiourea is a great urease inhibitor compared to ibuprofen, especially at meta-position with chloro-substituent. Chlorine is more electronegative and has smaller atoms, which may affect the urease inhibitory activity. The removal of carboxylic acid in ibuprofen (affect gastrointestinal) is replaced by ammonium moieties, which are slightly better than ibuprofen in terms of anti-inflammatory activity. Ibuprofen-amide derivatives also showed positive anti-inflammatory results compared to standard celecoxib, and the presence of halogen (Br) affected cell permeability, thus increasing the potency of FAAH/substrate-selective COX inhibitors. Ibuprofen silicon conjugate has high antioxidant activity. Ibuprofen with 1,3,4-oxadiazole gives promising results in the anticancer activity of breast cancer cells, especially in halogen-, methoxy-, and nitro-substituted compounds. Furthermore, ibuprofen with organotin complexes has better anticancer activity compared to the parent drug. According to the findings of this review article, the majority of the derivatives or metal complexes of acetaminophen and ibuprofen exhibited promising biological activities, although further research is necessary to fully exploit the potential of these compounds in developing novel therapeutics. This includes studying their safety, pharmacokinetics, and pharmacodynamics, as well as optimising novel modifications or metal complexes of current acetaminophen and ibuprofen to improve their therapeutic applications.

5. Acknowledgement

The authors wish to express their gratitude to the Malaysia Ministry of Higher Education (MOHE) for the support through Fundamental Research Grant Scheme (FRGS/1/2020/STG04/UNISZA/03/1).

6. References

Abd El-Halim, H. F., Mohamed, G. G., & Anwar, M. N. (2018). Antimicrobial and anticancer activities of Schiff base ligand and its transition metal mixed ligand complexes with heterocyclic base. Applied Organometallic Chemistry, 32(1), e3899. https://doi.org/10.1002/aoc.3899

Abourehab, M. A. S., Alqahtani, A. M., Almalki, F. A., Zaher, D. M., Abdalla, A. N., Gouda, A. M., & Beshr, E. A. M. (2021). Pyrrolizine/Indolizine-NSAID Hybrids: Design, Synthesis, Biological Evaluation, and Molecular Docking Studies. Molecules, 26(21), 6582. https://doi.org/10.3390/molecules26216582

Ahmadi, A., Khalili, M., Olama, Z., Karami, S., & Nahri-Niknafs, B. (2017). Synthesis and Study of Analgesic and Anti-inflammatory Activities of Amide Derivatives of Ibuprofen. Mini-Reviews in Medicinal Chemistry, 17(9), 799–804. https://doi.org/10.2174/1389557516666161226155951

Ahmed, E. F., El-baky, R. M. A., Ahmed, A. B. F., Gameel, N., Aziz, N. A., Fadl, G., & Gad, M. (2016). Evaluation of antibacterial activity of some non- steroidal anti-inflammatory drugs against Escherichia coli causing urinary tract infection. African Journal of Microbiology Research, 10(34), 1408–1416. https://doi.org/10.5897/AJMR2016.8179

Ahn, K., Johnson, D. S., & Cravatt, B. F. (2009). Fatty acid amide hydrolase as a potential therapeutic target for the treatment of pain and CNS disorders. Expert Opinion on Drug Discovery, 4(7), 763–784. https://doi.org/10.1517/17460440903018857

Ahsan, M. J. (2018). Synthesis and cytotoxicity evaluation of [(2,4-dichlorophenoxy)methyl]-5-aryl-1,3,4-oxadiazole/4H-1,2,4-triazole analogues. Turkish Journal of Chemistry, 42(5), 1334–1343. https://doi.org/10.3906/kim-1803-25

Akhondzadeh, S. (2016). The importance of clinical trials in drug development. Avicenna Journal of Medical Biotechnology, 8(4), 2016.

Al-Amiery, A. A., Kadhum, A. A. H., & Mohamad, A. B. (2012). Antifungal and antioxidant activities of pyrrolidone thiosemicarbazone complexes. Bioinorganic Chemistry and Applications, 2012(L). https://doi.org/10.1155/2012/795812

DOI:https//doi.org/10.22452/mjs.vol43no1.8
Malaysian Journal of Science 43(1): 86-112 (March 2024)

Alderawy, M. Q. A., Raheem Alrubaie, L. A., & Sheri, F. H. (2020). Synthesis, characterization of ibuprofen n-acyl-1,3,4 oxadiazole derivatives and anticancer activity against MCF-7 cell line. Systematic Reviews in Pharmacy, 11(4), 681–689. https://doi.org/10.31838/srp.2020.4.100

Alghamdi, A., & Nazreen, S. (2020). Synthesis, characterization and cytotoxic study of 2-hydroxy benzothiazole incorporated 1,3,4-oxadiazole derivatives. Egyptian Journal of Chemistry, 63(2), 471–482. https://doi.org/10.21608/ejchem.2019.17265.2059

Alkabodi, I., Almekhlafi, S., & Ibrahim, D. A. (2016). Synthesis and anti-inflammatory activity of novel aspirin and ibuprofen amide derivatives. Chemical and Pharmaceutical Research, 8(May 2019), 307–313.

AlKhalil, M., Al-Hiari, Y., Kasabri, V., Arabiyat, S., Al-Zweiri, M., Mamdooh, N., & Telfah, A. (2020). Selected pharmacotherapy agents as antiproliferative and anti-inflammatory compounds. Drug Development Research, 81(4), 470–490. https://doi.org/10.1002/ddr.21640

Amin, R. R., Abo-elkassem, M., & Anwar, A. (2017). Synthesis , Characterization , and Spectroscopic Studies for New Cu (II), Co (II), Zn (II), Fe (III) And Zr (II) Complexes of Oxytetracycline Antibiotic , In vitro Antimicrobial Assessment Studies. Research and Reviews : Journal of Pharmacy and Pharmaceutical Sciences, 6(1), 38–48.

Amir, M., Akhter, M. W., & Alam, O. (2016). Synthesis, characterization, and biological evaluation of furoxan coupled ibuprofen derivatives as anti-inflammatory agents. Monatshefte Fur Chemie, 147(3), 493–508. https://doi.org/10.1007/s00706-015-1557-x

Annerberg, A., Lwin, K. M., Lindegardh, N., Khrutsawadchai, S., Ashley, E., Day, N. P. J. J., Singhasivanon, P., Tarning, J., White, N. J., & Nosten, F. (2011). A Small Amount of Fat Does Not Affect Piperaquine Exposure in Patients with Malaria □ †. 55(9), 3971–3976. https://doi.org/10.1128/AAC.00279-11

Ansari, A., Ali, A., Asif, M., & Shamsuzzaman. (2017). Review: biologically active pyrazole derivatives. New Journal of Chemistry, 41(1), 16–41. https://doi.org/10.1039/C6NJ03181A

Antonenko, T. A., Gracheva, Y. A., Shpakovsky, D. B., Vorobyev, M. A., Tafeenko, V. A., Mazur, D. M., & Milaeva, E. R. (2022). Cytotoxic activity of organotin compounds containing non-steroidal anti-inflammatory drugs. Journal of Organometallic Chemistry, 960, 122191. https://doi.org/10.1016/j.jorganchem.2021.122191

Ashraf, Z., Mahmood, T., Hassan, M., Afzal, S., Rafique, H., Afzal, K., & Latip, J. (2019). Dexibuprofen amide derivatives as potential anticancer agents: Synthesis, in silico docking, bioevaluation, and molecular dynamic simulation. Drug Design, Development and Therapy, 13, 1643–1657. https://doi.org/10.2147/DDDT.S178595

Assefa, D. G., Zeleke, E. D., Bekele, D., Tesfahunei, H. A., Getachew, E., Joseph, M., & Manyazewal, T. (2021). Efficacy and safety of dihydroartemisinin – piperaquine versus artemether – lumefantrine for treatment of uncomplicated Plasmodium falciparum malaria in Ugandan children : a systematic review and meta - analysis of randomized control trials. Malaria Journal, 1–25. https://doi.org/10.1186/s12936-021-03711-4

Attia, M., Essa, E. A., Zaki, R. M., & Elkordy, A. A. (2020). An overview of the Antioxidant Effects of Ascorbic Acid and Alpha Lipoic Acid (In Liposomal Forms) as Adjuvant in Cancer Treatment. Antioxidants, 9(5), 1–15. https://doi.org/10.3390/antiox9050359

Ayipo, Y. O., Obaleye, J. A., & Badeggi, U. M. (2016). Novel metal complexes of mixed piperaquine-acetaminophen and piperaquine-acetylsalicylic acid: Synthesis, characterization and antimicrobial activities. Journal of the Turkish Chemical Society, Section A: Chemistry, 4(1), 313–313. https://doi.org/10.18596/jotcsa.287331

Ayipo, Y., Osunniran, W., Badeggi, U., Saheed, I., Jimoh, A., & Babamale, H. (2021). Synthesis, characterization and antibacterial study of Co(II) and Cu(II) complexes of mixed ligands of piperaquine and diclofenac. Journal of the Turkish Chemical Society Section A: Chemistry, 8(2), 633–650. https://doi.org/10.18596/jotcsa.898523

Babamale, H., Lawal, A., Rajee, O., & Oloyede, E. (2016). Synthesis , Characterization and Biological Activity Studies of Mixed Paracetamol- Ascorbic Acid Metal Complexes . Applied Science Environment, 20(4), 1157–1161. https://doi.org/http://dx.doi.org/10.4314/jasem.v20i4.32

Badea, G. I., & Radu, G. L. (2018). Introductory Chapter: Carboxylic Acids - Key Role in Life Sciences. In Carboxylic Acid - Key Role in Life Sciences (pp. 1–6). InTech. https://doi.org/10.5772/intechopen.77021

Bamigboye, M. O., Ejidike, I. P., & Ahmed, R. N. (2019). Antibacterial activities of Some Mixed Isoniazid-Ibuprofen Metal Complexes : Chelation and Characterization. Natural & Applied Science Journal, 2(2). https://doi.org/10.38061/idunas.631229

DOI:https//doi.org/10.22452/mjs.vol43no1.8
Malaysian Journal of Science 43(1): 86-112 (March 2024)

Barba, F. J., Esteve, M. J., & Frígola, A. (2014). Chapter 11 - Bioactive Components from Leaf Vegetable Products. In B. T.-S. in N. P. C. Atta-ur-Rahman (Ed.), Studies in Natural Products Chemistry (Vol. 41, pp. 321–346). Elsevier. https://doi.org/https://doi.org/10.1016/B978-0-444-63294-4.00011-5

Bateman, D. N., Carroll, R., Pettie, J., Yamamoto, T., Elamin, M. E. M. O., Peart, L., Dow, M., Coyle, J., Cranfield, K. R., Hook, C., Sandilands, E. A., Veiraiah, A., Webb, D., Gray, A., Dargan, P. I., Wood, D. M., Thomas, S. H. L., Dear, J. W., & Eddleston, M. (2014). Effect of the UK's revised paracetamol poisoning management guidelines on admissions, adverse reactions and costs of treatment. British Journal of Clinical Pharmacology, 78(3), 610–618. https://doi.org/10.1111/bcp.12362

Bhandari, S. V., Bothara, K. G., Raut, M. K., Patil, A. A., Sarkate, A. P., & Mokale, V. J. (2008). Design, Synthesis and Evaluation of Antiinflammatory, Analgesic and Ulcerogenicity studies of Novel S-Substituted phenacyl-1,3,4-oxadiazole-2-thiol and Schiff bases of Diclofenac acid as Nonulcerogenic Derivatives. Bioorganic and Medicinal Chemistry, 16(4), 1822–1831. https://doi.org/10.1016/j.bmc.2007.11.014

Biancatelli, R. M. L. C., Berrill, M., & Marik, P. E. (2020). The antiviral properties of vitamin C. Expert Review of Anti-Infective Therapy, 18(2), 99–101. https://doi.org/10.1080/14787210.2020.1706483

Bonakdar, A. P. S., Vafaei, F., Farokhpour, M., Esfahani, M. H. N., & Massah, A. R. (2017). Synthesis and anticancer activity assay of novel chalcone-sulfonamide derivatives. Iranian Journal of Pharmaceutical Research, 16(2), 565–568.

Caparrotta, T. M., Antoine, D. J., & Dear, J. W. (2018). Are some people at increased risk of paracetamol-induced liver injury? A critical review of the literature. European Journal of Clinical Pharmacology, 74(2), 147–160. https://doi.org/10.1007/s00228-017-2356-6

Chawla, G., Naaz, B., & Siddiqui, A. A. (2018). Exploring 1,3,4-Oxadiazole Scaffold for Anti-inflammatory and Analgesic Activities: A Review of Literature From 2005-2016. Mini-Reviews in Medicinal Chemistry, 18(3), 216–233. https://doi.org/10.2174/1389557517666170127121215

Chudobova, D., Dostalova, S., Ruttkay-Nedecky, B., Guran, R., Rodrigo, M. A. M., Tmejova, K., Krizkova, S., Zitka, O., Adam, V., & Kizek, R. (2015). The effect of metal ions on Staphylococcus aureus revealed by biochemical and mass spectrometric analyses. Microbiological Research, 170(June 2014), 147–156. https://doi.org/10.1016/j.micres.2014.08.003

Collignon, P. C., Conly, J. M., Andremont, A., McEwen, S. A., & Aidara-Kane, A. (2016). World Health Organization Ranking of Antimicrobials According to Their Importance in Human Medicine: A Critical Step for Developing Risk Management Strategies to Control Antimicrobial Resistance From Food Animal Production. Clinical Infectious Diseases, 63(8), 1087–1093. https://doi.org/10.1093/cid/ciw475

Cong, W., Sun, Y., Sun, Y. F., Yan, W. Bin, Zhang, Y. L., Gao, Z. F., Wang, C. H., Hou, G. G., & Zhang, J. J. (2021). Trifluoromethyl-substituted 3,5-bis(arylidene)-4-piperidones as potential anti-hepatoma and anti-inflammation agents by inhibiting NF-κB activation. Journal of Enzyme Inhibition and Medicinal Chemistry, 36(1), 1622–1631. https://doi.org/10.1080/14756366.2021.1953996

Corey, D. R. (2007). Chemical modification: The key to clinical application of RNA interference? Journal of Clinical Investigation, 117(12), 3615–3622. https://doi.org/10.1172/JCI33483

Dainese, E., Oddi, S., Simonetti, M., Sabatucci, A., Angelucci, C. B., Ballone, A., Dufrusine, B., Fezza, F., De Fabritiis, G., & Maccarrone, M. (2020). The endocannabinoid hydrolase FAAH is an allosteric enzyme. Scientific Reports, 10(1), 2292. https://doi.org/10.1038/s41598-020-59120-1

Damilola, A., Olagboye, S. A., & Akinwunmi, O. . (2019). Antimicrobial Activities of Novel Synthesized Cu(II) and Co(II) Mixed Ligand Complexes of Prednisolone and Paracetamol. International Journal of Scientific & Engineering Researc, 10(September). https://www.researchgate.net/publication/344429477_ANTIMICROBIAL_ACTIVITIES_OF_NOVEL_SYNTHESIZED_Cu_II_and_Co_II_MIXED_LIGAND_COMPLEXES_OF_PREDNISOLONE_AND_PARACETAMOL?channel=doi&linkId=5f746650299bf1b53e004bc5&showFulltext=true

Deplano, A., Cipriano, M., Moraca, F., Novellino, E., Catalanotti, B., Fowler, C. J., & Onnis, V. (2019). Benzylamides and piperazinoarylamides of ibuprofen as fatty acid amide hydrolase inhibitors. Journal of Enzyme Inhibition and Medicinal Chemistry, 34(1), 562–576. https://doi.org/10.1080/14756366.2018.1532418

Deplano, A., Karlsson, J., Svensson, M., Moraca, F., Catalanotti, B., Fowler, C. J., & Onnis, V. (2020). Exploring the fatty acid amide hydrolase and cyclooxygenase inhibitory properties of novel amide derivatives of ibuprofen. Journal of Enzyme Inhibition and Medicinal Chemistry, 35(1), 815–823. https://doi.org/10.1080/14756366.2020.1743283

DOI:https//doi.org/10.22452/mjs.vol43no1.8
Malaysian Journal of Science 43(1): 86-112 (March 2024)

Dinarello, C. A. (2010). Anti-inflammatory Agents: Present and Future. Cell, 140(6), 935–950. https://doi.org/10.1016/j.cell.2010.02.043

El-Sayed, S., Metwally, K., El-Shanawani, A. A., Abdel-Aziz, L. M., Pratsinis, H., & Kletsas, D. (2017). Synthesis and anticancer activity of novel quinazolinone-based rhodanines. Chemistry Central Journal, 11(1), 1–10. https://doi.org/10.1186/s13065-017-0333-x

Ennis, Z. N., Dideriksen, D., Vægter, H. B., Handberg, G., & Pottegård, A. (2016). Acetaminophen for Chronic Pain: A Systematic Review on Efficacy. Basic and Clinical Pharmacology and Toxicology, 118(3), 184–189. https://doi.org/10.1111/bcpt.12527

Fang, W. Y., Ravindar, L., Rakesh, K. P., Manukumar, H. M., Shantharam, C. S., Alharbi, N. S., & Qin, H. L. (2019). Synthetic approaches and pharmaceutical applications of chloro-containing molecules for drug discovery: A critical review. European Journal of Medicinal Chemistry, 173, 117–153. https://doi.org/10.1016/j.ejmech.2019.03.063

Fejzagić, A. V., Gebauer, J., Huwa, N., & Classen, T. (2019). Halogenating enzymes for active agent synthesis: First steps are done and many have to follow. Molecules, 24(21). https://doi.org/10.3390/molecules24214008

Garza-Cervantes, J. A., Chávez-Reyes, A., Castillo, E. C., García-Rivas, G., Ortega-Rivera, O. A., Salinas, E., Ortiz-Martínez, M., Gómez-Flores, S. L., Peña-Martínez, J. A., Pepi-Molina, A., Treviño-González, M. T., Zarate, X., Cantú-Cárdenas, M. E., Escarcega-Gonzalez, C. E., & Morones-Ramírez, J. R. (2017). Synergistic antimicrobial effects of silver/transition-metal combinatorial treatments. Scientific Reports, 7(1), 1–16. https://doi.org/10.1038/s41598-017-01017-7

Gerriets, V., Anderson, J., & Nappe, T. M. (2023). Acetaminophen. In StatPearls. http://www.ncbi.nlm.nih.gov/pubmed/24099020

Ghani, H., & Yousif, E. (2021). Chemistry of Some Organotin Compounds. Al-Nahrain Journal of Science, 24(3), 9–15. https://doi.org/10.22401/ANJS.24.3.02

Glomb, T., & Świątek, P. (2021). Antimicrobial Activity of 1,3,4-Oxadiazole Derivatives. International Journal of Molecular Sciences, 22(13), 6979. https://doi.org/10.3390/ijms22136979

Glomb, T., Szymankiewicz, K., & Świątek, P. (2018). Anti-Cancer Activity of Derivatives of 1,3,4-Oxadiazole. Molecules, 23(12), 3361. https://doi.org/10.3390/molecules23123361

Golonka, I., Oleksy, M., Junka, A., Matera-witkiewicz, A., Bartoszewicz, M., & Musiał, W. (2017). Selected Physicochemical and Biological Properties of Ethyl Ascorbic Acid Compared to Ascorbic Acid. Biol. Pharm. Bull., 40(8), 1199–1206. https://doi.org/10.1248/bpb.b16-00967

Gomaa, S. (2018). Adverse effects induced by diclofenac , ibuprofen , and paracetamol toxicity on immunological and biochemical parameters in Swiss albino mice. Basic and Applied Zoology, 79(5), 1–9. https://doi.org/10.1186/s41936-018-0025-7

Goodman, M. C., Xu, S., Rouzer, C. A., Banerjee, S., Ghebreselasie, K., Migliore, M., Piomelli, D., & Marnett, L. J. (2018). Dual cyclooxygenase–fatty acid amide hydrolase inhibitor exploits novel binding interactions in the cyclooxygenase active site. Journal of Biological Chemistry, 293(9), 3028–3038. https://doi.org/10.1074/jbc.M117.802058

Guo, Z.-R. (2012). [Modification of natural products for drug discovery]. Yao xue xue bao = Acta pharmaceutica Sinica, 47(2), 144–157. http://www.ncbi.nlm.nih.gov/pubmed/22512023

Haider, S., Alam, M. S., Hamid, H., Umar, S., Kumar, D., & Nazreen, S. (2018). Synthesis of novel amide containing Schiffs bases of 5-(4-chloro-phenyl)-furan-2-carboxaldehyde: Their in vivo anti-inflammatory, antioxidant and antinociceptive activities with ulcerogenic risk evaluation. Journal of Reports in Pharmaceutical Sciences, 7(1), 44–63.

Hassanzadeh, F., Jafari, E., Zarabi, M., Khodarahmi, G., & Vaseghi, G. (2020). Synthesis, cytotoxic evaluation, and molecular docking studies of some new 1, 3, 4-oxadiazole-based compounds. Research in Pharmaceutical Sciences, 15(5), 454. https://doi.org/10.4103/1735-5362.297848

Hazra, S., Paul, A., Sharma, G., Koch, B., da Silva, M. F. C. G., & Pombeiro, A. J. L. (2016). Sulfonated Schiff base Sn(IV) complexes as potential anticancer agents. Journal of Inorganic Biochemistry, 162, 83–95. https://doi.org/10.1016/j.jinorgbio.2016.06.008

He, X., Nie, Y., Zhong, M., Li, S., Li, X., Guo, Y., Liu, Z., Gao, Y., Ding, F., Wen, D., & Zhang, Y. (2021). New organoselenides (NSAIDs-Se derivatives) as potential anticancer agents: Synthesis, biological evaluation and in silico calculations. European Journal of Medicinal Chemistry, 218, 113384. https://doi.org/10.1016/j.ejmech.2021.113384

Hegde, P., Boshoff, H. I. M., Rusman, Y., Aragaw, W. W., Salomon, C. E., Dick, T., & Aldrich, C. C. (2021). Reinvestigation of the structure-activity relationships of isoniazid. Tuberculosis, 129, 102100. https://doi.org/10.1016/j.tube.2021.102100

DOI:https//doi.org/10.22452/mjs.vol43no1.8
Malaysian Journal of Science 43(1): 86-112 (March 2024)

Hernandez-Patlan, D., B.Solis-Cruz, Mendez-Albores, A., Latorre, Hernandez-Velasco, J. D., X., R., L.-A., & Tellez, G. (2017). Comparison of PrestoBlue â and plating method to evaluate antimicrobial activity of ascorbic acid , boric acid and curcumin in an in vitro gastrointestinal model. Applied Microbiology, 124(2), 423–430. https://doi.org/10.1111/jam.13659

Hill, R. G., & Rang, H. P. (2013). Drug Discovery & Development - Technology in Transition (R. G. Hill & H. P. Rang (eds.); 2nd ed.). Churchill Livingstone, ELSEVIER.

Hu, Y., Zhang, S., Zhao, F., Gao, C., Feng, L., Lv, Z., Xu, Z., & Wu, X. (2017). SC. European Journal of Medicinal Chemistry. https://doi.org/10.1016/j.ejmech.2017.04.002

Hughes, J. P., Rees, S., Kalindjian, S. B., Philpott, K. L., Philpott, K., & Building, H. (2011). Principles of early drug discovery Correspondence. https://doi.org/10.1111/j.1476-5381.2010.01127.x

Iqbal Farooqi, S., Arshad, N., Perveen, F., Ali Channar, P., Saeed, A., Javed, A., Hökelek, T., & Flörke, U. (2020). Structure and surface analysis of ibuprofen-organotin conjugate: Potential anti-cancer drug candidacy of the compound is proven by in-vitro DNA binding and cytotoxicity studies. Polyhedron, 192, 114845. https://doi.org/10.1016/j.poly.2020.114845

Iseh, A., Adegbola, A., & Adeagbo, B. (2017). Pharmacokinetic Characterization of Piperaquine in Nigerian Healthy Volunteers after Co-administration with a Commercial Brand of Moringa Tea. British Journal of Pharmaceutical Research, 15(4), 1–10. https://doi.org/10.9734/BJPR/2017/32723

Kafarski, P., & Talma, M. (2018). Recent advances in design of new urease inhibitors: A review. Journal of Advanced Research, 13, 101–112. https://doi.org/10.1016/j.jare.2018.01.007

Khanam, R., Ahmad, K., Hejazi, I. I., Siddique, I. A., Kumar, V., Bhat, A. R., Azam, A., & Athar, F. (2017). Inhibitory growth evaluation and apoptosis induction in MCF-7 cancer cells by new 5-aryl-2-butylthio-1,3,4-oxadiazole derivatives. Cancer Chemotherapy and Pharmacology, 80(5), 1027–1042. https://doi.org/10.1007/s00280-017-3414-6

Khosroshahi, A. M., Aflaki, F., Saemiyan, N., Abdollahpour, A., & Asgharian, R. (2016). Simultaneous determination of paracetamol, 4-Aminophenol, 4-Chloroacetanilid, Benzyl alcohol, Benzaldehyde and EDTA by HPLC method in paracetamol injection ampoule. Journal of Pharmaceutical and Health Sciences, 4(1), 61–69.

Kilburg, M., & Tyler, R. (2017). Ibuprofen Synthesis – Writing Anthology. https://central.edu/writing-anthology/2019/04/11/ibuprofen-synthesis/

Kingsley Ogemdi, I. (2019). A Review on the Properties and Uses of Paracetamol. International Journal of Pharmacy and Chemistry, 5(3), 31. https://doi.org/10.11648/j.ijpc.20190503.12

Kiriiri, G. K., Njogu, P. M., & Mwangi, A. N. (2020). Exploring different approaches to improve the success of drug discovery and development projects: a review. Future Journal of Pharmaceutical Sciences, 6(1). https://doi.org/10.1186/s43094-020-00047-9

Kleemiss, F., Justies, A., Duvinage, D., Watermann, P., Ehrke, E., Sugimoto, K., Fugel, M., Malaspina, L. A., Dittmer, A., Kleemiss, T., Puylaert, P., King, N. R., Staubitz, A., Tzschentke, T. M., Dringen, R., Grabowsky, S., & Beckmann, J. (2020). Sila-Ibuprofen. Journal of Medicinal Chemistry, 63(21), 12614–12622. https://doi.org/10.1021/acs.jmedchem.0c00813

Kowalska-Krochmal, B., & Dudek-Wicher, R. (2021). The Minimum Inhibitory Concentration of Antibiotics: Methods, Interpretation, Clinical Relevance. Pathogens, 10(2), 165. https://doi.org/10.3390/pathogens10020165

Kumari, R., Banerjee, S., Roy, P., & Nath, M. (2020). Organotin(IV) complexes of NSAID, ibuprofen, X-ray structure of Ph3Sn(IBF), binding and cleavage interaction with DNA and in vitro cytotoxic studies of several organotin complexes of drugs. Applied Organometallic Chemistry, 34(1), 1–24. https://doi.org/10.1002/aoc.5283

Kumawat, A., Raheem, S., Ali, F., Dar, T. A., Chakrabarty, S., & Rizvi, M. A. (2021). Organoselenium compounds as acetylcholinesterase inhibitors: Evidence and mechanism of mixed inhibition. Journal of Physical Chemistry B, 125(6), 1531–1541. https://doi.org/10.1021/acs.jpcb.0c08111

Kumria, R., Nair, A. B., Goomber, G., & Gupta, S. (2016). Buccal films of prednisolone with enhanced bioavailability. Drug Delivery, 23(2), 471–478. https://doi.org/10.3109/10717544.2014.920058

Lanquist, A. P., Gupta, S., Al-Afyouni, K. F., Al-Afyouni, M., Kodanko, J. J., & Turro, C. (2021). Trifluoromethyl substitution enhances photoinduced activity against breast cancer cells but reduces ligand exchange in Ru(II) complex †. https://doi.org/10.1039/d1sc03213e

Liew, S. K., Malagobadan, S., Arshad, N. M., & Nagoor, N. H. (2020). A review of the structure—activity relationship of natural and synthetic antimetastatic compounds. Biomolecules, 10(1), 1–28. https://doi.org/10.3390/biom10010138

DOI:https//doi.org/10.22452/mjs.vol43no1.8
Malaysian Journal of Science 43(1): 86-112 (March 2024)

Lobo, S. (2020). Is there enough focus on lipophilicity in drug discovery? Expert Opinion on Drug Discovery, 15(3), 261–263. https://doi.org/10.1080/17460441.2020.1691995

Ma, R., Guo, D.-X., Li, H.-F., Liu, H.-X., Zhang, Y.-R., Ji, J.-B., Xing, J., & Wang, S.-Q. (2019). Spectroscopic methodologies and molecular docking studies on the interaction of antimalarial drug piperaquine and its metabolites with human serum albumin. Spectrochimica Acta Part A: Molecular and Biomolecular Spectroscopy, 222, 117158. https://doi.org/https://doi.org/10.1016/j.saa.2019.117158

Maddila, S., Gorle, S., Sampath, C., & Lavanya, P. (2016). Synthesis and anti-inflammatory activity of some new 1,3,4-thiadiazoles containing pyrazole and pyrrole nucleus. Journal of Saudi Chemical Society, 20, S306–S312. https://doi.org/10.1016/j.jscs.2012.11.007

Madibone, K. S., Deshmukh, P. P., Navalkar, A., Maji, S. K., Badani, P. M., & Manjare, S. T. (2020). Cyclic Organoselenide BODIPY-Based Probe: Targeting Superoxide in MCF-7 Cancer Cells. ACS Omega, 5(23), 14186–14193. https://doi.org/10.1021/acsomega.0c02074

Malik, M. A., Dar, O. A., Gull, P., Wani, M. Y., & Hashmi, A. A. (2018). Heterocyclic Schiff base transition metal complexes in antimicrobial and anticancer chemotherapy. MedChemComm, 9(3), 409–436. https://doi.org/10.1039/c7md00526a

Marrs, W., & Stella, N. (2009). Measuring Endocannabinoid Hydrolysis: Refining our Tools and Understanding. AAPS, 11(No.2). https://doi.org/10.1208/s12248-009-9109-0

Martínez, M., Carranza, M. P., Massaguer, A., Santos, L., Organero, J. A., Aliende, C., De Llorens, R., Ng-Choi, I., Feliu, L., Planas, M., Rodríguez, A. M., Manzano, B. R., Espino, G., & Jalón, F. A. (2017). Synthesis and Biological Evaluation of Ru(II) and Pt(II) Complexes Bearing Carboxyl Groups as Potential Anticancer Targeted Drugs. Inorganic Chemistry, 56(22), 13679–13696. https://doi.org/10.1021/acs.inorgchem.7b01178

Mata, A. M. O. F. da, Carvalho, R. M. de, Alencar, M. V. O. B. de, Cavalcante, Melo, A. A. de C., & Silva, B. B. da. (2016). Ascorbic Acid in the Prevention and Treatment of Cancer. 62(7), 680–686. https://doi.org/10.1590/1806-9282.62.07.680

Mehta, N., Aggarwal, S., Thareja, S., Malla, P., Misra, M., Bhardwaj, T. R., & Kumar, M. (2010). Synthesis, pharmacological and toxicological evaluation of amide derivatives of ibuprofen. International Journal of ChemTech Research, 2(1), 233–238.

Mian, P., van den Anker, J. N., van Calsteren, K., Annaert, P., Tibboel, D., Pfister, M., Allegaert, K., & Dallmann, A. (2020). Physiologically Based Pharmacokinetic Modeling to Characterize Acetaminophen Pharmacokinetics and N-Acetyl-p-Benzoquinone Imine (NAPQI) Formation in Non-Pregnant and Pregnant Women. Clinical Pharmacokinetics, 59(1), 97–110. https://doi.org/10.1007/s40262-019-00799-5

Mihailović, N., Marković, V., Matić, I. Z., Stanisavljević, N. S., Jovanović, Ž. S., Trifunović, S., & Joksović, L. (2017). Synthesis and antioxidant activity of 1,3,4-oxadiazoles and their diacylhydrazine precursors derived from phenolic acids. RSC Advances, 7(14), 8550–8560. https://doi.org/10.1039/C6RA28787E

Mittapally, S., Taranum, R., & Parveen, S. (2018). Metal ions as antibacterial agents. Journal of Drug Delivery and Therapeutics, 8, 411–419. https://doi.org/9http://dx.doi.org/10.22270/jddt.v8i6-s.2063

Motwani, M. P., Bennett, F., Norris, P. C., Maini, A. A., George, M. J., Newson, J., Henderson, A., Hobbs, A. J., Tepper, M., White, B., Serhan, C. N., Macallister, R., & Gilroy, D. W. (2018). Potent Anti-Inflammatory and Pro-Resolving Effects of Anabasum in a Human Model of Self-Resolving Acute Inflammation. 104(4), 675–686. https://doi.org/10.1002/cpt.980

Mugesh, G., du Mont, W.-W., & Sies, H. (2001). Chemistry of Biologically Important Synthetic Organoselenium Compounds. Chemical Reviews, 101(7), 2125–2180. https://doi.org/10.1021/cr000426w

Mumtaz, A., Arshad, J., Saeed, A., Nawaz, M. A. H., & Iqbal, J. (2018). Synthesis, Characterization and Urease Inhibition Studies of Transition Metal Complexes of Thioureas Bearing Ibuprofen Moiety. Journal of the Chilean Chemical Society, 63(2), 3934–3940. https://doi.org/10.4067/s0717-97072018000203934

Murahari, M., Mahajan, V., Neeladri, S., Kumar, M. S., & Mayur, Y. C. (2019). Ligand based design and synthesis of pyrazole based derivatives as selective COX-2 inhibitors. Bioorganic Chemistry, 86, 583–597. https://doi.org/https://doi.org/10.1016/j.bioorg.2019.02.031

Nandanwar, S. K., & Kim, H. J. (2019). Anticancer and Antibacterial Activity of Transition Metal Complexes. ChemistrySelect, 4(5), 1706–1721. https://doi.org/https://doi.org/10.1002/slct.201803073

DOI:https//doi.org/10.22452/mjs.vol43no1.8
Malaysian Journal of Science 43(1): 86-112 (March 2024)

Narsinghani, T., & Sharma, R. (2017). Synthesis, anti-inflammatory activities and docking studies of amide derivatives of meclofenamic acid. Chemical Papers, 71(4), 857–868. https://doi.org/10.1007/s11696-016-0102-7

Nayak, S., Gaonkar, S. L., Musad, E. A., & Dawsar, A. M. AL. (2021). 1,3,4-Oxadiazole-containing hybrids as potential anticancer agents: Recent developments, mechanism of action and structure-activity relationships. Journal of Saudi Chemical Society, 25(8), 101284. https://doi.org/10.1016/j.jscs.2021.101284

Njus, D., Kelley, P. M., Tu, Y.-J., & Schlegel, H. B. (2020). Ascorbic Acid: The Chemistry Underlying Its Antioxidant Properties. Free Radical Biology and Medicine, 159, 37–43. https://doi.org/https://doi.org/10.1016/j.freeradbiomed.2020.07.013

Novilla, A., Mustofa, M., Astuti, I., Jumina, J., & Suwito, H. (2019). Cytotoxic Activity of Methoxy-4'amino Chalcone Derivatives Against Leukemia Cell Lines. Molecular and Cellular Biomedical Sciences, 3(1), 34. https://doi.org/10.21705/mcbs.v3i1.44

Ohashi, N., & Kohno, T. (2020). Analgesic Effect of Acetaminophen: A Review of Known and Novel Mechanisms of Action. Frontiers in Pharmacology, Frontiers Media S.A. https://doi.org/10.3389/fphar.2020.580289

Olszewska, P., Cal, D., Zagórski, P., & Mikiciuk-Olasik, E. (2020). A novel trifluoromethyl 2-phosphonopyrrole analogue inhibits human cancer cell migration and growth by cell cycle arrest at G1 phase and apoptosis. European Journal of Pharmacology, 871. https://doi.org/10.1016/j.ejphar.2020.172943

Osowole, A. A., Agbaje, O. B. A., & Ojo, B. O. (2014). Synthesis , characterization and antibacterial properties of some heteroleptic metal (II) complexes of paracetamol and vanillin. Asian Journal of Pharmaceutical and Clinical Research, 7(3).

Ouellette, R. J., & Rawn, J. D. (2018). 24 - Amines and Amides (R. J. Ouellette & J. D. B. T.-O. C. (Second E. Rawn (eds.); pp. 763–800). Academic Press. https://doi.org/https://doi.org/10.1016/B978-0-12-812838-1.50024-4

Ozawa, M., Kubo, T., Lee, S. H., & Oe, T. (2019). LC-MS analyses of N-acetyl-p-benzoquinone imine-adducts of glutathione, cysteine, N-acetylcysteine, and albumin in a plasma sample: A case study from a patient with a rare acetaminophen-induced acute swelling rash. The Journal of Toxicological Sciences, 44(8), 559–563. https://doi.org/10.2131/jts.44.559

Paul, E. D., Dallatu, Y. A., & Akwu, F. J. (2018). Antimicrobial, Acute Toxicity and Anti-inflammatory Investigations of Mg(II) Complex of Acetaminophen. 3(2), 959–963.

Pedro-Hernández, L., Martínez-Klimova, E., Cortez-Maya, S., Mendoza-Cardozo, S., Ramírez-Ápan, T., & Martínez-García, M. (2017). Synthesis, Characterization, and Nanomedical Applications of Conjugates between Resorcinarene-Dendrimers and Ibuprofen. Nanomaterials, 7(7), 163. https://doi.org/10.3390/nano7070163

Pérez, D. J., Díaz-Reval, M. I., Obledo-Benicio, F., Zakai, U. I., Gómez-Sandoval, Z., Razo-Hernández, R. S., West, R., Sumaya-Martínez, M. T., Pineda-Urbina, K., & Ramos-Organillo, Á. (2017). Silicon containing ibuprofen derivatives with antioxidant and anti-inflammatory activities: An in vivo and in silico study. European Journal of Pharmacology, 814, 18–27. https://doi.org/10.1016/j.ejphar.2017.07.046

Permala, J., Tarning, J., Nosten, F., & White, N. J. (2017). Prediction of Improved Antimalarial Chemoprevention with Weekly Dosing. Antimicrobial Agents and Chemotherapy, 61(5), e02491-16.

Ragab, F. A., Heiba, H. I., El-Gazzar, M. G., Abou-Seri, S. M., El-Sabbagh, W. A., & El-Hazek, R. M. (2017). Anti-inflammatory, analgesic and COX-2 inhibitory activity of novel thiadiazoles in irradiated rats. Journal of Photochemistry and Photobiology B: Biology, 166, 285–300. https://doi.org/10.1016/j.jphotobiol.2016.12.007

Ramachandran, A., & Jaeschke, H. (2019). Acetaminophen Hepatotoxicity. Semin Liver Dis, 39, 221–234. https://doi.org/10.1055/s-0039-1679919

Rashid, M., Rafique, H., Roshan, S., Shamas, S., Iqbal, Z., Ashraf, Z., Abbas, Q., Hassan, M., Ur, Z., Qureshi, R., Hassham, M., Asad, H. Bin, & Com, M. (2020). Enzyme Inhibitory Kinetics and Molecular Docking Studies ofHalo-Substituted Mixed Ester/Amide-Based Derivatives as JackBean Urease Inhibitors. https://doi.org/10.1155/2020/8867407

Rasmussen, S. A., Ceja, F. G., Conrad, M. D., Tumwebaze, P. K., Byaruhanga, O., Katairo, T., Nsobya, S. L., Rosenthal, P. J., & Cooper, R. A. (2017). Changing Antimalarial Drug Sensitivities in Uganda. Antimicrobial Agents and Chemotherapy, 61(12). https://doi.org/10.1128/AAC.01516-17

Reygaert, W. (2018). An overview of the antimicrobial resistance mechanisms of bacteria. AIMS Microbiology, 4(3), 482–501. https://doi.org/10.3934/microbiol.2018.3.482

DOI:https//doi.org/10.22452/mjs.vol43no1.8
Malaysian Journal of Science 43(1): 86-112 (March 2024)

Rizvi, F., Khan, M., Jabeen, A., Siddiqui, H., & Choudhary, M. I. (2019). Studies on Isoniazid Derivatives through a Medicinal Chemistry Approach for the Identification of New Inhibitors of Urease and Inflammatory Markers. Scientific Reports, 9(1), 1–14. https://doi.org/10.1038/s41598-019-43082-0

Rizzotto, M. (2012). Metal Complexes as Antimicrobial Agents. In A Search for Antibacterial Agents (pp. 74–89). InTech. https://doi.org/10.5772/45651

Roberts, E., Nunes, V. D., Buckner, S., Latchem, S., Constanti, M., Miller, P., Doherty, M., Zhang, W., Birrell, F., Porcheret, M., Dziedzic, K., Bernstein, I., Wise, E., & Conaghan, P. G. (2016). Paracetamol: Not as safe as we thought? A systematic literature review of observational studies. Annals of the Rheumatic Diseases, 75(3), 552–559. https://doi.org/10.1136/annrheumdis-2014-206914

Sangcharoen, N., Klaypradit, W., & Wilaipun, P. (2017). Antimicrobial activity optimization of nisin, ascorbic acid and ethylenediamine tetraacetic acid disodium salt (EDTA) against Salmonella Enteritidis ATCC 13076 using response surface methodology. Agriculture and Natural Resources, 51(5), 355–364. https://doi.org/https://doi.org/10.1016/j.anres.2017.12.005

Santis, M. De, & Saad, F. (2016). Corticosteroids in the Treatment of Metastatic Castration-resistant Prostate Cancer. Urology, 96, 156–164. https://doi.org/10.1016/j.urology.2016.02.010

Sasso, O., Migliore, M., Habrant, D., Armirotti, A., Albani, C., Summa, M., Moreno-sanz, G., Scarpelli, R., & Piomelli, D. (2015). Multitarget fatty acid amide hydrolase / cyclooxygenase blockade suppresses intestinal in fl ammation and protects against nonsteroidal anti-in fl ammatory drug-dependent gastrointestinal damage. FASEB, 29(6), 2616–2627. https://doi.org/https://doi.org/10.1096/fj.15-270637

Scarpelli, R., Sasso, O., & Piomelli, D. (2016). A Double Whammy : Targeting Both Fatty Acid Amide Hydrolase (FAAH) and Cyclooxygenase (COX) To Treat Pain and Inflammation. ChemMedChem, 11(12), 1242–1251. https://doi.org/10.1002/cmdc.201500395

Scattolin, T., Bortolamiol, E., Visentin, F., Palazzolo, S., Caligiuri, I., Perin, T., Canzonieri, V., Demitri, N., Rizzolio, F., & Togni, A. (2020). Palladium(II)-η 3 -Allyl Complexes Bearing N -Trifluoromethyl N -Heterocyclic Carbenes: A New Generation of Anticancer Agents that Restrain the Growth of High-Grade Serous Ovarian Cancer Tumoroids. Chemistry – A European Journal, 26(51), 11868–11876. https://doi.org/10.1002/chem.202002199

Seraj, F., Kanwal, Khan, K. M., Khan, A., Ali, M., Khalil, R., Ul-Haq, Z., Hameed, S., Taha, M., Salar, U., & Perveen, S. (2021). Biology-oriented drug synthesis (BIODS), in vitro urease inhibitory activity, and in silico studies on ibuprofen derivatives. Molecular Diversity, 25(1), 143–157. https://doi.org/10.1007/s11030-019-10032-x

Shakeel, A. (2016). Thiourea Derivatives in Drug Design and Medicinal Chemistry: A Short Review. Journal of Drug Design and Medicinal Chemistry, 2(1), 10. https://doi.org/10.11648/j.jddmc.20160201.12

Shenoy, N., Creagan, E., Witzig, T., & Levine, M. (2018). Ascorbic Acid in Cancer Treatment: Let the Phoenix Fly. Cancer Cell, 34(5), 700–706. https://doi.org/10.1016/j.ccell.2018.07.014

Shetty, A., & Dick, T. (2018). Mycobacterial Cell Wall Synthesis Inhibitors Cause Lethal ATP Burst. 9(August), 1–9. https://doi.org/10.3389/fmicb.2018.01898

Shoaib, M., Hussain, H., Shah, S. W. A., Umar, M. N., & Ullah, A. (2017). Synthesis, acute toxicity, analgesic activity & cytotoxicity of Some bisthiourea derivatives. Pakistan Journal of Pharmaceutical Sciences, 30(4), 1351–1356.

Singh, B. R., Yadav, A., & Ravichandran, K. (2021). Comparative Antimicrobial Activity of Aspirin, Paracetamol, Flunixin Meglumine, Tolfenamic Acid, Diclofenac Sodium and Pheniramine Maleate. Acta Scientific Veterinary Science, 3(September), 30–42.

Siwach, A., & Verma, P. K. (2020). Therapeutic potential of oxadiazole or furadiazole containing compounds. BMC Chemistry, 14(1), 1–40. https://doi.org/10.1186/s13065-020-00721-2

Stratan, E., Ţurcan, N., Crudu, V., Romancenco, E., Cotelea, T., Niţulescu, G. M., Chiriţă, C., & Moruşciag, L. (2018). Biological evaluation of new 2-phenethylbenzoyl thiourea derivatives as antituberculosis agents. Farmacia, 66(1), 97–106.

Straub, R. H., & Cutolo, M. (2016). Glucocorticoids and chronic inflammation. 6–14. https://doi.org/10.1093/rheumatology/kew348

Syahri, J., Yuanita, E., Nurohmah, B. A., Armunanto, R., & Purwono, B. (2017). Chalcone analogue as potent anti-malarial compounds againstPlasmodiumfalciparum: Synthesis, biological evaluation, and docking simulation study. Asian Pacific Journal of Tropical Biomedicine, 7(8), 675–679. https://doi.org/10.1016/j.apjtb.2017.07.004

DOI:https//doi.org/10.22452/mjs.vol43no1.8
Malaysian Journal of Science 43(1): 86-112 (March 2024)

Torfs, E., Piller, T., Cos, P., & Cappoen, D. (2019). Opportunities for Overcoming Mycobacterium tuberculosis Drug Resistance : Emerging Mycobacterial Targets and Host-Directed Therapy.

Turner, R. J. (2017). Metal-based antimicrobial strategies. Microbial Biotechnology, 10(5), 1062–1065. https://doi.org/10.1111/1751-7915.12785

Ullah, N., Huang, Z., Sanaee, F., Rodriguez-Dimitrescu, A., Aldawsari, F., Jamali, F., Bhardwaj, A., Islam, N. U., & Velázquez-Martínez, C. A. (2016). NSAIDs do not require the presence of a carboxylic acid to exert their anti-inflammatory effect – why do we keep using it? Journal of Enzyme Inhibition and Medicinal Chemistry, 31(6), 1018–1028. https://doi.org/10.3109/14756366.2015.1088840

Vedavathi, P., Sudhamani, H., & Raju, C. N. (2017). Synthesis and antimicrobial activity of new urea and thiourea derivatives of (2'-(1H-tetrazol-5-yl)biphenyl-4-yl)methanamine. Research on Chemical Intermediates, 43(5), 3251–3263. https://doi.org/10.1007/s11164-016-2823-1

Verghese, R. J., Mathew, S. K., & David, A. (2018). Antimicrobial activity of Vitamin C demonstrated on uropathogenic Escherichia coli and Klebsiella pneumoniae. Current Research in Scientific Medicine, 3(2), 88–93. https://doi.org/10.4103/jcrsm.jcrsm

Verma, A. K., Mittal, D., Goel, A., Shadija, L., & Singh, N. (2020). To Assess the Antimicrobial Action of Paracetamol. Acta Scientific Microbiology, 3(8), 65–71.

Wang, H., Zhai, Z.-W., Shi, Y.-X., Tan, C.-X., Weng, J.-Q., Han, L., Li, B.-J., & Liu, X.-H. (2019). Novel Trifluoromethylpyrazole Acyl Thiourea Derivatives: Synthesis, Antifungal Activity and Docking Study. Letters in Drug Design & Discovery, 16(7), 785–791. https://doi.org/10.2174/1570180815666180704103047

Yadav, A., Mohite, S., & Magdum, C. (2020). Synthesis, Characterization and Biological Evaluation of Some Novel 1,3,4-Oxadiazole Derivatives as Potential Anticancer Agents. International Journal of Scientific Research in Science and Technology, 275–282. https://doi.org/10.32628/IJSRST207234

Zhang, J., Tan, Y., Li, G., Chen, L., Nie, M., Wang, Z., & Ji, H. (2021). Coumarin Sulfonamides and Amides Derivatives: Design, Synthesis, and Antitumor Activity In Vitro. Molecules, 26(4), 786. https://doi.org/10.3390/molecules26040786

Zuegg, J., Solutions, S., Frei, S. A., Blaskovich, M. A. T., Willans, C. E., Wilson, J. J., & Cooper, A. (2020). Metal complexes as a promising source for new antibiotics. Chemical Science, 11, 2627–2639. https://doi.org/10.1039/c9sc06460e

DOI:https//doi.org/10.22452/mjs.vol43no1.8
Malaysian Journal of Science 43(1): 86-112 (March 2024)

MALAYSIAN JOURNAL OF SCIENCE
MJS
ISSN 1394-3065

Regular Issue

Malaysian Journal of Science 43(1): 113-122 (Mar 2024) https://mjs.um.edu.my

WATER TREATMENT USING NATURAL COAGULANTS: A REVIEW ON THE POTENTIAL UTILISATION OF BANANA WASTE

Abdassalam A. Azamzam[1a], Abdalahafid J. Alabdi[2a], Esam Bashir Yahya[3a], Japareng Lalung[4a]*, Mardiana Idayu Ahmad[5a]*, Mohd Rafatullah[6a]

Abstract: The massive industrial and agricultural development in the past few years has increased the pollution level of water bodies. Several studies have concluded that the global depletion of freshwater resources will result in difficulties accessing clean water. Plant-based water treatment techniques have attracted great interest in the past few years due to their safety and cost-effectiveness compared with chemical-based techniques. Natural coagulants have been extensively studied in terms of the type of plant and the mechanism of coagulation. Banana is one of the most famous tropical fruits from the Musa genus in the Musaceae family. It is widely consumed in Malaysia, especially Musa acuminata, Musa balbisiana, and Musa paradisiaca, resulting in tremendous amounts of biomass residue, including peels, stems, and leaves, with high potential use for wastewater treatment applications. This review aims to highlight the advantages of natural coagulants and to discuss the potential use of different banana wastes in water treatment applications.

Keywords: *Plant-based coagulant, banana wastes, water treatment, natural coagulant, waste biomass*

1. Introduction

Since the last century, with a dramatic increase during the Industrial Revolution, many industrial wastes have increased proportionally, increasing a worldwide primary source of severe pollution (Mohan et al., 2019). Air, water, and even soil have been polluted by anthropogenic activities. For instance, water pollution may occur due to the use of multiple chemical reagents, ranging from inorganic compounds to polymers and even organic products (Salmasi et al., 2020). Many developing societies lack appropriate wastewater treatment techniques, leaving waste without treatment. Many of these communities consume non-treated or badly treated water daily, which eventually affects their health and leads to severe waterborne disease (Ravindra et al., 2019).

Coagulation is a water treatment technique used to assist in colloidal particle removal (Lv et al., 2018), lime softening (Ghernaout et al., 2018), water clarification (López et al., 2021), sludge thickening (Atamaleki et al., 2020), and solid dewatering (Feng et al., 2022). Due to the potential cause of health problems, the use of chemical coagulants, such as alum, is not a preferable option (Bahrodin et al., 2021). Its use is restricted to turbidity removal, and it is not recommended for use in developing countries (Sulaiman et al., 2017). The use of plant-based materials as natural coagulants for water purification is simple, safe for human health, eco-friendly, and effective.

Authors information:
[a]School of Industrial Technology, Universiti Sains Malaysia, 11800 Penang, MALAYSIA. E-mail: azamzamabdassalam@gmail.com[1]; abdalhafid.j.alabdi@gmail.com[2]; essam912013@gmail.com[3]; japareng@usm.my[4]; mardianaidayu@usm.my[5]; mrafatullah@usm.my[6]
*Corresponding Author: japareng@usm.my; mardianaidayu@usm.my

In a previous study by Nath et al. (2021), the authors showed that several chemical coagulants have the ability to change the physicochemical properties of treated water. The same authors encouraged the use of natural coagulants to replace chemical ones. Several studies have concluded that natural coagulants show a significant improvement in the environment and ecosystem as a sustainable solution to wastewater treatment issues (Mumbi et al., 2018). The use of natural coagulants has been practiced since ancient times and has been proven in water treatment, while retaining natural benefits (Nandini and Sheba (2016).

Banana is one of the most consumed tropical fruits in Malaysia and many tropical countries (Soluri, 2021). The banana tree has been reported to produce around 3 to 20 fruits in a single cluster once in its lifetime. However, after consumption, this tree leaves a large amount of biomass that can be used for several applications. In our previous research, we investigated the potential use of banana peels in river water treatment applications and found great potential for such waste as a natural coagulant (Azamzam et al., 2022). Worldwide, the volume of bananas produced in 2020 has reached approximately 119.83 million tonnes, which increased from 117.53 million tonnes in 2019 (Duraiprasanth et al., 2022). Therefore, one million tonnes of peels are mostly discarded and are rarely utilised. It has been reported that Malaysians consume bananas, either ripe (fried banana) or unripe (fresh fruits), for making chips and juice (Aida et al., 2016). However, it has been reported that chip and juice factories generate tonnes of banana peel waste every year, which, in most cases, is not utilised and is dumped in landfills (Ahmad and Danish (2018). These wastes have a high quantity of beneficial organic compounds, including cellulose, lignin, pectin

Received: April 12, 2021
Accepted: April 14, 2023
Published: March 31, 2024

DOI:https//doi.org/10.22452/mjs.vol43no1.9
Malaysian Journal of Science 43(1): 113-122 (March 2024)

substances, pigments, and chlorophyll (Kandeeban and Malarkodi (2019). Banana stem juice has promising potential for use as a natural coagulant in water treatment (Hilal et al., 2004). İn the past few years, many review articles have been published discussing natural coagulants (Nath et al., 2020), polymeric coagulants (Nath et al., 2020), and plant-based coagulants (Choy et al., 2015). Several studies have been conducted on the potential use of banana wastes in water treatment applications, but they have never been reviewed. The present review attempts to deliver collective information about the potential use of banana waste materials as natural coagulants for water treatment. It also briefly discusses the advantages, disadvantages, and mechanisms of natural-based coagulants in water treatment applications.

2. Coagulation Treatment Method

Coagulation is an extensively used method for wastewater treatment that reduces turbidity and removes suspended colloidal particles. This method is usually performed using a sizeable chemical reactor that enters the basin and influences wastewater. The wastewater is then homogenised with a suitable coagulant agent and mechanically mixed until the sedimentation process takes place. Eventually, gravity settling is performed to remove the particulate matter (Amran et al., 2018). Concerted research and development efforts have been conducted in the past two decades to discover new plant species and constituents that can be used as natural coagulants, further boosting the effectiveness of existing plant-based natural coagulants (Liao et al., 2017). The coagulation process is a physicochemical process that reduces the repulsive potential of an electrical double layer of colloids using various coagulants. This will lead to the agglomeration and development of colloidal microparticles into larger particles or flocs (Mazloomi et al., 2019). This agglomeration can be formed by several mechanisms, including polymer bridging, charge neutralisation, and sweep coagulation, as discussed in the following section.

Coagulation Mechanisms

The coagulation process of both natural and synthetic coagulants can be performed using several mechanisms, including polymer bridging, sweep coagulation, double layer compression, and charge neutralisation (Bolto and Gregory (2007) as presented in Figure 1. Naceradska et al. (2019) investigated the removal mechanism of algal organic matter using Jar tests with either aluminium sulphate or polyaluminium chloride. The authors reported that high-molecular weight organic matter, such as saccharides, was more amenable to coagulation than lower weight compounds. The low surface charge of the removed fraction indicated that the prevailing coagulation mechanism was the adsorption of non-proteinaceous matter onto aluminium hydroxide precipitates. In comparison, Adeleke et al. (2021) showed different mechanisms for the natural coagulant *Moringa oleifera* and reported that the amino acid residues in *Moringa* had certain interactions with pollutant ligands, indicating that coagulation may occur.

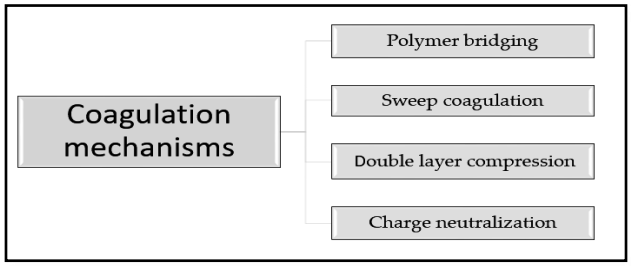

Figure 1. Diverse types of coagulation mechanisms. Reprinted from Bolto and Gregory (Bolto et al., 2007), with permission from Elsevier.

Many polysaccharides, such as cellulose, starch, gelatine, alginate, and chitosan, have been investigated as natural coagulants due to their biosafety to humans (Nath et al., 2020). The coagulation/ flocculation mechanism of these polysaccharides involves charge neutralisation and polymer bridging (Nath et al., 2020). In charge neutralisation, the positively charged coagulant attracts the negatively charged pollutant particles, which are adsorbed on its surface, neutralising the colloid particle charges. As shown in Figure 2, the surface charge difference between the pollutant and the coagulant leads to a decrease in electrostatic repulsion in the colloid particles, which then results in the attraction of the particles and coagulation (Henderson et al., 2008). In polymer bridging mechanisms, the adsorption of the particles takes place in a long chain of linear and high molecular weight polymers, leaving dangling heavy coagulant polymer segments to bridge all the particles of the pollutants together, as presented in Figure 2b (Diddens and Heuer (2019). Sweep coagulation is another mechanism that occurs in the presence of chemical coagulants (i.e., metal salts), which are usually added to the water at higher dosages than the solubility of the amorphous hydroxides, and the colloid particles eventually become entrapped within the precipitate and are removed from the suspension (Nan et al., 2016). High electrolyte concentrations in colloidal solutions cause double-layer compression. The colloids become unstable and increase the possibility of coagulation by lowering the colloid particles' repulsive force (Kristianto, 2017).

DOI:https//doi.org/10.22452/mjs.vol43no1.9
Malaysian Journal of Science 43(1): 113-122 (March 2024)

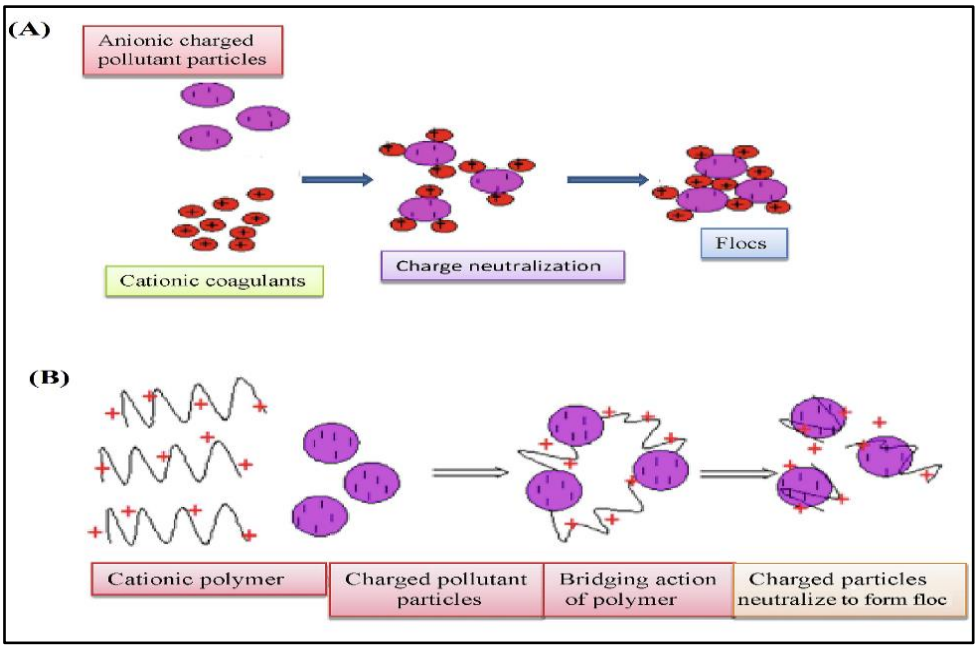

Figure 2. Coagulation mechanisms: (A) charge neutralisation and (B) polymer bridging. Reprinted from Nath et al. (2020) with permission from Elsevier.

The efficiency of coagulants in water treatment depends on the type of coagulants, their quantity, mixing conditions, and pH, as well as the properties of the solution to be treated, such as particle size, particle charges, the presence of divalent cations, the hydrophobicity level of the particles, and destabilising anions, such as sulphate ions, bicarbonate, and chloride (Sillanpää et al., 2018).

Synthetic and Inorganic Coagulants

Many synthetic and inorganic coagulants have been used in water treatment applications, such as metal salts and polymeric polysaccharides from a non-plant source, such as chitosan (Nath et al., 2020). Most polymeric coagulants are positively charged due to the presence of charged function groups on their surfaces (Rizal et al., 2020). Positively charged groups are called cationic polymer coagulants, and negatively charged polymers are called anionic polymer coagulants. In contrast, a mixture of two or more types of polymers is called a polyelectrolyte coagulant. Chitosan, for example, is one of the most frequently used polymers in different applications, including absorption. The presence of the cationic charge in their structure (i.e., amino groups) enables the polymer to efficiently absorb various metal ions (Alsharari et al., 2018). Metal salts and pre-hydrolysed coagulants have also been used in primary wastewater treatment (Theodoro et al., 2013).

Aluminium-based salts (such as aluminium sulphate and chloride) and ferric-based salts (such as ferrous sulphate and ferric chloride) are the most widely used metal saltwater treatment coagulants (Bahadori et al., 2013). Lately, the application of ferric-based coagulants is preferable compared to aluminium-based coagulants, which have been linked to many health risks. Ferric chloride and aluminium sulphate have excellent performance as wastewater treatment agents. Poly-ferric chloride, poly-ferrous sulphate, and poly-aluminium chloride are the most commonly used pre-hydrolysed coagulants. However, the use of these materials has the limitation of reducing the water pH to become close to acidic. Additionally, they have been reported to cause some health issues in humans after the consumption of water, such as presenile dementia and Alzheimer's disease (Gurumath and Suresh (2019). Another limitation of using metal salts as coagulant agents is the resulting large volume of sludge and the relatively high coagulant cost (Kristianto, 2017). Shi et al. (2004) reported that using ferric salt and poly-ferrous sulphate as coagulants could accelerate pipe corrosion. Table 1 presents an illustration of various non-plant-based coagulants applied for water treatment.

DOI:https//doi.org/10.22452/mjs.vol43no1.9
Malaysian Journal of Science 43(1): 113-122 (March 2024)

Table 1. Applications of synthetic and inorganic coagulants in water treatment applications

Coagulant	Type of pollutant	Type of water	Reference
Titanium salts	Sludge dewatering and algae-laden	Seawater and wastewater	(Shrestha et al., 2017; Zhang et al., 2017)
Titanium (III) chloride	Dissolved organic matter	Surface water	(Hussain et al., 2019)
polymeric zinc–ferric–silicate–sulphate	Humic acid, algae and oils	Wastewater	(Liao et al., 2017; Sun et al., 2017)
Ferric salts	Organic matter, sludge, and turbidity	Wastewater and drinking water	(Chua et al., 2020; Mazaheri et al., 2018)
Poly-ferric-titanium-silicate-sulphate	Organic dyes	Disperse and reactive dye wastewaters treatment	(Huang et al., 2020)
Aluminium salts	Organic matter and turbidity	Wastewater	(Mazloomi et al., 2019; Wan et al., 2019)
Titanium-Based Xerogel	Turbidity and cyanobacteria	Wastewater treatment of	(Wang et al., 2016; Wang, Wang et al., 2018)

Natural-Based Coagulants

Natural coagulants have been investigated with immense potential in water treatment applications (Ang and Mohammad (2020). The water treatment process removes suspended and colloidal materials and particles in water, such as organic matter, microbes, and inorganic matter (Jayalakshmi et al., 2017). Various plant-based materials have been used in many parts of the world, such as China, India, and even Africa (Asrafuzzaman et al., 2011; Kristianto, 2017). Due to the health, costs, and environmental aspects of many inorganic and synthetic coagulants, numerous studies have recently been conducted to search for a sustainable, eco-friendly, and non-toxic alternative to inorganic coagulants for water treatment purposes. The use of plant-based coagulants for water treatment has gained more interest as a natural, cost-effective, and renewable method that has been widely studied in the past few decades.

Plant-based coagulants have become more popular in recent research as an alternative and safer material to chemical and synthetic-based coagulants, especially in drinking water treatment. Table 2 presents a few examples of commonly used plants for water treatment. Plant-based coagulants are non-toxic, lower cost, safe, biodegradable, available, and sustainable; plant-based coagulants from different parts of plants have been utilised in water treatment, including roots, stems, fruits, fruit shells, leaves, and even seeds. In some plants, such as banana and *Moringa*, many parts of the plant tree have been utilised as natural coagulants.

Table 2. Plant-based coagulants and their applications.

Plants and their used parts	Treatment applications	Optimum result	Reference
Oryza sativa Rice starch	Treatment of palm oil mill	Removing up to 88.4% TSS at the small dosage of 0.55 g/L	(Teh et al., 2014)
Hibiscus sabdariffa Roselle seeds	Treatment of wastewater containing Congo red dye	Removing up to 91.2% of colour at 190 mg/L coagulant dosage at a 400 ppm dye concentration	(Yong and Ismail (2016)
Moringa oleifera Moringa seeds	Cyanobacteria and natural organic matter (OM) treatment	Removing 80% of chlorophyll a, 80–90% of dissolved OM, and 80% of cyanobacteria cells	(Teixeira et al., 2017)
Corchorus olitorius L. Nalta jute	Treatment of humic acid wastewater	Removing up to 95% turbidity and 100% of total organic carbon	(Altaher et al., 2016)
Ocimum basilicum Basil	Treatment of Landfill leachate	When combined with alum, it was able to reduce 64.4% of COD and 77.4% of water colour	(Rasool et al., 2016)
Zea mays Cornstarch	Treatment of kaolin and microorganisms	At a 0.5 mg/L dose, it was able to remove up to 98% of kaolin, *E. coli*, and *S. aureus*	(Liu et al., 2017)
Citrus sinensis Orange peel	Dairy wastewater treatment	At only 0.2 g/L, it was able to remove up to 97% turbidity	(Anju and Mophin-Kani (2016)
Artocarpus heterophyllus Jackfruit	Treatment of kaolin	60 mg/L dose was able to reduce turbidity by 43%	(Choy et al., 2017)

Abbreviations: TSS, Total suspended Solids; COD, Chemical Oxygen Demand

DOI:https//doi.org/10.22452/mjs.vol43no1.9
Malaysian Journal of Science 43(1): 113-122 (March 2024)

A plant-based coagulant is sustainable and cheaper than a chemical coagulant, as most chemical coagulants require other material to effectively treat high turbidity, which raises the cost of the treatment process and makes it difficult to use in developing countries (Antov et al., 2010). However, a significant increase in water organic material is one of the top disadvantages of using a plant-based coagulant, which results in the accumulation of microbial activity. This issue has been solved by the addition of chlorine at safe doses to sanitise treated water (Amran et al., 2018). The sedimentation time is another limitation that can be mentioned regarding plant-based coagulants, which require more time than chemical coagulants (Kumar et al., 2017).

3. Banana Wastes as a Bio-Coagulant

In recent years, the utilisation of banana waste as a bio-coagulant in water treatment has earned growing interest due to its eco-friendliness, sustainability, and biodegradability. A variety of banana waste, including banana peels, leaves and stems, fruit peels, and stem juice, has been investigated for removing water turbidity. Different banana parts, such as banana peels, piths, trunks, and leaves, have been studied in terms of utilising them in many applications, including water treatment (Mokhtar et al., 2019). Table 3 presents selected studies on banana waste as a bio-coagulant for water treatment applications.

Table 3. Recent studies on the use of banana waste as a natural coagulant in water treatment applications

Banana part	Type of water	Pollutants	Finding	Ref
Banana pith	River water	Physicochemical and heavy metal	Significant reduction in turbidity, COD, TSS, nitrates, sulphates, and heavy metals	(Kakoi et al., 2016)
Banana peels	Wastewater	Turbidity	Removal of up to 96% of water turbidity	(Azamzam et al., 2022)
Banana Pith Juice	Textile Wastewater	Turbidity and TSS	Slight reduction of TSS and significant removal of turbidity	(Gopika and Kani, 2016)
Banana peel	Storage water tanks	Turbidity and colour	A decrease in both turbidity and colour	(Fu et al., 2019)
Banana peel with fenugreek seeds	palm oil mill effluent	Turbidity	Better removal efficiencies than commercial flocculant	(Ling et al., 2018)
Banana Peel	Domestic wastewater	Turbidity, COD, and NH_4-N	89.9%, 80.0%, and 62.5% reduction	(Ting et al., 2022)
Banana Peel	Synthetic Wastewater	Turbidity	88% turbidity reduction under optimum conditions	(Mokhtar et al., 2019)
Lemon and Banana Peel	Synthetic raw water	Turbidity and BOD	Turbidity and BOD were significantly removed	(Subashree et al., 2018)
Banana peel gel	Acid mine drainage water	Heavy metal	Removed Cd, Cu, Pb, and Zn	(Yabuki et al., 2020)
Banana Pith Starch	River water treatment	Turbidity, colour, and TDS	Turbidity reduced by 94.4% and colour by 87.46%	(Yushananta and Ahyanti, 2022))

Banana Peels

Banana fruit peels have been analysed as coagulation agents for the removal of different physicochemical parameters (Mokhtar et al., 2019; Olaoye et al., 2018). Banana peel establishes approximately 40% of the overall weight of fresh banana fruit, generating a large amount of unusable waste (Pelissari et al., 2017). Banana peels contain many active organic compounds, such as polysaccharides, cellulose, pectin, and hemicellulose, in addition to pigments and other low molecular weight compounds (Khawas and Deka, 2016). They are an excellent source of starch, cellulose, galacturonic acid, and pectin, with different ratios based on banana type, analysis method, and maturation level (Chaturvedi et al., 2018). Chaturvedi et al. (2018) used the aqueous extract from banana peel and were able to remove up to 88% of water turbidity of household wastewater under the optimised conditions of the tested parameters. İn a separate study, the powdered extract of banana peels (*Musa paradisica*) removed up to 83% of water turbidity at all tested pH values, and the maximum removal of turbidity was recorded at a pH between 5 and 9, which was 98.8% (Daverey et al., 2019), suggesting the promising potential of utilising banana peels as a safe and cost-effective water treatment technique for turbidity removal. In our previous research, we found that the high positive charge in banana peel attracts the negatively charged particles that cause turbidity in the water (Azamzam et al., 2022). We used microwave treatment to enhance the attraction, which showed greater coagulation performance compared with the non-modified particles and the solution (Figure 3). The modification led to the formation of larger flocs around the banana peel particles and, thus, better precipitation. In a different study, Pathak and Mandavgane (2015) followed the same modification process and reported that the surface of their banana peel became rough and porous after microwave treatment, confirming its efficiency in releasing active compounds (Pathak and Mandavgane (2015). The results of these studies confirm that the mechanism of the banana peel coagulation process is performed by the charge neutralisation of different charges.

DOI:https//doi.org/10.22452/mjs.vol43no1.9
Malaysian Journal of Science 43(1): 113-122 (March 2024)

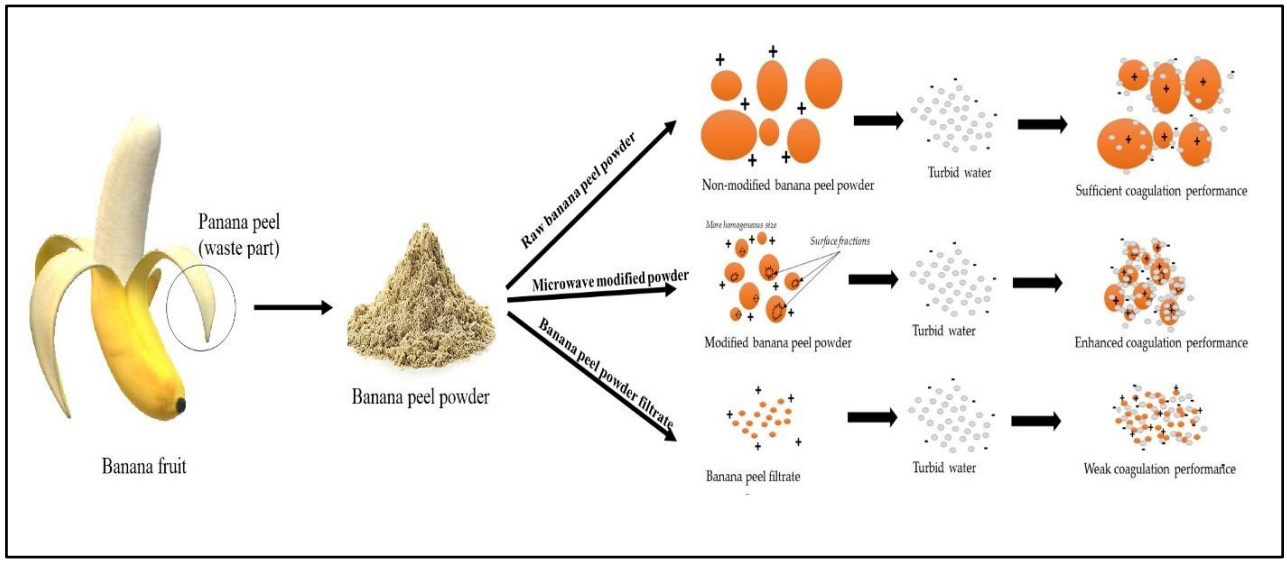

Figure 3. Coagulation mechanism of microwave-modified and non-modified banana peel particles. Adapted from Azamzam et al. (2022)

Banana Stem

The banana stem has been reported to be rich in polyelectrolytes that have not yet been significantly utilised for water treatment or any other economic purposes (Alwi et al., 2013). Two distinct methods have been reported for the mechanism of polyelectrolytes present in the banana pith, namely (i) bridging between particles and (ii) formation of bridges between particles (Kakoi et al., 2016). However, after harvesting banana fruit, the stem in most cases is left in the plantation as a mulching agent and fertiliser. The inner part of the stem is referred to as the pith, which is rarely used as food for livestock and, most of the time, is considered waste. After drying, powdered banana pith (Kakoi et al., 2016) is used for the direct removal of turbidity, suspended solids, and some heavy metals from river water. According to Feng et al. (2015), there are two steps in polyelectrolyte action: neutralisation of charges and the creation of bridges between particles. Chemically, banana pith is composed of a large number of significant functional groups, such as carboxylic, ether, and hydroxyl groups (Nayak et al., 2018).

The juice of banana pith has been used by Alwi et al. (2013) to reduce water physicochemical parameters, including turbidity, suspended solids, and chemical oxygen demand; they successfully reduced turbidity by 98.5%. They proposed that the juice contains inulin, which is the active coagulant agent responsible for creating bridges and thus decreasing the mentioned parameters. Namasivayam et al. (1993) reported that banana stems removed up to 87% of Rhodamine B from textile wastewater, even at low pH levels (pH 4). The use of banana stems has also been studied for the direct removal of red colour and acid brilliant blue, using the adsorption technique. It was able to absorb up to 5.92 mg of natural red and 4.42 mg of bright blue per gram of pith (Namasivayam et al., 1998), indicating the promising potential of using banana pith in adsorption and water treatment applications. Yushananta and Ahyanti (2022) synthesised banana pith starch using agricultural waste and used it for river water treatment applications. The authors also modified their isolated starch using cations from GTA (3-Chloro-2-hydroxypropyl trimethyl ammonium chloride) into the main chemical structure of starch using microwave radiation. Modified banana pith starch reduces up to 94.4% of water turbidity, in addition to 87.46% and 57.33% of colour and Total Dissolved Solids (TDS), respectively. These findings put additional value on banana waste, which can be further modified to enhance its water treatment performance.

4. Challenges and Propositions of Using Bio Coagulants in Water Treatment

Different types, parts, and composites of natural coagulants have been investigated for treating synthetic or wastewater, aiming to provide safer options than conventional chemical methods. The use of banana waste does not give the best results compared to other natural coagulants. Most natural coagulants generate flocs, but issues regarding the removal of those flocs have still not been settled. Composite coagulants can overcome many problems linked with a sole coagulant, including the generation of small flocs and the non-optimal removal of some parameters (Mohd-Salleh et al., 2019). Similarly, composite coagulants generate more recoverable aggregated flocs and more resistance to shear than aggregated flocs caused by non-composite coagulants (Wang, Yue et al., 2018). However, the materials induced the growth rate and antibiotic sensitivity mutations in the tested microorganisms (Yahya, Abdulsamad, et al., 2020). Most studies, such as Kalemelawa et al. (2012) and Mosa et al. (2015) focus on the good side of naturally occurring products and ignore the potential lousy side related to a human directly or indirectly. Therefore, more microbiological studies regarding the use of natural coagulants need to be done (Yahya, Alfallous, et al., 2020).

DOI:https//doi.org/10.22452/mjs.vol43no1.9
Malaysian Journal of Science 43(1): 113-122 (March 2024)

5. Conclusion

The use of renewable and sustainable sources of low-cost agricultural biomass waste, such as banana peels and stems, to produce natural coagulants is considered a better choice for water treatment. They can be used as a coagulant to treat various water parameters, such as turbidity, colour, COD, BOD, and even heavy metals. Future studies can be carried out to further investigate the efficiency of this plant-based treatment technique, which can be used as an option to overcome the issue of clean water scarcity, especially in rural areas.

6. Acknowledgement

The authors express their gratitude to the Ministry of Higher Education, Malaysia for the Fundamental Research Grant Scheme with Project Code: FRGS/1/2021/STG03/USM/02/8.

6. References

Adeleke V. T., Adeniyi, A. A., & Lokhat, D. (2021). Coagulation of organic pollutants by *Moringa oleifera* protein molecules: In silico approach. *Environmental Science: Water Research & Technology, 7*(8), 1453–1464.

Ahmad, T., & Danish, M. (2018). Prospects of banana waste utilization in wastewater treatment: A review. *Journal of Environmental Management, 206*, 330–348.

Aida, S., Noriza, A., Haswani, M., & Mya, S. (2016). A study on reducing fat content of fried banana chips using a sweet pretreatment technique. *International Food Research Journal, 23*(1), 68.

Alsharari, S. F., Tayel, A. A., & Moussa, S. H. (2018). Soil emendation with nano-fungal chitosan for heavy metals biosorption. *International Journal of Biological Macromolecules, 118*, 2265–2268.

Altaher, H., Tarek, E., & Abubeah, R. (2016). An agricultural waste as a novel coagulant aid to treat high turbid water containing humic acids. *Global Nest Journal, 18*(2), 279–290.

Alwi, H., Idris, J., Musa, M., & Ku Hamid, K. H. (2013). A preliminary study of banana stem juice as a plant-based coagulant for treatment of spent coolant wastewater. *Journal of Chemistry, 2013*.

Amran, A. H., Zaidi, N. S., Muda, K., & Loan, L. W. (2018). Effectiveness of natural coagulant in coagulation process: A review. *International Journal of Engineering & Technology, 7* (3.9), 34–37.

Ang, W. L., & Mohammad, A. W. (2020). State of the art and sustainability of natural coagulants in water and wastewater treatment. *Journal of Cleaner Production*, (262) 121267.

Anju, S., & Mophin-Kani, K. (2016). Exploring the use of orange peel and neem leaf powder as alternative coagulant in treatment of dairy wastewater. *IJSER, 7*(4), 238–244.

Antov, M. G., Šćiban, M. B., & Petrović, N. J. (2010). Proteins from common bean (*Phaseolus vulgaris*) seed as a natural coagulant for potential application in water turbidity removal. *Bioresource Technology, 101*(7), 2167–2172.

Asrafuzzaman, M., Fakhruddin, A., & Hossain, M. A. (2011). Reduction of turbidity of water using locally available natural coagulants. *ISRN Microbiology,* vol. 2011, 6 pages..

Atamaleki, A., Miranzadeh, M. B., Mostafaii, G. R., Akbari, H., Iranshahi, L., Ghanbari, F., & Salem, A. (2020). Effect of coagulation and sonication on the dissolved air flotation (DAF) process for thickening of biological sludge in wastewater treatment. *Environmental Health Engineering And Management Journal, 7*(1), 59–65.

Azamzam, A. A., Rafatullah, M., Yahya, E. B., Ahmad, M. I., Lalung, J., Alam, M., & Siddiqui, M. R. (2022). Enhancing the efficiency of banana peel bio-coagulant in turbid and river water treatment applications. *Water, 14*(16), 2473.

Bahadori, A., Clark, M., & Boyd, B. (2013). *Essentials of water systems design in the oil, gas, and chemical processing industries*. Springer Science & Business Media.

Bahrodin, M. B., Zaidi, N. S., Hussein, N., Sillanpää, M., Prasetyo, D. D., & Syafiuddin, A. (2021). Recent advances on coagulation-based treatment of wastewater: Transition from chemical to natural coagulant. *Current Pollution Reports, 7*(3), 379–391.

Bolto, B., & Gregory, J. (2007). Organic polyelectrolytes in water treatment. *Water Research, 41*(11), 2301–2324.

Chaturvedi, S., Kumari, A., Bhatacharya, A., Sharma, A., Nain, L., & Khare, S. K. (2018). Banana peel waste management for single-cell oil production. *Energy, Ecology and Environment, 3*(5), 296–303.

Choy, S., Prasad, K., Wu, T., & Ramanan, R. (2015). A review on common vegetables and legumes as promising plant-based natural coagulants in water clarification. *International Journal of Environmental Science and Technology, 12*(1), 367–390.

Choy, S. Y., Prasad, K. M. N., Wu, T. Y., Raghunandan, M. E., Yang, B., Phang, S.-M., & Ramanan, R. N. (2017). Isolation, characterization and the potential use of starch from jackfruit seed wastes as a coagulant aid for treatment of turbid water. *Environmental Science and Pollution Research, 24*(3), 2876–2889.

Chua, S.-C., Chong, F.-K., Malek, M., Ul Mustafa, M. R., Ismail, N., Sujarwo, W., Ho, Y.-C. (2020). Optimized use of ferric chloride and *Sesbania* seed gum (SSG) as sustainable coagulant aid for turbidity reduction in drinking water treatment. *Sustainability, 12*(6), 2273.

Daverey, A., Tiwari, N., & Dutta, K. (2019). Utilization of extracts of *Musa paradisica* (banana) peels and *Dolichos lablab* (Indian bean) seeds as low-cost natural coagulants for turbidity removal from water. *Environmental Science and Pollution Research, 26*(33), 34177–34183.

DOI:https//doi.org/10.22452/mjs.vol43no1.9
Malaysian Journal of Science 43(1): 113-122 (March 2024)

Diddens, D., & Heuer, A. (2019, July 21–26). *Ion transport mechanism in polymer electrolytes-Bridging the scales via molecular simulations and theory* [Paper presentation]. Electrochemical Conference on Energy and the Environment (ECEE 2019): Bioelectrochemistry and Energy Storage. Scotland Scottish Event Campus.

Duraiprasanth, T., Senthilnathan, S., Senthilkumar, R., Anandi, S., & Harishankar, K. (2022). How the banana farmers are efficient? An evidence from the Tiruchirappalli District of Tamil Nadu. *Methodology, 2022*. 363-368

Feng, L., Stuart, M. C., & Adachi, Y. (2015). Dynamics of polyelectrolyte adsorption and colloidal flocculation upon mixing studied using mono-dispersed polystyrene latex particles. *Advances in Colloid and Interface Science, 226*, 101–114.

Feng, Q., Guo, K., Gao, Y., Liu, B., Yue, Q., Shi, W., Gao, B. (2022). Effect of coagulation treatment on sludge dewatering performance: Application of polysilicate and their mechanism. *Separation and Purification Technology, 301*, 121954.

Fu, Y., Meng, X., Lu, N., Jian, H., & Di, Y. (2019). Characteristics changes in banana peel coagulant during storage process. *International Journal of Environmental Science and Technology, 16*(12), 7747–7756.

Ghernaout, D., Simoussa, A., Alghamdi, A., Ghernaout, B., Elboughdiri, N., Mahjoubi, A., El-Wakil, A. E.-A. (2018). Combining lime softening with alum coagulation for hard Ghrib dam water conventional treatment. *International Journal of Advanced and Applied Sciences, 5*(5), 61–70.

Gopika, G., & Kani, K. M. (2016) Accessing the suitability of using banana pith juice as a natural coagulant for textile wastewater treatment.

Gurumath, K., & Suresh, S. (2019). *Cicer arietinum* is used as natural coagulant for water treatment.

Henderson, R., Parsons, S., & Jefferson, B. (2008). Successful removal of algae through the control of zeta potential. *Separation Science and Technology, 43*(7), 1653–1666.

Hilal, N., Busca, G., Hankins, N., & Mohammad, A. W. (2004). The use of ultrafiltration and nanofiltration membranes in the treatment of metal-working fluids. *Desalination, 167*(1–3), 227–238.

Huang, X., Wan, Y., Shi, B., Shi, J., Chen, H., & Liang, H. (2020). Characterization and application of poly-ferric-titanium-silicate-sulfate in disperse and reactive dye wastewaters treatment. *Chemosphere, 249*, 126129.

Hussain, S., Awad, J., Sarkar, B., Chow, C. W., Duan, J., & van Leeuwen, J. (2019). Coagulation of dissolved organic matter in surface water by novel titanium (III) chloride: Mechanistic surface chemical and spectroscopic characterisation. *Separation and Purification Technology, 213*, 213–223.

Jayalakshmi, G., Saritha, V., & Dwarapureddi, B. K. (2017). A review on native plant based coagulants for water purification. *International Journal of Applied Environmental Sciences, 12*(3), 469–487.

Kakoi, B., Kaluli, J. W., Ndiba, P., & Thiong'o, G. (2016). Banana pith as a natural coagulant for polluted river water. *Ecological Engineering, 95*, 699–705.

Kalemelawa, F., Nishihara, E., Endo, T., Ahmad, Z., Yeasmin, R., Tenywa, M. M., & Yamamoto, S. (2012). An evaluation of aerobic and anaerobic composting of banana peels treated with different inoculums for soil nutrient replenishment. *Bioresource Technology, 126*, 375–382.

Kandeeban, M., & Malarkodi, M. (2019). Assessment of the farmers attitude towards banana cultivation and export in Coimbatore and Erode districts of Tamil Nadu. *International Journal of Farm Sciences, 9*(1), 49–51.

Khawas, P., & Deka, S. C. (2016). Isolation and characterization of cellulose nanofibers from culinary banana peel using high-intensity ultrasonication combined with chemical treatment. *Carbohydrate Polymers, 137*, 608–616.

Kristianto, H. (2017). The potency of Indonesia native plants as natural coagulant: A mini review. *Water Conservation Science and Engineering, 2*(2), 51–60.

Kumar, V., Othman, N., & Asharuddin, S. (2017). *Applications of natural coagulants to treat wastewater– A review* [Paper presentation]. MATEC Web of Conferences. Sibiu, Romania, June 7-9, 2017

Liao, Y., Tang, X., Yang, Q., Chen, W., Liu, B., Zhao, C., Zheng, H. (2017). Characterization of an inorganic polymer coagulant and coagulation behavior for humic acid/algae-polluted water treatment: Polymeric zinc–ferric–silicate–sulfate coagulant. *RSC Advances, 7*(32), 19856–19862.

Ling, D. C., Jewaratnam, J., & Kwong, C. J. (2018). Fenugreek seeds coagulant and banana peels flocculant for the treatment of palm oil mill effluent. *Research Communication in Engineering Science & Technology, 1*, 18.

Liu, Z., Huang, M., Li, A., & Yang, H. (2017). Flocculation and antimicrobial properties of a cationized starch. *Water Research, 119*, 57–66.

López, S. S., MacAdam, J., Biddle, M., & Jarvis, P. (2021). The impact of dosing sequence on the removal of the persistent pesticide metaldehyde using powdered activated carbon with coagulation and clarification. *Journal of Water Process Engineering, 39*, 101756.

Lv, D., Zheng, L., Zhang, H., & Deng, Y. (2018). Coagulation of colloidal particles with ferrate (VI). *Environmental Science: Water Research & Technology, 4*(5), 701–710.

Mazaheri, R., Ghazani, M. T., & Alighardashi, A. (2018). Effects of *Moringa peregrina* and ferric chloride ($FeCl_3$) on water treatment sludge dewatering. *Biosciences Biotechnology Research Asia, 15*(4), 975–980.

Mazloomi, S., Zarei, A., Nourmoradi, H., Ghodsei, S., Amraei, P., & Haghighat, G. A. (2019). Optimization of coagulation-flocculation process for turbidity removal using response surface methodology: a study in Ilam water treatment plant, Iran. *Desalination and Water Treatment, 147*, 234–242.

DOI:https//doi.org/10.22452/mjs.vol43no1.9
Malaysian Journal of Science 43(1): 113-122 (March 2024)

Mohan, S., Vidhya, K., Sivakumar, C., Sugnathi, M., Shanmugavadivu, V., & Devi, M. (2019). Textile waste water treatment by using natural coagulant (Neem-Azadirachta India). *International Research Journal of Multidisciplinary Technovation, 1*(6), 636–642.

Mohd-Salleh, S. N. A., Mohd-Zin, N. S., & Othman, N. (2019). A review of wastewater treatment using natural material and its potential as aid and composite coagulant. *Sains Malaysiana, 48*(1), 155–164.

Mokhtar, N., Priyatharishini, M., & Kristanti, R. (2019). Study on the effectiveness of banana peel coagulant in turbidity reduction of synthetic wastewater. *International Journal of Engineering Technology and Sciences, 6*(1), 82–90.

Mosa, Z. M., & Khalil, A. F. (2015). The effect of banana peels supplemented diet on acute liver failure rats. *Annals of Agricultural Sciences, 60*(2), 373–379.

Mumbi, A. W., Fengting, L., & Karanja, A. (2018). Sustainable treatment of drinking water using natural coagulants in developing countries: A case of informal settlements in Kenya. *Water Utility Journal, 18*, 1–11.

Naceradska, J., Novotna, K., Cermakova, L., Cajthaml, T., & Pivokonsky, M. (2019). Investigating the coagulation of non-proteinaceous algal organic matter: Optimizing coagulation performance and identification of removal mechanisms. *Journal of Environmental Sciences, 79*, 25–34.

Namasivayam, C., Kanchana, N., & Yamuna, R. (1993). Waste banana pith as adsorbent for the removal of rhodamine-B from aqueous solutions. *Waste Management, 13*(1), 89–95.

Namasivayam, C., Prabha, D., & Kumutha, M. (1998). Removal of direct red and acid brilliant blue by adsorption on to banana pith. *Bioresource Technology, 64*(1), 77–79.

Nan, J., Yao, M., Chen, T., Li, S., Wang, Z., & Feng, G. (2016). Breakage and regrowth of flocs formed by sweep coagulation using additional coagulant of poly aluminium chloride and non-ionic polyacrylamide. *Environmental Science and Pollution Research, 23*(16), 16336–16348.

Nandini, G. M., & Sheba, M. C. (2016). Emanating trends in the usage of bio-coagulants in potable water treatment: A review. *Seeds, 99*, 10.

Nath, A., Mishra, A., & Pande, P. P. (2021). A review natural polymeric coagulants in wastewater treatment. *Materials Today: Proceedings, 46*, 6113–6117.

Nayak, S., Sajankila, S. P., & Rao, C. V. (2018). Green synthesis of gold nanoparticles from banana pith extract and its evaluation of antibacterial activity and catalytic reduction of malachite green dye. *The Journal of Microbiology, Biotechnology and Food Sciences, 7*(6), 641.

Olaoye, R., Afolayan, O., Mustapha, O., & Adeleke, H. (2018). The efficacy of banana peel activated carbon in the removal of cyanide and selected metals from cassava processing wastewater. *Advances in Research*, 1–12.

Pathak, P. D., & Mandavgane, S. A. (2015). Preparation and characterization of raw and carbon from banana peel by microwave activation: Application in citric acid adsorption. *Journal of Environmental Chemical Engineering, 3*(4), 2435–2447.

Pelissari, F. M., Andrade-Mahecha, M. M., do Amaral Sobral, P. J., & Menegalli, F. C. (2017). Nanocomposites based on banana starch reinforced with cellulose nanofibers isolated from banana peels. *Journal of Colloid and Interface Science, 505*, 154–167.

Rasool, M. A., Tavakoli, B., Chaibakhsh, N., Pendashteh, A. R., & Mirroshandel, A. S. (2016). Use of a plant-based coagulant in coagulation–ozonation combined treatment of leachate from a waste dumping site. *Ecological Engineering, 90*, 431–437.

Ravindra, K., Mor, S., & Pinnaka, V. L. (2019). Water uses, treatment, and sanitation practices in rural areas of Chandigarh and its relation with waterborne diseases. *Environmental Science and Pollution Research, 26*(19), 19512–19522.

Rizal, S., Lai, T. K., Muksin, U., Olaiya, N., Abdullah, C., Yahya, E. B., Abdul Khalil, H. (2020). Properties of macroalgae biopolymer films reinforcement with polysaccharide microfibre. *Polymers, 12*(11), 2554.

Salmasi, F., Nouri, M., & Abraham, J. (2020). Upstream cutoff and downstream filters to control of seepage in dams. *Water Resources Management*, 34(12):1-18.

Shi, Y., Fan, M., Brown, R. C., Sung, S., & Van Leeuwen, J. H. (2004). Comparison of corrosivity of polymeric sulfate ferric and ferric chloride as coagulants in water treatment. *Chemical Engineering and Processing: Process Intensification, 43*(8), 955–964.

Shrestha, A., Naidu, G., Johir, M. A. H., Kandasamy, J., & Vigneswaran, S. (2017). Performance of flocculation titanium salts for seawater reverse osmosis pretreatment. *Desalination and Water Treatment*. 98 (2017) 92–97

Sillanpää, M., Ncibi, M. C., Matilainen, A., & Vepsäläinen, M. (2018). Removal of natural organic matter in drinking water treatment by coagulation: A comprehensive review. *Chemosphere, 190*, 54–71.

Soluri, J. (2021). *Banana cultures: Agriculture, consumption, and environmental change in Honduras and the United States*. University of Texas Press.

Subashree, R., Nagaraj, S., & Anusha, G. (2018). Investigation of coagulation activity of lemon and banana peel powder in water treatment. *ICRRDESH-17*. 46-49

Sulaiman, M., Zhigila, D. A., Mohammed, K., Umar, D. M., Aliyu, B., & Abd Manan, F. (2017). *Moringa oleifera* seed as alternative natural coagulant for potential application in water treatment: A review. *J. Adv. Rev. Sci. Res, 30*(1), 1–11.

Sun, Y., Zhu, C., Zheng, H., Sun, W., Xu, Y., Xiao, X., . . . Liu, C. (2017). Characterization and coagulation behavior of polymeric aluminum ferric silicate for high-concentration oily wastewater treatment. *Chemical Engineering Research and Design, 119*, 23–32.

DOI:https//doi.org/10.22452/mjs.vol43no1.9
Malaysian Journal of Science 43(1): 113-122 (March 2024)

Teh, C. Y., Wu, T. Y., & Juan, J. C. (2014). Potential use of rice starch in coagulation–flocculation process of agro-industrial wastewater: Treatment performance and flocs characterization. *Ecological Engineering, 71*, 509–519.

Teixeira, M. R., Camacho, F. P., Sousa, V. S., & Bergamasco, R. (2017). Green technologies for cyanobacteria and natural organic matter water treatment using natural based products. *Journal of Cleaner Production, 162*, 484–490.

Theodoro, J. P., Lenz, G. F., Zara, R. F., & Bergamasco, R. (2013). Coagulants and natural polymers: Perspectives for the treatment of water. *Plastic and Polymer Technology, 2*(3), 55–62.

Ting, W. C., Loh, Z. Z., Bahrodin, M. B., Awang, N. A., & Kadier, A. (2022). Assessment and optimization of a natural coagulant (*Musa paradisiaca*) peels for domestic wastewater treatment. *Environmental and Toxicology Management, 2*(1), 7–13.

Wan, Y., Huang, X., Shi, B., Shi, J., & Hao, H. (2019). Reduction of organic matter and disinfection byproducts formation potential by titanium, aluminum and ferric salts coagulation for micro-polluted source water treatment. *Chemosphere, 219*, 28–35.

Wang, W., Yue, Q., Li, R., Bu, F., Shen, X., & Gao, B. (2018). Optimization of coagulation pre-treatment for alleviating ultrafiltration membrane fouling: The role of floc properties on Al species. *Chemosphere, 200*, 86–92.

Wang, X., Li, M., Song, X., Chen, Z., Wu, B., & Zhang, S. (2016). Preparation and evaluation of titanium-based xerogel as a promising coagulant for water/wastewater treatment. *Environmental Science & Technology, 50*(17), 9619–9626.

Wang, X., Wang, X., Wei, Z., & Zhang, S. (2018). Potent removal of cyanobacteria with controlled release of toxic secondary metabolites by a titanium xerogel coagulant. *Water Research, 128*, 341–349.

Yabuki, L. N. M., Luko Sulato, K. S., Boniolo, M. R., Menegário, A. A., & Garcia, M. L. (2020). Diffusive gradients in thin films based on banana peel and moringa seeds binding gel disks for in situ measurement of Cd, Cu, Pb and Zn. *International Journal of Environmental Analytical Chemistry*, 102(4):1-25

Yahya, E. B., Abdulsamad, M. A., Allaq, A. A., Abdoallah, T., & Ermese, E. (2020). The effect of natural and petroleum based materials on the growth rate and antibiotic sensitivity of *Pseudomonas aeruginosa*. *International Journal for Research in Applied Sciences and Biotechnology, 7*(5), 295–298.

Yahya, E. B., Alfallous, K. A., Wali, A., Hameid, S., & Zwaid, H. (2020). Growth rate and antibiotic sensitivity effect of some natural and petroleum based materials on *Staphylococcus aureus*. *International Journal for Research in Applied Sciences and Biotechnology, 7*(5), 7–11.

Yong, M. Y., & Ismail, N. (2016). Optimisation of *Hibiscus sabdariffa* as a natural coagulant to treat Congo red in wastewater. *Journal of Engineering Science and Technology, 11*, 153–165.

Yushananta, P., & Ahyanti, M. (2022). Utilization of banana pith starch from agricultural waste as a cationic coagulant. *Jurnal Aisyah: Jurnal Ilmu Kesehatan, 7*(1), 165–172.

Zhang, W., Chen, Z., Cao, B., Du, Y., Wang, C., Wang, D., Xia, H. (2017). Improvement of wastewater sludge dewatering performance using titanium salt coagulants (TSCs) in combination with magnetic nano-particles: Significance of titanium speciation. *Water Research, 110*, 102–111.

DOI:https//doi.org/10.22452/mjs.vol43no1.9
Malaysian Journal of Science 43(1): 113-122 (March 2024)